Developing mitoribosomal profiling to investigate quality control of human mitochondrial protein synthesis

Maria Wesolowska

M. Sc.

Thesis submitted to Newcastle University
in candidature for the degree of Doctor of Philosophy

Newcastle University
Faculty of Medical Sciences
Wellcome Trust Centre for Mitochondrial Research
Institute for Cell and Molecular Biosciences
May 2015

Abstract

Mitochondria are essential organelles of nucleated cells that have the ability to conduct intra-organellar protein synthesis. Many aspects of this process are poorly understood especially the quality control and the rescue of stalled mitoribosomes.

My project was focused on investigating potential candidates involved in quality control and ribosome rescue, including the release factor protein C12orf65. The importance of this protein in mt-translation was confirmed in a patient harbouring a mutation in C12orf65 gene, which displayed a general decrease in de novo mt-translation with subsequent disruption in assembly of OXPHOS complexes I, IV and V. I investigated the consequences on mitochondrial homeostasis in such a cell line. However, for a molecular understanding of the mechanism of this protein's function a different, more focused approach was needed. To this end I applied ribosome profiling to mitochondria.

Ribosome profiling provides a genome-wide analysis of protein synthesis by deep-sequencing of the mRNA fragments protected by ribosomes. It allows monitoring of progression of translation in vivo and can be used to identify contributions by regulating factors. I optimized the protocol for use in human mitochondria, initially on a cell line with a mutation in mt-tRNAVal. The decrease in stability of the uncharged tRNAVal resulted in an increase in mitoribosomal density over the valine codons, consistent with ribosomal stalling. I then used the final protocol, proven effective to study defects in mitoribosome progression, on cells with siRNA depleted C12orf65. Reducing transcript levels to 30% of control gave modest differences in mitoribosomal profiles. The control profiles, however, allowed normal features of mitochondrial translation to be identified. Although the exact function of C12orf65 remains unknown its involvement in mitochondrial protein translation is clear. Further applications of mitoribosome profiling to depleted or mutant cell lines should elucidate mechanisms that rescue stalled mitoribosomes and the potential role of C12orf65.

Acknowledgments

First I would like to thank my supervisors Prof. Zofia Chrzanowska-Lightowlers and Prof. Robert Lightowlers for all the help, encouragement and inexhaustible patience they have given me throughout these years. I cannot thank you enough for giving me an opportunity to be a part of your team and working on this challenging project. I am grateful for you pushing me further and for all the time and energy you have spent teaching me how to be a better scientist. It was a privilege to learn from such kind, experienced and passionate people.

I would also like to thank members of my lab: Monika, Nicole, Christie, Fei, Kyle, Rawaa, Francesco, Tran, Casey and Martin for creating an incredibly friendly atmosphere. Having such a great group of friends made this experience unique. Thanks to your good energy, openness and support I enjoyed every day working in Lightowlers lab. I am also very grateful for all the technical help I received from John Grady during ribosome profiling analysis and his magical graph-producing skills.
Special thank you to Ola Pajak for all the help and guidance at the beginning of my project and teaching me her flawless lab technique. Also to Karolina Rygiel and Agata Rozanska for being my support group, sharing their experiences, giving me good advice and being there for me every time I needed to talk and complain.

I would like to thank Prof. Reuven Agami and his group for hosting me and kindly letting me learn in their facility, as well as for all the support with mitoribosome profiling development.

Last but not the least, I would like to thank my family, especially my future husband Wojtek for his love, support and patience. For giving me space and encouragement when I needed it the most and for bravely enduring my “thesis writing” phase. I love you, you are and always will be a source of inspiration for me.
I would also like to thank my parents for the enormous support throughout my whole life and teaching me that there are no limits to what I can accomplish.

Author's declaration

I declare that the data presented in this thesis is based solely on work carried out by the author, unless stated otherwise. Moreover, neither this thesis nor any of the data within it has been submitted before for any other degree or award. The contributions by others have been acknowledged, where appropriate.
Maria Wesolowska

Table of contents

List of figures

List of tables

Abbreviations

aa – amino acid (s)
aa – tRNA - aminoacyl-tRNA
ADP – adenosine diphosphate
APS – ammonium-persulphate
ArfA – an alternative ribosome factor A
ArfB – alternative ribosome factor B
A-site – aminoacyl-tRNA site within the ribosome
ATP – adenosine triphosphate
BN – Blue Native
bp – base pair(s)
BSA – bovine serum albumin cyt c - cytochrome c
CBB – Coomassie Brilliant Blue
cDNA – complementary DNA
C. elegans – *Caenorhabditis elegans*
CLIP – Crosslinking immunoprecipitation
CoQ – Coenzyme Q, ubiquinone
COX – Cytochrome *c* oxidase
CP – (ribosomal) central protuberance
cpm – counts per minute
cryo-EM – cryo-electron microscopy
CsCl – cesium chloride
C_T – threshold cycle
Cys – cystein
cyt – cytochrome
d – day(s)
DAB – 3,3'-diaminobenzidine
DDM – dodecylmaltoside
DEPC – diethyl pyrocarbonate
dH_2O – distilled water
D-loop – displacement loop
DMEM – Dulbecco's modified Eagle's medium DMSO - dimethyl-sulphoxide
DMSO – dimethyl-sulphoxide
DNA – deoxyribonucleic acid

dNTP – deoxynucleotide triphosphate

dsDNA – double stranded DNA

DTT – dithiothreitol

E. coli – *Escherichia coli*

EDTA – ethylene diamine tetra-acetic acid

EF(-G/-Ts/-Tu) - elongation factor (-G/-Ts/-Tu)

EGTA - ethylene glycol tetra-acetic acid

E-site - exit site within the ribosome

ETC – electron transport chain

FADH2 – reduced flavin-adenine dinucleotide

FCS – foetal calf serum

fMet – formyl-methionine

FPKM – fragments per kb of transcript per million reads

FRT – Flp-recombination-target

g – relative centrifugal force

GDP – guanine diphosphate

GoI – gene of interest

GRSF1 – G-rich sequence binding factor 1

GST – Glutathione-S-transferase

GTP – guanine triphosphate

h – hour(s)

H – heavy strand

H&E – hematoxylin and eosin staining

HEK293T – human embryonic kidney cells

HeLa – human cervical cancer carcinoma cells from Henrietta Lacks

HSP – heavy strand promoter

ICC – immunocytochemistry

IF – initiation factor

IMM/ IM – inner mitochondrial membrane

IMS – intermembrane space

IP – immunoprecipitation

IPTG – Isopro–yl β-D-1-thiogalactopyranoside

kb – kilo-base(pairs)

KCl – potassium chloride

kDa – kilo-Dalton

KOD – DNA polymerase from *Thermococcus kodakaraensis*

L– light strand

LB – Lysogeny broth

lcnRNAs – long non-coding RNAs

lincRNAs – long interspersed non-coding RNAs ()

LRPPRC – leucine-rich pentatricopeptide-repeat containing protein

LSP– light strand promoter

LSU – large subunit of the ribosome

M – matrix

MDa – mega-Dalton

MES – 2-(N-morpholino)ethanesulfonic acid

MESCs – mouse embryonic stem cells

Met – methionine

$MgSO_4$ – magnesium sulphate

min – minute(s)

MOPS – morpholinopropanesulfonic acid

MRGs – mitochondrial RNA granules

mRNA – messenger RNA

MRP(L/S) – mitochondrial ribosomal protein (of the LSU/ SSU)

mt – mitochondrial

mtDNA – mitochondrial genome

mtPAP – mitochondrial poly(A) polimerase

mtSSB – mitochondrial single stranded DNA-binding protein

MW – molecular weight

N – amino-terminus

NaCl – sodium chloride

NAD – nicotinamide-adenine dinucleotide

$NADH_2$ - reduced nicotinamide-adenine dinucleotide

NaOAc – sodium acetate

NBT – nitroblue tetrazolium

NEAA – non-essential amino acids

NGD – no-go mediated decay

NGS – next generation sequencing

NMD – nonsense mediated decay

NP-40 – Nonidet P-40, octyl phenoxy-polyethoxy-ethanol

NRD – non-functional 18S-rRNA decay

NRK- Normal Rat Kidney Epithelial Cells

NSD – non-stop mediated decay

nt – nucleotide(s)

NT – non targeting

OD – optical density

OM – outer mitochondrial membrane

O/N – overnight

ORF(s) – open reading frame(s)

OXPHOS – oxidative phosphorylation

PAGE – polyacrylamide gel electrophoresis

PAP – poly(A) polimerase

PAS – polypeptide accessible site

PBS – phosphate buffered saline

PES – polypeptide exit site

PCR – polymerase chain reaction

PMSF – phenylmethylsulphonyl fluoride

PNK – polynucleotide kinase

POLRMT – mitochondrial RNA polymerase

P-site – peptidyl-tRNA site within the ribosome

PTC – peptidyl-tRNA

PTH – peptidyl-tRNA hydrolase

PVDF – polyvinylidine fluoride

Q – ubiquinone

QH_2 – ubiquinol

qPCR (RT – qPCR) – quantitative real time PCR

RBP – RNA binding protein

RC – respiratory chain

RF – release factor

RFs – ribosome footprints

RITOLS – ribonucleotide incorporation throughout lagged strand

RNA – ribonucleic acid

RNA7 – *MT-ND4* and *MT-ND4L*

RNA14 – *MT-ATP6* and *MT-ATP8*

RNA15 – *MT-ATP6*, *MT-ATP8* and *MT-CO3*

rpm – revolutions per minute

RQC – ribosome dependent quality control

RRF – ribosome recycling factor

rRNA – ribosomal RNA

s – seconds

SD – standard deviation

SDH – succinate dehydrogenase

SDS – sodium-dodecyl-sulphate

siRNA – silencing RNA, small interfering RNA

SLIRP – stem-loop interacting RNA binding protein

SM – silent mutation

sprcRNAs – short polycistronic ribosome-associated coding RNAs

SSC – saline-sodium citrate

ssDNA – single stranded DNA

SSPE – saline sodium phosphate EDTA buffer

SSU – small subunit of the ribosome

TAE – tris-acetate EDTA

Taq – DNA polymerase from *Thermus aquaticus*

TBS – tris buffered saline

TBS-T – tris buffered saline, containing Tween-20 (0.1%)

TE – tris EDTA buffer

TE (ratio) – translational efficiency

TEMED – N, N, N', N'-tetramethylethylene-diamine

Tet – tetracycline

TFAM – transcription factor A

TFB1M and TFB2M – mitochondrial transcription factor B1 or 2 (synonym mtTFB1/2)

T_m – melting temperature

tmRNA – transfer messanger tRNA

TO – tetracycline operator

Tris – 2-Amino-2-hydroxymethyl-propane-1,3-diol

Triton X-100 – polyethylene glycol p-(1,1,3,3-tetramethylbutyl)-phenyl ether

tRNA – transfer RNA

T. thermophilus - *Thermus thermophilus*

Tween-20 – polyoxyethylene sorbitanmonolaurate

U – unit (enzyme activity; 1U = 1µmol/ min)

U2OS – human osteosarcoma cell line

uORFs – upstream open reading frames

UTR(s) – untranslated region(s)

UV – ultra-violet

V, Val – valine

VARS2/ VARS2L – mitochondrial valyl-tRNA synthetase

v/v – volume/ volume WT – wild type

w/v – weight/ volume

WT – wild type

Chapter 1

Introduction

1.1. Mitochondria – an overview

1.1.1. Origin and evolution

Mitochondria, specialized energy-converting organelles, are present in all known eukaryotic nucleated cells. Studies based on one of their specific features, the presence of an intraorganellar unique genome and its expression, suggested the eubacterial origin of mitochondria. The sequencing and phylogenetic analysis of mitochondrial DNA from a broad range of organisms resulted in proposing a single ancestor related to α-proteobacteria (Gray et al., 1999). According to the wildly accepted endosymbiotic hypothesis, this original bacteria was engulfed by another cell, the identification of which has proven controversial (Embley and Martin, 2006), forming a symbiotic relationship. This endosymbiont would, with time, evolve into the mitochondrion. One piece of evidence that strongly supports this course of action was provided by sequencing the genome of *Rickettsia prowazekii*, an α-proteobacteria and intracellular parasite. Phylogenic analysis of this organism's DNA showed that it is very closely related to mitochondria and that this similarity is greater than for any other microbe studied so far (Andersson et al., 1998). Although mitochondria may have originated from bacteria their genomes are much smaller than these found in their respective ancestors. Over time many of the organellar genomes have decreased their size due to the transfer of genes from mitochondria to nucleus. Many of these genes have become functional nuclear copies and their products are re-imported into the mitochondrion to perform their functions (Timmis et al., 2004).

1.1.2. Mitochondrial structure and functions

Similar to bacteria that they presumably originated from, mitochondria are surrounded by a double membrane (Fig. 1.1 A). The inner membrane (IMM) is highly infolded and forms specific structures called cristae. Parts between the cristae where the inner membrane runs parallel to the outer membrane (OM) are known as the inner boundary membrane. The gap between the OM and inner boundary membrane is called intermembrane space (approx. 20 nm width). The cristae membrane, protruding deep into the inside space of the organellum (matrix) is mainly tubular but can take many different forms. The parts of matrix enclosed by cristae membrane are called intermembrane space (IMS) or intercristal space and the points were the membrane joins with the

inner boundary membrane are called cristae junctions (Fig. 1.1 B) (Frey and Mannella, 2000). Mitochondria occupy up to 25% of the cytoplasmic volume (Ballard and Whitlock, 2004) and in most organisms they form a dynamic reticulum often in contact with other cellular compartments (Rizzuto et al., 1998). The mitochondrial network, as well as isolated organelles, are subject to constant rearrangements resulting from fusion, fission and motility events. These processes require constant membrane remodelling that is regulated by a number of proteins (Chan, 2006).

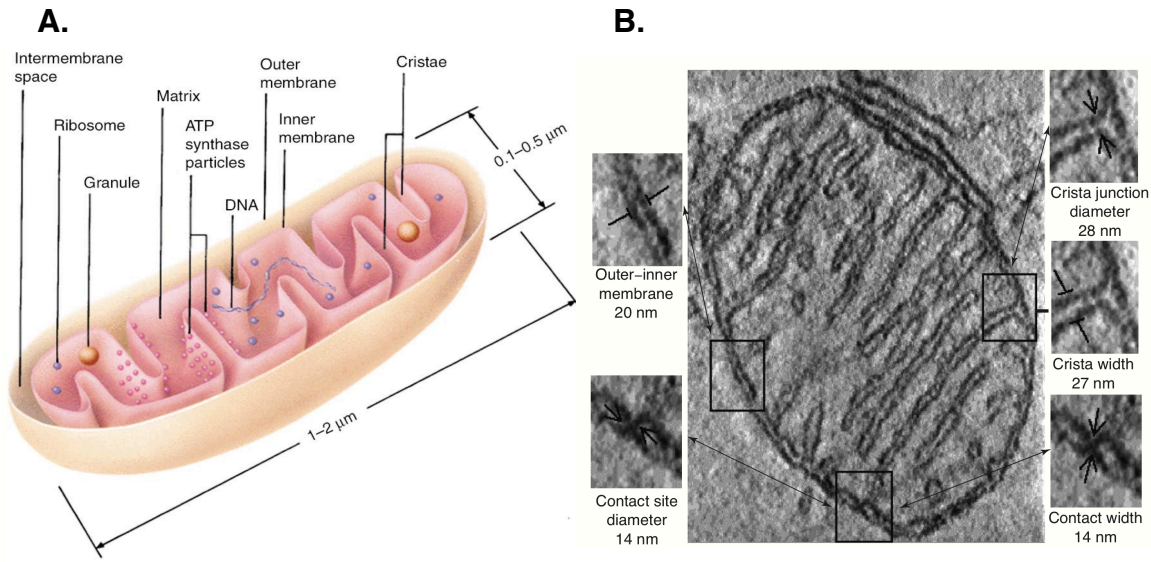

Figure 1.1 Organisation of the mitochondrial structures

A. Schematic representing internal structure of mitochondria. **B.** Electron microscopic image with details and measured dimensions of membrane structures inside mitochondria. Adapted from (Frey and Mannella, 2000).

Mitochondria perform many functions but synthesis of ATP by oxidative phosphorylation (OXPHOS) is a crucial and probably the most recognized role. This process is conducted via the transport of electrons through the series of protein complexes (respiratory chain, RC) embedded in the inner mitochondrial membrane. The electrons are transferred through the respiratory chain until finally they are transferred to the molecular oxygen. The passage of electrons is linked to the production of a proton gradient across the IMM, which is necessary for the F_OF_1 ATP synthase to produce ATP from ADP. The respiratory chain comprises of 4 protein complexes: complex I (NADH:CoQ oxidoreductase), complex II (succinate: ubiquinone reductase), complex III (cytochrome bc_1) and complex IV (cytochrome *c* oxidase). All complexes (except for complex II) have

components encoded in mitochondrial DNA as well as the nuclear genome. The electrons that are transferred across the RC are provided by reduced cofactors NADH and FADH2, produced during enzymatic reactions of glycolysis and tricarboxylic acid cycle (TCA). Complex I (reviewed in (Vogel et al., 2007) catalyzes the oxidation of NADH during which 2 electrons are released and passed through a flavin mononucleotide, iron-sulfur clusters and finally to ubiquinone (Q), which is reduced to ubiquinol (QH_2). During the transfer of these two electrons four protons are released to the intermembrane space across the IMM. Complex II (reviewed in (Cecchini, 2003) is a part of the Krebs cycle but it contributes to the respiratory chain by transferring electrons from succinate to the ubiquinone. During this process there is no proton translocation only supplying of the electrons to the electron transport chain (ETC). After the electrons are passed through complex I and II, QH_2 is reoxidised by complex III (reviewed in (Crofts, 2004). This reaction, called the Q-cycle, carries 2 electrons to the cytochrome *c* while releasing 2 protons across the membrane. The electron transfer is a 2-step process. First, one of the electrons from ubiquinol is carried to the cytochrome *c* on the membrane surface and the second electron passes to the ubiquinone at the matrix site of the complex. The uptake of the electron reduces ubiquinone to ubisemiquinone. When the second molecule of ubiquinol binds to the complex (again releasing 2 electrons and 2 protons) one of its electrons binds to another cytochrome *c* molecule while the second completes the reduction of the ubisemiquinone to ubiquinol. The final member of the electron transfer machinery is complex IV (reviewed (Yoshikawa et al., 2006), which receives electrons from the cytochrome *c*. These electrons are next passed on to the molecular oxygen (O_2), which is converted to water. For that reaction to fully occur 4 electrons are necessary but the cytochrome *c* can only transfer one at a time. Binding of just 1 electron to O_2 forms a dangerous reactive superoxide radical anion ($O_2^{\bullet -}$), which, if not contained, can damage the surrounding environment. Therefore the O_2 molecules are stored inside the complex in a bimetallic centre until it receives all 4 electrons. Only then it can be released as 2 molecules of water. The electrons pass through a chain of copper ions and hemes groups, which results in pumping protons across the membrane. For each O_2 molecule that is converted into water 4 protons are transferred through the membrane. The protons that are transferred to the IMM during the electron transfer form the electrochemical gradient, which is then

utilized by the last of the OXPHOS complexes, F_1F_O ATP synthase (Abrahams et al., 1994). The synthesis of ATP, which is assembled from ADP and P_i, is driven by proton flow back into the matrix. The production of ATP through oxidative phosphorylation is, therefore, more efficient than via anaerobic glucose metabolism, namely glycolysis.

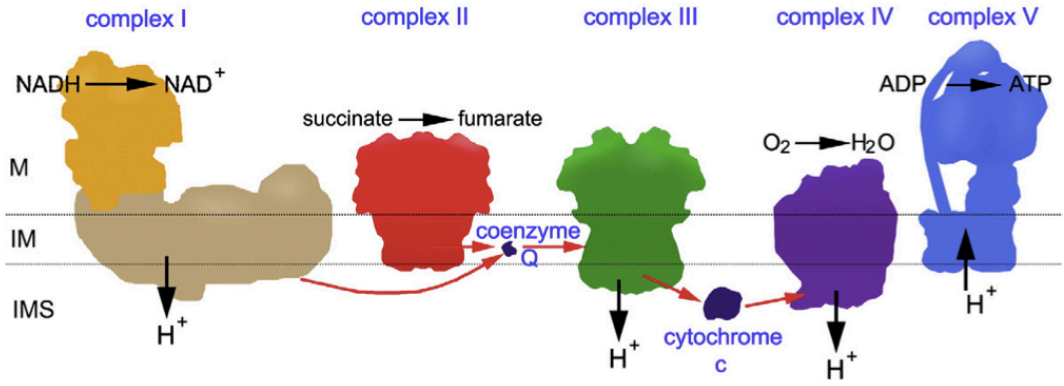

Figure 1.2. The schematic of oxidative phosphorylation

The schematic overview of OXPHOS with the simplified chemical reaction that is catalyzed by each of the complexes, adapted from (Dudkina et al., 2010). The electron transfer path is marked (red arrows) as well as the places where electron pumping occurs (black arrows). Positions of mitochondrial matrix (M), inner membrane (IM) and intermembrane space (IMS) are marked with black lines. Complex I (NADH:CoQ oxidoreductase) consists of 45 subunits, out of which 7 are encoded in mtDNA. Complex II (succinate: ubiquinone reductase), the smallest of all complexes is build of 4 subunits, all encoded in nuclear DNA. The products of redox reactions catalyzed by CI and CII is coenzyme Q (ubiquinone). Complex III (cytochrome bc_1) consists of 10 nuclear- and 1-mitochondrally encoded subunits. Cytochrome C shuttles electrons between CIII and Complex IV. CIV (cytochrome *c* oxidase), with 3 mitochondrial and 10 nuclear encoded subunits. The final complex, CV is a F_0F_1 ATP synthase is a multisubunit complex encoded in nuclear DNA except for 2 subunits.

However, ATP synthesis through OXPHOS is not the only function of mitochondria. These organelles take part in various processes within the cell including apoptosis (Martinou and Youle, 2011), calcium homeostasis (Celsi et al., 2009), and transduction of intra-cellular signals (Hüttemann et al., 2007). The only common function mitochondria of all species share is production of iron-sulphur clusters, crucial components of many essential enzymes (Lill, 2009).

1.1.3. Characteristics of mitochondrial genomes and mtDNA replication

The presence of the genome separate to the nucleus is one of the most profound characteristics of mitochondria. Mitochondrial genomes,

depending on the organism, vary in size from <6 kb in *Plasmodium falciparum* to ~ 367 kb in *Arabidopsis thaliana* (Gray et al., 1999; Unseld et al., 1997) and contents from 5 genes in *Plasmodium* to 97 in *Reclinomonas Americana* (Gray, 1999; Lang et al., 1997). They can also differ in shape, which in the majority of cases is circular but in some organisms linear genomes can be found (Nosek et al., 1998). Features of the human mtDNA are as follows: it is a small (16569 nucleotides), circular and double stranded DNA molecule, which encodes 13 polypeptides, 2 rRNAs and 22 tRNAs. The polypeptides are all subunits of the OXPHOS complexes. Coding sequences are placed on both strands of mtDNA, named H (heavy) and L (light) historically based on their buoyant densities in alkaline CsCl gradients (Clayton, 1991). The genetic information in humans and other mammals is very compact. There are no introns and the noncoding elements, including the regulatory sequences, are grouped in one place commonly named the displacement loop (D-loop), as it maintains a short nascent DNA sequence at the origin of leading strand replication (Clayton, 1991). D-loop contains promoters of transcription and replication (Anderson et al., 1981). In comparison, mitochondrial genomes of plants, which are much bigger than the mammalian ones, contain 80-90% non-coding sequences such as 5' and 3' untranslated regions introns, intronic and undefined ORFs, pseudogenes, and pieces of foreign DNA (chloroplast and nuclear) (Lang et al., 1999).

Often mitochondrial genome is characterized by having a higher mutation rate than the nuclear one (9-25 times) (Lynch et al., 2006). Mammalian mitochondrial DNA is maternally inherited, therefore the mutations in mtDNA can only be transmitted from mother to child but deletions seem to escape this and generally are not passed on. There are multiple copies of mtDNA in one cell (in somatic cell ~1000-10,000 per cell) and they can all be identical, a phenomenon called homoplasmy, where all copies are either wild type or harbouring a single specific mutation. If the mutation is present in only a subset of molecules it is termed heteroplasmy (Smeitink et al., 2001). The replication and turnover of the mtDNA was thought to be constant during the cell cycle with no specific connection to any of the phases (Bogenhagen and Clayton, 1977). However, this concept has recently been challenged when a link between the mitochondrial form and properties and the cell cycle was found in rat NRK cell line. (Mitra et al., 2009).

The replication of the mitochondrial genome is carried out by a set of proteins, the most important of them being the DNA polymerase γ, a helicase named Twinkle and mtSSB, which coats single stranded mtDNA (Graziewicz et al., 2006; Korhonen et al., 2003). The 2 main mechanisms that were proposed to describe the replication process are the strand-asymmetric / asynchronous and the bidirectional model. In the first one the replication is unidirectional and the synthesis of the lagging strand is delayed (Clayton, 1991; Robberson et al., 1972). The second model, describes the processes as bidirectional where a strand-coupled DNA synthesis occurs (Berk and Clayton, 1974; Holt et al., 2000). It is suggested that both mechanism coexist in mitochondria and the physiological conditions determine which one is utilized (Berk and Clayton, 1974; Bogenhagen and Clayton, 2003; Holt et al., 2000). However, there is a growing body of evidence that a third mtDNA replication mechanism named RITOLS (ribonucleotide incorporation throughout lagged strand) exists. In this model, replication is unidirectional and synthesis of lagging DNA strand involves a 'bootlace' mechanism during which RNA sequences are hybridized with it (Pohjoismäki et al., 2010; Reyes et al., 2013; Yasukawa et al., 2005).

1.1.4. Mitochondrial transcription, mtRNA processing and maturation

Even though mitochondria contain their own genome, its expression inside the organelle is not entirely independent of the rest of the cell. The polypeptides that are encoded in the human mtDNA are the subunits of the OXPHOS complexes (CI - *MT-ND1*, *MT-ND2*, *MT-ND3*, *MT-ND4, MT-ND4L*, *MT-ND5*, *MT-ND6*; CIII - *MT-CYB*; CIV - *MT-CO1*, *MT-CO2*, *MT-CO3*; CV - *MT-ATP6*, *MT-ATP8*). The rest of the genes encode both of the ribosomal RNAs and a complete set of tRNAs. All of the remaining ~1500 proteins (Nunnari and Suomalainen, 2012) required to generate and maintain a functional organelle are encoded in nuclear genome. Therefore more than 99% of all the necessary factors for replication, transcription (mt-transcription) and translation (mt-translation) and mitochondrial homeostasis, need to be imported from the cytosol (Glick and Schatz, 1991; Smits et al., 2010b). The transcription of human mtDNA is initiated from different sites on each strand. The L strand harbours only one promoter (LSP, position on the mtDNA marked on Fig. 1.3), whereas there are 2 promoters on the H strand (HSP1 and HSP2, also

referred to as H1 and H2, Fig. 1.3) (Montoya et al., 1982) located within 87 bp of each other. Transcription from all mentioned above promoters results in synthesis of polycistronic transcripts that are later processed by RNase P and Z (R. J. Temperley et al., 2010) to generate discreet coding sequences. Which transcripts originate from which promoter is presented on Fig. 1.3.

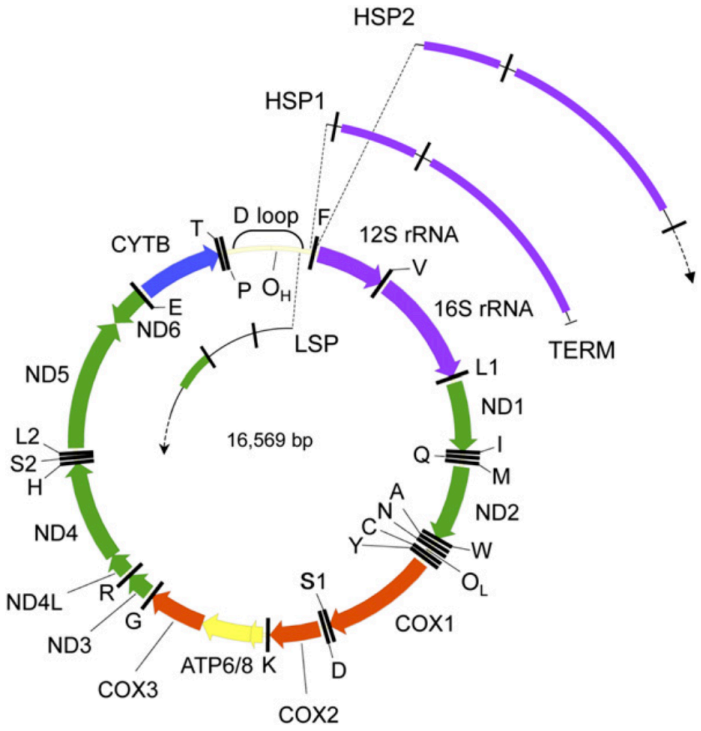

Figure 1.3. A schematic of transcription initiation of human mtDNA

The human mitochondrial genome is depicted as a circle with all the genes and initiation sites marked. The transcription of the L strand from the LSP promoter is presented as proceeding in the anticlockwise direction and the genes that are included in the polycistronic transcript that results from it are marked on the inside of the circle (tRNA genes depicted as black bars, *MT-ND6* in green). The genes transcribed from the H strand are marked at the outside of the circle and the process progresses in the clockwise direction. The polycistronic transcript originating from the HSP1 contains the two rRNA genes (12S and 16S rRNA in purple) and tRNAs F and V (black bars). The initiation from the HSP2 covers almost all of the H strand, including: 2 rRNAs, 13 tRNAs V, L1, I, M, W, D, K, G, R, H, S2, L2, and T (black) as well as 12 mRNAs: *MT-ND1*, *MT-ND2*, *MT-ND3*, *MT-ND4, MT-ND4L*, *MT-NG5* (in green), *MT-CO1*, *MT-CO2*, *MT-CO3* (orange), *MT-CYB* (blue), *MT-ATP6* and *MT- ATP8* (yellow). Adapted from (Bonawitz et al., 2006).

The most important components of the mt-transcription machinery are: RNA polymerase (POLRMT), transcription factor A (TFAM) and transcription factor B paralogues (TFB1M or TFB2M) (Bonawitz et al., 2006; Falkenberg et al., 2007). The polymerase consists of one unit and it contains 2 PPR motives (35 amino acid motifs) characteristic of RNA binding and processing functions. There is also a series of conserved motifs in the C-terminus that are found in

bacteriophage RNA polymerases (Masters et al., 1987) to which POLRMT has similarity. The proposed role of TFAM involves introducing conformational changes to mtDNA to facilitate binding of the RNA polymerase in the promoter region. This activity is sequence independent and allows binding, bending and unwinding of the DNA (Fisher et al., 1992). The direct interactions between TFAM and POLRMT result in formation of pre-initiation complex (pre-IC) in the promoter region. In order to initiate transcription pre-IC requires recruitment of TFB2M, that results in forming of the initiation complex (IC). The N-terminus of TFB2M reaches the active site of POLRMT, so that the later can bind an recognized the promoter (Morozov et al., 2015).

In addition to transcription activation, TFAM has another role in mitochondrial gene expression, namely it organizes mtDNA into the nucleoids. Within these protein complexes mtDNA is shaped into a U-turn via interaction with TFAM. Thus TFAM performs a dual role in transcription and organisation and maintenance of mtDNA (Ngo et al., 2011).

As for the remaining two transcription factors (TFB1M and TFB2M), the molecular mechanism of their action has not yet been fully defined (Sologub et al., 2009). However, the results in human mitochondria suggests that TFB2M plays a more important role in transcription than TFB1M, as it is involved in melting of the promoter and binding of a priming substrate (Sologub et al., 2009; Litonin et al., 2010). Although initially TFB1M demonstrated an ability to stimulate transcription initiation in *in vitro* studies (Falkenberg et al., 2002), it was not validated *in vivo*. Metodiev et al. showed that this protein is an essential methyltransferase of 12S rRNA and has no role in transcription (Metodiev et al., 2009).

After the polycistronic transcripts are generated from both mtDNA strands they are processed to produce individual transcripts. Since each protein coding or rRNA fragments is flanked by at least one tRNA gene, the formation of their characteristic cloverleaf structures was proposed as marker for endonucleolytic cleavage. This mechanism was termed the tRNA punctuation model (Ojala et al., 1981). Even though it does not explain all cleavage that occurs during mitochondrial tRNA processing it accounts for most of it (R. J. Temperley et al., 2010). There are 2 main enzymes involved in this process. RNase P that catalyses the cleavage at the 5’ ends of tRNAs (Holzmann et al., 2008). The processing of the 3’ ends is handled by RNase Z-like protein, ELAC2

(Dubrovsky, 2004). For the complete maturation, the resulting tRNA molecules require addition of the CCA nucleotides on the 3' terminus and aminoacylation by the correct aminoacyl-tRNA synthetase (Smits et al., 2010b).

The maturation of the mitochondrial mRNAs requires addition of a poly(A) tail. In human mitochondria all protein coding transcripts, except *MT-ND6,* are constitutively polyadenylated by addition of approximately 50 A residues (R. J. Temperley et al., 2010). For the majority of these transcripts, polyadenylation is necessary to complete the stop codon sequence as 7 of the 13 ORFs terminate with single U or UA nucleotides (Gagliardi et al., 2004). The poly(A) tail can also influence stability of mt-mRNAs, but its effect on each transcript differs (Chang and Tong, 2011; Nagaike, 2005; Tomecki et al., 2004). Recently published work of Wilson et al. provided additional insight into mechanisms regulated by the poly(A) modification through mutations that affect the activity of the mitochondrial poly(A) polymerase (mtPAP). Their results showed that changes to the length of the poly(A) tail can disrupt the post-transcriptional gene expression of mt-mRNAs and assembly of the respiratory chain complexes (Wilson et al., 2014).

In addition, the activity of the mtPAP was enhanced by the presence of the LRPPRC/SLIRP complex, which caused the poly(A) tail elongation. LRPPRC and SLIRP are two mitochondrial RNA binding proteins (RBP). They form a complex that binds the majority of the mt-mRNAs and is involved in maintenance of the poly(A) tails (Chujo et al., 2012; Ruzzenente et al., 2012; Sasarman et al., 2010). MtPAP was also found colocalizing with mt-RNA in discreet foci (Wilson et al., 2014), termed mitochondrial RNA granules (MRGs), which were first described by (Jourdain et al., 2013). MtPAP showed the same pattern of distribution as the marker of MRGs, GRSF1 protein. This protein belongs to a family of RNA processing proteins. Its role and presence in MRGs, where it colocalizes with RNase P and nascent mtRNAs, was investigated by (Jourdain et al., 2013) and (Antonicka et al., 2013). Integrity of these granules influenced the mtRNA maintenance and generation of the functional RNAs. GRSF1 was identified as an important factor in processing of the precursor RNA species (containing or lacking the tRNAs transcripts). It was suggested that these precursor species accumulate in the MRGs and are then released after the appropriate processing (Jourdain et al., 2013). Another study focusing on GRSF1 and its role in mitochondrial RNA processing granules proposed

an additional function for this protein. In the work by Antonicka et al. GRSF1 was found binding long non-coding RNAs (lcnRNAs) that originated from the mtDNA L-strand. In addition, the knockdown of GRSF1 resulted in disruption of the ribosome function and biogenesis (Antonicka et al., 2013). The mitochondrial RNA granules are most likely the place where processing and maturation of mt-transcripts occurs, which is necessary to prepare transcripts for the subsequent step in gene expression, namely, translation.

1.2. Translation

The protein synthesis system that operates in mitochondria, despite the presence of unique features, resembles more closely prokaryotic type of translation than the one from eukaryotic cytosol (Smits et al., 2010b). Many aspects of this process are still ucharacterised but those that are well described reveal features distinguishing mitochondrial translation from other systems. The necessary components for mitochondrial protein synthesis, apart from the mRNA template, include mitoribosome, 22 tRNAs with the enzymes required for their aminoacetylation, as well as various protein factors that facilitate mRNA recognition, translation initiation, elongation, termination and mitoribosome recycling (described in detail in the following subsections). All 13 polypeptides that are synthesised in human mitochondria are subunits of the OXPHOS complexes. However, the mitochondrially encoded proteins constitute only a small portion of all OXPHOS complexes subunits. The remaining proteins are encoded in nuclear genome and they are transported to mitochondria through the import system (Harbauer et al., 2014).

Therefore generation of the fully assembled OXPHOS complexes requires coordination of protein synthesis in both mitochondrial and cytosolic compartments. The mitochondrially-encoded proteins are highly hydrophobic and they are inserted into the inner mitochondrial membrane. The protein called Oxa1L (Oxa1 in yeast) plays the major part in the insertion process and it binds the nascent polypeptides at an early stage (Hell et al., 2001). Oxa1L is binding the mitoribosome via its C-terminus (Haque et al., 2010). This interaction is thought to facilitate the insertion of the proteins to the IMM (Szyrach et al., 2003). Although, Oxa1 is crucial for protein insertion, other factors' involvement is also highly likely (Ott and Herrmann, 2010). In addition, a significant proportion of mammalian mitochondrial ribosomes was found bound to the

inner mitochondrial membrane (Liu and Spremulli, 2000). Such positioning could enable delivery of mt-encoded proteins to their place in OXPHOS complexes.

1.2.1. Mitoribosomes - architecture and functions

Mitoribosomes are unique multi RNA-protein complexes that differ in structure from both prokaryotic and eukaryotic counterparts. In addition, there is also a significant variation between mitoribosomes from different organisms, which sets the mammalian mitoribosomes apart from others (O'Brien, 2003). They are composed of two subunits; small (28S; mt-SSU) and large (39S; mt-LSU) that together form a 55S monosome (O'Brien, 1971). Even though the sedimentation coefficient of a mitochondrial monosome is lower than that of bacterial one (55S as opposed to 70S) due to more porous structure, mitoribosomes' molecular weight is higher (Sharma et al., 2003). They also have a different rRNA/protein ratio (O'Brien, 2002). Mitoribosomes contain more proteins but two times less rRNA making the ratio 69% protein to 31% rRNA, whereas in bacterial ribosomes it is 33% protein and 67% rRNA (O'Brien, 2002; Sharma et al., 2003). In addition, human and other mammalian mitoribosomes lack the 5S rRNA that is present in large subunits of bacterial and cytosolic ribosomes (O'Brien, 2003). The small subunit of the mammalian mitoribosome is compose of 29 proteins and 12S rRNA, which is 950 nucleotides long, whilst the mt-LSU is made up of 52 proteins and 16S rRNA (1560 nucleotides) (Mears et al., 2006; Sharma et al., 2003). Almost half of these 81 proteins are specific to the mitochondrial ribosome, the rest have bacterial homologues (Sharma et al., 2003). The recent cryo-electron microscopy (cryo-EM) images of mammalian LSU gave near atomic resolution and so allowed very detailed reconstruction of its structure. This combined with cross-linking experiments revealed the exact positions of many mt-specific proteins (Greber et al., 2014, 2013). The following cryo-EM reconstruction of the human mt-LSU with the 3.4 Å resolution showed new, specific features (Brown et al., 2014) and confirmed the reduction in rRNA, which is evenly distributed throughout the whole structure, not specified to one particular place or randomly distributed losses. As a result of the loss of parts of rRNA, mitoribosomes have much more porous structure in comparison to the bacterial and cytosolic counterparts. Small portions of the missing 16S domains are compensated by the presence of

the mt-specific proteins that stabilize the structure in the absence of rRNA. However, the majority of mt-specific proteins are placed in new positions (Brown et al., 2014). In mammalian mitoribosomes the solvent exposed side tends to contain more of these proteins (Fig. 1.4 A), whereas the core is more conserved (Fig. 1.4 B) and is formed with homologues of bacterial proteins (Greber et al., 2013). The mitochondrial specific changes were also found in the part of the LSU called the central protuberance (CP), which contains mt-exclusive proteins. One of these proteins is ICT1, which was previously characterised as a mitoribosomal protein (Richter et al., 2010b) but only recently its exact position in CP was revealed (Greber et al., 2013). In bacterial ribosomes 5S rRNA is a part of central protuberance. However, since the 5S is not present in mammalian mitoribosomes, its place in CP is taken by a different RNA species, namely tRNA (Fig. 1.4 C) (Brown et al., 2014; Greber et al., 2014). The exact type of the tRNA, which functions as a scaffold for CP, is not yet clear. The porcine mt-LSU reconstruction identified it to be $tRNA^{Phe}$ (Greber et al., 2014), the human mt-LSU, however, was shown to contain the $tRNA^{Val}$ instead (Brown et al., 2014). The latter could be easily explained by the composition of the genes encoded in the mt-transcripts. The mt-$tRNA^{Val}$ gene is flanked by the 16S rRNA gene at the 3' end of the tRNA gene (Fig. 1.3). The $tRNA^{Phe}$ is flanked by the 12S rRNA gene at the 5' end of the tRNA gene but the whole fragment of mtDNA containing both of the mention tRNAs and rRNAs is proposed to be transcribed from the additional H strand transcription promoter (Fig. 1.3 HSP1). The general structure of the CP is remodelled due to the lack of the 5S and its binding partners as well as the presence of the tRNA (Brown et al., 2014; Greber et al., 2014).

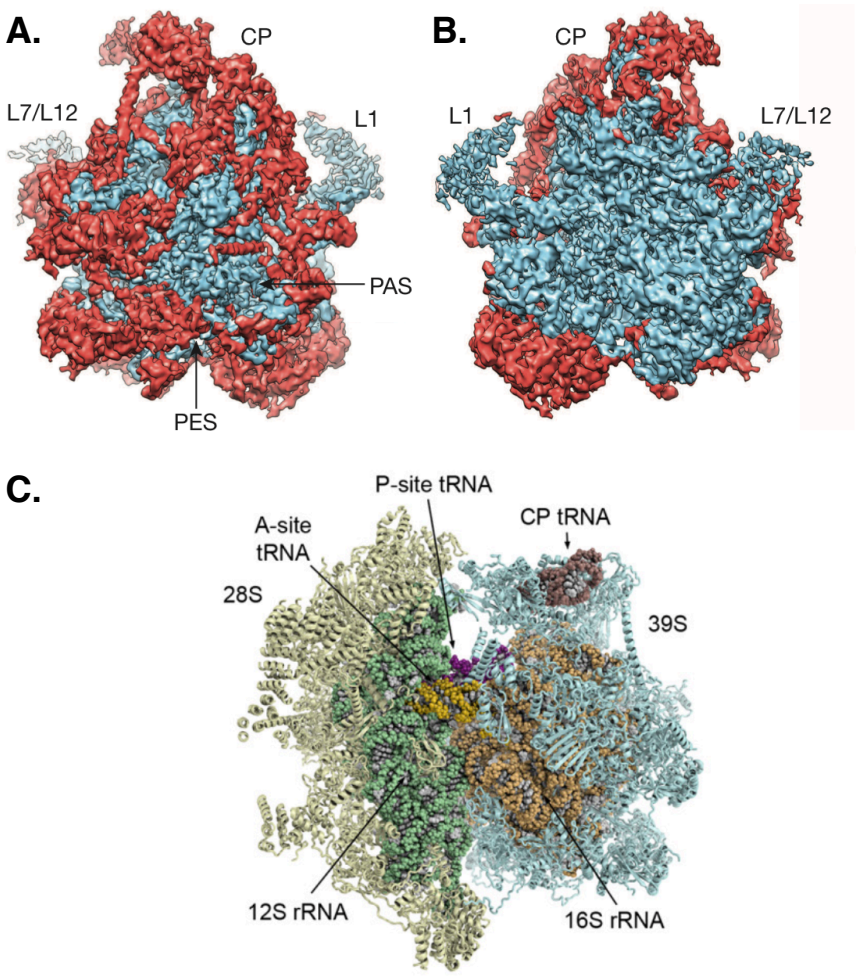

Figure 1.4. Overall structure of the 39S large subunit (A, B) and 55S mammalian mitoribosome (C)

A. The structure of the large mitoribosome subunit viewed from the solvent side with depiction of conserved (in blue) mitochondrial specific elements (red). The positions of central protuberance (CP), polypeptide accessible site (PAS), polypeptide exit site (PES), L1 and L7/L12 stalk. Adapted from (Greber et al., 2013). **B.** The interface site view of mt-LSU with the same color code as in A. **C.** A complete 55S mitoribosome structure divided in large 39S and small 28S subunits. Proteins of the 39S subunit are presented in blue, 16S rRNA in orange and tRNA in CP in brown. In small subunit proteins are visualized in pale yellow, 12S rRNA in light green, A-site tRNA in yellow and P-site tRNA in purple. Adapted from (Greber et al., 2015).

Another part of the mitoribosome that was identified to contain very characteristic features is the polypeptide exit tunnel, where the nascent polypeptide leaves the ribosome. In human mitoribosomes the overall path of this tunnel is similar to the bacterial/cytosolic ones. However, inside is much more hydrophobic and it is possible that there are strong interactions with also hydrophobic nascent polypeptides. The exit tunnel can also be a place where the helical tertiary structures of the mt-peptide start to form as observed in cytosolic ribosomes (Brown et al., 2014). As for the exact protein composition of

the mammalian mitoribosomal polypeptide exit tunnel, the ring that surrounds it is conserved and has corresponding bacterial homologues. However, there is a second layer of proteins that is specific to mitochondria only (MRPL44 and MRPL45) (Greber et al., 2013). The remodelling and mt-specific proteins present at the exit site may be a result of adaptation to the unique mitochondria translation system. It seems that these changes allow binding of the maturation factors and docking of the mitoribosomes to IMM (Brown et al., 2014; Greber et al., 2013).

The recently presented cryo-EM structure of the small subunit of the mitoribosome in 7-Å resolution (Kaushal et al., 2014) revealed the importance of the mitochondrial-specific extensions of homologous MRPs. These protein parts are involved in forming contacts with fully mt-specific MRPs. A lot of elements interacting with mRNA and tRNA are lined with the mt-specific proteins, which confirms the adaptation of the mitoribosome to the specific of mt-translation. Also there was a higher number of proteins involved in the formation of intersubunit connections (Kaushal et al., 2014). These observations were confirmed with proceeding publication of the higher resolution (3.6 Å) cryo-EM structures of SSU, in a context of a fully assembled monosome (Greber et al., 2015). An additional structure of an intact monosome (3.5 Å) presented even more details of mt-SSU consistent with aforementioned publications (Amunts et al., 2015). As in case of the mt-LSU, large pieces of small subunit rRNA were lost in mitoribosome in comparison to the bacterial one (Amunts et al., 2015; Greber et al., 2015). Many helices of rRNA that are involved in interaction with tRNA (P and A sites) in bacterial and cytosolic ribosomes are lost in mitoribosomes. The most recent structures of mitoribosomes shed light on the highly flexible nature of the mt-SSU that facilitates taking different conformations necessary for its function. In addition, the structure of the mRNA channel was resolved, which identified mitoribosome specific remodelling of both entry and exit sites. The most important element in the channel was protein uS5m (MRPS5) that seemed to be in contact with mRNA (Amunts et al., 2015; Greber et al., 2015). In contrast to mRNA channel, the tRNA decoding centre appeared to be well conserved between mitoribosomes and bacterial counter parts (Greber et al., 2015).

1.2.2. Translation initiation

The first step of the protein synthesis is called translation initiation and it requires recognition of the start codon in mRNA by the ribosome. This codon is then placed in the ribosomal P site where it is bound by the initiator $tRNA^{Met}$ carrying methione in its formylated form. This action, as well as the following steps of the initiation in mitochondria, is still poorly understood. Distinctive features of the 5' ends of mammalian mt-transcripts such as short (≤ 3) unstructured 5' sequences (Montoya et al., 1981), the absence of a prokaryotic Shine-Dalgarno sequence or eukaryotic 7-methylguanylate cap (Grohmann et al., 1978) makes the comparison with any known model impossible. In prokaryotic and cytosolic translation in eukaryotes, these special features serve as the markers for the binding of the small ribosomal subunit and forming of the preinitiation complex. With such short 5' untranslated region, and no modifications it is difficult to identify what attracts mitoribosomes to the start codons of mt-transcripts. There is a hypothesis that the very lack of specific features or long 5' UTRs is the signal, which gets recognized by the small mitoribosomal subunit (Haque et al., 2008; Jones et al., 2008) and that the process is facilitated by one of the initiation factors, mtIF3. This factor has an ability to induce dissociation of the mitoribosomal into large and small subunits in order to facilitate binding of the mRNA and initiator tRNA (Koc and Spremulli, 2002). Recently published structures of small subunit of the mitoribosome suggest the possible mechanism of how the mRNA is connected to the mt-SSU during initiation. Based on the architecture of the mRNA entry channel it was proposed that the 5' end of the transcript is threaded through the entry with assistance of mt-specific MRPs MRPS5 and MRPS39 (Greber et al., 2015)

Mitochondria utilize the formylated methionine for the initiation of translation but it is carried by the same tRNA species that facilitates incorporation of the methionine during elongation. When initiation codon AUG is position in ribosomal P site, $fMet\text{-}tRNA^{Met}$ is incorporated into the ribosome with the help from GTP-dependant second initiation factor, mtIF2 (Christian and Spremulli, 2010). In any characterized mitochondrial translational systems there are no equivalents of IF1, which is considered a universal initiation factors for both bacterial and eukaryotic cytoplasmic systems (Christian and Spremulli, 2012). In *E. coli* IF1 blocks the A site of the small ribosomal subunit during the initiation (Allen et al., 2005). In mitochondrial system, the mtIF2 is thought to perform

this function as well as the previously described facilitating of the initiator tRNA binding (Christian and Spremulli, 2012). The mRNA binding is directed through the mRNA entry gate in mt-SSU (Sharma et al., 2003) and is though to occur prior to the fMet-tRNA^{Met} recognition (Christian and Spremulli, 2010). The mRNA with AUG codon in mitoribosomal P site, fMet-tRNA^{Met} and factors mtIF2 and mtIF3 form an initiation complex, which is additionally stabilized by the interactions of codon:anticodon binding between tRNA and start codon (Christian and Spremulli, 2010). In the next step the mt-LSU joins the small subunit to form the 55S monosome, the GTP from mtIF2 is hydrolysed to GDP and both initiation factors are released, which marks the end of the initiation process (Haque et al., 2008; Smits et al., 2010b).

1.2.3. Translation elongation

After the initiation step is over the mitoribosome proceeds to the elongation phase when new amino acids are added to the growing polypeptide chain. For each incorporated residue the following reactions have to take place: aminoacyl-tRNA binding, peptide bond formation and ribosome translocation, which moves it 3 nt along the mRNA (towards 3' end) to a position ready for the next cycle. With a few exceptions, the elongation phase of mitochondrial translation is similar to the bacterial model from *E. coli* (Cai et al., 2000). In general this step of protein synthesis is more conserved than the initiation or termination (Christian and Spremulli, 2012). The first factor engaged in this process in mitochondria, mtEF-Tu, is the homologue of the main bacterial elongation factor. Its active, GTP-bound form captures the aminoacyl–tRNA (aa-tRNA) creating a ternary complex. This complex enters the mitoribosomal A site where the fidelity of the codon-anticodon binding is assured in a process named tRNA decoding. In bacterial ribosomes the correct pairing of codon and anticodon is recognised by specific bases of ribosomal 16S rRNA. These bases (G530, A1492 and A1493) make contact with the minor groove of codon-anticodon helix and recognise the correct geometry of the Watson-Crick binding. Only the geometry at first two positions is closely monitored, allowing for the non-canonical (wobble) base pairing at the third (Ogle and Ramakrishnan, 2005). The correctly selected tRNA causes conformational changes of the ribosomal decoding centre that closes tightly around it (Demeshkina et al., 2012). This induces the hydrolysis of the GTP and

GDP-bound mtEF-Tu is released from the ribosome. MtEF-Tu goes through cyclic changes between active (bound with GTP) and inactive forms (containing GDP) that are regulated by another factor, mtEF-Ts (Sprinzl, 1994; Woriax et al., 1997). Mt-EF-Ts induces the exchange of the GDP in inactive mtEF-Tu to GTP, thus activating the protein and preparing it to bind another aa-tRNA. When a codon in the A site is correctly decoded by a corresponding aa-tRNA, a new peptide bond is formed. The C-terminus of the peptide is released from the P site tRNA and joined with the N-terminus of the A site tRNA in reaction called transpeptidation. The catalysis of this reaction is performed by the ribosome itself, in a part of the large subunit called the peptidyl transferase centre (PTC). In mammalian mitoribosome the PTC is built with 16S rRNA and is highly conserved between mitochondria, prokaryotes and eukaryotic cytosol. The modelled structures that contained tRNA in P and A site showed that interactions between them and 16S rRNA in PTC are also conserved (Greber et al., 2014). After the polypeptide bond is formed and the protein chain is attached to the A site tRNA, another elongation factor, mtEF-G1 catalyses the translocation of the ribosome 3 nucleotides toward the 3' end of mRNA. During this step the peptidyl-tRNA moves from the A site to the P site and the deacylated tRNA from the P site is removed (Smits et al., 2010b). In bacterial and cytosolic translation, the deacylated tRNA is moved from P to E site. However, the exact mechanism behind the release of the deacylated tRNA in mammalian mitoribosome is not clear (Sharma et al., 2003). Most important rRNA domains, that in bacterial ribosome are responsible for interactions with tRNAs in the E site are missing from the mammalian ribosome. The only one part of the E site that is conserved is the tRNA's CCA-3' terminus binding pocket (Greber et al., 2014). In the model of human mt-LSU the same 3' part of the tRNA was shown bound to the ribosome, which confirms that a vestigial E site may be present but the interactions between it and tRNAs are much weaker than in bacteria (Brown et al., 2014).

1.2.4. Translation termination and mitoribosome recycling

The elongation cycles continue until one of the stop codons UAA, UAG and UGA (in prokaryota and eukaryotic cytosol) reaches the ribosomal A site (Nakamura et al., 1996; Tate and Brown, 1992). There is no tRNA that would recognize a stop codon, hence a special type of protein factor is required

that would bind the A site of the ribosome instead. These proteins belong to the class I release factors (RF). In bacteria the 2 types of release factors are distinguished: RF1, which recognizes UAA and UAG codons and RF2 that interacts with UAA and UGA stop codons (Müller et al., 2012). Eukaryota and archaebacteria require only one class I release factor named eRF1 and aRF1 respectively (Dontsova et al., 2000; Frolova et al., 1999; Konecki et al., 1977). The specific, codon recognition function of RF in bacteria is determined by the characteristic motifs in domain 2 (Laurberg et al., 2008), namely PXT in RF1 and SPF in RF2 (Ito et al., 2000). Upon stop codon recognition release factors undergo structural rearrangements resulting in the conformation that places the loop between domains 3 and 4 in the ribosomal peptidyl transferase centre (Fig. 1.5 A and B) (Laurberg et al., 2008). This loop contains another motif unique to release factors, a tri-peptide GGQ (glycine-glycine-glutamine). The GGQ motif is highly conserved, present in all class I release factors and is indicative of their function, which is ribosome dependent peptidyl-tRNA hydrolase activity (Frolova et al., 1999). Placing of the GGQ in the PTC triggers structural changes to the ribosome, which then result in the hydrolysis of the bond between the nascent peptide and the P site tRNA that is docking it to the ribosome (Laurberg et al., 2008; Trobro and Åqvist, 2007). After the peptide is released the class II release factor help to dissociate the class I RF from the ribosome. In bacteria the class II release factor is a small, G-protein named RF3 that facilitates the removal of the RF1/RF2 after the completed peptidyl-tRNA hydrolysis (Freistroffer et al., 1997). Then the ribosome recycling (RRF) factor with the elongation factor EF-G promote dissociation of the ribosome to separate subunits (Zavialov et al., 2005). Eukaryotic cells utilize a different mechanism of recycling of the ribosome. The homologue of RF3, eRF3, stimulates the eRF1 release activity in a GTP-dependent manner but not its dissociation (Alkalaeva et al., 2006; Jackson et al., 2012; Kisselev and Buckingham, 2000). The eukaryotic homologue of RF3, eRF3, stimulates the eRF1 release activity in a GTP-dependent manner. (Alkalaeva et al., 2006; Jackson et al., 2012; Kisselev and Buckingham, 2000). These two protein factors form a stable ternary complex with GTP (eRF1-eRF3-GTP). Hydrolysis of GTP results in release of eRF3 and allows eRF1 to assume the conformation necessary for peptidyl-tRNA hydrolysis (des Georges et al., 2014). After eRF3 dissociates an ABC-type ATPase ABCE1 binds the ribosome and stimulates the peptide release

by eRF1 (Preis et al., 2014). Finally, ABCE1 cooperates with eRF1 to dissociate ribosomal subunit, thus there is a functional coupling of the translation termination and ribosome recycling (Jackson et al., 2012; Pisarev et al., 2010).

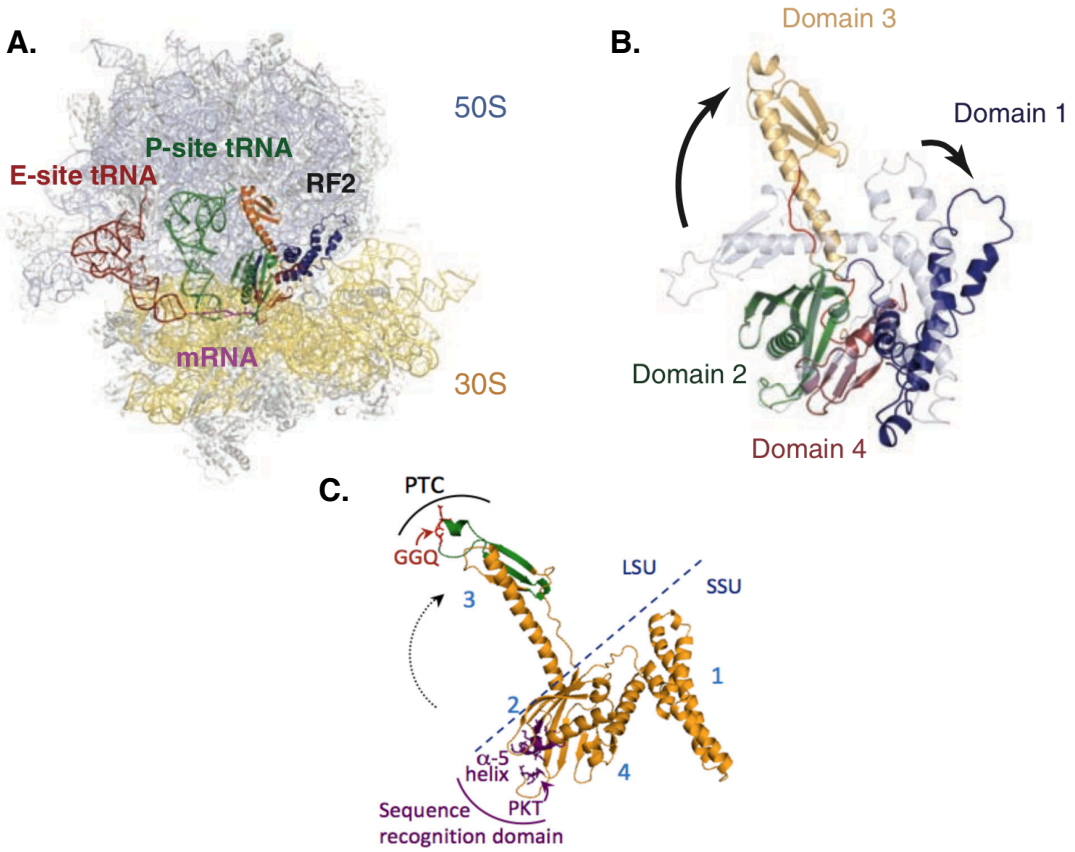

Figure 1.5. Structures of release factors RF2 and mtRF1a

A. Overview of the bacterial ribosome (50S in grey, 30S in yellow) with release factor (RF2) bound to the A-site, E-site tRNA (red), P-site tRNA (green) and mRNA template in purple. Adapted from (Weixlbaumer et al., 2008). **B.** Structure of bacterial RF2 free form (in grey) and bound to ribosome (each domain in different color) aligned together to show differences in conformation. Black arrows demonstrate the movement of domains after binding to ribosome. **C.** Structure of mitochondrial release factor mtRF1a modeled on bacterial RF2. Conformation of the protein is representing the ribosome-bound state with relative positions of LSU, SSU and peptidyl transferase centre (PTC). The position of GGQ motif in domain 3 (red) and sequence recognition elements (α-5 helix, PKT, purple) are detailed. Adapted from (Chrzanowska-Lightowlers et al., 2011).

The process of translation termination in mitochondria differs from that described above. Most species' mitochondria utilize only two out of three canonical stop codons, namely UAA and UAG (Soleimanpour-Lichaei et al., 2007), whereas UGA encodes tryptophan (Lee et al., 1987). However, in human mitochondria 2 of the transcripts (*MT-CO1* and *MT-ND6*) have either AGA or AGG following the open reading frame instead. This resulted in the assumption that human mitochondria were characterised by a set of four stop codons. The first candidate for the mitochondrial release factor that

emerged from the bioinformatics survey, was a protein called mtRF1 (Zhang and Spremulli, 1998). However, it failed to present the release factor activity with any of the canonical stop codons. Thus a new candidate protein was proposed, mtRF1a (Fig. 1.5 C), which displayed the peptide release activity both *in vitro* and *in vivo* but only for the canonical UAA and UAG codons (Soleimanpour-Lichaei et al., 2007). Termination of the translation of *MT-CO1* and *MT-ND6* is achieved through a -1 single nucleotide frameshift, which changes codon in mitoribosomal A-site from the AGA/AGG into canonical UAG. This frameshift allows for the canonical mechanism of termination facilitated by mtRF1a to occur. (R. Temperley et al., 2010). Therefore mtRF1a operates as a universal mitochondrial release factor and terminates translation of all 13 polypeptides.

A candidate for the mitochondrial ribosome recycling factor, class II factor, has been proposed from bioinformatics data (Zhang and Spremulli, 1998), namely mtRRF, which displayed necessary *in vitro* and *in vivo* activity (Rorbach et al., 2008a). In contrast to bacterial translational system where both translocation of the ribosome and disassembly of its subunits are carried by one protein EF-G, in mitochondria these two functions are divided between 2 proteins: mt-EFG1 and mtEFG2 (Tsuboi et al., 2009). As discussed in section 1.2.3 mtEFG1 is involved in translocation. Therefore, the role of mtEFG2 is to assist mtRRF in recycling of the mitoribosomal units during post-termination step. The GTPase activity displayed by mtEFG2 is required after the subunits are separated in order to release mtRRF and mtEFG2 (Tsuboi et al., 2009). The subunits remain separated due to binding of the initiation factor mtIF3 to the mt-SSU (Christian and Spremulli, 2012).

1.3. Stalling of ribosomes - rescue mechanisms in bacteria

Not every translational event results in complete protein synthesis. Some ribosomes can be arrested at various points of translation and fail to undergo the canonical process of termination and subunit recycling, a phenomenon known as ribosome stalling (Garza-Sánchez et al., 2008). When ribosomes are arrested and unable to resume translation it poses a threat to cell viability as it reduces available pool of ribosomes and therefore affects translation efficiency (Chadani et al., 2010; Jørgensen and Kurland, 1990). Such stalled ribosomes have to be either degraded or recycled with a help of external factors. As a

consequence of ribosome rescue the mRNA template as well as the nascent polypeptide (in most cases unfinished) are also removed and often degraded (Guydosh and Green, 2014). Stalling can occur either at the 3' end of the transcript, when there is a lack of functional stop codon (non-stop mRNA) or during elongation. In both cases it leaves the ribosome with an empty A-site (Keiler et al., 1996; Vivanco-Domínguez et al., 2012). The non-stop RNA species can be caused by premature termination of transcription or by nuclease cleavage (Keiler et al., 1996). The stalling of the elongating ribosomes is triggered by the features of tRNAs, mRNAs or the nascent polypeptide. The shortage of the particular aminoacyl-tRNA can result in stalling over the corresponding codon (Vivanco-Domínguez et al., 2012) as well as the presence of rare codons (Gouy and Gautier, 1982). The forming of the secondary structures as hairpins and pseudoknots (Somogyi et al., 1993; Wen et al., 2008) is also thought to impede the progression of ribosomes. Finally, the features of the nascent polypeptide, such as accumulation of positive charges that could interact with the exit tunnel, are other possible stalling factors (Charneski and Hurst, 2013).

1.3.1. tmRNA- mediated ribosome rescue

Mechanisms able to rescue stalled ribosomes thereby maintaining translation efficiency have been developed in many bacterial species. The most common system, *trans*-translation, utilizes a specific RNA molecule, named tmRNA that has functions of both tRNA as it is shaped to resemble tRNA structure, charged with alanine and mRNA as it encodes a short ORF (SsrA) (Hayes and Keiler, 2010). This molecule recognizes and enters the A-site of the stalled ribosome (Fig. 1.6 A) and accepts the nascent polypeptide on the alanine residue attached to the tRNA-like component (Fig. 1.6 B). Next, it resumes the translation of that peptide using the short ORF in mRNA part as a template (Fig. 1.6 C) (Hayes and Keiler, 2010; Keiler et al., 1996; Withey and Friedman, 2003). As a result the polypeptide with an added SsrA tag is released from the ribosome by canonical termination at the SsrA ORF stop codon and the ribosome is recycled (Fig. 1.6 D). The tagged protein, which most likely is truncated as its translation was interrupted, is recognized and degraded by proteases (Janssen and Hayes, 2009). Factors essential for the trans-

translation to occur are EF-Tu and small protein SmpB (Barends et al., 2000; Kurita et al., 2007; Moore and Sauer, 2007). When the ribosome is stalled by reasons other than the non-stop mRNA, the cleavage of the transcript is necessary prior to the tmRNA-mediated action (Roche and Sauer, 1999), (Garza-Sánchez et al., 2008). One of the identified factors that is involved in this process is a RelE toxin, which catalyses the cleavage of the 3' end side of the mRNA, close to the stalled ribosome. As a result, the substrate for tmRNA/SmpB is created (Pedersen et al., 2003). However, the participation of toxins in trans-translation occurs only upon strong amino acid starvation. Moderate conditions invoke toxin-independent cleavage of the 3' mRNA (Li et al., 2008).

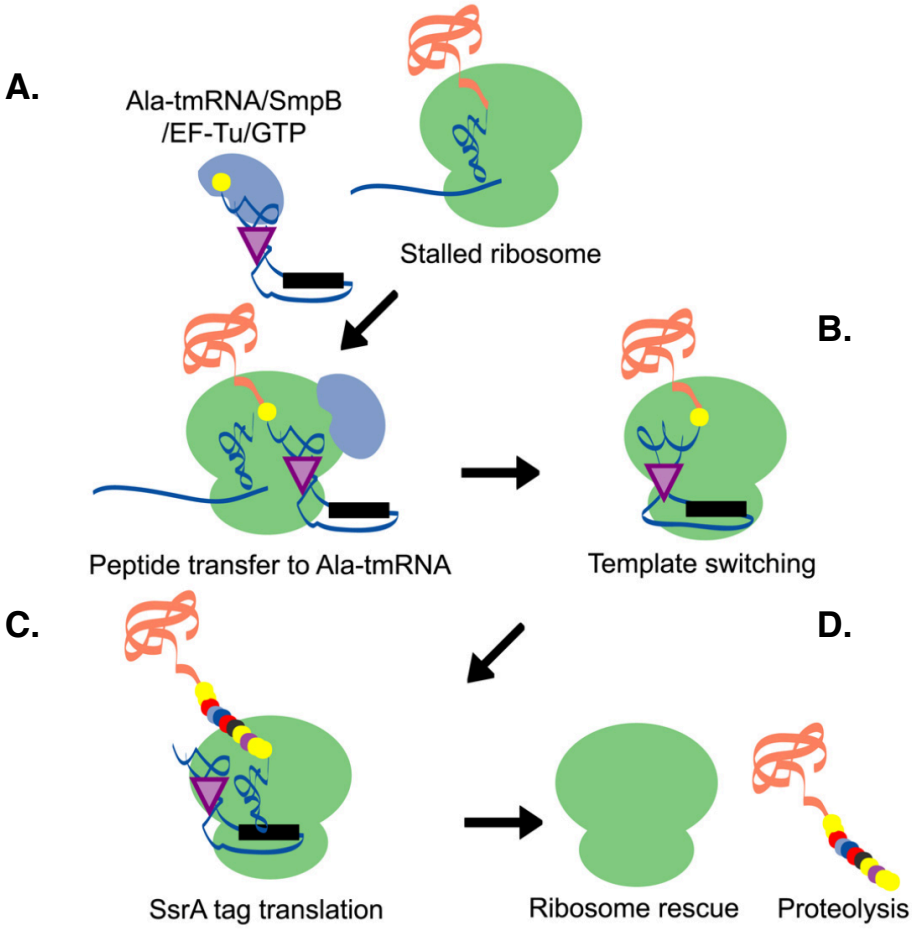

Figure 1.6. Overview of tmRNA-mediated rescue of stalled ribosomes

Mechanism of tmRNA function presented in separate steps. **A.** Recognition of the stalled complex by the aminoacylated-tmRNA facilitated by SmpB and EF-Tu. **B.** Change of the template for the ORF-part of tmRNA. **C.** Addition of the SsrA tag as a result of translation of tmRNA ORF. **D.** Release of the tagged-protein followed by proteolysis. Image adapted from (Shimizu, 2014).

1.3.2. ArfA and YaeJ - alternative rescue strategies

Although tmRNA is present in all sequenced eubacterial genomes, it is not the exclusive rescue system for many species. For example *E. coli* harbour an alternative rescue mechanism of stalled ribosomes on non-stop mRNA that involves protein called ArfA (Alternative release factor A) (Chadani et al., 2010). This protein lacks the GGQ motif, therefore in order to hydrolyse the peptidyl-tRNA bond in the stalled complex it recruits the release factor RF2. ArfA binds the large subunit of the ribosome and directs RF2 to the ribosomal A-site resulting in the process similar to the canonical translation termination (Chadani et al., 2012; Shimizu, 2012). However, the exact molecular mechanism of the rescue conducted by ArfA and RF2 is still unknown (Abo and Chadani, 2014).

A second identified alternative mechanisms involved in rescue of stalled ribosomes is based on protein factor called YaeJ (or ArfB), which was utilized in non-stop mRNA and in case of rare-codon clusters (Y. Handa et al., 2010). Contrary to ArfA, YaeJ contains the GGQ motif (Fig. 1.7 A), which it utilizes to catalyse the peptidyl-tRNA hydrolysis in stalled ribosomes and enable the recycling of the ribosomal subunits (Y. Handa et al., 2010). Despite the similarities between the catalytic domain of YaeJ and class I release factors, the former differs in structure from the RFs. YaeJ lacks the codon-recognition domain which results in much shorter amino acid sequence (approximately 140 aa instead of 360). Therefore the function of this protein can be described as a codon-independent but ribosome depending peptidyl-tRNA hydrolase (Chadani et al., 2011; Y. Handa et al., 2010). Studies on the crystal structure show that it utilizes its basic-residue rich C-terminal tail as a sensor to detect the presence of mRNA in entry channel downstream of ribosomal A-site. When the entry channel is empty YaeJ binds to large subunit, which results in placing GGQ-containing domain in ribosome PTC and hydrolysis of peptidyl-tRNA (Fig. 1.7 B). This process utilizes the same mechanism as the canonical translation termination (Gagnon et al., 2012). Mutational analysis of the C-terminal tail amino acid sequence identified the residues important for the binding of the stalled ribosome (Kogure et al., 2014).

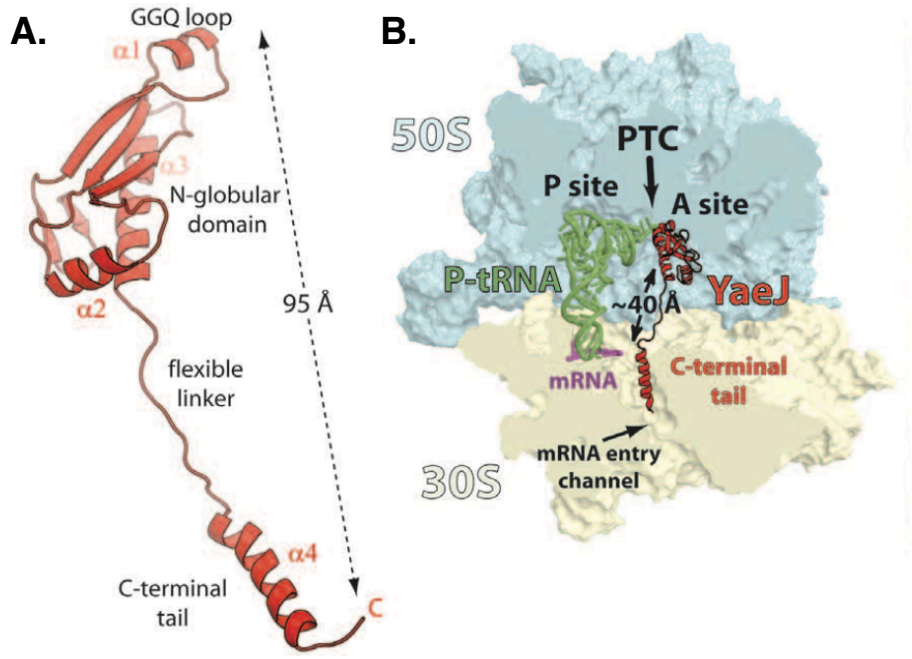

Figure 1.7. Structure of YaeJ bound to the 70S ribosome

A. Conformation of YaeJ in a ribosome bound-state with labeled domains. **B.** Position of YaeJ (red) in an empty A-site of a stalled 70S ribosome. Large subunit (50S) presented in light blue, small (30S) in pale yellow, P-site tRNA in green and mRNA in purple. N-terminal domain is placed in the A-site of the large subunit, C-terminal domain placed in empty mRNA entry channel of small subunit. Adapted from (Gagnon et al., 2012)

In conclusion, *E. coli* cells were identified with at least 3 different ribosome rescue mechanisms, which supports the prediction that ribosome stalling is detrimental for the cell. According to the present model, the tmRNA remains the primary rescue strategy with ArfA and YaeJ-mediated mechanism acting as a fail-safe (Abo and Chadani, 2014).

1.4. Stalling of ribosomes - rescue mechanisms in eukaryotes

The mechanisms of mRNA and protein synthesis quality control are also present in eukaryotic cells, although no homologues of tmRNA have been found. Instead, a few different translation-dependent mechanisms have been characterized that are triggered by the ribosome stalled during elongation or termination (Isken and Maquat, 2007). One of the common stalling-inducing features is an absence of the stop codon. Lack of an in frame stop codon (non-stop mRNA) can be caused by an error in transcription or accidental cleavage at the 3' end of the mRNA. There are even genes identified to produce such transcripts as a result of a natural expression (Sparks and Dieckmann, 1998).

Other reasons for the presence of non-stop mRNAs are endonucleolytic cleavage or chemical damage (Meaux and Van Hoof, 2006). Non-stop mRNAs are likely to cause ribosome stalling at their 3' end with the polypeptide-tRNA still covalently bound to the P site. These mRNAs are rapidly degraded in mammalian and yeast cytosol by the mechanism called non-stop mediated degradation (NSD) (Graille and Séraphin, 2012). The process utilizes nucleolytic activity of the exosome as well as the SKI complex with Ski7 associated factors (Fig. 1.8 B) (Schaeffer and van Hoof, 2011; van Hoof et al., 2002).

A second mRNA quality control mechanism, named nonsense mediated decay (NMD), induces the degradation of the transcripts with a premature stop codon. The stalled translation complex recruits exoribonucleases as well as the cytoplasmic exosome that degrade the aberrant transcript (Cole et al., 2009).

When ribosome stalling is triggered by other than defective stop codons, transcripts are degraded with a mechanism called no-go decay (NGD). The substrates for the NGD are usually mRNAs that cause stalling at positions other than the 3' end. Hence the system requires an endonucleolytic cleavage of the mRNA close to the stalled ribosome, which is followed by exonuclease degradation of the remaining mRNA by Xrn1 and exosome (Fig. 1.8 C). Transcripts with internal poly(A) sequences, as well as those chemically damaged mRNAs are also potential targets of NGD (Graille and Séraphin, 2012). Finally, there is an indication that NGD also targets transcripts containing strong secondary structures within the open reading frame (Doma and Parker, 2006).

Defective mRNAs are not the only cause of the disruption of the translational progression. Ribosomal defects, including mutations, chemical damage and errors at biogenesis can also result in stalling, as these dysfunctional ribosomes fail to conduct translation efficiently (Fig. 1.8 D) (Graille and Séraphin, 2012). In yeast these defective ribosomes are stalled at sense codons during elongation and are removed with the mechanism called non-functional 18S-rRNA decay (NRD) (Cole et al., 2009; LaRiviere et al., 2006).

In yeast, all surveillance pathways described above have a common feature, namely the involvement of Dom34:Hbs1 complex (Graille and Séraphin, 2012). The orthologues of the first component, Dom34 are found in many eukaryotic species, in humans is called Pelota (Atkinson et al., 2008). Both Dom34 and

Pelota share similarities in both structure and sequence with termination factor eRF1 (Graille et al., 2008). Dom34 structure mimics tRNA in the way eRF1 does. However, it does not contain the GGQ motif responsible for the peptidyl-tRNA hydrolysis and unlike eRF1 its N-terminal domain folding suggests an ability to bind RNA (Graille and Séraphin, 2012). The second component of the complex is a GTPase related to the eRF3 (Carr-Schmid et al., 2002). The Dom34-Hbs1 complex, when bound to the ribosome, resembles the ribosome-bound eRF1–eRF3 complex (Becker et al., 2011). Through their interaction with the ribosomal A site, Dom34-Hbs1 triggers dissociation of the subunits and peptidyl-tRNA drop-off from stalled ribosomes (Shoemaker et al., 2010)(Becker et al., 2011). The subsequent GTP hydrolysis results in Hbs1 dissociation and conformational changes in Dom34. These actions lead to the recruitment of the Rli1 (in mammals ABC1), which triggers ATP-dependent ribosomal subunit dissociation and recycling (Pisareva et al., 2011; Shoemaker et al., 2010). Rescue of ribosomes is also linked to degradation of nascent proteins that were translated by the stalled complex. This process involves recruitment of the ribosome dependent quality control complex (RQC) that includes ubiquitin ligase Ltn1 and other factor facilitating recognition and removal of the polypeptide (Brandman et al., 2012; Defenouillère et al., 2013; Verma et al., 2013).

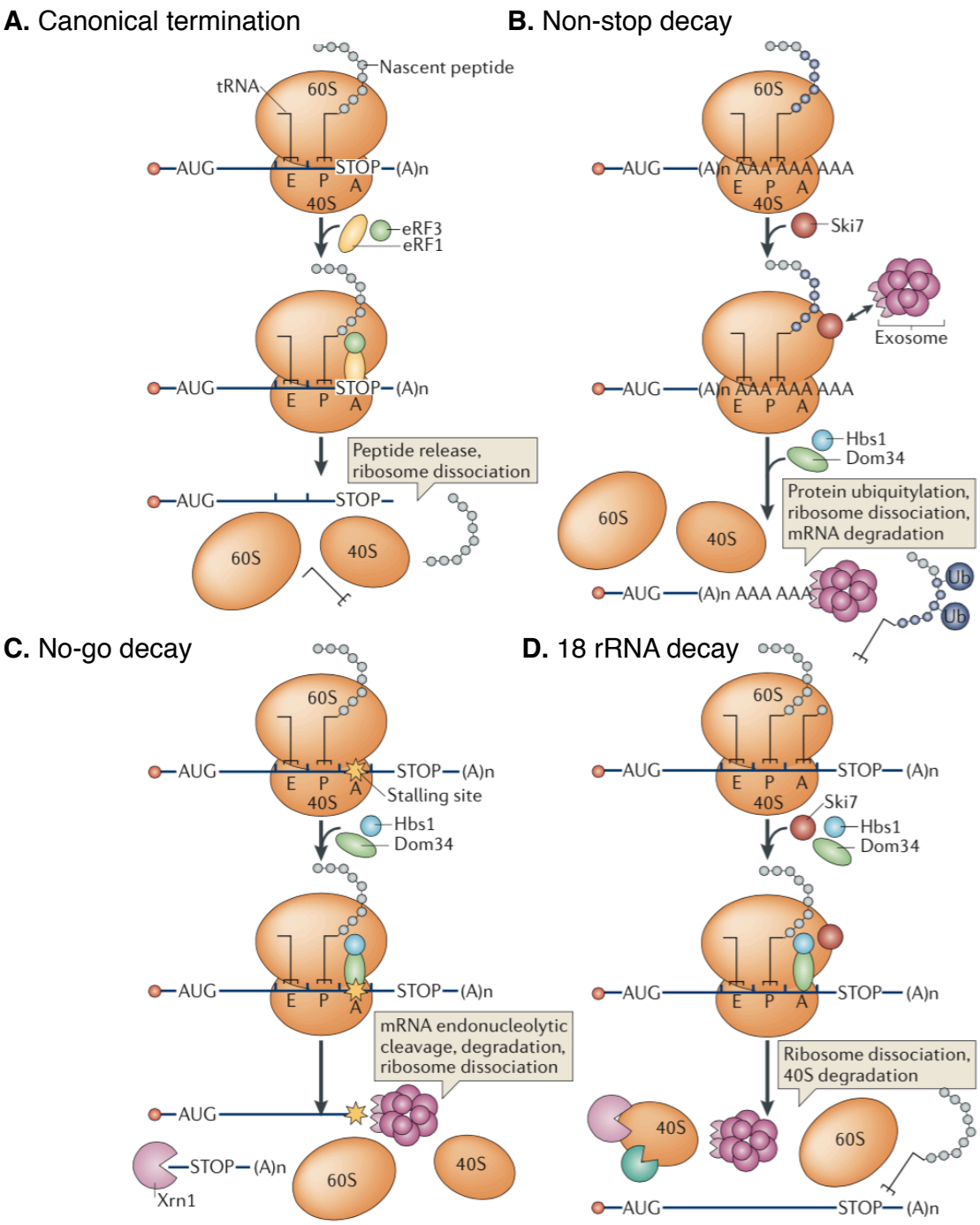

Figure 1.8. Mechanisms of quality control of translation in eukaryota

A. Termination of translation of a canonical template by release factor 1 (eRF1), followed by eRF3-GTP. **B.** Overview of the non-stop mRNA decay pathway. In the absence of stop codon ribosome is stalled during translating the poly(A) tail, synthesizing a polylysine extension to the nascent polypeptide. The stalled complex is resolved by Ski7- exosome and Dom34-Hbs1.The ribosome recycling is coupled with degradation of the peptide and mRNA. **C.** Ribosomes stalled within an ORF are rescue as a part of no-go decay pathway. The mechanism involves endonucleolytic cleavage followed by 5'-3' degradation with Xrn1. The proteins that carry the release of the nascent polypeptide and recycling of the ribosome are Dom34 and Hbs1. **D.** Ribosomes that are unable to carry translation due to defects of small subunit (40S) are bound by Dom34, Hbs1 and Ski7, which result in 18S rRNA degradation. Adapted from (Graille and Séraphin, 2012).

1.5. Translational recoding

Ribosome stalling is not the only non-canonical event that can occur during protein synthesis. There are programmed mechanisms, collectively known as translational recoding, that affect the progression of the ribosome, resulting in the change in the linearity of the genetic information readout or decoding of a particular codon (Gesteland and Atkins, 1996). These alternative ways of decoding mRNA compete with standard translation and result in 2 or more different polypeptides from one transcript. Although, there are many mechanisms of translational recoding this section will focus on 3 major types: 1) -1 or +1 frameshifting, 2) ribosome hopping and 3) stop codon readthrough (Namy et al., 2004). During the frameshift ribosome slides over one nt (upstream or downstream), which results in translation of an overlapping ORF. The frameshift is usually triggered by the presence of a slippery sequence in mRNA that favours the misalignment of the tRNA and a stimulator element, often decreasing the speed of translation, such as pseudoknot (Kontos et al., 2001). An example of such frameshift in Prokaryotes is *prfB* gene that encodes the RF2 protein and harbours -1 signal necessary for the expression of the functional protein (Craigen and Caskey, 1986).

A second type of recoding, ribosome hopping (or bypassing) involves detachment of the ribosome from the mRNA and continuing of translation at a different spot on template. So far the only one well-characterized example of this phenomenon is a bypass of 50 nt sequence in gene *60* of T4 bacteriophage (Herr et al., 2000; Huang et al., 1988). However, recently a number of programmed bypassing sites were identified in mitochondria of yeast *Magnusiomyces capitatus* (Lang et al., 2014; Nosek et al., 2015).

Finally, the last form of translational recoding is a readthrough of the stop codon. It requires a specific sequence context near the termination site that allows recognition by tRNA and carrying of the translation beyond it (Namy et al., 2004). The context can be interpret as: 1) the base immediately downstream from the stop codon, 2) last 2 amino acid residues of the nascent polypeptide, 3) presence of the stimulating elements downstream from the stop codon as secondary structures (Bertram et al., 2001). The readthrough of the stop codon allows synthesis of a protein of extended length and alternative biochemical features. The most common form of the programmed suppression of the stop codon is decoding of UGA triplet with selenocysteine identified in

both prokaryotes and eukaryotes (Namy et al., 2004). However, the readthrough can also involve decoding with canonical amino acid (Jungreis et al., 2011; Namy et al., 2004). Many examples of genes that undergo the suppression of the stop codon were recently identified in *Drosophila melanogaster* (Jungreis et al., 2011).

1.6. Stalling of ribosomes and mammalian mitochondria

1.6.1. What do we know ?

So far no mechanism accountable for the rescue of stalled mitoribosomes has been identified. However, there is no evidence for mitochondrial protein synthesis to be error-free. On the contrary, mitoribosomes are anticipated to encounter issues with progression, such as stalling, but the cause and the ways to overcome it are yet to be determined. As discussed in section 1.2, given the presumed α-proteobacterial origin of mitochondria (Gray et al., 1999) many processes involved in mt-genes expression are modelled on the bacterial system (Smits et al., 2010b). However, so far no tmRNA-like apparatus was found in mitochondrial genomes. There was a tRNA species that resembled upstream part of the tmRNA identified in the mt-genome of a primitive species *Reclinomonas americana* (Keiler et al., 2000). The tRNA fragment, however, was not coupled with an open reading frame, which suggested lack of function. Therefore it is unlikely that the mechanisms of ribosome rescue similar to tmRNA would be present in any mitochondrial genome. The unique features of the mitochondrial genome and protein synthesis apparatus suggest that various aspects of these processes including quality control would exhibit mitochondrial-specific characteristics. Especially distinctive features of mitoribosome architecture (1.2.1) would most likely determine the special quality control pathways. Despite the uniqueness of the mitochondrial translational system, the analysis of mt-proteins with bacterial homologues of known function in quality control may still be the best way to commence the search for potential rescue factors. This approach can be enforced with additional identification of factors transiently interacting with mitoribosome. The only candidates for the rescue of mitoribosomes proposed so far are members of so called mitochondrial release factor family. The family was identified through bioinformatics screening based on the shared feature: presence of the GGQ motif (Richter et al., 2010a; Rorbach et al., 2008a). As presented in

section 1.2.4, the highly conserved GGQ motif is characteristic to all class I release factors (Frolova et al., 1999). Human mitochondrial release factor family consists of 4 proteins but only one of them, mtRF1a, is a *bona fide* release factor that operates during termination of all mt-polypeptides translation (Soleimanpour-Lichaei et al., 2007; R. Temperley et al., 2010). However the function of the remaining 3 members: mtRF1, ICT1 and C12orf65 is still unknown. Each member of this family will be characterised and discussed in details in the following subsection.

1.6.2. Mammalian mitochondrial release factor family

mtRF1

The first member of the mitochondrial release factor family is protein mtRF1, which is exclusively present in vertebrates and originated from mtRF1a gene duplication (Soleimanpour-Lichaei et al., 2007; Young et al., 2010). As discussed in 1.2.4, this protein was primarily a candidate for a canonical release factor but eventually failed to display the peptidyl-tRNA hydrolysis activity both *in vitro* and *in vivo* (Soleimanpour-Lichaei et al., 2007). The structure of mtRF1 resemble the bacterial class 1 RFs, as well as the mtRF1a, with which it shares 39% of sequence similarity (Huynen et al., 2012). It contains both of the functionally important domains: the GGQ domain and stop codon recognition domain. The latter, however, varies from the prokaryotic recognition sequence (hexapeptide PEVGLS instead of tripeptide PXT) (Duarte et al., 2012; Huynen et al., 2012). The 3D modelling of mtRF1 predicted that it could bind to the empty A-site of the mitoribosome in the absence of mRNA. Based on this observation an involvement of mtRF1 in the rescue of the stalled mitoribosomes with an empty A-site was proposed (Huynen et al., 2012). However, the exact role, especially in the context of mt-translation quality control is yet to be uncovered (Chrzanowska-Lightowlers et al., 2011; Huynen et al., 2012).

ICT1

Of all members of mitochondrial release factor family ICT1 (Immature Colon Carcinoma Transcript-1), has been the most successfully characterised so far. It was first identified as a downregulated transcript in colon carcinoma cell line during *in vitro* differentiation and at that point no connection to mitochondria was made (van Belzen et al., 1998, 1995). The following experiments

conducted in my host lab characterised ICT1 as a protein associated with mtRRF (Rorbach et al., 2008a). Further analysis of ICT1 structure showed that the mature protein (175 aa) lacks the codon recognition sequences but contains functional GGQ domain. ICT1 retained the peptidyl-tRNA hydrolysis activity but it is codon-independent (Richter et al., 2010b). Interestingly this protein was also identified as an integral part of the mitoribosome, which was recently confirmed in the cryo-EM structures of the mt-LSU supported by the cross-linking proteomic analysis (Fig. 1.9) (Greber et al., 2013) as discussed in 1.2.1. The presence of ICT1 in mitoribosome was consistent with observed disruption of ribosome structure and decrease in *de novo* mt-protein synthesis due to ICT1 depletion (Richter et al., 2010b). The solution structure analysis of ICT1 showed 3 main parts of the protein namely: 1) N-terminal mt-targeting signal, 2) structured domain containing GGQ motif and 3) unstructured C-terminal tail enriched with positively charged amino acids (Yoshihiro Handa et al., 2010). The GGQ-containing domain topology, β_1-β_2-α_1-β_3- α_2 resembles the one in bacterial RF2, except for the additional α-helix inserted between β2 and β3 in ICT1.

ICT1 has a bacterial homologue, which is a previously described protein YaeJ (1.3.2). Comparison of structures between ICT1 and YaeJ showed high level of similarity but not complete (Gagnon et al., 2012; Yoshihiro Handa et al., 2010; Kogure et al., 2014). The main difference is present in the N-termini, as ICT1 is a mitochondrial protein with targeting sequence. Although both proteins contain an additional insertion in the GGQ-domain, in case of YaeJ it is a β-strand not a α-helix (Kogure et al., 2014). The C-terminal tail of YaeJ, which structure and composition were important for the ribosome binding function and PTH activity are conserved in ICT1 (Kogure et al., 2014). All shared features between ICT1 and YaeJ that also distinguish these 2 proteins from canonical RFs suggest a similar, potentially conserved function. YaeJ, as ICT1, was characterized with codon-independent peptide release activity (Kogure et al., 2014; Wesolowska et al., 2014). However, YaeJ is not an integral part of a ribosome, nor can it substitute for ICT1 and stably interact with the mitoribosome (Wesolowska et al., 2014). This result clearly distinguishes the mechanism of action of these proteins. YaeJ is expected to transiently interact with an empty A-site of the ribosome, where it is able to catalyze the release of the peptide from the stalled complex (Gagnon et al., 2012; Kogure et al., 2014).

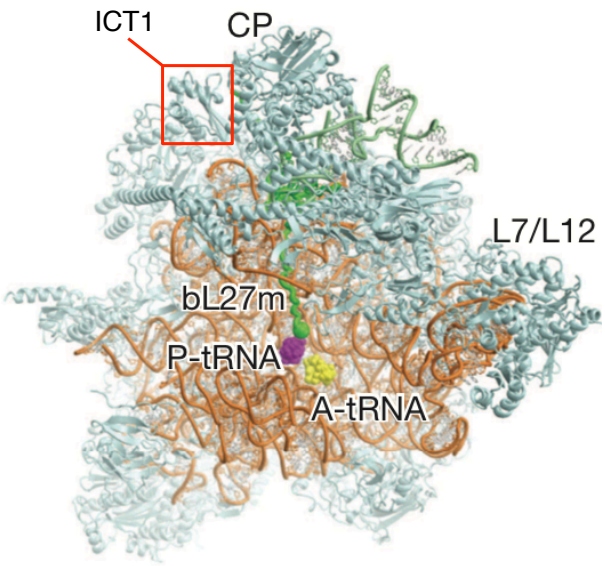

Figure 1.9. Position of ICT1 in the mt-LSU

Structure of the large mitoribosomal subunit (subunit interface side). Ribosomal 16S RNA is depicted in orange, mitoribosomal proteins in cyan. The position of ICT1 in the central protuberance (CP) is boxed in red, A-site and P-site tRNAs are presented in purple and yellow respectively. Adapted from (Greber et al., 2014).

ICT1 is placed in the mitoribosomal central protuberance far from the peptidyl transferase centre (Fig. 1.9), which prevents the unrestricted PTH activity (Greber et al., 2013). Therefore, in order for ICT1 to utilize the GGQ motif, the mitoribosome would require significant conformational changes to the structure. Despite the growing evidence and similarities to known ribosome rescue factors, the involvement of ICT1 in relieving of stalling, as well as the exact mechanism of action are yet to be confirmed.

C12orf65

The last member of the mitochondrial release factor family, a protein called C12orf65, was first characterised in case of 2 unrelated patients with Leigh syndrome (Antonicka et al., 2010). Both patients harboured frameshift mutations (210delA and 248delT) in *C12orf65* gene resulting in a premature stop codon. In each case patients' skin fibroblasts showed impairment of mt-protein synthesis, lower CIV activity and defects in CI, IV and V assembly. Since then a number of different patient reports have been published (Buchert et al., 2013; Haruo Shimazaki et al., 2012; Spiegel et al., 2014; Tucci et al., 2013) confirming the importance of this protein for proper mitochondrial translation (discussed more thoroughly in chapter 4).

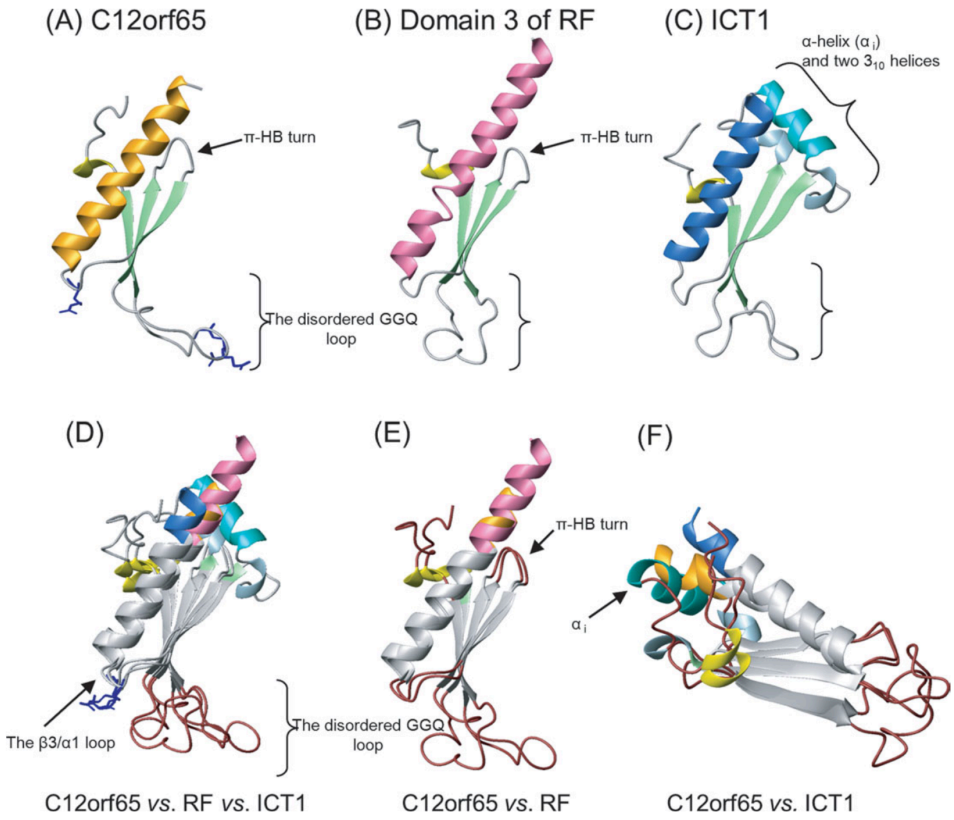

Figure 1.10. Comparison of the GGQ domain structures from C12orf65, ICT1 and bacterial class I release factor.

Individual structures of GGQ domains of C12orf65 (A) bacterial RF (B) and ICT1 (C). The exact position of the GGQ motif is depicted by brackets in all 3 structures. The additional α-helix insertion in ICT1 (C) also presented by brackets. Alignment of the all 3 structures (D), C12orf65 and RF (E) and C12orf65 and ICT1 (F) in order to facilitate comparison of topological features. Adapted from (Kogure et al., 2012)

The solution structure of C12orf65 was resolved and showed high similarity to ICT1. As ICT1, C12orf65 consists of 3 major parts (N-terminal part with targeting sequence, GGQ domain and C-terminal tail). It also lacks the codon recognition domain, hence it is much smaller than canonical release factors (~190 residues instead of ~360) (Kogure et al., 2012). The structure of the GGQ domain displays the following topology: 3_{10}-β_1−β_2−β_3−α_1 with the GGQ motif is located in a loop between β_1 and β_2 (Fig. 1.10 A). As the GGQ domain of C12orf65 lacks the insertion between β2 and β3, it resembles the bacterial RF2's domain 3 more closely than the GGQ domain in ICT1 (Fig. 1.10 D). Differences between C12orf65 and ICT1 are also visible in their mitochondrial localization as C12orf65 was identified as a free matrix protein, not a part of mitoribosome (Antonicka et al., 2010). Finally, unlike ICT1, C12orf65 did not display PTH activity *in vitro* (with or without the presence of a stop codon)

(Antonicka et al., 2010). However, the *in vitro* experiments were performed on bacterial 70S ribosomes, hence it is possible that the lack of 55S mitoribosome or some mitochondrial specific factors was impeding the C12orf65 function. Interestingly, overexpression of ICT1 in patient fibroblasts was able to partially rescue the pathological phenotype (Antonicka et al., 2010). This result suggested that these proteins may share some functions or take part in similar processes.

Apart from the patient case, the potential function of C12orf65 was also studied in HeLa cells with siRNA-mediated knockdown (Kogure et al., 2012). Lack of C12orf65 caused a decrease in cell growth as well as lower complex IV activity. It therefore, confirmed that C12orf65 is necessary for cell viability and proper mitochondrial function (Kogure et al., 2012). The same experiments were performed on ICT1-depleted cells and they also displayed cell and mitochondrial function defects. However, the lack of ICT1 had more detrimental effect than the lack of C12orf65 (Kogure et al., 2012). These results together with the partial-rescue with ICT1 overexpression in C12orf65 patient fibroblasts (Antonicka et al., 2010) suggest the possibility that both proteins may have overlapping but not identical functions. As observed in *E. coli*, where at least 3 different ribosome rescue mechanisms exist it is possible that mitochondria are also equipped with multiple tools to alleviate stalling.

1.7. Aims of this study

The main goal of the first part of my PhD project was to characterise the function of C12orf65 and explore its role in mitochondrial translation. The strong indication that C12orf65 is essential for synthesis of mitochondrial proteins was based on patient reports, mainly (Antonicka et al., 2010). As presented in my introduction (1.6) there are a number of pieces of evidence that suggest the potential involvement of C12orf65 in quality control of mt-translation. The investigation of C12orf65 function in relation to this hypothesis was commenced by Dr. Aleksandra Pajak. Thus my objective was to carry on experiments in order to broaden the knowledge on the role of C12orf65.

Main goals for experiments included in this part of my project were as follows:

- Complete characterisation of C12orf65 mitochondrial distribution.
- Establish if the C12orf65 GGQ motif is functional and necessary for the

cell viability utilizing cell lines expressing mutated forms of this protein (AGQ and GSQ mutations).

- Investigate the effect of C12orf65 depletion on mt-translation (*de novo* protein synthesis and steady state levels of mt-proteins).
- Investigate how mitochondrial transcripts are affected in C12orf65 depleted cells.

In order to expand characterisation of C12orf65 function an additional set of experiments was performed utilizing immortalized skin fibroblast of a patient who was diagnosed with 210delA mutation in *C12orf65*. This mutation was predicted to cause a frameshift change to the gene sequence that would result in premature stop codon. A patient harbouring the exact same mutation was described in the report by (Antonicka et al., 2010). The initial biochemical analysis of patient fibroblasts (carried in Mitochondrial NCG Diagnostic Service) showed decrease in complex IV activity. The clinical presentation varied from the original report, so I performed a series of experiments focused on identification of changes to mitochondrial gene expression in this patient's cells at the molecular level.

Experimental aims for the analysis of patient cell line in the second part of my project included:

- Comparison of the growth rate between patient and control cell lines.
- Assessment of the mitochondrial protein synthesis levels (*de novo* translation and steady state levels of mt-proteins).
- Investigation of the changes to the levels of mitochondrial transcripts.

The third and last part of my project was focused on addressing the challenges involved in investigation translation quality control in mitochondria. Given the hypothesis that C12orf65 is a potential candidate to rescue stalled mitoribosomes it was necessary to develop an appropriate tool to study changes to ribosome progression. A method called ribosome profiling was selected for this purpose. Ribosome profiling was developed to combine advantages of nuclease protection assay with deep sequencing (Ingolia et al., 2009). Fragments of mRNA that are protected by ribosomes from RNase digestion are sequenced and aligned to reference genome. Results represent the map of ribosome distribution across transcripts (ribosome profiles) and

allow genome-wide analysis of translation *in vivo*. Differences in ribosome densities within particular transcript can be used to infer variation in ribosome progression: high number of ribosomes at specific region is likely to be a result of slower ribosome movement within it (Ingolia, 2014). At the beginning of my project there were no published cases of ribosome profiling conducted on mitochondria. Therefore, my first aim was to adjust the present protocols (Ingolia, 2010; Ingolia et al., 2012) in order to apply them on mitoribosome protected fragments. The new protocol was designed for sequencing using IonTorrent^{TM}. This approach was later adjusted for Illumina platform according to the first published results of ribosome profiling in human mitochondria (Rooijers et al., 2013). The objective of this part of my project was to apply optimized protocol to analyse mitoribosome profiles from wild type cell lines.

These experiments were aimed to provide the following information:

- Identify a general pattern for the mitoribosome distribution across mt-transcripts.
- Identify naturally occurring regions were there is a higher accumulation of mitoribosomes.
- Test for specific mRNA sequences that would cause stalling (such as overlapping sequences in bicistronic transcripts).

Finally the mitoribosome profiling experiments were applied to cell lines where stalling of mitoribosomes was expected. First of the cell lines carried a C25U mutation in mt-tRNA^{Val} that reduced levels of its aminoacylated form (Hornig-Do et al., 2014; Rorbach et al., 2008b). Due to deficiency of mt-tRNA^{Val} mitoribosomes were expected to stall during translation of valine codons. In addition, the cell line version selected for these experiments was stably transfected with valyl-tRNA synthetase (VARS2) which was shown to partially rescue the tRNA^{Val} deficiency (Hornig-Do et al., 2014).

The experiments on mt-tRNA^{Val} mutant cell line aimed to establish:

- If mitoribosomes stall on valine codon in the mutant cell line
- Is the stalling prevented by overexpression of VARS2?
- Develop data analysis approach for identification of stalling sites in mitoribosome profiles.

The second cell line used in the final part of my PhD project was depleted of C12orf65 via siRNA treatment. The analysis of mitoribosome profiles from this cell line was compared to non-targeting control in order to answer:

- Is there more evidence of mitoribosome stalling in the absence of C12orf65 than in control cells?
- Can involvement of C12orf65 in the rescue of stalled mitoribosomes be confirmed based on these experiments?

The following chapters will describe results of experiments performed to address the presented questions for each part of my PhD project.

Chapter 2

Materials and methods

2.1. Mammalian cell culture

2.1.1. Culturing and storage of cells

Cell lines used in this study:

- HEK293T FLP-IN TRex (Invitrogen)
- U2OS wild type
- 143B.206
- T1V1 *trans*-mitochondrial cybrid with m.1624C>T mutation in mt-tRNA^{Val}, stably expressing mitochondrial valyl-tRNA synthetase (VARS2)
- HEK293T inducibly expressing FLAG tagged C12orf65 wild type with silent mutation in *C12orf65*
- HEK293T inducibly expressing FLAG tagged C12orf65 AGQ mutant with silent mutation in *C12orf65*
- HEK293T inducibly expressing FLAG tagged C12orf65 GSQ mutant with silent mutation in *C12orf65*
- Immortalised patient fibroblasts with c.210delA, p.(Gly72Alafs*13) mutation in C12orf65
- Immortalised Control fibroblasts

HEK293 WT, U2OS WT, 143B cell lines used in this study were grown as monolayer cultures in Dulbecco's Modified Eagle's Medium (SIGMA 6429) supplemented with 10% foetal calf serum (FCS), 1x nonessential amino acids (NEAA) and 50 µg/ml uridine. The basic culture was performed in 75 cm^2 vented flasks under standard conditions (37°C, 5% CO_2, humidified atmosphere) with 15 ml of DMEM. Growth medium was changed every 3 days and when cells reached 80% of confluency they were split and reseeded in new flasks. Cells were stripped by incubation in PBS / 1 mM EDTA and pelleted by centrifugation at 220x g for 4 min. Pellets were then resuspended in growth media and 1/2 -1/10 (depending on initial confluency) was reseeded in new flasks.

Stable transfection cell lines expressing FLAG tagged variants of C12orf65 were grown as untransfected cell lines with addition of Blasticidin^S (10 µg/ml final concentration, in order to retain the tetracycline repressor) and Hygromycin^B (100 µg/ml final concentration, to repress growth of cells devoid of expression construct) every third passage. During culturing of T1V1 cell lines

addition of Hygromycin^{B} was omitted. Immortalised patient and Control fibroblasts were also grown in DMEM (SIGMA 6429, supplemented with 10% FCS, 1x NEAA and 50 µg/ml uridine). For passage of these cell lines 1x Trypsin (Sigma) in PBS/EDTA solution was used. Cells were split maximum 1:5.
In order to store cell lines, cells grown in 75 cm^2 flasks to ~ 80% confluence, were stripped, pelleted and resuspended in ice-cold FCS with 10% DMSO. Cell suspensions were kept on ice for ~5 min and then transferred to cryopreservation tubes, placed in polystyrene container, overnight at -80°C. Afterwards they were transferred to liquid nitrogen.

2.1.2. Mycoplasma testing

Mycoplasma test were kindly performed by Mrs. Debra Jones using MycoAlert® Mycoplasma Detection Kit (Lonza) following the manufacturer's instruction. In case of an infection, cells were treated with Plasmocin (1:1000) for minimum 2 weeks and the Mycoplasma test was repeated.

2.1.3. Cell counting

For the experiments comparing fibroblast cell growth on different carbon sources, cells cultured in a standard way (2.1.1) were seeded in 6-well plates (2 ml of media per well). To investigate the growth on galactose, medium after one day was replaced with DMEM lacking glucose, supplemented with 0.9 mg/ml galactose and dialyzed FCS. For testing the growth on glucose, cells were cultured in the standard DMEM. At chosen time points cells were counted by adding 10 µl of cell suspension mixed with 0.4% Trypan blue solution (Sigma, in order to distinguish between live and dead cells) to haemocytometer (Hawksley, depth 0.1 mm, 1/400 mm^2). Mean values of the counts taken from 8 peripheral squares were calculated and the count was multiplied by 10,000, giving the amount of cells/ml.

2.1.4. siRNA transfection to mediate transcript depletion

siRNA mediated depletion was performed in 6-well or in 24-well plates on wild type HEK293-Flp-In^{TM} cells or on stable transfected cell lines named: HEK-C12orf65-WT, HEK-C12orf65-AGQ or HEK-C12orf65-GSQ cell lines. For the 6-well plates 100,000 of cells were seeded per well (in 1.25 ml DMEM) on the day of transfection. For the experiments in 24-well plates 30,000 cells in 400 µl

of DMEM per well were seeded a day before transfection. For each transfected well a tube was prepared containing a mixture of Opti-MEM® + Glutatmax™ (Gibco 51985-026), siRNA (siC12orf65 or non-targeting, 20 μM stock) and Lipofectamine RNAiMAX (Invitrogen) in proportions as described in Table 2.1. The mix was incubated at room temperature for 10-20 min and then added to cells. The siRNA treatment for the ribosome profiling experiments was performed in 15 cm diameter dishes on wild type HEK293-Flp-In™. The siRNA mixture (Table 2.1) was incubated in plates for 20 min at room temperature, after which the cells (in 20 ml DMEM) were added.

In each case, after 3 days cells were harvested or re-transfected for another 3 days. The re-transfection was carried by removing the old media and adding the same volume of the fresh one with the same amount of siRNA and transfections reagents.

Table 2.1. Proportions of siRNA treatment mixture

Reagent	24-well plate	6-well plate	15 cm diam. dish
Opti-MEM	100 μl	250 μl	4.5 ml
siRNA (20 μM)	1.5 μl	3.75 μl	66.6 μl
Lipofectamine	0.8 μl	2 μl	36 μl

Each siRNA was custom synthesised by Eurogentec (Table 2.2) and stored at -20 °C as 20 μM or 100 μM stocks in RNase free water.

Table 2.2. Sequences of all siRNAs used in this project

Name	Sequence
siRNA- C12orf65	5'-GGG AGA AGC UGA CGU UGU U dTdT
siRNA NT	siRNA non-targeting negative control duplex OR-0030-NEG05

2.1.5. Transient transfection and generation of stable cell lines (HEK293, U2OS)

Stable cell lines were generated by integration of the sequences from pcDNA5/FRT/TO, tetracycline inducible expression vector (Invitrogen) with the gene of interest (GoI). Two types of cell lines, HEK293-Flp-In™ T-Rex™ and U2OS-Flp-In™ T-Rex™, were transfected with pcDNA5/FRT/TO/GoI and pOG44 vectors (Ampicillin and Hygromycin^B resistant) using the 1:5 or 1:7.5 ratio, following the protocol from Superfect Transfection Reagent Handbook

(Qiagen). Stable transfection reactions were carried in 6-well plates seeding 100000 cells/well.

Transient transfection of U2OS cells was performed only with pcDNA5/FRT/TO vector containing the gene of interest (2 µg DNA) and Superfect Transfection Reagent using 1:7.5 ratio according to the manufacturer's instructions. Transient transfection reactions were carried in the 24-well plates seeding 25000 cell per well.

2.2. Bacterial cell manipulation

2.2.1. Bacterial culture

All bacterial strains were grown in LB media or on LB agar plates (detailed below). For plasmid amplification, bacteria were grown at 37°C, overnight in suspension, with aeration in the presence of appropriate antibiotics. For the long term storage at -80°C, bacteria were suspended in LB media with 15% glycerol (v/v).

Lysogeny Broth (LB) medium, pH 7.5:

1% Bacto-tryptone

0.5% Yeast extract

1% NaCl

for plates : 2% agar

2.2.2. Bacterial transformation

The α-select chemically competent cells (BIO-85025, Bioline) were transformed with pcDNA5/FRT/TO/FLAG-tagged protein GoI expression vector according to the manufacturer's instructions. Selection of the transformants was performed overnight on the LB plates (2.2) with 100 µg/ml ampicillin. Transformed strains with the plasmid of interest were stored at -80°C (as in 2.2).

2.2.3. Plasmid DNA purification

Positively transformed cells were grown in 5 ml LB with ampicillin overnight at 37°C. The plasmids were isolated using GeneJET Plasmid Miniprep Kit (Thermo Scientific) according to the manufacturer's instructions and eluted with 50 µl of elution buffer.

2.3. Cloning and DNA manipulation

2.3.1. PCR

PCR reactions that required proofreading polymerase activity (in order to amplify fragments for cloning) were performed with KOD hotstart polymerase (Novagen) in 50 µl of volume (Table 2.3 A and B). Other amplification reactions were carried with DreamTaq polymerase (Thermo Scientific, FEREP0701) in 20 µl of volume (Table 2.4 A and B). Primers used in this study are listed in the specific subsection.

Table 2.3. Components and conditions for PCR with KOD hotstart polymerase

A.

Components [stock]	Volume
KOD buffer [10x]	5 µl
dNTPs [2 mM]	5 µl
$MgSO_4$ [25 mM]	3 µl
Forward primer [10 µM]	1.5 µl
Reverse primer [10 µM]	1.5 µl
H_2O	30 µl
KOD Polymerase [1U/ µl]	1.5 µl
Template (cDNA)	3 µl

B.

Stage	Temperature	Time
Hold	94˚C	5 min
30 cycles	95˚C	1 min
	54˚C	1.5 min
	72˚C	2.5 min
Hold	72˚C	7 min
Hold	4˚C	∞

Table 2.4. Components and conditions for PCR with DreamTaq polymerase.

A.

Components [stock]	Volume
DreamTaq buffer [10x]	2 µl
dNTPs [2 mM]	2 µl
Forward primer [10 µM]	0.15 µl
Reverse primer [10 µM]	0.15 µl
H_2O	14.5 µl
Dream Taq polymerase [5 U/ µl]	0.125 µl
Template (15 ng DNA)	1 µl

B.

Stage	Temperature	Time
Hold	95˚C	3 min
35 cycles	95˚C	1 min
	52˚C	1 min
	72˚C	1 min
	72˚C	8 min
Hold	4˚C	∞

2.3.2. Electrophoresis

Regular 1% agarose and low-melt 1% agarose gels were prepared as follows: agarose was dissolved in the 1x TAE buffer (40 mM Tris acetate, 1 mM EDTA pH 8.0) in a microwave. After cooling, either ethidium bromide (0.5 µg/ml final concentration) or GelRed (Biotium, 1:10000 dilution) was added in order to visualize DNA by UV light. Samples, mixed with loading dye (1 µl of 10x buffer per sample, as described below) were loaded on the gel along the 1 kb ladder (molecular weight marker). The gel electrophoresis was carried at constant voltage (60- 80V) in 1x TAE buffer.

10x loading buffer:

- 0.25% bromophenol blue
- 0.25% xylene cyanol FF
- 30% (v/v) glycerol

2.3.3. Purification of PCR products

PCR products were size selected via electrophoresis in 1% low melting agarose gel. Next, they were extracted from gels and purified using the QIAquick Gel extraction kit (Qiagen) according to the manufacturer's instructions.

2.3.4. Digestion with restriction enzymes

The restriction digestion with both XhoI (1U per reaction, NEB) and HindIII (0.5U per reaction, Roche) was performed in the 20 µl final volume using buffer 2 (B7002S, New England Biolabs), following the manufacturers' protocol. Samples were incubated at 37°C for 3 h.

2.3.5. Dephosphorylation

Vectors subjected to dephosphorylation were treated with alkaline phosphatase (Roche) for 30 min at 37°C supplemented with 0.5 % SDS in 100 mM Tris- HCl pH 9.0. The enzyme was denatured by incubation at 50°C for 30 min.

2.3.6. Phenol/chloroform purification

The volume of each sample was increased to 100 µl with dH_2O and then 100 µl of phenol pH 7.9 was added. Samples were mixed by vortexing and centrifuged for 2 min at 14,000 x g. The aqueous, upper phase was removed, transferred to a new tube and an equal volume of chloroform was added. Samples were vortexed and centrifuged again. DNA from the aqueous phase was precipitated with 0.3 M sodium acetate (final concentration), 96% ethanol (2.5x sample volume) and 1 µl of linear acrylamide by incubation at -80°C for at least 1h. The samples were then centrifuged at 20,000 g, 4°C for 30 min. After ethanol was removed, the DNA pellets were resuspended in 10 µl of sterile dH_2O.

2.3.7. Ligation

The ligation of the digested PCR product and the linear vector (molar ratio of insert to vector 1:3) was conducted using Rapid DNA Ligation kit (Thermo Scientific) according to the manufacturer's protocol. Samples (20 µl final volume) were incubated for 5 min at 22°C.

2.3.8. Measurement of DNA concentration

DNA concentration of samples diluted in either dH_2O or TE buffer was measured using NanoDrop Spectrophotometer ND-1100. For double stranded DNA a millimolar extinction coefficient of 50 was used and 40 for RNA, 30 for ssDNA.

2.3.9. Sequencing

Sequencing was kindly performed by Mrs. Charlotte Alston using 3130*xl* Genetic Analyzer (Applied Biosystems) and BigDye® Terminator v3.1 kit according to the manufacturer's instructions. Sequencing of PCR reactions were conducted as follows: 1 µl sequencing primer (5 µM stock, listed in Table 2.5), 500 ng DNA, 1.5 µl 5x Sequencing Buffer v3.11 and 3 µl BigDye

Terminator v3.1 were made up to the final volume of 20 µl. The PCR reaction conditions are described in Table 2.6.

Table 2.5. Sequencing primers

Name	Sequence (5'-3')
CMV Forward	CGCAAATGGGCGGTAGGCGTG
BGH Reverse	TTAGAAGGCACAGTCGAGG

Table 2.6. Sequencing PCR conditions

Stage	Temperature	Time
Hold	95˚C	5 min
30 cycles	95˚C	30 s
	50˚C	10 s
	60˚C	4 min
Hold	4˚C	∞

PCR products were precipitated in 96 well plate. To each sample 10 µl Hi-Di was added then they were incubation at 95°C for 2 min and loaded on the analyser. SeqScape v2.6 software (Applied Biosystems) to analyse data.

2.4. RNA manipulation

All experiments involving RNA were performed using DEPC-treated water. DEPC was added to dH_2O at the final concentration of 0.1% and then autoclaved.

2.4.1. RNA isolation

RNA isolation from human cells was conducted using Trizol Reagent (Invitrogen) following manufacturer's instruction. The pellet of harvested cells was resuspended in 0.5 ml (or 1 ml, depending on pellet volume) of Trizol and the solution was incubated for 5 min at room temperature. Then 0.1 ml (0.2 ml) of chloroform was added and each sample was vortexed for 15 s and centrifuged at 12000 x g at 4°C. The clear supernatant was collected and transferred into a new tube with 0.25 ml (0.5 ml) of isopropanol. Samples were mixed and then incubated at room temperature for 10 min. RNA was pelleted by centrifugation for 15 min, 12000 x g at 4°C. Pellets were washed with 0.5 ml (1 ml) 75% ethanol, centrifuged for 5 min, 7500 x g at 4°C. Final pellets were resuspended in 10-30 µl of DEPC-H_2O.

2.4.2. Northern blotting

RNA samples (20 µl final sample volume) containing 1-4 µg of RNA in 8 µl of DEPC-H_2O, 1x MOPS, 35% (v/v) formamide and 5.5% (v/v) formaldehyde. First samples were incubated at 55°C for 15 min, then cooled down and 1x RNA loading buffer and ethidium bromide (0.1 µg/ µl final concentration) were added. Samples were electrophoresed in the 1.2% (w/v) denaturing agarose gel (1x MOPS pH 7.2, 0.9% formaldehyde). The separation of the samples was performed in 1x MOPS buffer pH 7.2 (50 V) for approximately 6 h. The samples were transferred onto the GeneScreen Plus membrane overnight in 10x SSPE buffer. After transfer, the membrane was vacuum dried at 80°C for 2h followed by incubation with prehybridisation buffer (50% v/v formamide, 5x SSPE, 1% w/v SDS and 5x Denhardt's solution) for minimum 2 h at 42°C.

The probes for labeling specific mt-transcripts were prepared as follows: DNA fragment in DEPC-H_2O (9 µl volume) was denatured at 95°C for 4 min, then placed on ice and mixed with 3 µl random hexamer mix (containing dGTP, dATP, TTP and 5x buffer), 5 U Klenow DNA polymerase I and 2 µl of [^{32}P]-dCTP (~ 10-20 µCi, PerkinElmer NEG513H). Reactions were incubated at 37°C for 1 h.

The volume of samples was increased to 50 µl with DEPC-treated water and purification was conducted using illustra Microspin G-25 spin columns (GE Healthcare) according to the manufacturer's instructions. The activity of purified probes was measured with a Cerenkov counter and minimum of 500000 cps was added 10 ml hybridisation buffer. Membranes were incubated with the probe in hybridization buffer overnight at 42°C, then washed twice with 2x SSPE for 15 min at room temperature. The final wash was performed for 15 min at 65°C with 2x SSPE / 2% SDS buffer. Next membranes were exposed to a Phosphor-Imager screen. The visualisation and analysis of the signal form radiolabelled RNA species was conducted using Typhoon™ PhosphoImager and ImageQuant software (GE Healthcare). For the purpose of reprobing of membranes they were washed twice with boiling 0.1x SSC and once with 0.1x SSC/ 0.1% (w/v) SDS in order to strip previous signals. Next, membranes were prehybridised as described above prior to adding a new probe.

10x MOPS-buffer (pH 7.2)

0.4 M Morpholinopropanesulfonic acid (MOPS)

0.1 M NaOAc

10 mM EDTA

20x SSPE (pH 7.4)

3 M NaCl

0.2 M NaH_2PO_4

20 mM EDTA

10x RNA loading buffer

50% (v/v) glycerol

1 mM EDTA

0.25% (w/v) bromophenol blue

0.25% (w/v) xylene cyanol

5x random hexamer mix

250 mM Tris/ HCl (pH 7.5)

50 mM $MgCl_2$

5mM DTT

0.5 mM dATP

0.5 mM dGTP

0.5 mM dTTP

20x SSC

3M NaCl

0.3 M Na-citrate

2.4.3. Reverse transcription

Reverse transcription reactions on total RNA were carried using either Super Script® VILO™ Mastermix (Life Technologies, 11755050) or SuperScript® III First-Strand Synthesis System (Life Technologies 18080-051). In both cases reactions were performed according to the manufacturer's instructions in 20 µl volumes, using 300 ng of total RNA template and random hexamers (for SuperScript® III First-Strand Synthesis System only).

2.4.4. Quantitative real time PCR

The qPCR reactions were carried on cDNA templates. A list of all primers used is presented in Table 2.7. Dilution of template depended on the primers used (C12orf65: undiluted; VARS2L 1:10; 18S rRNA 1:100). Fast start essential DNA green Master kit (Roche, 06 402 712 001) was used. Each reaction was made up to 20 µl in the following way: 2 µl of cDNA template, 1 µl forward primer (10 µM stock), 1 µl reverse primer (10 µM stock), 6 µl dH_2O and 10 µl Fast start essential DNA green Master reagent (2x concentrated stock). LightCycler® Nano (Roche) was used with the reaction conditions as in Table 2.8.

Table 2.7. List of primers for qPCR

Type	Name	Sequence (5'-3')	T_m
C12orf65 Forward	C12RTFor	GTTTCTCGCATGCGCAGTCAGT	51.6°C
C12orf65 Reverse	C12RTRev	TCAGCGGAGGATTCGCAA	53.4°C
VARS2L Forward	VARS2LqPCRFor	CTGATGCAGAGGTTGTGGTAG	49.2°C
VARS2L Reverse	VARS2LqPCRRev	GCCCGTGTAGATGTGTGTATC	49.2°C
18S rRNA Forward	18S For	GTAACCCGTTGAACCCAATT	60°C
18S rRNA Reverse	18S Rev	CAATCCAATCGGTAGTAGCG	62°C

Table 2.8. Profile and analysis condition for LightCycler® Nano software

Stage	Temperature	Ramp	Time
Hold	95˚C	5	600 s
45 cycles	95˚C	5	10 s
	60˚C	4	10 s
	72˚C	5	15 s ☑
Melting: initiation	65˚C	4	50 s
Melting: final	95˚C	0.1	1
Hold	4˚C	-	-

☑ data generated after this step

Analysis: automatic quantification, T_m calling

2.5. Protein manipulation

2.5.1. Preparation of cell lysate

Pellets of harvested cells were washed once with PBS and resuspended in cold lysis buffer (50 mM Tris pH 7.4, 130 mM NaCl, 2 mM $MgCl_2$, 1 mM PMSF, Protease Inhibitor Cocktail EDTA-free (Roche), 1% Nonidet P-40). Samples were incubated on ice for 15 min, vortexed 30 s and centrifuged at 1100 x g, 2 min 4°C. In order to digest nucleic acids approximately 1 U of Benzonase® Nuclease (70746) was added per 100 µl. Supernatant was collected to a separate tube and stored at -80°C (longer than a few weeks) or -20°C (more immediate use).

2.5.2. Mitochondrial isolation and lysis

Mitochondria were isolated from cells grown in 75 or 225 cm^2 flasks and harvested at ~80% confluency. Pellets were washed with Dulbecco's PBS and

resuspended in homogenisation buffer (0.6 M Mannitol, 10 mM Tris pH 7.4, 1 mM EGTA) supplemented with 0.1% BSA and 1 mM PMSF. The homogenisation was carried in Glass Col Homogeniser (15 passes) and the suspension was centrifuged at 400 x g, 10 min, 4°C in order to separate mitochondria (in supernatant) from unbroken cells (pellets). These two steps were repeated 3 times and the supernatants collected after each repeat were centrifuged at 11000 x g, 10 min, 4°C. Pelleted mitochondria were washed in 1 ml homogenisation buffer (lacking BSA). Where required mitochondria were lysed using lysis buffer from the Sigma FLAG-IP kit (50 mM Tris pH 7.4, 150 mM NaCl, 1 mM EDTA, 1% Triton X-100) supplemented with Protease Inhibitor Cocktail EDTA-free (Roche), 1 mM PMSF and 10 mM $MgCl_2$. Lysis conditions were as follows: 30 min lysis with agitation at 4°C and centrifugation 12000 x g, 10 min 4°C.

2.5.3. Bradford measurement of protein concentration

Measurement of protein concentration was carried using Bradford Assay. Cell or mitochondrial lysate (1 µl) were diluted in dH_2O (800 µl final volume). In parallel a series of BSA standard dilutions (in 800 µl H_2O) was prepared with following concentrations: 0, 2, 5, 10, 15 and 20 mg/ml. To each sample (experimental and standard) 200 µl of Bradford reagent (BioRad) was added, and voretxed. Next, 200 µl of each solution was loaded on the 96-well plate (experimental samples 4 times, standard in duplicates) and analysed in Microplate Reader (Elx800) measuring the absorbance of 595 nm.

2.5.4. Blue native PAGE

Mitochondria isolated from patient and control fibroblasts grown in 1x 300 cm^2 flasks (2.5.2) were resuspended in solubilisation buffer (50 mM NaCl, 50 mM imidazole-HCl, 2 mM 6-aminohexanoic acid, 1 mM EDTA, 1 mM PMSF). Next, protein concentration was measured (2.5.3) and the detergent, dodecylmaltoside (DDM, Sigma), was added at concentration 3.2 g/ g of protein. Solubilisation was carried on ice for 20 min, then samples were centrifuged at 20000 x g, 20 min, 4°C and the supernatant was transferred to a new tube. Protein concentration was measured again and samples containing equal amount of protein (25 µg) were prepared by adding Coomassie G250 solution in solubilization buffer at detergent/dye ratio of 10 g/g. Samples

were separated on a 4.5 - 16 % gradient BN-PAGE (Table 2.9) under following conditions: 150 V, 4°C, approximately 4 h. The gel chamber was filled with deep blue cathode buffer (50 mM tricine, 7.5 mM imidazole, 0.02% Coomassie blue G-250, pH 7), which after approximately 20 min of electrophoresis was changed into slightly blue cathode buffer (50 mM tricine, 7.5 mM imidazole, 0.002% Coomassie blue G-250, pH 7). The bottom chamber was filled with anode buffer (25 mM imidazole-HCl pH 7.0). Gels were transferred to PVDF membranes (activated with 100% methanol) in Mini Trans-Blot (Bio-Rad, 1.5 h, 4°C 150mA with constant stirring) using transfer buffer (25 mM Tris, 200 mM glycine, 10% methanol). After transfer the blot was fixed in 8% acetic acid for 15 min in room temperature and immunostained (2.5.6) with antibodies specific to each complex (Table 2.10).

Table 2.9. BN-PAGE gels composition (3.5 ml final volume)

Stock solutions	**4.5%**	**16%**
ReadySol IEF 40% T, 3% C Acrylamide solution (GE Healthcare)	1.7 ml	6 ml
100% glycerol	-	3 ml
3x gel buffer (75 mM Imidazole-HCl, pH 7.0 and 1.5M 6-aminohexanoic acid	5 ml	5 ml
dH_2O	8.243 ml	0.935 ml
TEMED	27 µl	19 µl
10% APS	2.7 µl	1.9 µl

Table 2.10. Primary antibodies used in Western blotting analysis of BN-PAGE

Name	**Complex**	**Company**	**Cat. No.**	**Dilution**	**Secondary**	**Conditions**
NDUFB9	CI	Abcam	AB11928	1:1000	mouse	O/N 4°C
70kDa	CII	Mitosciences	MS204	1:1000	mouse	O/N 4°C
Core2	CIII	Abcam	Ab14745	1:1000	mouse	O/N 4°C
COX4	CIV	Abcam	Ab14744	1:1000	mouse	O/N 4°C
ATP5 A	CV	Abcam	Ab14748	1:1000	mouse	O/N 4°C

2.5.5. SDS-PAGE

Proteins from samples (lysates from cell and mitochondria, sucrose gradient fractions) were separated on 12 or 14% Tris-glycine SDS-PAGE (Table 2.11).

Prior to loading samples were denatured in 1x (final concentration) loading buffer at 95°C for 3 min. Electrophoresis was carried in 1x running buffer at 15 mA per 1 gel, alongside Spectra Multicolour Broad Range Protein Ladder (Thermo Scientific).

Table 2.11. SDS-PAGE gels composition (5 ml final volume)

Stock solutions	**12% resolving gel**	**14% resolving gel**	**3.75% stacking gel**
30% acrylamide: bisacrylamide (29:1)	2 ml	2.333 ml	0.625 ml
3.75 M Tris-HCl (pH 8.5)	0.5 ml	0.5 ml	-
0.5 M Tris-HCl (pH 6.2)	-	-	1.25 ml
dH_2O	2.395 ml	2.062 ml	3.02 ml
10% SDS	50 µl	50 µl	50 µl
TEMED	5 µl	5 µl	5 µl
10% APS	50 µl	50 µl	50 µl

5x SDS-PAGE loading dye:
312.5 mM Tris-HCl pH 6.8
10% SDS
50% glycerol
0.05% bromophenol blue
0.25 M DTT

1x running buffer:
192 mM glycine
25 mM Tris
0.1 % SDS

2.5.6. Western blot

Samples resolved on gels were immobilised on PVDF membrane (Immobilion-P, Milipore, activated with 100% methanol) using Mini Trans-Blot (Bio-Rad) for wet transfer under following conditions: 1 h, 100 V, 4°C with constant stirring. After transfer, membranes were blocked with 5% milk in T-TBS buffer for 1 h at room temperature.

1x Transfer buffer
25 mM Tris
192 mM glycine
0.02% SDS
15% methanol

T-TBS
20 mM Tris-HCl pH 7
0.5 M NaCl
0.1% Tween 20

The blocked membranes were incubated with primary antibodies (Table 2.12 A) overnight at 4°C and then washed 3x for 10 min with T-TBS. Incubation with secondary antibodies (Table 2.12 B) proceeded for 1 h at room temperature followed by the same washing procedure. Signals were detected with a use of ECL Plus reagent (Amersham) when visualised on X-ray films or Phosphoimager, or with ECL Prime kit (Amersham) for visualisation with ChemiDoc-MP (Bio-Rad), protocol according to manufacturer's instruction.

Table 2.12. Primary antibodies used in this study

A.

Protein	Size [kDa]	Company	Cat. number	Dilution	Secondary
C12orf65	15	Eurogentec	custom	1:500	rabbit
C12orf65	15	Santa Cruz	Sc-6024	1:200	goat
C12orf65	15	Abnova	FLJ386663	1:500	mouse
CII 70kDa	70	MitoSciences	MS204	1:1000	mouse
ClpX	65	Abcam	Ab68338	1:1000	rabbit
Core2/UQCRC2	42	Abcam	Ab14745	1:1000	mouse
COX2	20	Molecular Probes	A6404	1:1000	mouse
DAP3	45	Abcam	AB11928	1:1000	mouse
FLAG M2	1	Sigma	F1804	1:1000	mouse
HSP60	60	BD Biosciences	611562	1:1000	mouse
ICT1	20	ProteinTech	10403-1-AP	1:1000	rabbit
Lon-P	110	Sigma	HPA002192	1:1000	rabbit
MRPL3	39	Abcam	AB39268	1:2000	goat
MRPL45	35	ProteinTech	15682-1-AP	1:1000	rabbit
MRPS26	25	ProteinTech	15989-1-AP	1:1000	rabbit
MRSP27	45	ProteinTech	17280-1-AP	1:1000	rabbit
mtRF1	48	Eurogentec	custom	1:2000	rabbit
NDUFB8	20	MitoSciences	MS105	1:1000	mouse
Porin/VDAC1	39	Abcam	Ab14734	1:10000	mouse
SLIRP	12	Abcam	Ab51523	1:1000	rabbit

B.

Name	Raised in	Company	Cat. number	Dilution
Anti-Mouse/HRP	rabbit	Daco	P0260	1:2000
Anti-goat/HRP	rabbit	Daco	P0449	1:2000
Anti-Rabbit/HRP	swine	Daco	P0339	1:3000

2.6. Affinity purification of antibodies

2.6.1. Expression and purification of GST-tagged fusion protein

Liquid LB medium (1 l, supplemented with 100 µg/ml ampicillin) was inoculated with Rosetta cell culture (4x 5 ml) carrying pGEX vector with recombinant C12orf65 N-terminal GST fusion protein (generated by Dr. Pajak). Bacteria were grown at 37°C in a orbital shaker (200 rpm) until the culture reached OD_{600} = 0.4-0.6. At that point bacteria were induced with 1 mM (final concentration) IPTG (isopropyl-1-thio-b-D-galactopyranoside) overnight at 16°C. Cells were then harvested by centrifugation at 5000 rpm (GST rotor), 4°C 15 min. Pellets were washed with PBS (with 1x protease inhibitor cocktail (Roche), 1 mM PMSF, 1 µl Benzonase® Nuclease (70746)), resuspended by vortexing and incubated on ice for 20 min. The cell suspension was then sonicated with 15x 10 s pulses (Soniprep 150, 18 microns amplitude) and centrifuged at 30,000 x g in 4°C for 30 min. Collected supernatants were filtered (0.45 µm) and added to a column with 0.6 ml Glutathione Sepharose 4B beads. The column was then washed with sterile PBS and dH_2O, prior to the overnight incubation at 4°C with agitation. This was followed by another series of washings: 5 times with 10 ml PBS (with proteinase inhibitor cocktail and 1 mM PMSF) and 5 times with 10 ml PBS. In order to elute the protein from the column, 600 µl of PBS containing 25 µl PreScission Protease, 1 mM EDTA and 1mM DTT was added and the elution fractions were collected to separate tubes.

2.6.2. Purification of antibodies using NHS-activated sepharose

After the purification of the C12orf65 protein, a column with NHS-Activated Sepharose 4 Fast Flow (GE Healthcare) was prepared. Beads (1 ml) were added to 10 ml BioRad column and washed 3 times with cold 1 mM HCl. Next, the purified protein in elution buffer (4 mg of protein) was incubated on the column overnight at 4°C. After the incubation the flowthrough was saved and

the column was incubated with 0.1 M Tris-HCl pH 7.4 overnight, 4°C. Prior to application of the final bleed from the immunisation (generated by Eurogentec, Speedy protocol for Custom Anti-protein Polyclonal Antibody Production), the column was incubated with 8 M urea in PBS (3 h, 4°C with agitation) and washed twice with 10 ml PBS. The serum (7 ml) was added on the column and incubated overnight at 4°C with agitation. The flowthrough was saved and the incubation with 7 ml of serum was repeated. Finally, after the second flowthrough was collected, beads were washed 2 times with PBS, once with Tris-buffer/pH 8.0 (50 mM Tris-HCl pH8.0, 0.1% Triton X-100, 0.5 M NaCl), once with Tris-buffer/pH 9.0 (50 mM Tris-HCl pH 9.0, 0.1 % Triton X-100, 0.5 M NaCl) and once with sodium-phosphate-buffer/pH 6.3 (50 mM sodium phosphate pH 6.3, 0.1% Triton X-100, 0.5 M NaCl). The final elution of the antibodies was carried with 5 ml of Glycine-buffer/pH 2.5 (50 mM glycine pH 2.5, 0.1% Triton X-100 and 0.15 M NaCl) that was added to the column, followed by immediate neutralization with 1ml of 1 M Tris-HCl pH 9.0. The eluted antibodies were then dialyzed twice against 1L of PBS at 4°C, overnight with stirring. In order to reduce the volume of dialysed antibodies Aquacide II (Calbiochem) was used. The reduced antibodies sample (1.250 ml) was supplemented with 10% glycerol and 0.02% of sodium azide for long term storage at -20°C.

2.7. Isokinetic sucrose gradients

Sucrose gradients were prepared in Ultra Clear open top tubes in 1 ml volume. Two different sucrose solutions (10% and 30% w/v) were prepared in 1x sucrose gradient buffer (see below). 0.5 ml of 10% solution was added to each tube. Then, with a use of a syringe, 0.5 ml of 30% solution was loaded carefully on the bottom of tube so that both solutions formed separate layers. Gradient was obtained in tilted tube rotation using 55 s programme (Biocomp Gradient Maker instrument). Tubes with gradients were incubated for 1 h at 4 °C prior to loading. Samples (cell or mitochondrial lysates, maximum of 700 µg of protein) were loaded carefully on top of gradients and separated by centrifugation in Optima TLX Ultracentrifuge (BECKMAN) using TLS55 rotor under following conditions: 39000 rpm (100000 xg), 2 h 15 min at 4 °C (accel.= 1, decel.=4). After centrifugation from each gradient sample 10 fractions of 100 µl (the volume of the 11th fraction depended on the volume of lysate input) were

taken, stored in separate tubes and labelled: 1-11 starting from the top of gradient. If the gradient centrifugation was followed by SDS-PAGE, 12 µl of each fraction was taken, mixed with 3 µl of 5x SDS-PAGE loading dye (2.5.5) and stored at -20°C.

1x sucrose buffer:

625 mM	Tris-HCl (pH 7.2)
500 mM	NH_4Cl
125 mM	MgOAc
100 mM	KCl
1 mM	PMSF

2.8. Immunocytochemistry

U2OS cell were grown on glass cover slips placed on the bottom of 24-well plates. First, cells were fixed with formaldehyde solution in PBS (4% final concentration) for 10 min at room temperature. Then the cells were permeabilized with "Abdil" buffer (0.1% v/v Triton-100, 3% w/v BSA final concentration in PBS) for 30 min at room temperature. The primary antibodies diluted in the "Abdil' buffer were added to the samples on cover slips and incubated for 1 h at room temperature. Next samples were washed with PBS with 0.1% Triton X-100, 3 times for 5 min at room temperature and incubated with secondary antibodies diluted in "Abdil" buffer for 1 h. Finally samples were washed again 3x 5 min with PBS and 0.1% Triton X-100 and mounted on the glass slide using Vectashield Mounting medium with DAPI (hard set, H-1500, Vector). Cells were visualised on Axiovert 200M (Zeiss) microscope under bright field and using appropriate filters.

2.9. [^{35}S]-methionine/cysteine metabolic labelling

patient and control fibroblasts were grown in 25 cm^2 flasks to ~70% confluence. Prior to the metabolic labeling, cells were incubated with methionine/cysteine free DMEM twice for 10 min at 37°C. Next, they were incubated with the same medium supplemented with 10% dialyzed FCS, 2 mM L-glutamine, 1 mM sodium pyruvate, 50 µg/ml uridine and 100 µg/ml final emetine dihydrochloride for 30 min at 37°C. From each flask 0.5 ml of medium was removed and 20 µl of [^{35}S]-methionine/cysteine mix added (PerkinElmer; 125 µCi/ml EasyTag^{TM}

express [^{35}S] protein labeling mix NEG-772, 73% L-met, 22% L-cys). Incubation was carried for 1 h at 37°C, after which the metabolic labeling medium was removed. Cells were harvested with PBS/1 mM EDTA and centrifuged at 250 x g, 4 min, 4°C. Pellets were washed once and resuspended in ice-cold PBS with Protease Inhibitor Cocktail (EDTA-free, Roche) and 1 mM PMSF. Cell suspensions were snap frozen and stored at -80°C, until SDS-PAGE separation.

Prior to electrophoresis, samples were thawed on ice, protein concentration was measured and aliquots of equal protein content (50 µg) were mixed with loading buffer (1x final concentration, 2.5.5). Next, samples were incubated 1 h at room temperature with 12 U Benzonase® Nuclease (Novagen) and separated on 15% (w/v) SDS-PAGE. Unless stated otherwise in the subsection, after electrophoresis gels were fixed overnight with fixing buffer (3% v/v glycerol, 10% v/v glacial acetic acid, 30% v/v methanol). Visualisation of nascent proteins was carried with PhosphorImager and analysed using Image-Quant software (GE Healthcare). In order to asses equality of samples' loading, after the visualisation gels were rehydrated and stained with Coomassie Brilliant Blue (CBB) using 0.2% (w/v) Coomassie Blue R solution in 45% (v/v) methanol, 10% (v/v) and glacial acetic acid. Staining was carried out for 15 min at room temperature. Next, gels were destained twice for 10 min in CBB destaining solution (45% (v/v) methanol and 10% (v/v) acetic Acid). Images were taken with CCD camera system.

2.10. Statistics analysis

Calculation of standard deviation of all the mean values obtained from the data in this project were carried using t-test available at: http://www.graphpad.com/quickcalcs/ttest1.cfm.

The significance of the difference between results were specified as:

$p > 0.05$ as not statistically significant

$p = 0.01$ to 0.05 as significant (*)

$p = 0.001$ to 0.01 as very significant (**)

$p < 0.001$ extremely significant (***).

Chapter 3

Characterisation of C12orf65

3.1. Introduction

One of the primary questions underlying my project was to define the function of C12orf65. The attempts to characterize this protein function were included in patient reports (Antonicka et al., 2010) (Haruo Shimazaki et al., 2012) and in the study on the solution of the C12orf65 crystal structure (Kogure et al., 2012). The former two publications (especially (Antonicka et al., 2010) included a detailed analysis of the effect of mutations in C12orf65 on the mitochondrial gene expression. The mutations, namely homozygous 1 bp deletions different in both patients (246delA and 210delA), resulted in premature stop codons but did not affect the levels of the *C12orf65* transcript. However, the effect on the stability of the protein was unknown (Antonicka et al., 2010). In the second study a homozygous nonsense mutation (C394T, (Haruo Shimazaki et al., 2012) resulted in a truncated, stable form of the protein (Haruo Shimazaki et al., 2012). The most outstanding changes to the mitochondrial gene expression were observed in *de novo* mitochondrial protein synthesis (where a generalized decrease was seen in patient samples), assembly and activity of the OXPHOS complexes (disruption of CI, IV and V formation, decrease of complex IV activity) (Antonicka et al., 2010; Haruo Shimazaki et al., 2012). Further functional studies were performed on cells following C12orf65 depletion using siRNA (Kogure et al., 2012). The described effects of the lack of C12orf65 included increase in cell death (65%) and lower complex IV activity compared to controls (decreased by 52% in isolated mitochondria). These results clearly show the importance of C12orf65 for the cell and mitochondrial function but what is the exact role of this protein?

Investigation of the C12orf65 function was started by a former member of my host laboratory Dr. Aleksandra Pajak as a part of her PhD thesis. She was able to establish that the depletion of the C12orf65 caused a growth defect of HEK293 or HeLa cells when cultured in media containing galactose. These conditions, forcing cells to respire, are known to be a very sensitive test of potential mitochondrial defects. Both cell lines presented slower growth rate and unusual morphology after 3 days of C12orf65 depletion, although the effect was more profound in HeLa cells than in HEK293T. These cells also displayed changes to the mitochondrial network as assessed by non-quench mode fluorescent staining using the membrane potential dye, TMRM. Mitochondrial distribution was more compact and clustered around the nucleus after the

depletion. However, the observed changes to the cell morphology were not caused by the decrease in the steady state levels of mitochondrially encoded proteins. The steady state levels of COXII, a subunit of complex IV, was not affected by the C12orf65 depletion, neither was the nuclear NDUFB8. The latter protein, even though it is imported from the cytosol, is a surrogate marker for the assembly of the complex I. No changes to the levels of these two proteins suggested that there may be correct assembly of the complex I and IV. The detrimental result of the C12orf65 depletion could not be attributed to a decrease in the levels of MRPs, which remained stable even after 6 days of the treatment. However, the changes to the mitochondrial gene expression were visible when the steady state levels of mitochondrial transcripts were tested. Northern blot analysis showed an accumulation of the mt-mRNAs (*RNA14*, *MT-ND1*, *MT-CO1*, *RNA15*) and mt-rRNA. This increase became more profound after 6 days of depletion. The accumulated mitochondrial mRNAs were not associated with the monosome, but rather with separate mitoribosomal large subunit. Further, the lack of C12orf65 did not affect the composition of the mitoribosome, or caused the accumulation of the free ribosomal subunits, which might have been suggested by the upregulation of the rRNAs. There was also no evidence of the C12orf65 being a part of the mitoribosome, but a transient interaction cannot be ruled out.

This work, especially when put in the context with already published data (Antonicka et al., 2010; Kogure et al., 2012; Haruo Shimazaki et al., 2012) strongly suggests the involvement of the C12orf65 in mitochondrial gene expression. The objective of my experiments on the C12orf65 was to carry on the characterization of the protein function in the cells depleted of it.

3.2. C12orf65 colocalizes with mitochondria

The patient reports and resolving of the crystal structure are not the only context in which C12orf65 was noticed. In the study by (Antonicka et al., 2013) a novel mitochondrial function of the protein GRSF1 was identified and it co-immunoprecipitated with C12orf65. This former protein is involved in posttranscriptional processing and storage of mt-mRNAs as a part of RNA processing granules in mitochondria. The possibility of C12orf65 being a part of these granules could not be verified due to the lack of sufficiently specific and sensitive antibodies that would be suitable for immunocytochemistry (ICC).

Therefore, to test this hypothesis I performed ICC on C12orf65-FLAG expressing cells, which allowed me to use FLAG antibodies instead of those recognizing C12orf65. The objective of this experiment was to confirm the mitochondrial localization of C12orf65 and investigate the pattern of this protein distribution. There was a possibility that if the distribution was highly discreet, further ICC co-staining with GRSF1 antibodies would give the potential to identify any colocalization of the two proteins, indicating that C12orf65 may be sequestered in RNA processing granules. Even though a stable HEK293 cell line with the potential to inducibly express C12orf65-FLAG was available, it was not used because of the issues with imaging of HEK cells. For this type of experiments it is advised to use more flat cells, like U2OS, where the intracellular features are more clearly visualised. Since there was no stable U2OS cell line that could inducibly express C12orf65-FLAG, I made a transient transfection with the plasmid pcDNA5/FRT/TO/C12orf65-FLAG that contained a wild type FLAG tagged copy of C12orf65 (generated by Dr. Aleksandra Pajak; detailed protocol for transfection is described in 2.1.5). Briefly, U2OS cells were seeded on glass cover slips (round, dim. 13 mm) put inside the 24-well plate, at a density of 25000 cells per well. On the same day, one set of cells was transfected with plasmid (2 µg), the other was left as an untreated control. The ICC was performed the next day, based on the protocol (2.8) kindly delivered by Dr. Alexis Jourdain (University of Geneva). The procedure and the following imaging were performed with supervision from Dr Jorge Oliveira (University of Porto).

First the live cells were incubated with MitoTracker Red (CM-H_2XRos, Molecular Probes; final conc. 400 nM, 30 min) in order to stain the mitochondrial network. The trial epifluorescent images were taken and confirmed sufficient intensity of the signal to proceed with the procedure. Next, cells were fixed and immunostained (2.8). Detection of FLAG tag was performed with monoclonal anti-FLAG antibodies (1:200, Sigma F1804) and secondary goat anti-mouse antibodies conjugated with fluorescent dye (Alexa 488; Invitrogen, A11001). These cover slips were next mounted on glass slides using hard set mounting medium with DAPI (to stain the nuclei). The fluorescent signal from different dyes (red MitoTracker stained mitochondria, green C12orf65-FLAG and blue DAPI-labelled nuclei) was detected through epifluorescence microscopy (Axiovert 200M, Zeiss). Z stack Images were taken (with help from Dr.

Oliveira, Fig. 3.1) using appropriate filters independently (for Alexa488: excitation λ=493 nm, emission λ=520 nm; for DAPI ex. λ=359 nm, em. λ=461 nm; for MitoTracker Red CM-H_2XRos ex. λ=579 nm, em. λ=599 nm). These images could be superimposed to a 'Merged' image (Fig. 3.1). The successfully transfected cells were visualized through the signal from the green channel (coming from C12orf65-FLAG). On the merged images this signal fully colocalized with the signal derived from mitochondria. Untransfected cells displayed only the blue DAPI staining of nuclei and MitoTracker red mitochondria.

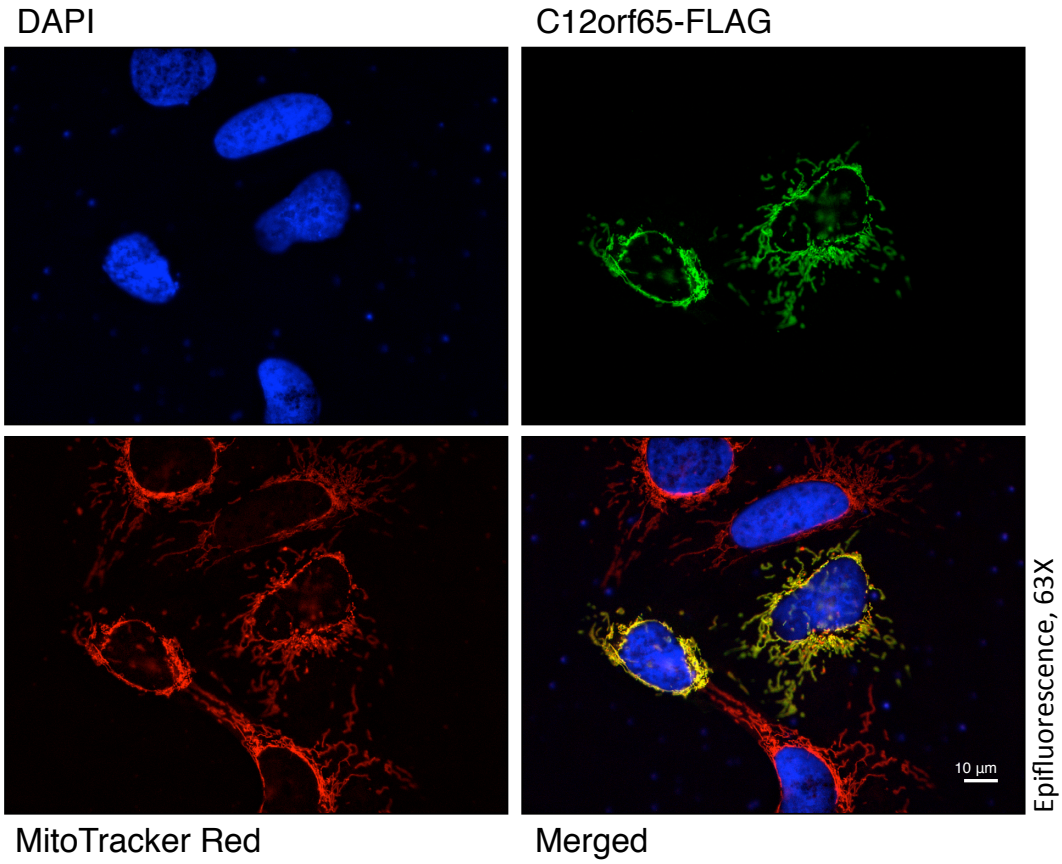

Figure 3.1. C12orf65 is localized to mitochondria

Fixed U2OS cells transiently expressing C12orf65-FLAG were analyzed via immunocytochemistry using antibodies against FLAG and visualized with fluorescent Alexa 488 conjugated secondary antibodies (green). The nuclei were stained with DAPI (blue) and the mitochondrial network was labeled with MitoTracker Red (red). Presented data comes from sigle Z-stack images.

The signal detected from FLAG antibodies was very intense due to the strong expression of the C12orf65 and it exceeded the strength of the mitochondrial labeling. Due to the strong promoter and a transient unregulated expression

the amount of C12orf65 protein significantly exceeded the physiological amount, which is undetectable using the antibodies available (that can detect 20 ng by western). Since the signal was saturated it was not possible to determine if the distribution of this protein was in discreet foci, which could resemble the pattern displayed by proteins associated with RNA processing granules. To answer this question in the future it will be necessary to create a stable cell line with morphology that is suitable for microscopy and that would allow titration of induced C12orf65-FLAG expression. Also the use of confocal microscopy instead of just the epifluorescent would be advised because it allows collecting serial optical sections and eliminate background information away from focal plane. As a result, images come from thin sections and the out of focus fluorescent light is rejected. Scanning a number of sections within one sample can be used to build a sharp 3D image. In addition, it allows special discrimination between full co-localization and signals from separate sources in close proximity. In order to address these issues I then created a stable U2OS cell line with inducible expression of the C12orf65-FLAG that could be used in the future to help determine whether C12orf65 colocalises with the RNA processing granules.

The stable transfection was performed (2.1.5) with the C12orf65-WT-FLAG construct in pcDNA5/FRT/TO vector together with pOG44 plasmid (encoding the Flp recombinase). U2OS-Flp-in cells in 6-well plates (seeded 60000 cells/ well) were transfected and selection of successful transformants achieved with hygromycin^{B} (100 µg /ml). Clones of the cells that survived selection were isolated, propagated separately in 25 cm^2 flasks and tested for the expression of the gene of interest. Induction of the C12orf65-FLAG expression was conducted with 1 µg /ml tetracycline for 3 days. Total cell lysate was prepared from induced cells and uninduced controls and equal amounts (50 µg) were separated by SDS-PAGE (2.5.5). After transfer to membranes the proteins of interest were immunodetected with antibodies and the results are presented in Fig. 3.2.

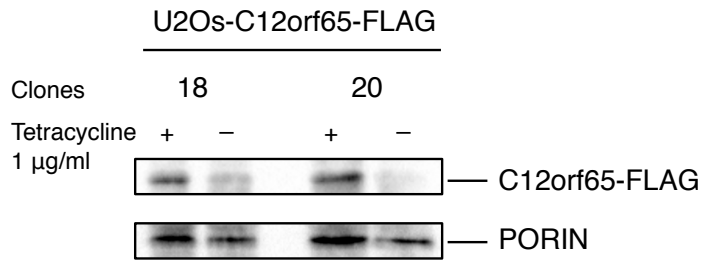

Figure 3.2. C12orf65-FLAG expression in the sable transfection U2OS cell line

The U2OS cell line was stably transfected with C12orf65-FLAG (2.1.5). After 3 days of induction with tetracycline the total cell lysate (50 µg per lane) of induced and uninduced control cells was analysed via western blot using anti-FLAG antibodies. The detection with porin served as a loading control. Visualization of signals was by chemiluminescence and CCD camera capture.

Two clones (No 18 and 20) were tested using α-FLAG to confirm expression of C12orf65-FLAG and porin as a loading control. Both clones displayed positive expression of the C12orf65-FLAG corresponding to the stronger signal from FLAG antibodies in induced cells (Fig. 3.2, lanes marked '+ Tetracyline') in comparison to the control (- Tetracycline). Although the loading of the samples is not perfectly even, as is evident from the porin signal, the fold increase in FLAG signal is greater than the difference observed in porin signal, confirming that there is inducible expression of C12orf65-FLAG. A faint but detectable signal is present in the uninduced control and is the result of the "leaky" expression. This is not uncommon and occurs when the Tet operator upstream from the promoter controlling the expression of the construct is not completely blocked by the Tet repressor. In such cases even without addition of tetracycline there is a possibility of uncontrolled expression. This should not, however, affect the ICC imaging as the levels of the product are very low. The clones presented here were, therefore, suitable be used for these experiments. Moreover, the expression levels of C12orf65 could be titrated by applying different concentrations of doxycycline. This antibiotic is known to induce expression of the gene of interest in a much more controllable way than tetracycline, which essentially switches on expression at maximum levels.

3.3. Comparison of purified and commercially available C12orf65 antibodies

One of the difficulties of working on C12orf65 is the lack of good commercially available antibodies. In order to address this problem Dr. Aleksandra Pajak

generated a fusion C12orf65-GST protein, which after removal of the GST tag was sent to be used as an antigen in a rabbit immunization programme (Eurogentec). The antibodies were subsequently affinity purified from the 2 batches of antisera. Affinity and specificity were tested by western blotting using recombinant antigen and the following samples of HEK293 mitochondria: wild type untransfected, C12orf65 depleted (via siRNA), overexpressing C12orf65-FLAG. The initial results were very promising. At a dilution of 1:200 the antibodies could detect the recombinant protein (20 ng), and endogenous C12orf65 in 10 µg of mitochondrial lysate. Although there were a number of unspecific bands, the one corresponding to C12orf65 was easily confirmed by a comparison with the overexpressing cell line and the one with C12orf65 depletion. However, these purified antibodies appeared to be very unstable during storage both at 4°C as well as -20°C, making reproducibility a problem. I continued this work by repeating the affinity purification step making the following adjustments to the commonly used protocol (2.6). First, double the amount (14 ml) of antiserum was used (#94 that previously gave a better result in terms of specificity). Second, the protein was denatured with 8 M urea while still attached to NHS-activated beads, in order to better expose the epitopes. Finally, in order to increase the concentration of the protein, the eluted antibodies were dialyzed and the final volume was reduced using Aquacide. Glycerol (10%, final concentration) and sodium azide (0.02% final concentration) were added and aliquots of the purified antibody were stored at -20ºC.

The specificity of these purified antibodies was tested by western blotting on total cell (Fig. 3.3, lane 4) and mitochondrial (Fig. 3.3, lanes 5-8) lysates. Different dilutions of the recombinant C12orf65 protein were used as positive controls (Fig. 3.3, lanes 1-3).

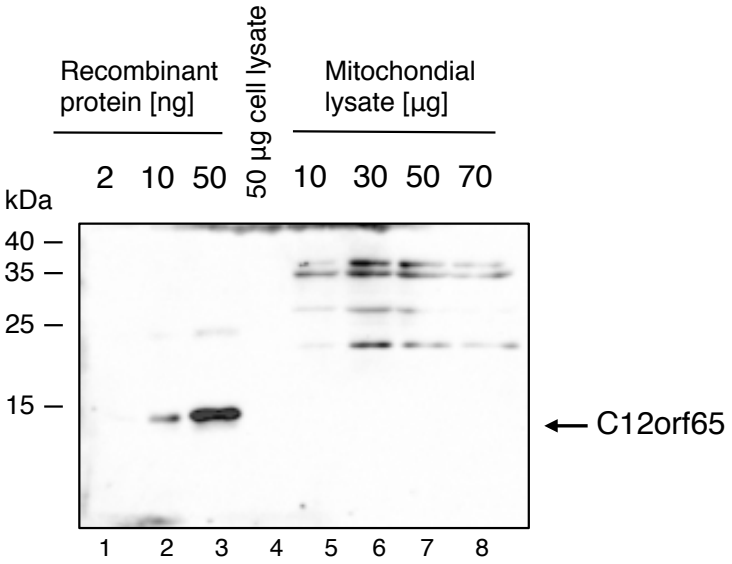

Figure 3.3. Affinity purified antibodies do not recognize the endogenous levels of C12orf65

Samples of wild type HEK293 total cell lysate (lane 4), mitochondrial lysate (lanes 5-8) and recombinant C12orf65 protein (lanes 1-3, as positive control) were separated by 15% SDS PAGE. Purified C12orf65 antibodies (1:200) were used to test their efficacy in western blot analysis.

The purified antibodies recognized the recombinant protein with very weak recognition of 2 ng but clear signal for 10 and 50 ng (Fig. 3.3 lane 1-3). Unfortunately, it was unable to detect the endogenous levels of C12orf65 in cell lysate (50 µg) nor when tested against high amounts (70 µg) of mitochondrial lysate (Fig. 3.3, lane 8). It seems, therefore, that the purification did not increase the sensitivity of the antibodies. In addition, the antibodies specificity was low as indicated by the presence of multiple bands. The affinity purified antibodies cannot be used in experiments and commercial antibodies became available.

The antibodies offered by Santa Cruz Biotech (SC-242028) and Abnova (FLJ38663) were tested. These antibodies were used at a 1:200 (Santa Cruz) and 1:500 (Abnova) dilution on HEK293 cell line inducibly expressing C12orf65-FLAG. Both types of antibodies were able to detect C12orf65 in mitochondrial lysate in induced cells (50 µg) and recognize the recombinant protein (10 ng). However, detection in uninduced cell lines was obscured by the abundance of unspecific signal, especially close to expected size of the protein (data not shown). Addition of the signal enhancing reagent SuperSignal® (Life Technologies, 46640) did not improve specificity of the binding. The comparison of the 3 types of used antibodies shows that none of them was sufficient to detect the endogenous form of the protein. For the following experiments, the

levels of the C12orf65 could not be detected with western blot analysis. Instead, the transcript levels measurements with qPCR had to be used.

3.4. C12orf65 is not an integral part of mitoribosome

Of the mitochondrial release factor family of proteins, two have lost the sequence recognitions domains, namely C12orf65 and ICT1. The latter has become incorporated into the mitoribosome (Richter et al., 2010b), unlike its bacterial homologue YaeJ, which interacts transiently with stalled ribosomes (Gagnon et al., 2012). The mechanisms of C12orf65 action and its relation to mitoribosomes are unknown. The preliminary data from Dr. Pajak thesis suggested C12orf65 is not an integral part of mitoribosome and any potential interaction is only transient. In order to definitely exclude that, like ICT1, C12orf65 is incorporated to the mitoribosome (either monosome or any subunit) mitochondrial ribosomes were analyzed on sucrose gradient prior to the western blot analysis. In this experiment cell lysate is centrifugated in isokinetic sucrose gradient (10-30%, 2.7) and its components (including the content of mitochondria) are separated based on their buoyant density. Single mitoribosomal subunits or fully assembled monosome binding partners can be immunodetected and analysed as they are collected with different fractions of the gradient. Since the endogenous levels of C12orf65 were known to be low, and the antibodies were not efficient enough to detect these, the experiment was done on the stable cell line expressing FLAG tagged version of C12orf65 (HEK-C12orf65-FLAG). The position of small (mt-SSU, 28S) and large mitoribosomal subunit (mt-LSU, 39S) were detected with antibodies for one of their components (DAP3 and MRPL3 respectively, Fig. 3.4).

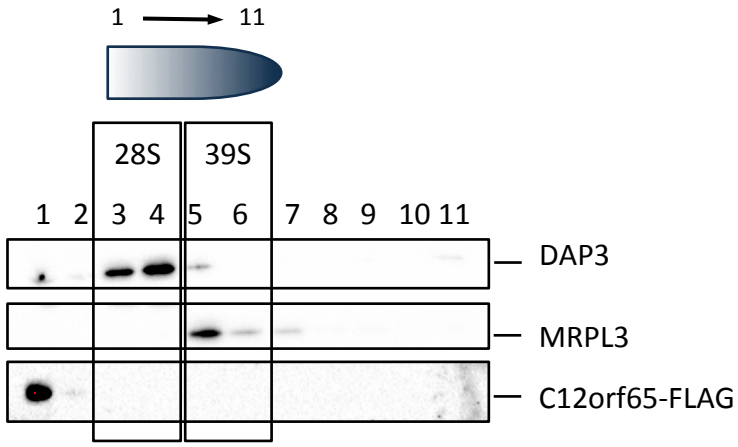

Figure 3.4. C12orf65 is not detectable in the separate mitoribosomal subunits

HEK-C12orf65-FLAG cells were induced for 3 days (1 µg/ml tetracycline) and the lysate (700 µg) was separated on the isokinetic sucrose gradient (10-30 %, 2.7). Fractions (1-11) were taken from the top down and all fractions were electrophoresed on 12% PAG followed by western blotting. Immunodetection was performed using antibodies specific to proteins from small and large mitoribosome subunit (DAP3 and MRPL3 respectively). The presence of the overexpressed C12orf65-FLAG was detected with α-FLAG antibodies.

Fractions 3 and 4 (Fig. 3.4), where the highest concentration of DAP3 protein was found were also most likely containing small ribosomal subunit (28S, SSU). Position of the large subunit (39S, LSU) was determined by the signal from MRPL3 to be in fractions 5 and 6. Unfortunately, the presence of the monosome could not be detected which is not uncommon when analysing cell lysates and observed in my host lab. However, even without the detectable levels of monosomes, it was ppossible to determine if there is an interaction of C12orf65 with separate subunits. The signal from C12orf65-FLAG was only present in fraction 1 and 2 (but much weaker), which correspond to the free protein not attached to any ribosomal subunit. Therefore it was concluded that C12orf65 is not permanently associated with the free mitoribosomal subunits (small or large) and if any such interaction occurs it is only transient.

3.5. Is the GGQ motif important for C12orf65 function?

After investigating a possible interaction of C12orf65 with mitoribosomes, another feature of the protein was tested, namely the functionality of the GGQ motif. The presence of this well conserved and highly specific sequence is the reason for characterizing C12orf65 as a member of mitochondrial release factor family. The GGQ motif is present in all class I release factors and is unambiguously associated with ribosome dependent PTH activity (Frolova

et al., 1999). Previous experiments by Dr. Pajak started investigating if the GGQ motif in C12orf65 is functional. If it were then the potential ribosome-dependent peptidyl-tRNA hydrolysis activity would be another argument for proposing C12orf65 as a candidate ribosome rescue factor. It has been previously established, by testing AGQ and GSQ *E. coli* mutants that the first two residues are essential for the release activity (Frolova et al., 1999). Therefore, Dr. Pajak created two constructs of C12orf65 in pcDNA5/FRT/TO vector, each one containing either AGQ or GSQ mutation, to generate stable-transfection cell lines. In order to be able to deplete the endogenous protein but not newly incorporated mutated form, silent mutations (SM, five single bp mutations) were introduced by site directed mutagenesis to the construct sequence. The lack of complementarity across this SM sequence protected the mutant C12orf65 from the siRNA. In addition, the sequence of FLAG tag was also included to enable detection of the expressed proteins on Western blots. Finally, Dr. Pajak confirmed the import of the encoded proteins into mitochondria.

I used these constructs generated by Dr. Pajak and repeated generation of stable cells lines as described above (2.1.5). Wild type HEK293-Flp-In TRex cells were seeded in the 6-well plates (160000/ well) and on the next day transfected with the pOG44 plasmid and either pcDNA5-C12orf65-AGQ-SM-FLAG or pcDNA5-C12orf65-GSQ-SM-FLAG. Two days later antibiotic selection started using Hygromycin B (100 µg/ml). After approximately 3 weeks selection, the remaining resistant colonies of cells (clones) were isolated, propagated independently and subsequently tested for expression of the transfected constructs. For each protein expressing cell line C12orf65-AGQ-FLAG (Fig. 3.5 A) or –GSQ-FLAG (Fig. 3.5 B) 4 clones were tested. Expression of the proteins of interest was induced with tetracycline (1 µg/ml) for 3 days in each cell line. In addition, an identical set of uninduced cells was cultivated alongside the induced ones. The expression was confirmed with western blotting (50 µg of total cell lysate per sample) targeting the FLAG tag. Porin served as a loading control.

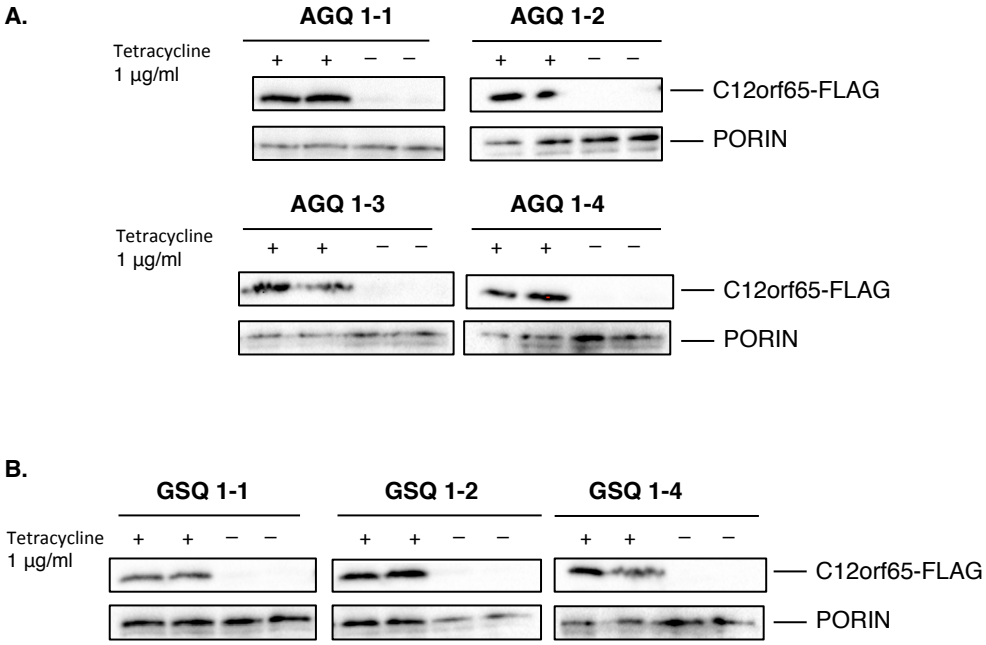

Figure 3.5. Generation of the cell lines expressing C12orf65 mutants

Western blot analysis was performed on total cell lysates (50 µg) from induced (1 µg/ml tetracycline, 3 days) and uninduced HEK-C12orf65-AGQ-FLAG (**A**) or –GSQ-FLAG (**B**) cell lines. Each cell line originates from an individual clone of transfected cells isolated during selection (labelled from 1-1 to 1-4). Expression was confirmed by immunodetection of the FLAG tag, equality of the loading was tested with porin antibodies. Each sample was run as a duplicate. Only clones positively expressing the gene of interest are included.

Each of the tested HEK-C12orf65-AGQ cell lines expressed the protein of interest (Fig. 3.5 A). Only in cell line 'AGQ 1-1' there is a faint signal from C12orf65-FLAG in uninduced control samples lanes. This is an evidence of a very subtle "leaky" phenotype. For the GSQ cell lines only 1 failed to express the C12orf65-GSQ-FLAG (cell line 'GSQ 1-3', data not shown), the rest displayed high levels of expression.

Further experiments involved testing if the overexpression of the mutated forms of C12orf65 would have a dominant negative effect on the cell growth. However, it was important to first investigate if the excess of wild type C12orf65, on its own, would be toxic for the cells. In order to test this, a cell line expressing the wild type form of C12orf65 (HEK-C12orf65-WT-SM-FLAG clone 3-2, produced by Dr. Pajak) was used alongside the newly generated C12orf65-AGQ (clone 1-1) and GSQ (clone 1-1) mutants. The growth of the induced and uninduced cells from the aforementioned cell lines was monitored and compared (Fig. 3.6 A). In parallel, 2 sets of all 3 cell lines were cultivated for the purpose of confirming the expression by western blot analysis (50 µg cell lysate/sample). As described previously, the expression of these 3 C12orf65

forms (WT, AGQ and GSQ) was validated by immunodetection via FLAG and compared with uninduced cells (Fig. 3.6 B).

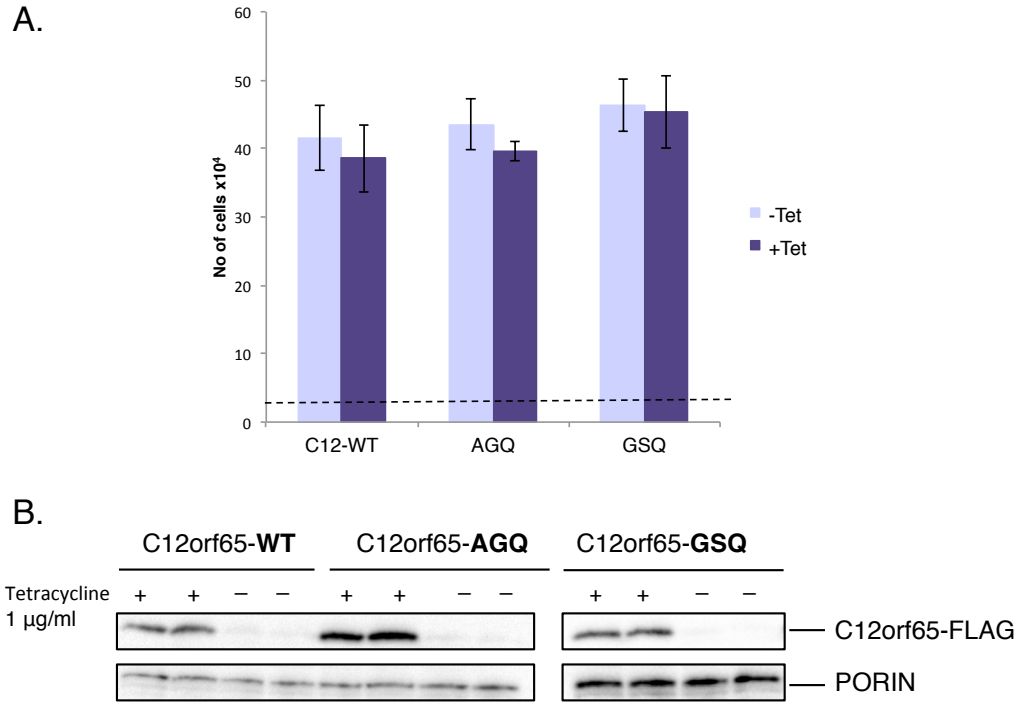

Figure 3.6. Cell growth rate is not affected by overexpression of WT or mutated forms of C12orf65

A. Growth of 3 different cell lines was monitored, those overexpressing wild type C12orf65 (C12orf65-WT), the AGQ mutant (C12orf65-AGQ) and the GSQ mutant (C12orf65-GSQ). Equal numbers of cells (30000, represented by the dashed line) were seeded in a 24-well plate. One set of cells was induced with tetracycline (1 µg/ml; purple), second identical set was left untreated (uninduced control; lilac). The number of cells in each condition (average and standard deviation of 3 wells) after 3 days of overexpression is graphically represented. **B.** Expression of the proteins of interest (wild type and GGQ-mutant C12orf65) was confirmed by western blot analysis (50 µg cell lysate) via FLAG tag immunodetection. Each sample was loaded as duplicate. Porin was used as a loading control.

The expression of all 3 forms of C12orf65, validated with FLAG detection was positive (Fig. 3.6 B). The levels of these proteins exceeded any potential traces of uninduced expression (as defined by a very faint signal seen in uninduced cell lines). The comparison between induced and uninduced C12orf65-WT expressing cells (Fig. 3.6 A) showed no difference to the cell growth, which suggests that the much higher than physiological levels of C12orf65 is not harmful to the cells. The same observation was made in both mutant-expressing cell lines, as the doubling time of cells in uninduced and induced cell lines was very similar and also comparable to wildtype. These results indicate that the presence of high levels of the C12orf65 with mutations in the GGQ motif does not have a dominantly negative effect on the cell. However, it is

still possible that the GGQ in C12orf65 is functional and necessary for the normal cell growth. It is important to remember that in these experiments the endogenous, wild type protein is still present and therefore can be sufficient to maintain the function suppressing the effect of the mutation.

In order to better characterize whether the mutation of the GGQ recessively affects the cell viability, a further experiment was performed. The same 3 cell lines were seeded in 24-well plates (30000/ well) expressing wild type C12orf65 ('C12-WT', clone 3-2), C12orf65 AGQ mutant ('AGQ', clone 1-1) and GSQ mutant ('GSQ', clone 1-1) as before all cell lines were induced to express their form of C12orf65 (1 µg/ml, 3 days). This time, one set of cell lines was depleted of C12orf65 mediated via siRNA ('siC12') and a second parallel set was treated with non-targeting control siRNA ('NT'). As all three cell lines expressed *C12orf65*–containing the silent mutation, the expressed C12orf65 protein was immune to the C12-targetted siRNA. The endogenous mRNA, however, would still be targeted and depleted. This approach aimed to replace the endogenous C12orf65 so that the expressed form would dominate. The overexpression of the WT form was included as a control in this experiment to investigate if the siRNA transfection procedure together with simultaneous replacement with overexpressed C12orf65 is harmful to the cell. This control aimed to identify if the exogenous C12orf65 impairs function, potentially due to the presence of a C-terminal FLAG-tag. It was important to establish this in order to accurately interpret the results derived from the GGQ-mutations. These growth rate experiments were performed as those described previously (Fig 3.8).

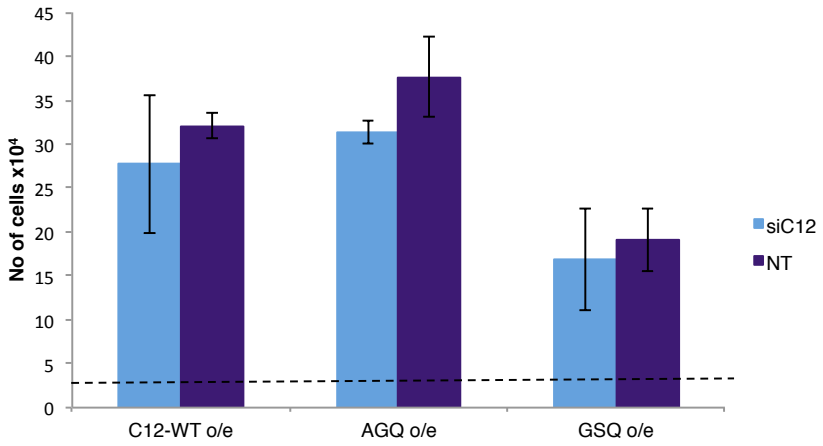

Figure 3.7. Replacement of the WT C12orf65 with GGQ-motif mutants does not affect the cell growth.

Cells were induced to express various forms of C12orf65 (wild type, AGQ mutant and GSQ mutant; tetracycline 1 µg/ml, 3 days in plate (30000 cells/15.6 mm diameter well, indicated by the dashed line). One set of cells were C12orf65 depleted (siC12) and the control cells were treated with non-targeting siRNA (NT). Cell numbers were determined after 3 days and are presented graphically (expts performed in triplicate, mean +/- SD).

No significant difference between the C12orf65 depleted and control samples was observed (Fig. 3.7). This indicated that replacing the endogenous form of C12orf65 with either the WT or GGQ mutated forms does not impair the cell growth. However, prior to accepting this interpretation, it was necessary to confirm both that overexpression of the transfected C12orf65 was successful, and that the endogenous version was actually depleted. To answer the first question western blotting analysis was performed on cell lysate from each cell line (50 µg) either induced or uninduced. FLAG tag immunodetection validated the C12orf65-FLAG expression in all tested cell lines (Fig. 3.8). This confirmed that the lack of growth defect was not due to unsuccessful production of the mutant and WT C12orf65.

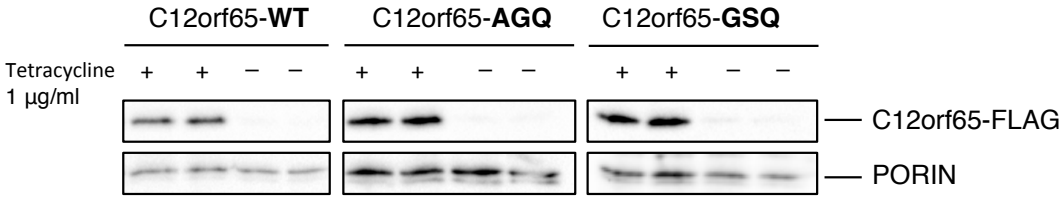

Figure 3.8. Confirmation of expression of WT and GGQ-mutant C12orf65-FLAG proteins

Cell lysates (50µg) from all 3 cell lines (induced and uninduced, each sample was run in duplicate) were analysed by western blot. Antibodies to the FLAG moiety validated the overexpression. Porin immunodetection was used as a loading control.

Having confirmed the overexpression of the proteins of interest the next step was to investigate the level of the endogenous C12orf65 depletion by qPCR (2.4.4). The primers used in this analysis were specific to the region upstream of the coding sequence (CDS), which was not included in the C12orf65 construct cloned in pcDNA5 vector used for the stable transfections. Therefore, this experiment was designed to detect only the endogenous form of C12orf65 and was used subsequently to estimate the level of depletion as follows:

$$2^{-\Delta\Delta C_T} = \frac{2^{\Delta C_{T\ C12orf65}}}{2^{\Delta C_{T\ 18S\ rRNA*}}}$$

Where:

$$\Delta C_{T\ C12orf65} = C_{T\ siNT} - C_{T\ siC12orf65}$$

$$\Delta C_{T\ 18S\ rRNA} = C_{T\ siNT} - C_{T\ siC12orf65}$$

* 18S-rRNA reference gene

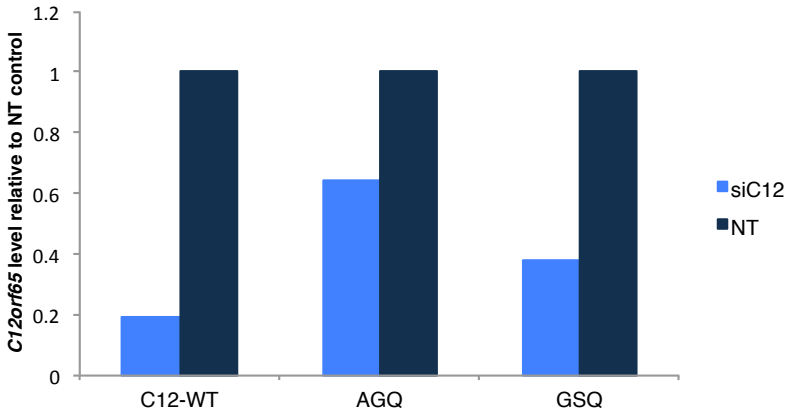

Figure 3.9. Detection of the endogenous levels of C12orf65 in induced cell lines.

RNA was isolated from each of the cell lines induced to express wild type C12orf65, or AGQ and GSQ mutants. qPCR analysis was used to measure the level of depletion of endogenous *C12orf65* transcript in all samples. *C12orf65* levels were calculated based on mean value of 3 technical repeats and normalized to 18S rRNA levels. Results were represented in relation to the expression in NT cells.

In the C12orf65-WT overexpressing cell line (Fig. 3.9, C12-WT) the level of depletion was around 80% (indicating that there was only 20% of the endogenous *C12orf65* transcript remaining). This result confirms that when the endogenous form of the protein is severely depleted and replaced with the exogenous form, the cell growth is not impaired (Fig. 3.7). In the case of the GGQ-mutant cell lines (AGQ and GSQ), the depletion was not as effective (only 35% reduction for the AGQ and 60% for the GSQ, Fig. 3.9). Both of these cell

lines did not display any major change to the growth rate (Fig.Fig. 3.7), which could be explained by the fact that they still retained a relatively high (especially AGQ- 65%) level of the endogenous, wild type C12orf65. This could suggest that approximately 40% of wild type C12orf65 is sufficient to sustain the function and normal cell growth.

3.6. Effect of C12orf65 depletion on *de novo* synthesis of mitochondrial proteins

Another critical experiment to determine the function of C12orf65 was the effect of depletion on *de novo* mitochondrial protein synthesis. Studies on the patient fibroblasts carrying the C12orf65 mutations shows that the resulting phenotype often includes a decrease in the levels of newly synthesized mitochondrial proteins (Antonicka et al., 2010; Haruo Shimazaki et al., 2012). In order to compare the results of a patient mutation and depletion of C12orf65, wild type HEK293 were treated with C12orf65 siRNA (2.1.4), followed by [^{35}S]-methionine/cysteine metabolic labeling of mitochondrial proteins (standard protocol used in my host lab, 2.9). The cells were cultivated and treated in 6-well plates (90000 cells/ well, 3 wells/ siRNA treated for 6 days, 6 wells for 3-days treatment). On the final day of the siRNA treatment they were metabolically labeled with [^{35}S]-methionine/ cysteine with prior emetine inhibition of cytosolic translation. Under these conditions only newly synthesized mtDNA-encoded polypeptides would be visualized. Equal amounts of cell lysate from each condition were separated by 15% SDS-PAGE. Signals from radiolabelled newly-synthesised mt-proteins were detected and visualised by PhoshoImager and ImageQuant software (Fig. 3.10).

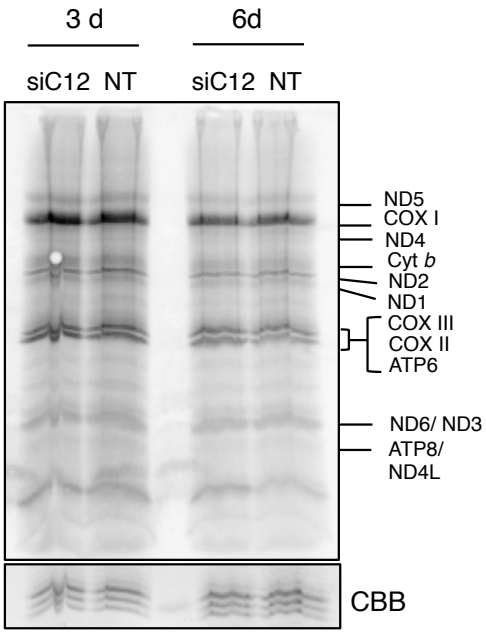

Figure 3.10. *De novo* protein synthesis in mitochondria following C12orf65 depletion

HEK293 wild type cells were treated with C12orf65 siRNA (siC12) or nontargeting siRNA (NT) for 3 or 6 days (3d or 6d). They were subsequently metabolically labelled with [^{35}S]-methionine/ cysteine with parallel inhibition of cytosolic translation (as described in 2.9). Samples (50 µg total cell protein) were separated by 15% SDS-PAGE. Signals from newly synthesised mt-proteins were detected via PhosphoImaging (upper panel). Prior to the imaging, the gel was stained with Coomassie brilliant blue (CBB, lower panel) to confirm loading.

Visualisation of the metabolic labeling of the newly-synthesized mt-proteins (Fig. 3.10 upper panel) shows no general difference between the depleted and control samples. Coomassie staining of the gel (Fig. 3.10, bottom panel) indicates the protein levels in each sample. Here it confirmed even loading of the samples. To correctly interpret this result, however, a confirmation of the depletion must also be made. For this purpose, in parallel to metabolic labeling, cells were cultured with siRNA treatment (siC12 and NT, 3 and 6 days) to provide material for qPCR analysis of *C12orf65* levels. Estimation of the depletion level was conducted as described previously (Fig. 3.9 and section 2.4.4). The comparison of the *C12orf65* levels between the depleted (Fig. 3.11, siC12) and control cells (NT) shows that after 3 days there was 40% of the transcript remaining. The longer siRNA treatment resulted in an increase of *C12orf65* levels to 60%. This suggested that the re-transfection with siRNA after 3 days was not as successful and failed to maintain or further decrease the level of the transcript. However, even in the sample with higher level of depletion (3d, 40% of control) there are no changes in *de novo* mt-protein

synthesis in comparison to the control. This result can be explained in the same way as the GGQ mutant experiments. It is possible that 60% depletion is insufficient to cause a deleterious phenotype in cells and affect the synthesis of mitochondrial proteins.

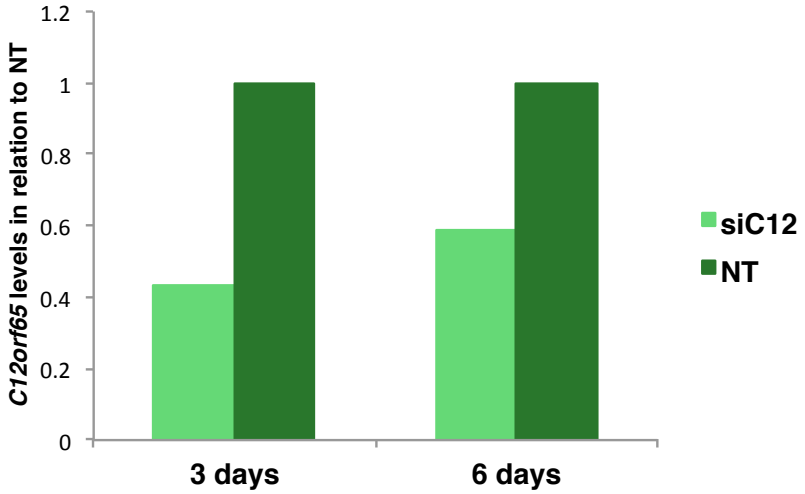

Figure 3.11. Estimation of the level of *C12orf65* depletion in the *de novo* mt-translation experiment

RNA was extracted from cells cultured and treated in parallel to those used in metabolic labelling. Depletion of *C12orf65* was analysed by qPCR to estimate residual *C12orf65* levels. *C12orf65* levels were calculated based on mean value of 3 technical repeats.. Results, normalized to 18S rRNA levels, were represented in relation to the expression in NT cells.

3.7. Does depletion of C12orf65 cause accumulation of mitochondrial transcripts?

It had been observed by Dr. Pajak that the steady state levels of mt-RNAs were elevated after C12orf65 was depleted and that this effect was even stronger after longer siRNA treatment. In order to confirm this observation, I replicated this experiment by depleting wild type HEK293 cells (seeded in 6-well plates at 100000/ well with siRNA against C12orf65 (siC12, 3 and 6 days). Control cells were treated with non-targeting siRNA (NT). At the end of the treatment total RNA was isolated from cells, equal amounts (4 µg) were separated on denaturing agarose gel and subjected to Northern blot analysis (as described in 2.4.2).

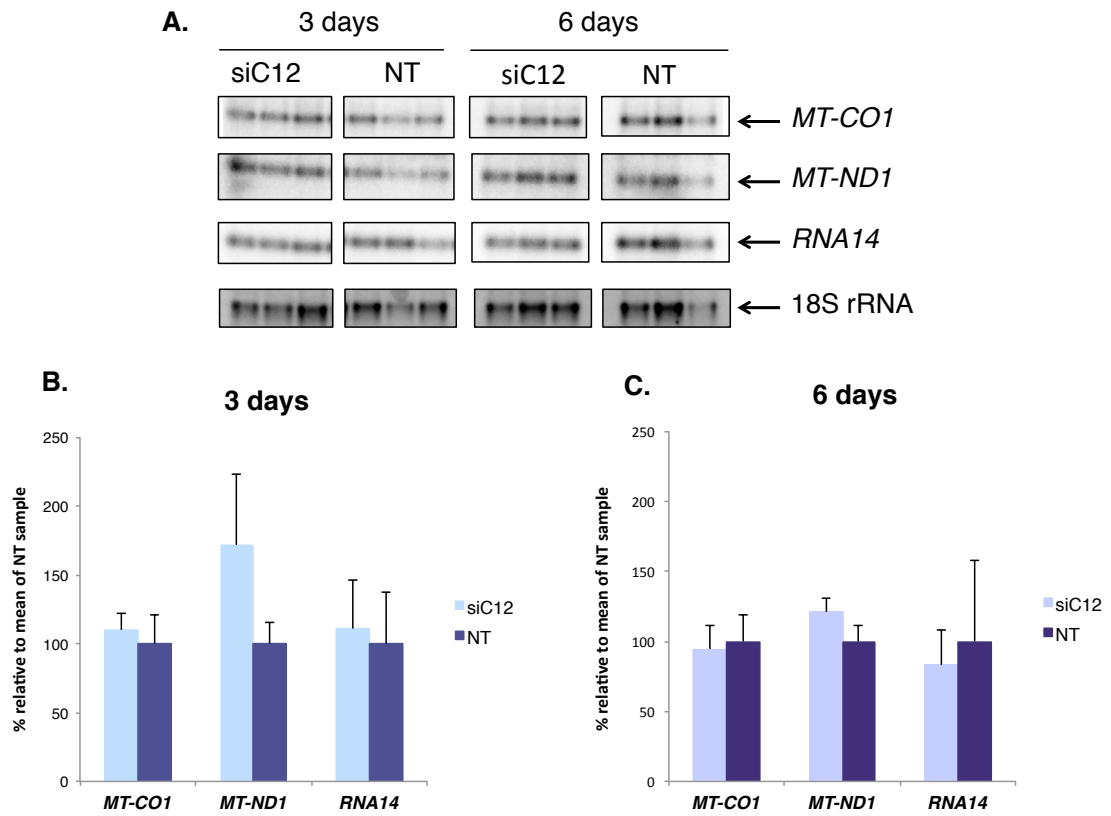

Figure 3.12. Levels of the mitochondrial transcripts are not affected by C12orf65 depletion

A. Total RNA (4 μg) isolated either from C12orf65-depleted (siC12) or control (NT) HEK293 cells (3-day and 6-day treatment), was subjected to Northern blot analysis with the indicated probes. The probes were targeting mitochondrial-encoded transcripts (2.4.2). **B.** Quantification of mt-mRNA steady state levels after 3 days of siRNA treatment (siC12) was calculated using ImageQuant software and presented as the percentage of the control sample (NT) sample. Levels of cytosolic 18S RNA, detected by retained intercalated ethidium bromide on the membrane after transfer, were used as the loading control to normalise intensity of each signal. The graph presents the mean and standard deviation of three independent experimental repeats. **C.** The signal quantification and normalisation of the samples treated for 6 days was performed as in B.

The mt-mRNAs were visualized with specific probes to compare the steady state levels between the depleted samples (Fig.3.12 A, siC12) with non-targeting control (Fig.3.12 A, NT). Signal from each probe was normalized against the loading control: 18S rRNA ethidium bromide signal. The calculated relative amounts of mt-mRNA (*MT-CO1*, *MT-ND1*, *RNA14*) are presented as histograms (Fig 3.12 B, 3 day depletion; Fig. 3.12 C, 6-days). The histograms (Fig. 3.12 B and C) showed a very clear result where, with the exception of *MT-ND1* transcripts, the steady state levels of mt-mRNAs did not differ significantly between the depleted (siC12) and control (NT) samples. The lack of significant difference between the siC12 and NT samples was unexpected, especially for

the 6-days depletion, as they contradicted those of Dr. Pajak. The latter clearly showed an increase in the levels of mt-mRNAs that was even more prominent after 6 days of C12orf65 depletion. However, as in previous experiments to determine GGQ functionality (Fig. 3.8 and 3.9) and *de novo* mt-protein synthesis (Fig. 3.10 and 3.11), the validation of the depletion was essential for accurate interpretation of this data. The remaining RNA from the samples used for the Northern blot was analysed by qPCR (as in Fig. 3.9 and 2.4.4).

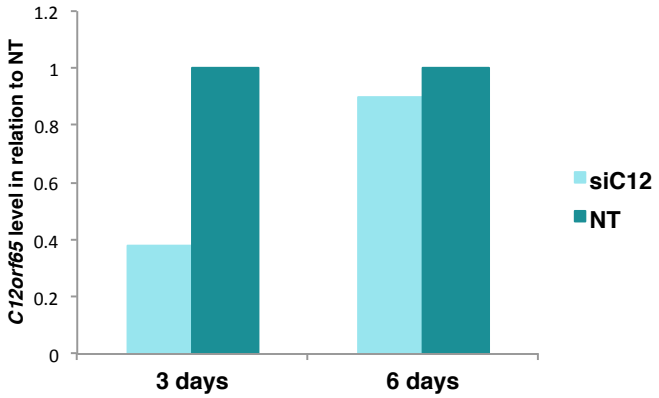

Figure 3.13. Estimation of the level of *C12orf65* depletion in the samples used for Northern blot analysis

RNA used in the Northern blot analysis (3 and 6 days of C12orf65 depletion) was analysed by qPCR to estimate the level of *C12orf65* depletion. *C12orf65* levels were normalized to 18S rRNA levels and represented as the remaining transcript after depletion (siC12) in relation to the level in non-targeting control (NT) cells.

Similar to the depletion verification performed on *de novo* mt-translation samples (Fig. 3.11) approximately 40% *C12orf65* remained after 3 days of siRNA treatment (Fig.3.13, siC12, 3 days). The re-transfection for the 6-days sample again did not result in further reduction of the targeted transcript. On the contrary, the amount of the *C12orf65* transcript elevated (~ 90%) almost to the levels in the non-targeting control samples (Fig. 3.13 siC12, 6 days). These results suggest that the reduction of the *C12orf65* level to 40% of the control is not enough to cause the accumulation of the mt-mRNA transcripts as observed in previous experiments by Dr. Pajak and (Antonicka et al., 2010).

3.8. Discussion

The experiments described above were designed to complement the work of Dr. Pajak who started the characterisation of the C12orf65 function in HEK293 and HeLa cell lines. One of her most striking observations was that upon

depletion of C12orf65 the steady state levels of the mt-RNAs were elevated. A similar phenotype was then described in the patient report (Antonicka et al., 2010) as a result of the 248delT and, to much less extent, 210delA *C12orf65* mutations. However, she did not observe the decrease in steady state levels of the mitochondrially-encoded proteins that was characteristic to these patients (Antonicka et al., 2010).

In my experiments, I aimed to further characterise the function of this protein. In order to identify if there is any association of C12orf65 with the mitochondrial RNA processing granules as reported by (Antonicka et al., 2013) I generated a stable U2OS cell line that could inducibly express wild type C12orf65-FLAG. A good antibody would facilitate investigations, so I performed a comparison of our custom synthesised affinity purified antisera (Fig. 3.3) and the commercially available C12orf65 antibodies. Unfortunately, none one of these 3 antibodies was specific and sensitive enough to recognize the endogenous form of the protein in 50 µg of cell lysate or similar amounts of purified mitochondria. In the cell lines tested, C12orf65 protein is expressed at a very low level and even using the enhancer, immunodetection could not detect the protein. Unless the method can be further improved, the levels and specifically changes in levels of C12orf65 protein cannot be estimated by western blotting. Potentially a more sensitive enhancer than SuperSignal® reagent would solve this problem. The reagent reported to be useful with C12orf65 antibodies was Can Get Signal immunostain (Toyobo, (Kogure et al., 2012), however this could not be supplied to the UK. Further, I generated the 2 stable cell lines that could inducibly express the mutated forms of C12orf65 GGQ sequence (AGQ and GSQ, Fig. 3.5). These cell lines were next used to investigate if the conserved GGQ motif had retained functionality. Unfortunately, in order to determine that, it was necessary to completely deplete cells of the wild type C12orf65 and replace it with the overexpressed, mutated versions. This, however, was not successful because the levels of the C12orf65 depletion were approximately 60% of control and this was not sufficient to lose activity of the wild type protein (Fig. 3.9). A similar issue with insufficient depletion of C12orf65 was observed in *de novo* mt-translation assay (Fig. 3.11) and during measurement of the steady state levels of mt-transcripts (Fig. 3.13). In all three cases, the remaining C12orf65 (not less than 40% of control) could have prevented the development of the expected, pathological phenotype. It was, therefore, impossible to

determine if the lack of change to the cell viability and mitochondrial function was because they do not depend on the presence of C12orf65 or simply because depletion did not cross the low threshold required to trigger pathology. This hypothesis seems to be supported by the observation by (Kogure et al., 2012) where the cell and mitochondrial defects were observed with 90% depletion of C12orf65. Perhaps, if the level of depletion was as high in my experiments, the results would better show the importance of the C12orf65 and its motifs for cell and mitochondrial function. In order to achieve this it would be critical to refine the siRNA depletion of C12orf65, which was used in my experiments (2.1.4). I had already modified the protocol used by Dr. Pajak by increasing the final concentration of siRNA from 0.33 μM to 0.5 μM. I have also used a newly synthesised batch of siRNA, increased time of incubation to 4 days and tested a different than lipofectamine transfection reagent (INTERFERin® reagent, Polyplus 409-10). None of these changes resulted in higher than 70% depletion level. Potentially increasing the amount of siRNA even further or changing the siRNA sequence to that used by (Kogure et al., 2012) would improve the depletion level. The re-transfection for the 6-days treatment is another step that needs optimization. In the described protocol (2.1.4) the conditions were optimised for the 3-days incubation. For longer treatments a fresh siRNA solution was added on the third day. To increase the efficiency of this step the concentration of siC12 could be increased and a reverse transfection method employed so that cells would be resuspended and reseeded again to prevent them from growing in clumps rather than left adherent, and this would improve the access of the siRNA to all cells. However, if the level of the depletion cannot be improved, an alternative approach could be used to perform the experiments on cells (preferably HeLa as they had a stronger susceptibility to depletion) grown in galactose containing medium rather than glucose. It has been observed by Dr. Pajak, that under these conditions the growth defect is visible and potentially the anticipated features of a deleterious phenotype would also be observed.

At this point the function of C12orf65 is still not clear. Obvious comparisons can be drawn between the C12orf65 and ICT1 because of the structural similarities (Kogure et al., 2012). In addition, in (Antonicka et al., 2010) the patient phenotype was partially rescued by overexpression of the ICT1 construct, which

indicates some reciprocity of the two proteins' functions. However, the experiments described in Kogure et al. unambiguously show that the effects of ICT1 downregulation are much more severe than in the case of C12orf65 depletion (Kogure et al., 2012). Unlike ICT1, C12orf65 is not a part of the mitoribosome and it seems to be lacking the peptidyl-tRNA hydrolysis activity *in vitro* (Antonicka et al., 2010). Differences between C12orf65 and ICT1 structures, such as the lack of the additional α-helix in the former or the varying distribution of the protein specific residue clusters and electrostatic charges (Kogure et al., 2012), could account for the different features of these two proteins. However, to better understand the function of C12orf65 it needs to be studied in the model that is truly devoid of this protein and would better reflect the changes that are caused by its absence. Further experiments to generate such a cell line could use for example CRISPR/Cas9 system in order to knockout the *C12orf65* gene with high efficiency.

Although the insufficient C12orf65 depletion potentially prevented the anticipated changes to mitochondrial translation and transcription, it did, however, reveal a very important feature of C12orf65. It seems that presumably very low levels of C12orf65 are sufficient to maintain its function. It is also possible that C12orf65 protein is highly stable and even if synthesis of its new molecules is impaired by siRNA, these produced before the treatment are still present and functional. However, considering the former possibility is true it could mean that C12orf65 function is highly specialised and it is involved in rare occurring events. An example of such event would be a very specific type of mitoribosome stalling. Finally, it could also further confirm the possibility of C12orf65 and ICT1 having overlapping functions. Therefore, the deficiency of one factor can be partially recompensed by the activity of the other, preventing the changes to mitochondrial gene expression.

Chapter 4

Molecular analysis of the effect of c.210delA *C12orf65* mutation - patient case

4.1. Introduction

Due to its classification as a mitochondrial release factor family member, my host laboratory was already studying C12orf65 and its role in human mito-protein synthesis. Further focus on C12orf65 and its potential role in mitochondrial protein synthesis was brought by multiple published reports on patients harbouring pathogenic mutations in the encoding gene. One example described the case of two unrelated patients with Leigh syndrome, optic atrophy (loss of optic disc nerve fibres) and ophthalmoplegia (paralysis of the extraocular muscles) that were both the result of a 1 bp deletion in *C12orf65* (Antonicka et al., 2010), causing a frameshift and premature termination. Another group of patients described by Shimazaki and colleagues (H. Shimazaki et al., 2012) displayed a milder phenotype that was dominated by optic atrophy and neuropathy. Impairment of motor functions caused by peripheral neuropathy and spasticity were observed to develop later. In these patients the symptoms were all results of a nonsense mutation (c.394C>T, p.R132X) that produced a truncated form of C12orf65. Since these two patient reports, three other studies have been published that broaden the knowledge of C12orf65 related phenotypes. The first study by Spiegel et al. (Spiegel et al., 2014) described the case of seven patients from two consanguineous families, each carrying a pathogenic *C12orf65* mutation. Affected members of family A (3 males and 1 female) displayed slowly progressing bilateral optic atrophy with variability in visual acuity. They developed gait disturbances, spastic paraparesis and hyper reflexia in the legs. There were no changes in the brain MRI. Patients from family B (one male and two females) showed delayed development that progressed into mild-to-moderate intellectual disability. Patients were diagnosed with severe optic atrophy resulting in blindness. In addition, possibility of peripheral neuropathy was suggested due to progressive spastic paraparesis (lower limb spasticity), limitation in walking and foot deformations. Brain MRI of two of these patients revealed presence of lesions.

In the second study (Tucci et al., 2013) two members of a consanguineous family were diagnosed with slowly progressing axonal neuropathy, bilateral optic atrophy, muscle loss and weakness. These phenotypes were consistent with Charcot-Marie Tooth disease type 6 (CMT6) and were the consequence of c.346delG, p.V116X mutation introducing premature stop codon in *C12orf65*

gene. The last report (Buchert et al., 2013) compares two cases of patients with mild cognitive impairment, spastic paraplegia and feet malformations. As in the case of previous reports, the mutation underlying these phenotypes was c.415C>T, causing a premature stop codon in *C12orf65* gene.

As an addition to the clinical description of patient conditions, three of these reports included molecular characteristics of the phenotypes. The most detailed analysis (Antonicka et al., 2010) investigated steady state levels of mtDNA encoded proteins and RNAs, as well as activity and structure of OXPHOS complexes. The results revealed a decrease in complex IV activity in patients' fibroblasts and severe disruption of complex I, IV and V assembly. There was also a decrease in steady state levels of mitochondrially-encoded proteins as a result of uniformly affected mt-protein synthesis. Similar observations were made in the study by Shimazaki et al. (H. Shimazaki et al., 2012), where a general defect of mitochondrial translation was reported. The activity of complex IV but also complex I were decreased as well as levels of fully assembled complexes I, III and IV. In case of patients with CMT6 phenotype (Tucci et al., 2013), the complex V defect was reported based on disruption of the complex structure and decrease in its activity. The mitochondrial membrane potential in one of the patients was reduced without any change to the morphology of the organelle.

During this project an opportunity arose to analyse samples from a previously uncharacterized patient with a *C12orf65* mutation. The genetic defect in this patient samples was primarily analysed in the Mitochondrial Diagnostic Service, Newcastle. I carried out the analyses to investigate how dysfunction of C12orf65 protein affects patient's mitochondrial homeostasis, especially mitochondrial gene expression. The overarching aim of this investigation was to better understand the function of the protein by characterising the patient's molecular phenotype caused by the *C12orf65* mutation in skin derived fibroblasts.

4.2. Clinical and diagnostic presentation (courtesy of the Mitochondrial NCG Diagnostic Service and associated clinicians)

Patient report (courtesy of Dr. Grainne Gorman):

Presentation

A 45 year old man presented acutely falling at home, with reduced Glasgow coma scale (GCS 6 out of 15). He was found to be in type II respiratory failure and warranted ITU admission and intubation and ventilation. He developed massive hematemesis and required urgent laparotomy and repair of a perforated duodenal ulcer. He was slow to wean from the ventilator and was noted to have difficulty swallowing.

He had a term birth and normal development until aged 2 years at which stage he underwent anaesthetic and surgery for hypospadias. He sustained a perioperative respiratory arrest and was noted to have a visual defect, dysarthria, mild fixed limb spasticity and cognitive developmental delay subsequently. He underwent a tendon lengthening procedure at age 14 years with no untoward sequelae. He was diagnosed with schizoaffective disorder in his second decade of life requiring multiple hospital admissions.

Six months prior to his acute admission, he was noted to have deteriorated physically with shortness of breath on exertion and worsening mobility requiring two sticks to mobilise with the need for a wheelchair for longer distances. His dysarthria had also progressively worsened.

On examination, he had bilateral ptosis, nystagmus and bilateral optic atrophy. He had mild facial muscle weakness, palatal myoclonus, a reduced gag reflex, dysarthria and was unable to protrude his tongue. He had severe muscle wasting of upper and lower limbs with marked distal muscle atrophy. Upper and lower limb reflexes were pathologically brisk. Ankle and plantar reflexes were absent.

He had a protracted hospital stay and remained ventilator dependent via a trachyostomy related to gross disturbance of central respiratory drive compounded by respiratory muscle weakness. Bulbar function remained profoundly poor, necessitating the placement of a percutaneous endoscopic gastrostomy feeding tube.

Initial investigations

Neurophysiological evaluation was consistent with an axonal neuropathy.

Initial neuropathy screen including serum protein electrophoresis, copper, caeruloplasmin, acylcarnitines, carnitine, phytanic acid, very long chain fatty acids, alpha-fetoprotein and urinary organic acids were normal.

MRI of the head showed extensive swelling and abnormal high T2-weighted signal changes centrally within the medulla and dorsal pons (Fig. 4.1). Additional small foci of restricted diffusion were seen within this and the cerebellar hemispheres. Brain MRS showed a lactate peak, with reduced NAA and raised choline in a voxel centred over the brain stem consistent with a diagnosis of Leigh's syndrome.

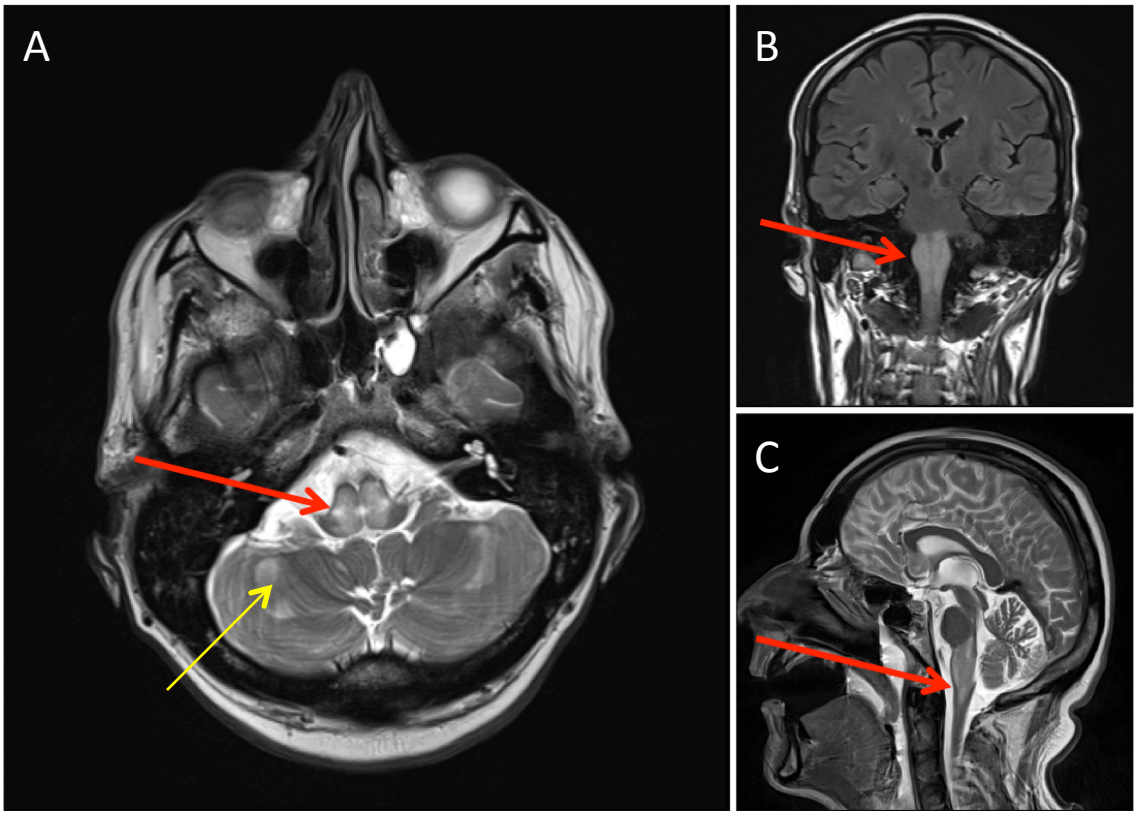

Figure 4.1. Results of the patient's brain MRI

MRI of the head shows extensive swelling and abnormal high T2-weighted signal changes centrally within the dorsal pons (**A**, red arrow) and medulla (**B**, **C** red arrows). Additional small foci of restricted diffusion are seen within this and the cerebellar hemispheres (**A**, yellow arrow).

To investigate the possibility of mitochondrial disease, histochemical and biochemical analyses of patient fibroblasts and skeletal muscle samples were performed in the Mitochondrial NCG Diagnostic Service. The hematoxylin and eosin staining (H&E) revealed normal morphology and integrity of muscle fibers (Fig. 4.2 A). Activity of cytochrome *c* oxidase (COX) was investigated by addition of 3,3'-diaminobenzidine (DAB), which would cause dark brown staining of the cells with functional COX. Lack off the brown staining in patient muscle sample indicates severe complex IV deficiency. Succinate dehydrogenase (SDH) activity was visualized by reduction of nitroblue

tetrazolium (NBT) to blue formazan end product. Sequential double-labeling (COX/SDH) allowed for final identification of cells with dysfunctional COX as these not saturated by DAB and retaining the blue staining. The complex IV deficiency was confirmed by spectrophotometric respiratory chain enzymes activity assays (Fig. 4.2 B). Activity of complex IV was reduced to 20% of control values in muscle samples and to 50% in fibroblasts. The spectrophotometric assay was performed by Dr. Langping He as described in (Kirby et al., 2007).

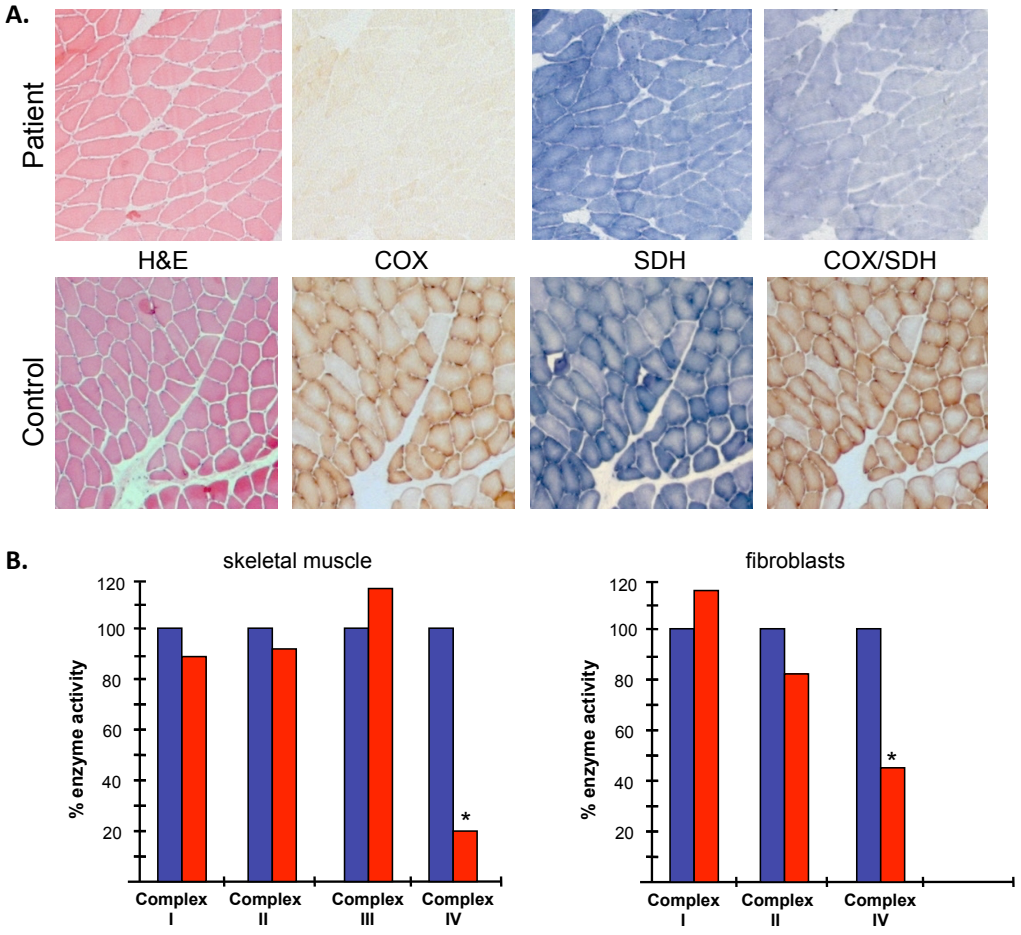

Figure 4.2. Histopathological and biochemical analysis of C12orf65 patient fibroblasts and skeletal muscle reveals complex IV defect

A. Histochemical analysis of cytochrome *c* oxidase (COX) in patient muscle was performed as described in (Old and Johnson, 1989) by Mr. Gavin Falkous. For comparison, a panel of images of control samples from a separate experiment was included. The morphology and integrity of the muscle tissue was determined by hematoxylin and eosin staining (H&E). Cytochrome *c* oxidase (COX) activity was assessed by staining with 3,3'-diaminobenzidine (DAB), whereas the succinate dehydrogenase (SDH) activity was visualized by nitroblue tetrazolium (NBT) staining. Sequential double-staining (COX/SDH) was performed for final assessment of COX activity **B.** Respiratory chain enzyme activity in skeletal muscles and fibroblasts were determined in control (blue) and patient (red). Results, normalised to citrate synthase, were based on three independent measurements and are shown as percent of the control mean value. The significance was assessed based on reference range.

The biochemical analysis of patient muscle and skin samples indicated a disruption in mitochondrial function. In order to identify the genetic origin of the patient's pathogenic phenotype molecular genetic diagnostics were performed. Sequencing of mtDNA excluded depletion, rearrangements, and no point mutations in mtDNA were identified. These experiments were performed in the Mitochondrial Diagnostics Service by Dr. Langping-He, Dr. Emma Watson and Ms. Anna Butterworth respectively. The next step of analysis, sequencing of the *SURF1* gene (the most common cause of Leigh syndrome), was performed in the laboratory of Prof. Garry Brown in Oxford and its results also showed no mutations. Since the genetic cause of the patient's condition was not in mitochondrial DNA, exome capture was performed and the results were analysed in the laboratory of Prof. Patrick Chinnery (Wellcome Trust Centre for Mitochondrial Research, Institute of Genetic Medicine, Newcastle University), to investigate nuclear encoded mitochondrial proteins. The analysis identified a mutation in the *C12orf65* gene as the most likely factor causing the patient's disorder. It was chosen based on the fact that another case was reported with the same genetic defect (Antonicka et al., 2010) resulting in mitochondrial disease. As both patient's parents were unaffected, the pathogenic mutation could only be recessive and the identified *C12orf65* mutation was homozygous which further justified the choice. This left the potentially pathogenic mutation being the one in the *C12orf65* gene. The mutation singled out by exome capture, was confirmed by Sanger sequencing performed by Mrs Charlotte Alston in the Mitochondrial Diagnostics Service (Fig. 4.3).

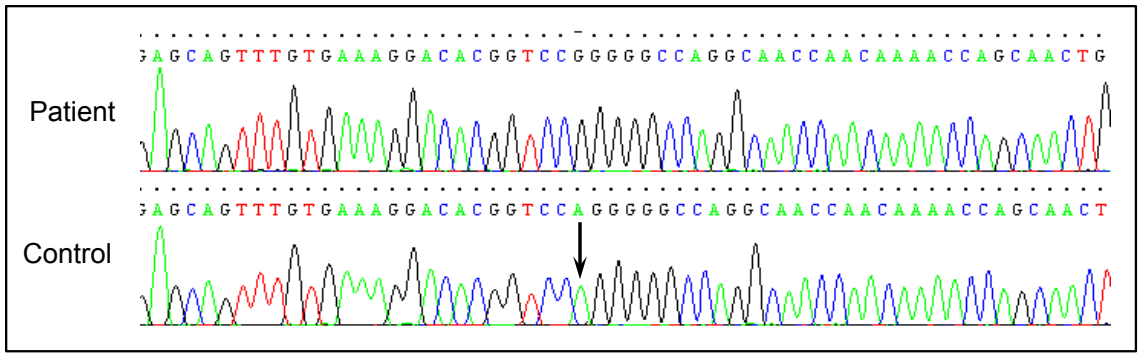

Figure 4.3. Sequence analysis of patient DNA samples

Electropherogram of Sanger sequencing. Sequencing of the *C12orf65* gene was performed for the patient (upper panel) as well as normal controls (example shown in lower panel. The arrow points at the position of the nucleotide (A) in control sample that is deleted from the patient's genome.

The mutation was a deletion of 1 bp in position 210 (c.210delA) resulting in a frameshift and premature stop codon. The first amino acid affected by the frameshift is glycine in position 72 and the stop codon occurs 13 residues downstream from the pathogenic deletion (p.Gly72Alafs*13). The resulting protein would be predicted to be truncated, consisting of only 84 amino acids, not 166 as the full-length form. Additionally this mutation occurs just before the well conserved GGQ motif (highlighted in Fig. 4.4 panel A; described in detail in 1.2.4 and 1.6.2), changing its amino acid sequence to GAR (boxed in Fig. 4.4 B below).

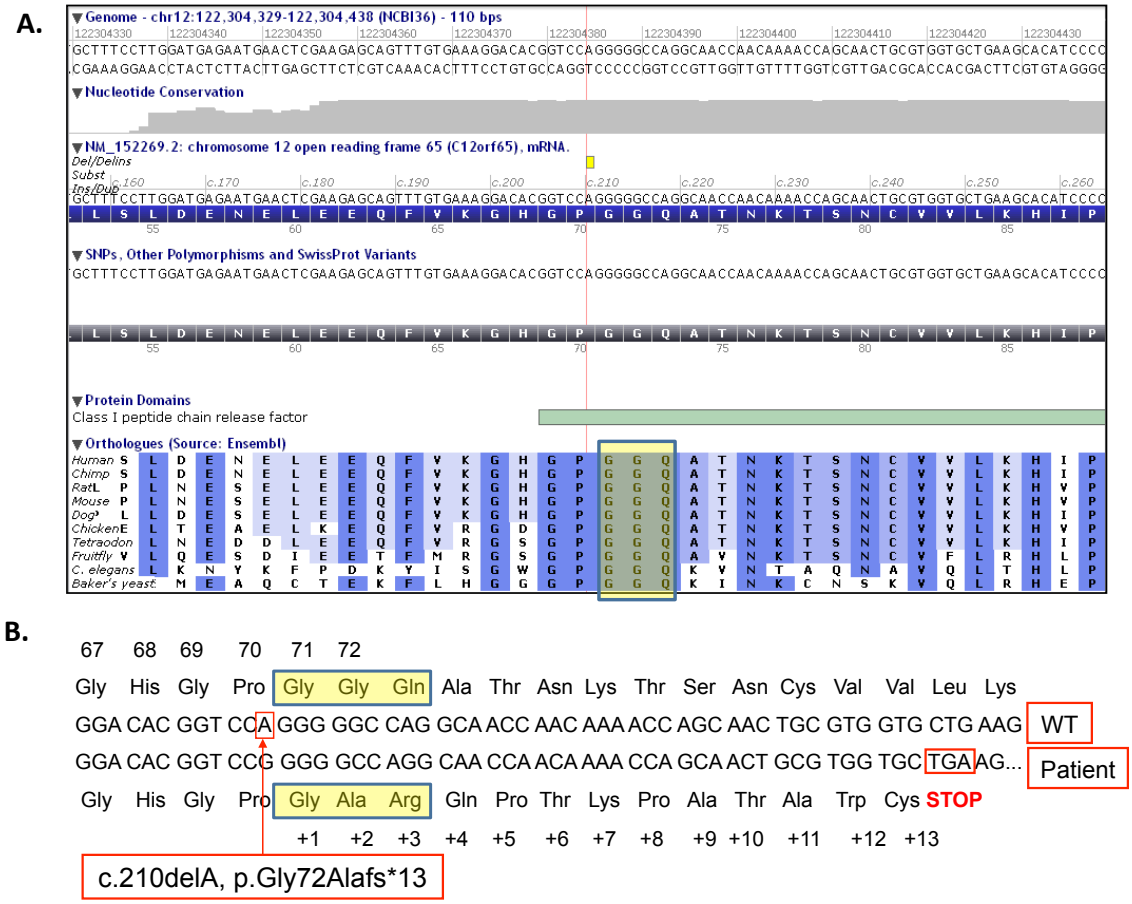

Figure 4.4. Prediction of c.210delA mutation effect on C12orf65 protein

A. Effect of c.210delA on C12orf65 protein predicted by Alamut Visual software. The red line indicates the place of mutation in the genome and resulting protein sequence. Bottom panel represents conserved motifs present in C12orf65 protein sequence, as well as the position of the mutation in relation to putatively functional GGQ motif (highlighted by the yellow box). **B.** Prediction of how the C12orf65 amino acid sequence is affected by c.210delA mutation. The frameshift caused by the deletion changes amino acid composition starting from two residues downstream. The most important functional consequences are highlighted (altered GGQ motif with yellow box, premature stop codon with red). The analisis was perfomed by Mrs. Charlotte Alston in the Mitochondrial Diagnostic Service.

4.3. c.210delA mutation in *C12orf65* causes an OXPHOS defect and impaired growth of patient's fibroblasts in medium containing galactose

For further investigations, patient skin fibroblasts obtained from biopsies were immortalized by the Neuromuscular Biobank, (Institute of Genetic Medicine, Newcastle University by Ms. Mojgan Mohammed Reza). The method of immortalization utilised a retroviral vector encoding the E6/E7 early region gene from HPV and geneticin as a selection agent. This process allows the extended divisions when culturing of fibroblast cell lines, which are required to generate sufficient amount of material for experiments. In addition to the patient, a control skin fibroblast cell line (sample: M08828-12) derived from a non-familial, healthy person was immortalized in parallel. After the immortalization, cells from both patient and control fibroblasts were transported back from the Institute of Genetic Medicine in a 6-well plate to start the selection process. Selection was necessary in order to preserve only those cells that were successfully immortalized. Wells of unimmortalized cells (1 well of each cell line) were also placed in selective media as a control for efficiency of the transfection and to identify when selection process was complete as all the untransfected cell would be dead. The concentration of the selection agent, geneticin was chosen based on the previous experiments by Dr. William C. Wilson. DMEM medium containing 400 µg/ml of geneticin was added to all the cells (un- and immortalized), which were then cultured until all unimmortilized cells died. Throughout the selection process the medium with geneticin was changed every two days. The immortalized cell lines were labelled: "C12orf65-MUT SW/IMM" for the patient (in this study referred to as "patient") and "DC/IMM" for the control (referred to as "Control 1"). Both cell lines were propagated and multiple aliquots were stored in liquid nitrogen for the future experiments.

In order to answer the question of whether the mutation in C12orf65 affects the patient's cell doubling time, growth curves for both cell lines were produced. Parallel experiments were conducted using standard growth medium containing either glucose, or galactose as the only source of carbon (as described in 2.1.3). Galactose-based medium was used to force cells to utilise OXPHOS for ATP production. In these conditions defects of mitochondrial functioning and their effect on cell growth were enhanced causing impaired growth in

comparison to control cells.

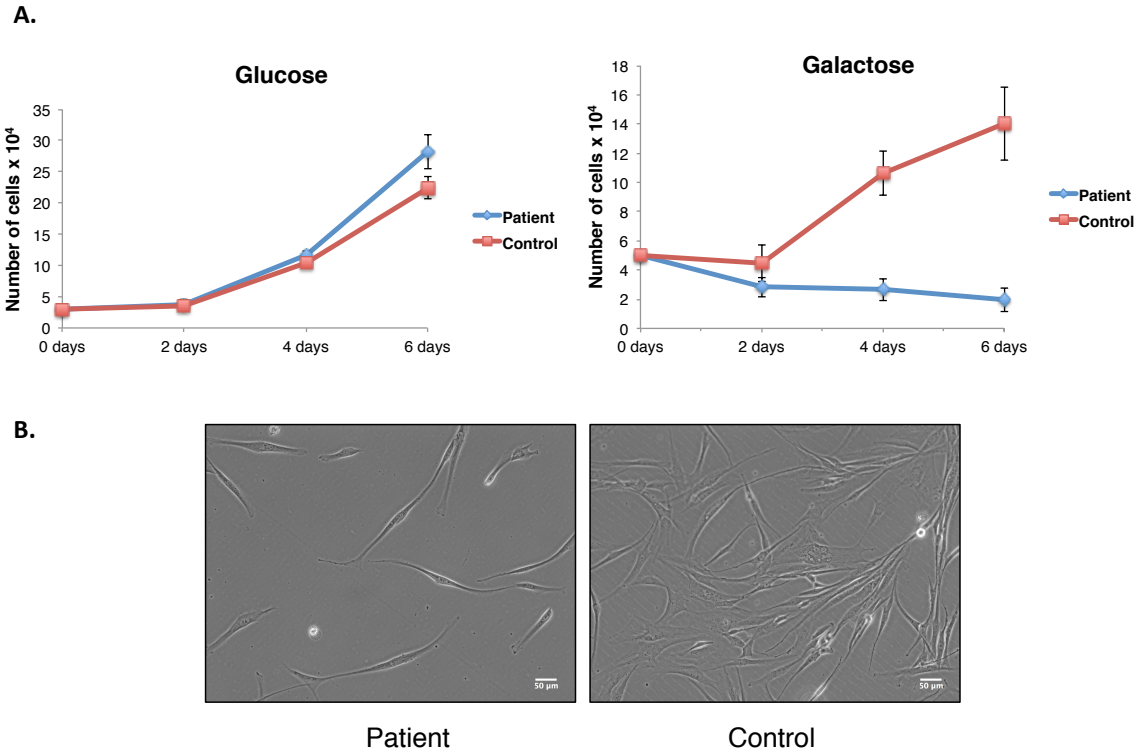

Figure 4.5. Comparison of patient's and control fibroblasts growth on different sources of carbon.

A. Equal number of patient or control fibroblasts were seeded and then counted at the same time points (2, 4 and 6 days) in two different growth media (as described in 2.1.3). Growth curves were produced based on average from 3 experimental repeats.
B. Differences in density and morphology of the patient and control fibroblasts is detectable by bright field light microscopy. Equal number of cells were seeded and the panels presented are after 6 days growth in galactose medium.

When grown in standard, glucose-containing medium both cell lines exhibited similar growth rates. However, when the source of carbon was changed to galactose, the growth of patient cells appeared to be completely inhibited. The number of cells at the last time point was lower than the initially seeded number, suggesting accelerated cell death. These results show that c.210delA mutation in *C12orf65* indeed causes mitochondrial OXPHOS defects and confirms the role of this protein in normal cell functioning.

4.4. c.210delA mutation in *C12orf65* causes disruption of complex I, IV and V assembly

After identification of the mitochondrial defect, further investigation was conducted to characterize more specifically how OXPHOS is affected by the *C12orf65* mutation. BN-PAGE analysis was performed to assess respiratory chain complexes assembly. Mitochondria were isolated from patient and control fibroblasts and solubilised with dodecylmaltoside (as described in 2.5.4). Samples (12.5 µg) were separated on a gel 4.5-16% gradient gel in imidazole-containing buffer under native conditions in order to preserve OXPHOS complexes intact. Western blot analysis then allowed for the detection of the fully and potentially partially assembled respiratory chain complexes using antibodies specific to a single subunit. Any potential disruption of complex formation could be identified as decrease in amount of its subunit or aberrant migration.

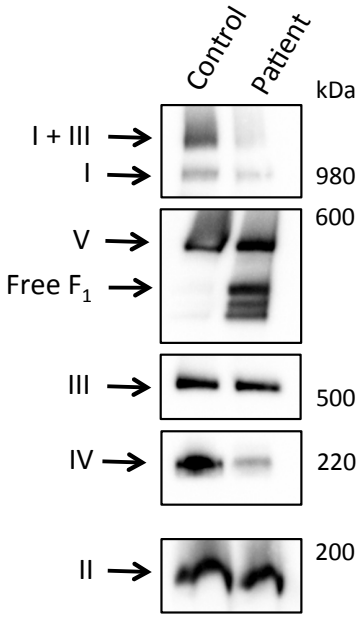

Figure 4.6. BN-PAGE analysis revealed changes in OXPHOS complexes in patient fibroblasts with c.210delA *C12orf65* mutation

Equal amounts of mitochondrial lysate (12.5 µg per lane) from patient and control fibroblasts were loaded on 4.5-16% gradient polyacrylamide BN gel. After transfer, Western blot analysis was used to visualize all OXPHOS complexes with subunit specific antibodies as follows: complex I (NDUFA9), complex III (Core 2) and complex II (SDHA 70 kDa), complex IV (COX4) and complex V (α-subunit).

Results of BN-PAGE analysis showed visible differences in amounts of protein complexes between patient and control samples (Fig. 4.6). The most severely affected complexes are complex I, IV and V. In case of complex I and IV, the

assembly defect manifests itself as lower amounts of proteins. Impaired complex V formation is represented by detection of free F_1 subunits detached from the rest of the complex. There is also a minor defect of complex III, visible also in combination with complex I deficiency, where it results in lower levels of supercomplex I+III. As expected, levels of complex II are not affected as it consists of exclusively nuclear encoded subunits, in comparison to all other OXPHOS complexes that contain components coded by mtDNA. Thus any potential disruptions to mitochondrial gene expression can cause defects in their formation.

4.5. *C12orf65* mutation causes a decrease in steady state levels of complex I and IV subunits.

To further investigate what defects of OXPHOS and mitochondrial function are caused by the *C12orf65* mutation, analysis of the steady state levels of mitochondrial and mitochondrially encoded proteins was performed. Solubilised mitochondria were subjected to SDS-PAGE (2.5.5) and Western blotting (2.5.6) using a panel of antibodies (Fig. 4.7 A and C).

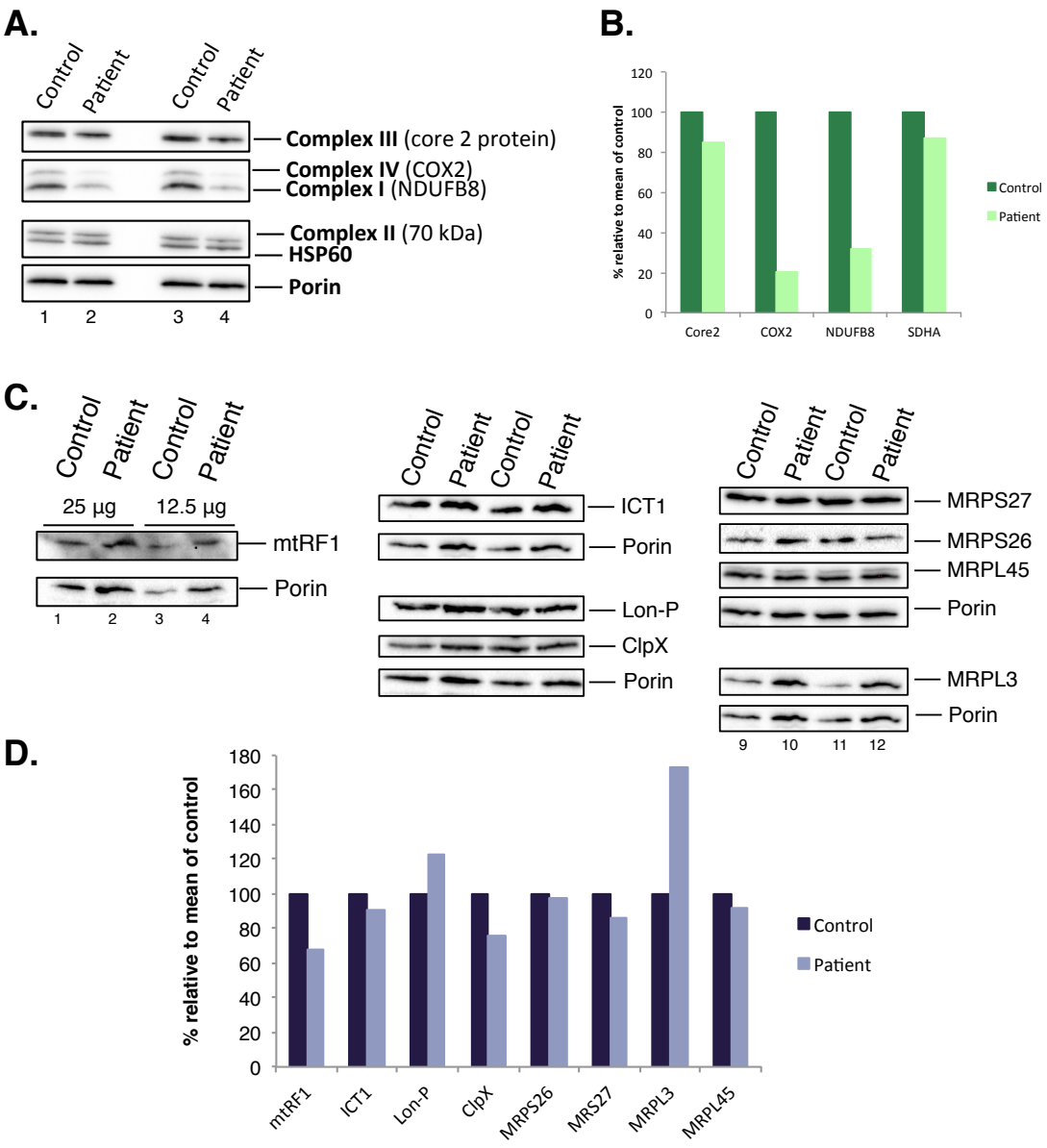

Figure 4.7. Comparison of steady state levels of mitochondrial proteins was assessed in patient and control fibroblasts

Mitochondrial lysates of patient and control fibroblasts (12.5 µg per lane) were separated on 12% SDS-PAGE, each sample was loaded twice as technical repeats (lanes 1 and 3 for control, 2 and 4 for patient) **A.** Levels of subunits of respiratory chain complexes were detected with antibodies specific to nuclear encoded NDUFB8 (complex I), SDHA 70kDa (complex II), Core2 (complex III) and mitochondrially encoded COX2 (complex IV) porin and HSP60 were used as loading controls. **B.** Histograms, were generated from the densitometric measurements of the westerns in panel A. Mean value of the signals from two repeats was calculated for patient and control. Results of patient samples were presented in relation to the signal of the control. **C.** Levels of mitochondrial release factor family members (mtRF1 and ICT1), mitochondrial proteases (Lon-P, ClpX) and mitoribosomal proteins (small subunit: MRPS26 and MRPS27 or large subunit: MRPL3 and MRPL45) were investigated. In each case porin was used as a loading control. **D.** Densitometric measurements of the signal from panel C. were presented as histograms with the mean value of the signal from patient sample represented in relation to the mean signal of the control.

Visual inspection, supported by densitometry analysis (Fig 4.7 B), showed a severe decrease in levels of mitochondrially encoded COX2 (subunit of complex IV), which suggests a disruption in mt-translation in the patient sample. Lower levels of NDUFB8 (complex I subunit) support this observation. Although NDUFB8 is encoded in the nuclear genome, it is incorporated with all mt-encoded subunits into the membrane-anchored part of the complex I (Perales-Clemente et al., 2010) and is sensitive marker of complex I assembly. Thus a decrease in its levels indicates that the levels of mitochondrially encoded subunits could also be reduced. In addition the western blot results showed no significant reduction in levels of nuclear encoded Core 2 (subunit of complex III) or SDHA (70 kDa subunit of complex II). All these results are consistent with the defects of OXPHOS complexes identified during BN-PAGE analysis (Fig. 4.6) with complex I and IV being the most affected and no observed changes to complex II, which is fully encoded by the nuclear genome. These results further support the observation that the decrease in steady state levels of respiratory chain complexes in the patient samples was due to defects of mitochondrially encoded components. The mutation in *C12orf65* was most likely causing disruption in mitochondrial translation but if it was due to the decrease in *de novo* protein synthesis or the increase in the turnover then this could be confirmed by [^{35}S]-Met/Cys metabolic labelling.

In addition to respiratory chain subunits the following groups of mitochondrial proteins were also studied: release factor family, mitochondrial proteases and mitoribosomal proteins (MRPs). The steady state levels of release factor family members were analysed in order to investigate if the mutation of C12orf65 would trigger a potential compensation mechanism. However, patient sample showed no increase in levels of neither mtRF1 nor ICT1 (Fig 4.7 C, quantified in Fig. 4.7 D). On the contrary, there was a moderate decrease in levels of mtRF1. Comparison of the levels of mt-proteases (Lon-P, ClpX) was performed to detect if in the absence of functional C12orf65 there is an increase in protein degradation. Only slight changes in levels of these two proteins were observed (increase of Lon-P signal and decrease of ClpX in patient sample, Fig. 4.7 C and D) suggesting that there is no additional elevation of proteolytic activity caused by C12orf65 mutation. Finally, the steady state levels of MRPs from both small and large ribosomal subunits were investigated. With the exception of MRPL3 which showed an increase in patient samples, there were no

changes between patient and control samples (Fig. 4.7 C and D). These results indicated that the C12orf65 mutation did not affect the mitoribosomal biogenesis or turnover.

4.6. *C12orf65* c.210delA mutation causes a decrease in mitochondrial *de novo* protein synthesis

The observed detrimental effects on the composition and levels of OXPHOS complexes, as well as their subunits described above, suggest that this mutation in C12orf65 may result in a disruption of mitochondrial protein synthesis. This could be caused either by a defect of *de novo* synthesis or by accelerated mt-protein turn over. To investigate this hypothesis, [^{35}S]-methionine/ cysteine metabolic labelling was performed under conditions where cytosolic protein synthesis was inhibited with emetine to facilitate visualisation of only the newly formed 13 mtDNA-encoded polypeptides. The patient and two control cell lines were incubated with [^{35}S]-labelled methionine/cysteine (2.9). Samples from each labelled cell line, containing equal amounts of protein were separated on 15% SDS-PAGE. Signals from radiolabelled newly-synthesised mt-proteins were detected by PhosphoImager and ImageQuant software.

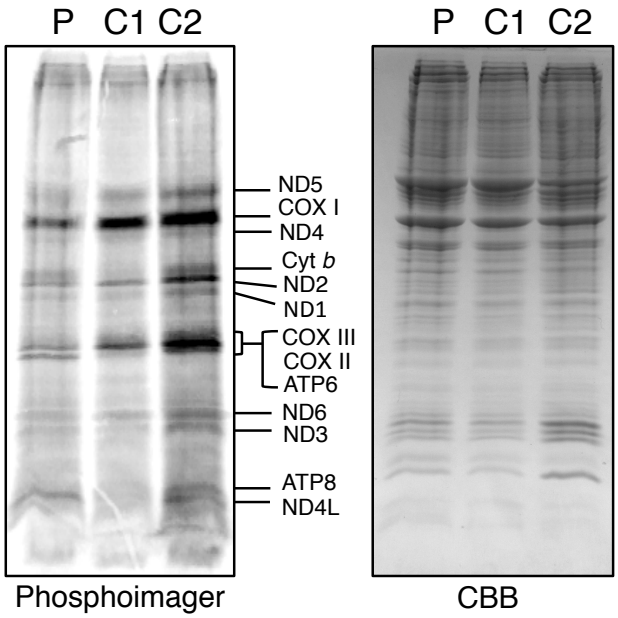

Figure 4.8. Decrease of the *de novo* mitochondrial protein synthesis in patient samples with c.210delA *C12orf65* mutation

patient (P) and two control fibroblast cell lines (C1 and C2) were metabolically labelled with [^{35}S]-methionine/ cysteine with parallel inhibition of cytosolic translation. Equal amounts of radiolabelled samples (50 µg of total cell protein) were separated by 15% SDS-PAGE. Signal from newly synthesised mt-proteins was detected via phosphoImaging (Phosphoimager, left panel). Prior to the imaging, the gel was stained with Coomassie brilliant blue (CBB, right panel) to confirm even loading.

Comparison of the results of the [^{35}S]- methionine/ cysteine metabolic labelling between the patient sample (Fig. 4.8 'P') and control cell lines (C1 and C2) showed the general decrease of the signal in the patient sample. The difference was more profound in comparison with C2 sample. However, this was caused by overloading of the control 2 sample, confirmed based on the Coomassie blue staining of the gel (Fig. 4.8 'CBB'). The decrease of the signal in patient sample was observed for all mitochondrially encoded proteins with exception of COX2/3/ATP6 triad and ATP8/ND4L. In both cases regions of higher signal in the patient sample seemed to be of lower motility than the corresponding areas in control samples. Hence it was impossible to assess whether they were a result of increase in translation or represent truncated/degraded form of polypeptide. The result of [^{35}S]- methionine/ cysteine metabolic labelling suggested that the C12orf65 mutation impairs the *de novo* protein synthesis in mitochondria with a varying effect on different polypeptides.

4.7. The c.210delA mutation in *C12orf65* causes accumulation of mitochondrially encoded transcripts

It is clear that the mutation in C12orf65 causes a defect in translation of mitochondrial proteins but is this an indirect effect with the primary defect being in the transcription of mt-mRNA? In some other contrary cases, inhibition of translation can cause accumulation of transcripts (R. Temperley et al., 2010). To investigate whether changes in the steady state levels mitochondrial transcripts were responsible for the changes in protein synthesis, mt-RNAs were analysed via Northern blot.

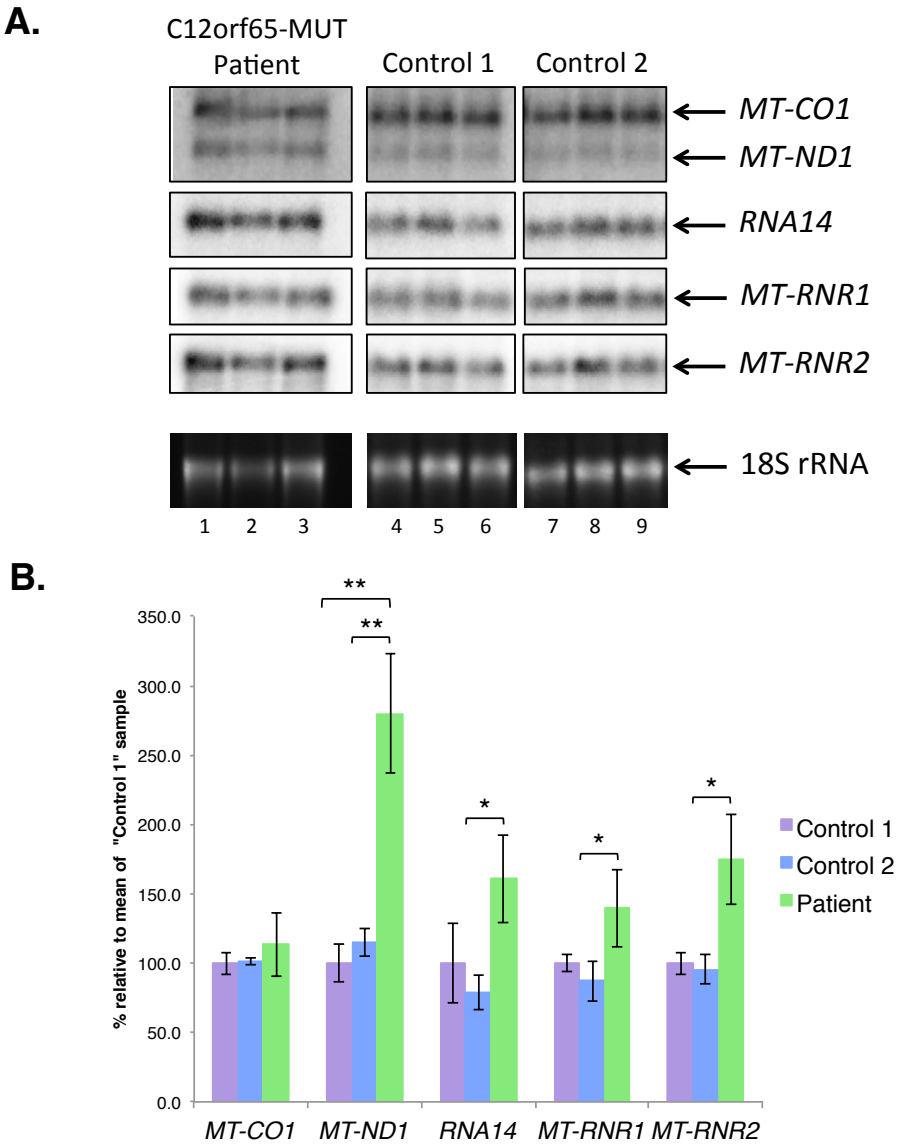

Figure 4.9. Steady state levels of mitochondrial transcripts are altered in C12orf65 patient.

A. Total RNA (4 μg) isolated either from patient or control fibroblasts, was subjected to Northern blot analysis with the indicated probes. The probes were designed to target mitochondrial-encoded transcripts (2.4.2). **B.** Quantification of mt-RNA steady state levels was calculated using ImageQuant software and presented as the percentage of the patient sample. Levels of 18S cytosolic RNA, detected by retained intercalated ethidium bromide on the membrane after transfer, were used as the loading control to normalise intensity of each signal. The graph consists of a mean and standard deviation of three independent experimental repeats (*p <0.05, **p<0.01, ***p<0.001).

Visualisation with probes specific to different mt-transcripts allowed comparison of their amounts between patient and control samples (Fig 4.9 A). After the normalization with 18S as a loading control (signal from the ethidium bromide stained samples visible on the membrane after the transfer), relative amounts of mt-mRNA (*MT-CO1*, *MT-ND1*, *RNA14*) and mt-rRNA (*MT-RNR1*, *MT-RNR2*) were calculated and presented as histograms (Fig 4.9 B). The measurement

of the signals was performed with ImageQuant software which is only a semi-quantitative method but the generated histograms clearly showed the difference between patient's and control's steady state levels of mt-transcripts. In case of mitochondrial messenger RNA, levels of both *MT-ND1* and *RNA14* were elevated in patient sample (2.7x and 1.7x respectively, relative to control 1 levels). However, increase in levels of *MT-CO1* in patient samples was not as profound (1.2x in relation to control 1). Similarly to mRNAs, patient sample showed increase in levels of mitochondrial ribosomal RNAs (1.4x for *MT-RNR1* and 1.7x for *MT-RNR2* in comparison to control 1). These results suggest the accumulation of mitochondrial transcripts in patient fibroblast as the result of *C12orf65* mutation.

4.8. Discussion

Many cases of patients with *C12orf65* mutations have been published so far. Interestingly, these reports show a wide variety of clinical presentations. The common features for most of these patients' phenotypes are optic atrophy often with ophthalmoplegia, peripheral neuropathy accompanied by muscle weakness and spasticity and abnormalities in brain MRI and MRS. The severity of phenotypes ranges from mild to acute but with the predominance of the former. Out of 15 reported cases only one patient died at a young age (Antonicka et al., 2010), the majority of them were diagnosed as adults and were still alive at the time of publication of the reports (Buchert et al., 2013; H. Shimazaki et al., 2012; Spiegel et al., 2014; Tucci et al., 2013).

The characterisation of patient samples in my project clearly indicated that the c.210delA *C12orf65* mutation resulted in an OXPHOS defect. It was manifested by a decrease in cytochrome *c* oxidase (COX) activity in skeletal muscle and skin fibroblasts (Fig. 4.2) and confirmed by impaired growth of fibroblasts on galactose medium (Fig. 4.5). The observed decrease in COX activity was consistent with the defect of complex IV assembly (Fig. 4.6). In addition, BN-PAGE analysis revealed that respiratory chain complexes I, V and, to a lesser extent, complex III were also affected. In case of complex V, immunoblotting detected the presence of free F_1 subunit, which was the result of severe assembly defect (Fig. 4.6). These results were reflected in decreased steady state levels of complex I, III, IV and V subunits (Fig. 4.7 A and B). The reduction

in steady state levels of these proteins was not, however, coupled with an upregulation of mitochondrial proteolytic activity. Levels of mitochondrial proteases ClpX and Lon-P were not changed between the patient and control (Fig. 4.7 C). The C12orf65 mutation had an effect only on the OXPHOS complexes that contain mitochondrially-encoded subunits. Complex II, which is composed entirely of subunits synthesised in cytosol, was not affected. These observations indicated impairment of mt-translation further confirmed by the decrease in *de novo* mitochondrial protein synthesis (Fig. 4.8). However, the reduction in levels of newly synthetises mt-proteins, observed in [^{35}S]-methionine/cysteine metabolic labelling, was not uniform. There was a visible increase in the signal in vicinity of COX3/COX2/ATP6 triplet and ATP8/ND4L. This result could be caused by either upregulation of translation or accumulation of the truncated form of unidentified polypeptide. A similar observation was made during characterisation of the mutation in mitochondrial poly(A) polymerase where the same pattern of differences in *de novo* mt-translation between patient and control was present (Wilson et al., 2014).

The final characterised feature of the patient's phenotype described in this section was accumulation of mitochondrial transcripts (Fig. 4.9). This result suggested a possible compensation mechanism for defects in mt-translation. Another explanation would be a disruption to RNA degradation mechanism. Increase in levels of mt-transcripts in patient sample was observed for both mRNAs and rRNAs. The surplus of the ribosomal RNAs was not coupled with an increase in mitoribosomal biogenesis as the levels of MRPs were not changed (Fig. 4.7 C). Increase in steady state levels of mitochondrial transcripts was also observed by Dr. Pajak due to depletion of C12orf65 via siRNA. The steady state levels of mitoribosomal proteins in that study were also not changed.

The molecular analysis of the patient samples conducted for this project is consistent with the published reports, especially with characterisation of patients from Antonicka et al. study (Antonicka et al., 2010). In this report the mutation in patient 1 is identical with the genetic defect of patient described in my project. Both cases displayed the same defects in assembly of OXPHOS complexes, with complex I, IV and V most severely affected. Also the characteristic detachment of F_1 subunit from complex V is consistent between the two reports, as well as observed in patients reported by Tucci et al. (Tucci et al., 2013).

Number of additional features characterised as a result of C12orf65 mutation in my project were also consistent with published patient reports. For example, decrease in complex IV activity was present in multiple patient cases (Antonicka et al., 2010; H. Shimazaki et al., 2012; Spiegel et al., 2014; Tucci et al., 2013). The increase in steady state level of mt-transcripts was among the effects of C12orf65 mutation in patients characterised in (Antonicka et al., 2010). The results of *de novo* mt-protein synthesis are also consistent between different studies, where mutations in C12orf65 are causing a general decrease in *de novo* mt-translation (Antonicka et al., 2010; H. Shimazaki et al., 2012). The specificity of the C12orf65 mutation effect on mt-translation was confirmed in (Antonicka et al., 2010) by the successful rescue experiment. Overexpression of wild type C12orf65 in patient cell lines resulted in increase in *de novo* translation levels and partial suppression of the other defects.

The most recent publication characterises mutation in C12orf65 as a new cause for Behr syndrome and proposes to re-evaluate classification of the already published cases of C12orf65 mutations (Pyle et al., 2014). However, the unusual clinical presentation of the patient described in my project varies from the definition of Behr syndrome, especially due to lack of early (less than 10 years) onset of optic atrophy.

Results of this study, as well as the published data strongly suggest involvement of C12orf65 in mitochondrial translation. Mutations in C12orf65 are clearly impairing protein synthesis in mitochondria, which is reflected by decrease in *de novo* mt-translation. Resulting deficiencies in mitochondrially-produced proteins could be the reason for the observed disruption in complex assembly, which would then lead to the decrease in their activity. The final outcome is the mitochondrial defect manifested by the range of symptoms from nervous system and skeletal muscles, two of the most energy-demanding tissues. Like in many cases of mitochondrial diseases the consequence of the organellar defect can be tissue specific and despite the clear evidence of a role for C12orf65 in mitochondrial translation, the nature of its involvement is still unknown.

Chapter 5

Mitoribosome profiling - preliminary protocol for use with IonTorrent sequencing

5.1. Introduction

The study of cell lines with depleted or mutated C12orf65 allowed characterisation of the consequent defect but did not yield sufficiently definitive results to explain the function of the protein. The methods used for these experiments were not enough to reveal the role of C12orf65 as a potential ribosome rescue factor. For this purpose, different methodology needed to be used that would provide more insight into the direct interactions of mitoribosomes with mt-mRNA and be sensitive enough to detect changes to ribosome progression after loss of a protein involved in translation. The chosen method that had the potential to answer these questions was ribosome profiling. Ribosome profiling is a relatively new technique for studying translation *in vivo,* combined with high throughput Next Generation Sequencing (NGS). Before this methodology was pioneered, investigation of the levels of gene expression was conducted through assessing the amount of transcribed and translated mRNA by northern/qPCR/microarray and westerns respectively. The development of Next Generation Sequencing contributed to the advancement of this field and provided immeasurable benefits to genomic and transcriptomic analysis. This led to the creation of the RNAseq methodology, which replaced microarrays in assessment of gene expression levels. However, the measurement of transcripts levels is not sufficient to analyse the actual process and levels of translation. To study how much of the generated mRNA is actually being translated it is necessary to focus only on levels of mRNA bound to ribosomes. One of the approaches used to obtain this type of data was polysome profiling. More than just one ribosome can translate a single transcript at the same time creating what are called polysomes (Mašek et al., 2011). The mRNA translated by polysomes can be separated on sucrose gradient based on its differences in density. The method allows to distinguish between fractions of free mRNA and transcripts occupied by one or multiple ribosomes (Arava et al., 2003; Mašek et al., 2011). The number of the ribosomes attached to a given transcript is a reflection of the efficiency of its translation. Polysome profiling can also be linked with variety of the methods to expand the information recovered (Northern, western blotting, qPCR, genome-wide microarrays) (Arava et al., 2003; Kuhn et al., 2001; Mašek et al., 2011). However, this technique is laborious and limited in generating quantitative data and because of difficulties in resolving fractions that contain high amount of ribosomes, therefore

quantitative analysis of translation has always been problematic. In addition, polysome profiling data is unable to determine the exact positions of ribosomes on a transcript (Ingolia, 2014). Positions of ribosomes were historically studied by nuclease protection assay (Steitz, 1969), many data were generated this way, defining the specific sequences occupied by ribosomes. Before development of microarrays and NGS, this method could only be used *in vitro* on one specific sequence of template. For comprehensive analysis of *in vivo* translation another method had to be designed. Ribosome profiling combines the aforementioned techniques, taking the advantages that each of them provides. Nuclease protection allows for determination of sequences occupied by ribosomes, while NGS provides depth and scope of sequence analysis similar to RNAseq. Fragments of mRNA protected by ribosomes from ribonucleolytic cleavage (ribosome footprints, RFs) are deep sequenced and their sequences are then aligned with the genome (Fig. 5.1).

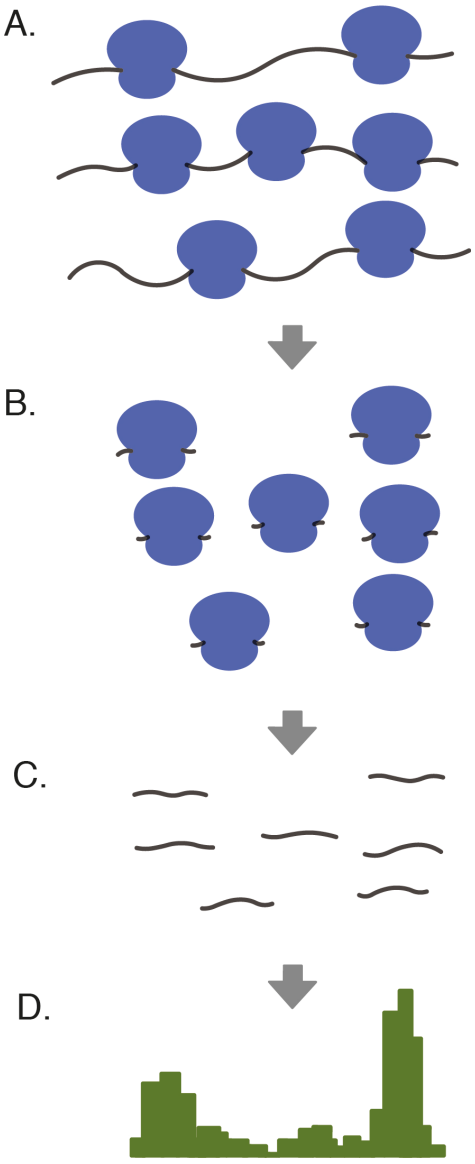

Figure 5.1. Schematic overview of the ribosome profiling principle

Cell lysate (**A**) is treated with ribonuclease, which digests mRNA, leaving fragments protected by translating ribosomes intact (**B**). Pieces of the mRNA protected by ribosomes (**C**) are isolated based on their size (~ 30 nt) and converted into a cDNA library. Deep sequencing of the library and alignment with the reference genome results in ribosome profiles (**D**).

This alignment is presented as histograms of footprint density, which corresponds to ribosome occupancy across each aligned transcript. Analysis of these histograms in combination with RNAseq data enables the intensity of translation and the exact positions of translating ribosomes to be defined.

The first published ribosome profiling experiments were performed in yeast and provided a genome-wide, detailed measurement of translation *in vivo*

(Ingolia et al., 2009). The data generated provided insights into how ribosome densities change in position-specific manner. The resulting ribosome profiles allowed identification of characteristic ribosomal accumulation near the beginning of the transcript. Additionally, the data revealed the previously undetected presence of ribosomes on many short sequences upstream of known CDS. These upstream open reading frames (uORFs), many of which were uncharacterized, initiated from non-AUG codons and so it had previously been presumed that these were not translated. Finally, the ribosome profiling protocol was utilized to define changes in translation efficiency caused by starvation/nutrient deprivation and therefore it aided in characterizing regulatory and compensatory mechanisms invoked during this process. The complete methodology (Ingolia, 2010) included: 1) incubation of the cells with cyclohexamide to inhibit elongation and prevent ribosomes running off during the experiment, 2) treatment of the cell lysate with ribonuclease (RNase One) for the protection assay, 3) separation of ribosomes containing fragments of protected mRNA (ribosome footprints), 4) isolation and size separation of the ribosome footprints (~ 30 nt), 5) conversion of isolated mRNA fragments into dsDNA sequencing library, 6) deep sequencing of the library on an Illumina platform and finally 7) alignment with the yeast genome and bioinformatics analyses to generate ribosome profiles.

Since the first publication in 2009, ribosome profiling is progressively gaining more applications in a growing number of organisms including bacteria (Li et al., 2012), *C. elegans* (Stadler and Fire, 2011) and *D. melanogaster* (Dunn et al., 2013). The first published application in a mammalian genome was carried out on mouse embryonic stem cells (MESCs) by (Ingolia et al., 2011). Modification of the protocol allowed the authors to determine rates of translation elongation (pulse-chase experiments using inhibitory antibiotics) and to identify strong pause sites. This study, together with two others (Lee et al., 2012; Fritsch et al., 2012) revealed many unannotated products of translation from uORFs, sprcRNAs (short polycistronic ribosome-associated coding RNAs) and 5' end of long interspersed non-coding RNAs (lincRNAs) in mammalian cells.

Various applications of ribosome profiling have generated results that have helped to expand knowledge on different aspects of translation. Among many others, ribosome profiling enabled investigation and characterization of different mechanisms of co-translational folding of proteins in bacteria (Oh et al.,

2011) and mammals (Han et al., 2012). The genome-wide study by (Dunn et al., 2013) provided evidence of stop codon readthrough in *Drosophila melanogaster*, a phenomenon also observed in viruses. Investigations of different stress factors revealed a mechanism in which translation is affected in response to protein misfolding (Liu et al., 2013), heat shock (Shalgi et al., 2013) or oxidative stress (Gerashchenko et al., 2012). Ribosome profiling has also been successfully applied to medical purposes to investigate genomics of prostate cancer (Hsieh et al., 2012). It was used to characterize translation regulation of gene expression downstream of the mTOR oncogenic signalling and help to identify translationally controlled mRNAs regulating invasion and metastasis.

The aim of my study was to optimize and apply ribosome profiling to human mitochondria. At the start of my project there were no published data on ribosome profiling in mitochondria so the available protocols required adjustments to accommodate the specifics of organellar translation. In addition, the essential steps that needed very careful optimization were purification of mitochondria and isolation of mitoribosomes protecting mRNAs. The final aspect that needed modification were the generated libraries, which had to be made compatible with IonTorrent^{TM} sequencing as this was the NGS system available in our facility and for a small genome such as the human mtDNA would provide sufficient coverage to give meaningful results. Moreover, IonTorrent sequencing had been previously used for deep sequencing of mitochondrial DNA libraries with success (CLIP experiments by (Hornig-Do et al., 2014). This chapter will provide a detailed description of the methodology I had to develop in order to generate the profiles from the mitoribosome protected fragments. It will also present the preliminary results of deep sequencing.

5.2. Optimization of mitoribosome footprints generation

My initial protocol for mitoribosome profiling was based on the original publication by Ingolia (Ingolia et al., 2009) described later in greater detail in (Ingolia, 2010). Because the aim of this experiment was to capture and analyse fragments of mRNA protected only by mitochondrial, not cytosolic ribosomes, a number of changes to the protocol were considered necessary. The main adjustments included inhibition of mt-translation by chloramphenicol instead

of cyclohexamide, isolation and purification of mitochondria prior to RNase treatment and separation of mitoribosomes via sucrose gradient. The first part of optimization was focused on generating mitoribosomal footprints and investigating efficiency of the chosen protocol. Experiments were performed utilizing wild type HEK293 cell lines. For each mitoribosome profiling experiment 2x 225cm^2 flasks of HEK293 cells (at 80-95% confluence) were used. Prior to isolation of the mitochondria, cells were treated with chloramphenicol (final concentration 5 µg/ml, 1 h, 37°C). Next cells were harvested and the pellets were washed with Dulbecco's A PBS, supplemented with chloramphenicol. Chloramphenicol was present in all the buffers used during generation of ribosome footprints in order to maintain inhibition of translation elongation throughout the whole of the procedure. Mitochondria from chloramphenicol-treated cells were isolated as described in 2.5.2. The only difference was addition of chloramphenicol (50 µg/ml final) to the homogenisation buffer and lack of PMSF. To minimise contamination with cytosolic ribosomes the outer mitochondria membrane was "shaved" by treatment with DNase I and proteinase K (described below). DNase was added to reduce the viscosity of sample that was often observed after the mitochondria isolation. PMSF was omitted, as it would inhibit the activity of proteinase K. For the shaving procedure, mitochondrial pellets were resuspended in 250-300µl of homogenisation buffer (lacking BSA and PMSF) and the protein concentration was estimated by Bradford assay. Subsequently $MgCl_2$ and $CaCl_2$ were added to final concentrations of 10 mM and 1 mM respectively as the presence of Mg^{2+} and Ca^{2+} ions is necessary for DNase activity. For 4 - 5mg of mitochondrial protein 2U of DNase I (AMPD1, SIGMA) was used and incubated for 15 min at room temperature. Proteinase K (Invitrogen) was then added in proportion of 5 µg of enzyme per 1 mg of mitochondrial proteins. After 30 min of incubation on ice, the reaction was quenched by addition of 1 mM PMSF and the sample was centrifuged (11000 g, 5 min, 4°C). Finally the pellet was washed with Homogenisation Buffer (-BSA, +PMSF, 2.5.2) and resuspended in 100 µl of the same buffer. A fraction ($^1/_{10}$) of mitochondrial solution was retained for RNA isolation (to estimate RNA contents in isolated mitochondria), the remaining $^9/_{10}$ was used for membrane lysis. To solubilize mitochondrial membranes, organellar solution was pelleted and, depending on the pellet volume, resuspended in 100-175µl of Lysis Buffer (2.5.2). The sample was

incubated for 30 min at 4°C, with agitation on a rotator and then centrifuged (12000 g, 5 min, 4°C). The supernatant was transferred into a new tube and protein concentration was determined by Bradford assay (2.5.3). The lysate was divided into aliquots of a maximum volume of 100µl, each containing 300-700 µg of proteins. Each part had the same amount of proteins and an equal volume.

The estimation of the RNA concentration in mitochondrial lysate was necessary to determine the amount of ribonuclease to be used in the protection assay. The 10µl of mitochondrial solution left before lysis was resuspended in 500µl of Trizol reagent (Invitrogen), and RNA isolated following manufacturer's instructions. The final pellet was resuspended in 15 µl of DEPC-treated water followed by measurement of the RNA concentration by NanoDrop (Labtech). Based on these results, the amount of RNA in the remaining mitochondrial solution was calculated.

For the ribonuclease protection assay 7U of RNase One (Promega) was used per 100 µg of mitochondrial RNA. Only one aliquot of mitochondrial lysate was treated with RNase, the second was left untreated as a control to compare the effect of the enzyme on ribosome composition. Reactions were performed in the presence of 5 mM EDTA, at 20°C for 10 min (shaking heatblock). The temperature used for this reaction was lower than the optimal 37°C and RNase activity was stopped by loading samples on sucrose gradient.

Separation on an isokinetic 10% to 30% sucrose gradient was performed as in 2.7. After centrifugation, aliquots (100 µl) of the samples were taken from the top (fraction 1, see Fig. 5.2), which partitioned into 11 fractions (volume of fraction 11 was equal to the volume of loaded sample). Samples from each fraction (12 µl with 3 µl of 5x SDS-PAGE loading buffer, 2.5.5) were then analysed via western blot (2.5.6). Immunoblotting of these samples with antibodies for mitoribosome proteins served as indicator of the monosome position within the gradient (Fig. 5.2). The positions of small and large mitoribosomal subunits were detected using DAP3 and MRPL3 antibodies, respectively.

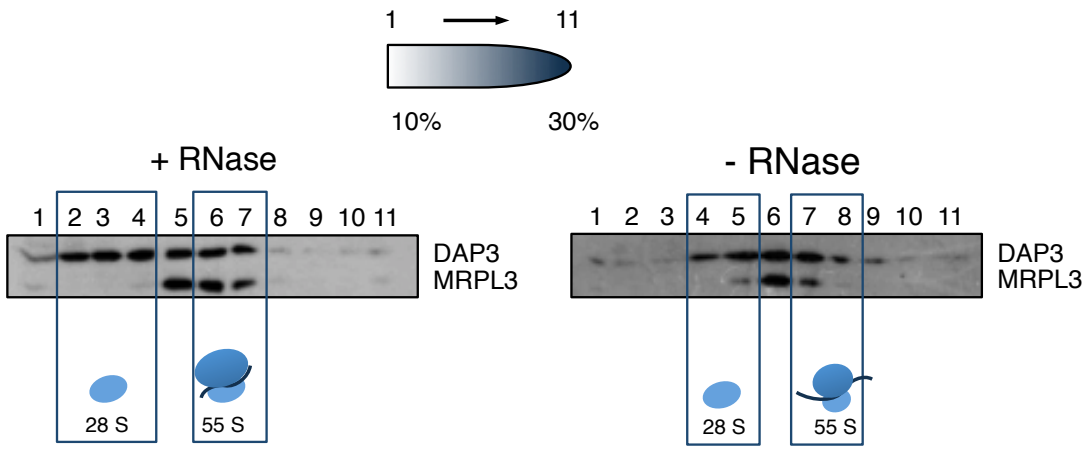

Figure 5.2. Migration profile of mitoribosomal proteins is altered after RNase treatment.

Equal amounts of cell lysate (300 - 700 µl) from HEK293 treated with RNase ("+RNase") or untreated ("-RNase") were separated on isokinetic sucrose gradients (10% - 30%). Western blotting was used to analyse each fraction (12 µl) for the presence of 28S small (DAP3) or 39S large (MRPL3) mitoribosomal subunit. Signals from each antibody indicated which fractions contained monosomes (55S).

Prior to the RNase treatment (Fig. 5.2, sample '-RNase', right panel) the signal from DAP3 antibodies representing the position of small subunit was present in fractions 4 and 5. The fractions containing the 55S monosome were identified as 7 and 8. However, after the RNase digestion ('+RNase' left panel) the positions of the subunits, as detected by antibody probing, shifted towards the less dense fractions of the gradient. The small subunit was identified in fractions 2, 3 and 4 and monosome in fractions 6 – 7. The fraction 5 contains most likely free large subunits. The change in the position of small subunit and monosome was most likely caused by the digestion of mt-mRNA with RNase I. As observed in numerous experiments conducted in my host lab, mitochondrial transcripts are detected in sucrose gradient fractions corresponding to free mitoribosomal subunits as well as the whole monosome. The treatment with RNase would remove the unprotected parts of these mRNAs associated with mitoribosomes (free subunits and monosomes). This action would result in changing the molecular weight (MW) of mitoribosomal subunits and monosomes.

The rest of each gradient fraction (~ 88 µl) was used directly after gradient separation to isolate RNA, using hot acid phenol: chloroform extraction (Ingolia, 2010). This procedure allowed samples to be stored as precipitated in isopropanol. Only fractions that were identified to contain monosomes were processed further. Each of the samples was mixed with SDS (1% final volume)

and heated to 65°C, then mixed with 1 volume of pre-heated (65°C) acid phenol: chloroform solution (5:1, pH 4.5) and incubated at 65°C for 5 min (thermomixer with maximum shaking). Samples were placed on ice for another 5 min then centrifuged (16 000 g, 2 min, 4˚C). The aqueous phase was recovered, mixed with 1 volume of acid phenol: chloroform solution and incubated at room temperature (thermomixer with vigorous shaking). Next, samples were centrifuged (16 000 g, 2 min, 4˚C), the aqueous phase was again recovered and re-extracted by mixing with 1 volume of chloroform: isoamyl alcohol (24:1). After another centrifugation the final aqueous phase was transferred into new tubes and mixed with 2 volumes of 96% ethanol, NaOAc (300 mM final conc) and 2 µl linear acrylamide. At this point samples were stored at -80˚C until the western blot results were obtained that would indicate which fractions contained monosomes. Only these fractions were chosen for the next part of the experiment.

5.3. Optimisation of library preparation

Methodology used to optimize library preparation was based on Ingolia's original protocol (Ingolia et al., 2009) further detailed in (Ingolia, 2010). According to this protocol the first step to create a sequencing library was polyadenylation of the 3'-end of the template. This was necessary to enable reverse transcription with a specific construct that served as a primer (RT primer, labelled "MITOPROF-RT", Fig. 5.3).

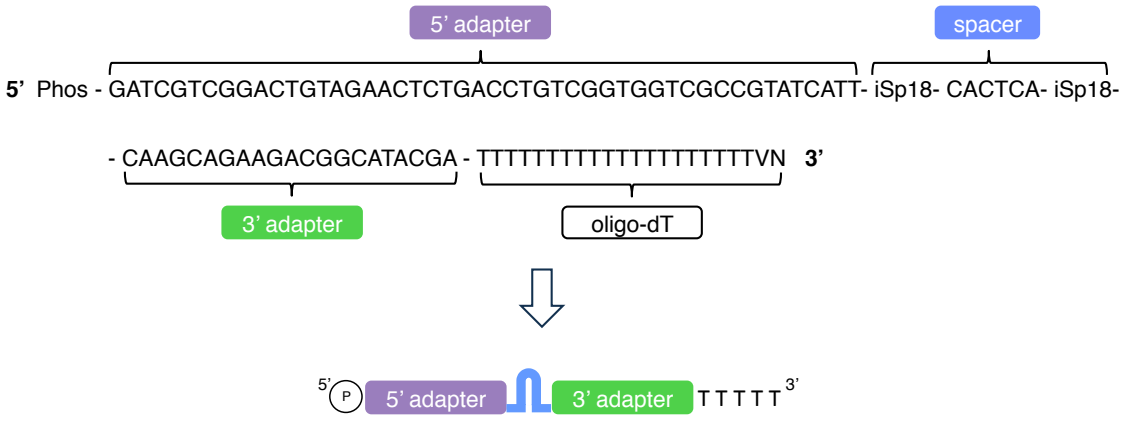

Figure 5.3. Sequence and features of the reverse transcription primer

The RT primer (MITOPROF-RT) sequence was build of 4 parts (each bracketed). The 5' and 3' adapters were separated by a flexible spacer sequence consisting of 2 internal Sp18 modifications (polyethylene glycol) and 6-nt insert. The oligo-dT_{20} tract is added at 3' end of the molecule. V and N stand for degenerate positions corresponding to A/C/ G or A/C/G/ T respectively. The 5' end of the primer was phosphorylated. A simplified overview of the whole primer sequence is depicted below.

The reverse transcription primer contained an oligo-dT stretch of 20 dTs, which would be complementary to the poly(A) tail thus facilitating priming of the construct on the endogenous transcripts. The rest of the primer sequence included adapters for 3' and 5'-end of library products. Both adapters were of defined sequence and served as priming sites for subsequent PCR amplification of cDNA. Between the two adapters there was a 6-nt sequence flanked by two polyethylene glycol modifications (Sp18 spacers). Sp18 spacers were introduced to form a hairpin loop (Durand et al., 1990) that would provide a full block to polymerases (Ingolia, 2010). The phosphorylation of the 5' end facilitated internal ligation (explained in more depth in Fig. 5.4). Trialling this methodology with a synthetic RNA as the initial template is described in detail below.

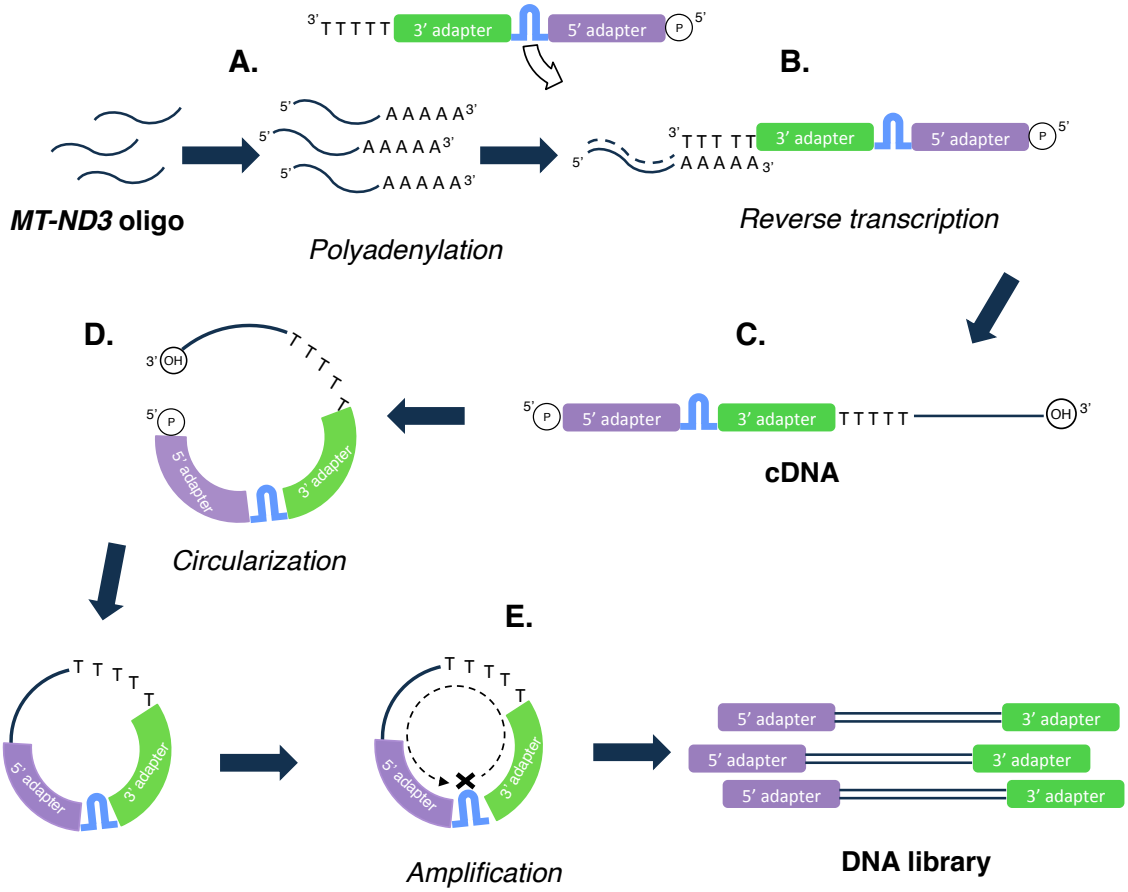

Figure 5.4. Schematic of methodology used to optimize library preparation

A synthetic 40-nt long oligo-RNA (*MT-ND3*) was used as a test template for the sequencing library preparation. *In vitro* polyadenylation (**A**) of the template introduced a priming site for reverse transcription with oligo-dT containing RT primer (**B**). The primer sequence became part of the reverse transcribed cDNA, together with the *MT-ND3* sequence (**C**). In order to connect the 5'-adapter with the template in direct way, the cDNA molecule was circularized (**D**). PCR amplification of the circular cDNA generated double stranded DNA library (**E**).

The principle of this methodology is as follows:

Reverse transcription using the RT (MITOPROF-RT, Fig. 5.3) primer generated a cDNA molecule that contained, starting from the 5' end: 5'-adapter, spacer, 3'-adapter, oligo-dT tract followed by the template fragment (ribosome footprint, Fig. 5.4 C) Next, cDNA strands were circularized by CircLigase ssDNA II enzyme (Epicentre Biotechnology) to link the 5'-end adapter directly with the template and close the molecule (Fig. 5.4 D). The circularised cDNA molecules were then amplified via PCR using primers specific to each adapter sequence. Due to the presence of two internal Sp18 modifications to the 6-nt spacer a stable secondary structure was formed between the adapters (detailed in blue in Fig. 5.3 and 5.4). This structure blocked the progression of the DNA polymerase (Fig. 5.4 E). Thus, linear double stranded PCR products containing only one copy of the template were generated. These products were used as a sequencing library.

As mentioned earlier, I decide to carry out the optimization using a synthetic 40-nucleotide oligo-mt-mRNA (first 40 nucleotides of *MT-ND3* transcript from 5' end), to mimic a ribosome footprint. This oligo-RNA served as a test template for library preparation and was advantageous for optimization of this part of ribosome profiling protocol. This also allowed concurrent optimisation of actual mitoribosome footprint production. Availability of this synthetic oligo allowed for multiple repeats of the optimization experiments, which used the identical starting template and so could give confidence in the reproducibility of the technique. In addition, the possibility to control the initial concentration of the template was also beneficial to this stage of the project, as it permitted identification of the optimal and minimum amount of starting material necessary to successfully generate a library. First, the polyadenylation step was optimized. To do this different concentrations of *E. coli* poly(A) polymerase (PAP) were tested (0.2, 0.5, 1 and 2 U/µl of enzyme solution), different reaction times (5 and 10 min) as well as the equipment (thermomixer and thermocycler). Further, to decrease the volume of the sample, the buffer used was more concentrated than in the original protocol (5x instead of 2x). Optimization of this reaction condition was very important to achieve the desirable poly(A) tail length, which according to (Ingolia, 2010) is between 25 – 35 nucleotides. This amount is long enough to facilitate priming via oligo-dT but the length of the poly(A) tail should

not exceed it. Following the initial experiments, optimal conditions were defined as given:

5x PAP buffer

12.5 µl 10x poly(A) polymerase reaction buffer (NEB)
5 µl 10 mM ATP
1.25 µl SUPERase-In (20 U/ µl, Ambion AM2694)
6.25 µl DEPC H_2O

The 5x PAP buffer was used to dilute the enzyme (original concentration of 5 U/µl) in two steps. First it was diluted to 1 U/µl of enzyme solution (1 U/µl PAP enzyme mix 1, as described below). This dilution was then used in second step to prepare 0.2, 0.5 U/µl of enzyme solution mixes. The original 5 U/µl enzyme concentration was also used to prepare the 2 U/µl of enzyme solution mix. Optimal enzyme concentration was 0.2U/µl (0.2 U/µl PAP enzyme mix 2, prepared as described below).

1 U/µl PAP enzyme mix 1

9 µl DEPC-treated H_2O
3 µl 5x PAP buffer
3 µl *E. coli* poly(A) polymerase (PAP, NEB M0276S)

0.2 U/µl PAP enzyme mix 2

3 µl DEPC-treated H_2O
1 µl 5x PAP buffer
1 µl 1 U/µl enzyme mix 1

In order to denature samples, 1 µl of *MT-ND3* oligo [125 ng/µl] was mixed with 6 µl DEPC-treated H_2O.and incubated for 2 min at 80°C, then placed on ice to cool down. Next, 2 µl of 5x PAP buffer and 1 µl 0.2 U/ µl PAP enzyme mix 2 were added. Reactions were performed in the thermocycler at 37°C for 10 min and stopped by adding 40 µl of 10 mM EDTA. Finally samples were precipitated at -80°C over night, by addition of 110 µl 96% ethanol, 5 µl 3M sodium acetate and 2 µl linear acrylamide.

After precipitation samples were centrifuged for 30 min at 4°C, 16000 g. Pellets were resuspended in 10 µl DEPC-treated H_2O, mixed with 15 µl denaturing loading dye (defined below) and denatured at 55°C for 5 min. In parallel, size marker samples were prepared. 0.5 µl of tRNAs (100 ng/µl, size approximately 70 nt, the same as the desirable polyadenylation product), 1 µl of *MT-ND3* (125 ng/µl stock concentration) and 0.5 µl of ssRNA ladder (NEB, ND364S) were mixed with DEPC-treated H_2O to final volume of 3 µl with 2 µl denaturing loading dye. These samples were denatured at 65°C for 5 min and kept on ice until loaded.

All samples were loaded on 18% denaturing polyacrylamide gel and electrophoresed in 1x TBS buffer (defined below). Afterwards, the gel was stained with SybrGold (Invitrogen, SS-11494) 1:10000 in TBS for 20 min and visualized on a standard UV transilluminator, images were captured by CCD camera.

18% denaturing PAG (15 ml stock solution)

27 g urea
33 ml 30% acrylamide: bisacrylamide (29:1)
5.5 ml 10x TBE

for 10 ml gel:
10 ml stock solution
72 µl 10% APS
16 µl TEMED

10x TBE (1 litre)

108 g Tris base
55 g Boric acid
40 ml 0.5M EDTA (pH 8.0)

Denaturing loading dye (1 ml)

900 µl formamide
100 µl 10x TBE
Bromophenol blue

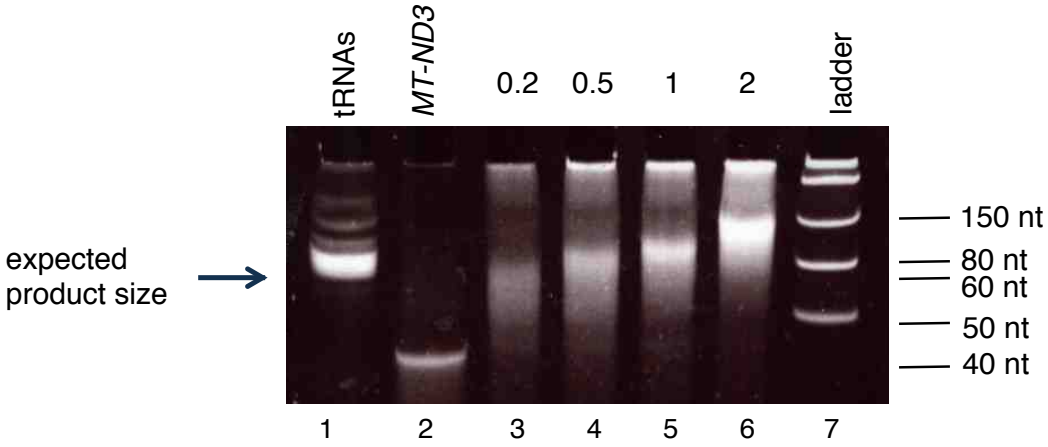

Figure 5.5. *In vitro* polyadenylation conditions were established to obtain optimal poly(A) extension of the ribosome profiling template

A 40-nt long oligo-RNA fragment served as a template for initial optimisation of the *in vitro* polyadenylation assay. Different amounts of enzyme were used in order to obtain a poly(A) tail of the desired length (25- 35 residues). Products of the polyadenylation reactions were separated on 18% denaturing polyacrylamide gels. The expected size of the final product (depicted by the arrow) was approx. 70 nt, with the same anticipated migration as the tRNA mix used as a size marker.

Comparison of product sizes revealed that under the optimal conditions (0.2U/µl of enzyme, 10 min, and reaction in thermocycler), the poly(A) tail length was approximately 30 residues, giving the desirable-sized end product of 70 nt (Fig. 5.5 lane 3). Higher amounts of enzyme caused excessive elongation of the poly(A) tail.

Next step of optimization focused on reverse transcription. *In vitro* polyadenylation assay was performed on *MT-ND3* oligo using the optimal conditions defined above. After precipitation, the RNA pellets were resuspended in in 9µl DEPC-treated H_2O and the entire sample was mixed with: 2.5 µl DEPC H_2O, 1 µl 10 mM dNTP mix, 1 µl 50 mM RT primer "MITOPROF-RT" described earlier. Samples were then denatured at 65˚C for 5 min and put on ice. Next 4 µl 5x First Strand Buffer, 1 µl SUPERase-In, 1 µl 0.1 M DTT and 1 µl SuperScript III reverse transcriptase (200 U/µl; Invitrogen) were added. Reactions were performed at 48˚C for 30 min, and then stopped by adding 2.3 µl 1N NaOH and incubation at 98˚C for 15 min (procedure adapted from (Ingolia, 2010). Reaction products were loaded on 18% polyacrylamide gel (as in previous experiment) to separate the cDNA product from the unextended primer.

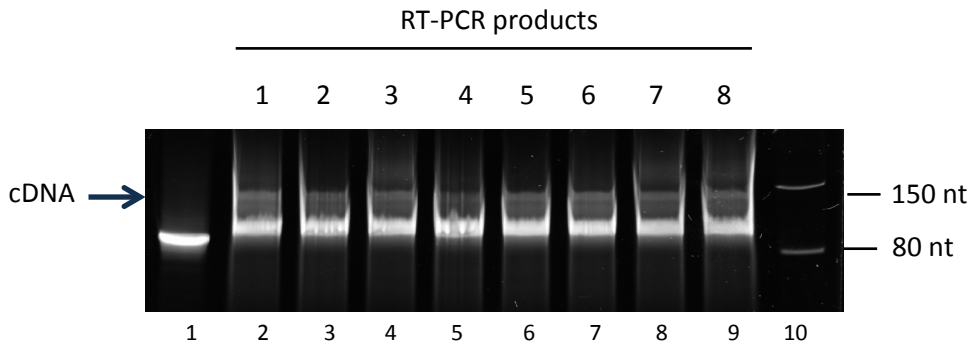

Figure 5.6. Reverse transcription using MITOPROF-RT primer generated correct sized cDNA products

Products of polyadenylation of *MT-ND3* oligo were reverse transcribed (8 identical repeats) using MITOPROF-RT primer. These samples (lanes 2 - 9) were separated by 18% denaturing PAGE. Products of the desirable size (120-140 nt, depicted by the arrow) contained cDNA of *MT-ND3* oligo with incorporated primer. The intense band of ~ 100 nt size corresponds to unincorporated primer. The untreated *MT-ND3* oligo (lane 1) and molecular weight markers were electrophoresed alongside (lane 10)

Bands of ~120-140 nt length (Fig. 5.6) were excised from gels and eluted as follows. Gel pieces, were transferred into 0.5 ml tubes with a hole in the bottom and the tube was put in 1.5 ml microcentrifuge tube. By centrifugation (16 000x g, 2 min, 4˚C), gel pieces were crumbled to facilitate elution. RNA/DNA elution buffer (400 µl, described below) was added to each tube and elution was performed overnight at 4˚C on rotating wheel. After incubation the elution was filtered from gel pieces by centrifugation through glass wool filled tubes (0.5 ml tube with a hole put in 1.5 ml tube) at 2000 g, 2 min, 4˚C. The DNA was precipitated in 2 volumes of 96% ethanol and 2 µl linear acrylamide at -80˚C for 2 h minimum. DNA pelleted after precipitation was resuspended in 12 µl of DEPC-treated H_2O, ready for circularisation as described below.

RNA/DNA elution buffer

300 mM NaOAc pH 5.5

1 mM EDTA

1 µl SUPERase-In (20 U/ µl concentrated) per 400 µl

After the reverse transcription, the following step in optimization of library preparation was cDNA circularisation. It was necessary to internally ligate cDNA in order to introduce adapters on both ends of the target sequence in one reaction instead of two. The resuspended cDNA samples were mixed with: 2 µl 10x CircLigase buffer, 2 µl 50 mM $MnCl_2$, 4 µl 5M betaine, 1 µl CircLigase

ssDNA II enzyme (100 U/µl; Epicentre Biotechnology). Reaction was performed as described below (adapted from (Ingolia, 2010).

Table 5.1. Conditions of circularization reaction

Temperature	Time
60˚C	60 min
80˚C	10 min
4˚C	∞

Circularized cDNA samples were then amplified by PCR reaction with primers specific to the adapters sequences (Table 5.3). For each sample 5x reaction mix was prepared. As different cycle profiles needed to be tested 4 aliquots of mix (16.7 µl each) were prepared in separate tubes. All tubes were placed in thermocycler to perform PCR reaction. It was essential to prevent 'overamplification' of the PCR products, which presented a risk of creating concatamers (Ingolia, 2010). Therefore 4 reactions were prepared and each aliquot was amplified through a different number of cycles (6, 8, 10 and 12). Comparison of the length of the PCR reaction products after different cycle profiles allowed the optimal number of cycles to be identified before undesirable overamplification occurred. In order to do that, at the end of 6th cycle the first of the 4 samples was removed from thermocycler and 4 µl of loading dye was added. The next were removed after the 8th, 10th and 12th cycle. All samples were analysed following electrophoresis on 10% nondenaturing polyacrylamide gels (Fig 5.7).

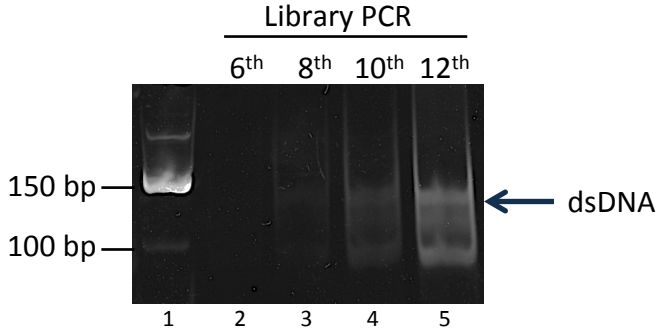

Figure 5.7. Library PCR optimization generated correctly sized products

Circularized cDNA samples were amplified via PCR with primers specific to both adapters. Different amount of reaction cycles were tested (6, 8, 10 and 12) for each of the experimental samples. Image contains results of only one, representative sample amplified in 4 separate reaction terminated after the 6th, 8th, 10th or 12th cycle (lanes 2-5). A molecular marker (lane 1) was included in electrophoresis. The arrow depicts dsDNA product of the expected ~140 bp size.

The expected size of this PCR reaction products was ~140 bp. The band present below the desirable product (~100 bp) contains unamplified cDNA template. The optimal number of PCR cycles was selected for each of the samples (based on the amount of the product). From all aliquots of PCR products only these with the bands of the highest intensity, ~140 bp length and no evidence of overamplification (multiple bands, bigger in size) were chosen. They were captured and eluted from gel as described previously. These purified DNA samples were ready for IonTorrent™ (Invitrogen) library preparation.

Table 5.2. Composition of the library PCR reaction mix

Components	5x reaction mix
nH_2O	57.6 µl
5x Phusion buffer	16.7 µl
10 mM dNTPs	1.7 µl
50 mM LibraryFor primer	0.8 µl
50 mM LibraryRev primer	0.8 µl
Circularized product	0.8 µl
Phusion DNA polymerase (2 U/µl; Finnzymes)	5 µl

Table 5.3. Sequence of library PCR primers

Name	Sequence
LibraryFor	5'-AAT-GAT-ACG-GCG-ACC-ACC-GA-3'
LibraryRev	5'-CAA-GCA-GAA-GAC-GGC-ATA-CGA-3'

10% nondenaturing PAG (55 ml)

5 ml 30% acrylamide: bisacrylamide (29:1)

1.5 ml 10x TBE

8.4 ml H_2O

150 µl 10% APS

15 µl TEMED

Nondenaturing loading dye (1.2 ml)

600 µl glycerol

600 µl 10x TBE

Bromophenol blue

Xylene cyanol

5.4. IonTorrent analysis of ND3 library

In order to complete optimization, the generated library PCR products containing *MT-ND3* fragment were next prepared for IonTorrent™ deep-sequencing. The oligo RNA, which served as a template for these optimization experiments contained part of the sequence of one of actual mitochondrial transcripts. This allowed for the sequenced data to be aligned with the mitochondrial gnome and was predicted to generate a single accumulation of the reads at the beginning of *MT-ND3.* Because the adapter sequences used to generate the library were taken directly from (Ingolia, 2010) where the deep-sequencing was performed on Illumina® platform not IonTorrent™ , amplified PCR products required an additional processing. The IonTorrent™ specific adapters had to be ligated to library products in order to facilitate additional amplification and sequencing. These procedures were planned according to manufacturer's instructions. However, the protocols provided by IonTorrent™ (Ion Plus Fragmented Library Kit) lacked many details of the reaction mixes included in the kits, especially the information on how or if the template needs to be phosphorylated. To solve this problem and maximise the efficiency of the adapter ligation two strategies were used: 1) the library PCR on circular cDNA was repeated using phosphorylated primers and 2) the "end repair" step of the Ion Plus Fragmented Library Kit protocol was included prior to ligation. The end repair step is necessary for libraries generated from fragmented whole genomic DNA, which is a different method than the one used in ribosome profiling. However, it was possible that this step also included the phosphorylation of the template so it was decided to apply it to this library. As a result, two sets of libraries (amplified via un- and phosphorylated primers) containing *MT-ND3* fragment were converted into IonTorrent™ compatible libraries. This allowed for comparison between the two approaches and their efficiency. During the end repair step, library PCR products were resuspended in nuclease-free water to final volume 79 µl, and mixed with 20 µl of 5x end repair buffer and 1 µl End Repair Enzyme. Samples were incubated for 20 min at room temperature. Next the samples were purified using Qiagen Nucleotide Removal (Qiagen, #28304) kit according to the manufacturer's instructions. The purified product was eluted with 35 µl elution buffer and used in ligation step. Reaction was prepared as described in Table 5.4.

Table 5.4. Components of ligation reaction

Components	N=1
DNA (purified PCR products)	35 µl
10x Ligase Buffer	10 µl
Ion P1 Adapter	2 µl
Ion Xpress™ Barcode	2 µl
dNTP mix	2 µl
Nuclease-free Water	39 µl
DNA Ligase	2 µl
Nick repair polymerase	8 µl
Total volume	100 µl

The barcodes were used at this stage of processing in order to enable sequencing of the two libraries (amplified via un- and phosphorylated primers) on one chip. For the "unphosphorylated" sample the Ion Xpress™ Barcode No 6 was used whereas the "phosphorylated" sample was ligated with barcode No 12. Ligation reaction was performed as described in Table 5.5.

Table 5.5. Condition of the ligation reaction

Temperature	Time
25˚C	15 min
72˚C	5 min
4˚C	∞

Products of the ligation were then purified with 400 µl Agencourt® AMPure® XP reagent (4x volume of the sample) according to the Ion Plus Fragment Library kit protocol. Pellets were resuspended in 25 µl of Low TE buffer and the samples were amplified with primers specific to IonTorrent™ adapters, as described in Tables 5.6. and 5.7.

Table 5.6. Components of the amplification reaction

Components	N=1
Platinium® PCR SuperMix High Fidelity	100 µl
Library Amplification Primer Mix	5 µl
Unamplified library	25 µl
Total volume	130 µl

Table 5.7. Condition of the amplification reaction

Stage	Temperature	Time
Hold	95˚C	5 min
9 cycles	95˚C	15 s
	58˚C	15 s
	70˚C	1 min
Hold	4˚C	∞

The amplified libraries were purified using Agencourt® AMPure® XP reagent as described previously. Finally, pure libraries were resuspended in 20 µl of Low TE buffer and kept at -20˚C. The sequencing on IonTorrent™ was performed by Dr. Helen Tuppen according to the manufacturer's instructions.

The alignment of the sequencing results with the reference genome (mtDNA) was performed automatically by the IonTorrent software. The resulting *.bam files were then visualized with an open-access IGV software (http://www.broadinstitute.org/igv, (Thorvaldsdóttir et al., 2013). As the only template used in the sequenced library was a fragment of *MTND*3 transcript (first 40 nt from 5' end), it was expected that all sequencing reads would be grouped at that region of mtDNA. However, the assessment of quality of the sequencing run (a built-in feature of the IonTorrent software) showed that in both samples (with and without phosphorylation of primers) only 4% of the reads were aligned to the mtDNA. The visual analysis of the alignment in the IGV software revealed that these reads were mostly localized to the beginning of *MTND3*. The number of the aligned reads was much lower than expected, especially considering that the library should have consisted of the homogenous population of a single sequence. The possible reason for this result was the presence of the 5' and 3' adapter sequences (from the RT primer "MITOPROF-RT") that are not specific to IonTorrent application. The alignment step has a programmed specified number of the allowed mismatches between the sequencing read and the reference genome. Reads that contain more mismatches than the threshold value are being automatically excluded from the analysis. Having an unknown sequence (adapter sequences "5' adapter" when sequencing from the 5' end of the product or "3' adapter" from the other end, Fig. 5.8 A) preceding the *MTND3* sequence could possibly exceed the allowed mismatches number. As a result, these reads could have been filtered out by the software, even though they contained a fragment of an actual mtDNA

sequence. In order to test this hypothesis the alignment was repeated but this time the mtDNA genome was replaced with the exact sequence of the *MTND3* template with both adapters and poly(A) tract (Fig. 5.8 A labelled as "ND3 construct"). In this setting, the majority of the reads should have been recognized and aligned giving the real representation of the content of the sequencing library.

Figure 5.8. Alignment with predicted library product sequence

Analysis of the sequencing results was performed by alignment to the exact library product sequence. The predicted library product sequence consisted of 4 parts (**A**, ND3 construct), starting from 5' end: 5' adapter, *MT-ND3* oligo fragment, poly(A) tail and 3' adapter. **B.** Screenshot of the alignment results of one of the samples visualized in the IGV software. Red arrow no. 1 depicts the position of the reference sequence and genome coordinates in the application window. Arrow no. 2 points at the histogram with the density of the reads aligning to reference sequence at each position (scale 0 ~ 20000). Arrow no. 3 points at the data track for the "Unphosphorylated" sample that shows each of the aligning reads (grey horizontal bar) with possible mismatches (in colour or black). The data track for the "Phosphorylated" sample is depicted with arrow no. 4. **C.** Information about the quality of the alignment provided by the software. These metrics include data on the total number of aligned base pairs, the average coverage depth of the alignment to the reference sequence and what percentage of all base pairs was aligned.

The visualisation of the alignment in IGV software showed reads covering the whole of the reference sequence. 81% of the reads aligned to the "ND3 construct" sequence, which accounts for 6.4M aligned basepairs and 49344.6X coverage of the reference sequence (Fig. 5.8 C specifications taken from

the run information). The quality of the alignment was similar for both of the samples (Fig. 5.8 B arrow 3, Unphosphorylated; and arrow 4 Phosphorylated), which indicated that the 5' end phosphorylation of the primers was not necessary for the successful preparation of libraries. There are areas where the coverage is more scarce mainly around position 90 bp of the "Phosphorylated" sample (Fig. 5.8.B arrow 4). This was most likely a result of the reads truncation due to the presence of the poly(A) sequence. When the polynucleotide sequence is long (as in case of this construct 20 nt) it is not easy for the system to detect the exact number of residues incorporated and also the quality of reads tends to decrease downstream of the polynucleotide tract. The uncovered space in this alignment was most likely caused by filtering out the reads that were sequenced from the 3' end (indicated by the direction of the arrow at the end of the grey bars) the quality of which dropped after the poly(A) tail sequencing. However, regardless of the issues with the poly(A) presence, the high amount of the successfully aligned reads meant that the library preparation and sequencing methodology optimization was completed and can be used on real mitoribosome footprints.

5.5. Generation of mitoribosome profiles from HEK293 WT cells

After the successful optimization of each step of the ribosome profiling for human mitochondria, I performed the complete protocol on HEK293 wild type cells using methods described in detail in 5.2 for the generation of the ribosomal footprints and 5.3 for library preparation. Mitochondria were isolated from 2x 225 cm^2 confluent flasks of HEK293 that were first treated with the chloramphenicol. After the shaving step with DNase I and Proteinase K, $^9/_{10}$ of the mitochondrial pellet volume was lysed and the protein concentration was estimated by Bradford measurement. The remaining $^1/_{10}$ was used to Isolate and measure RNA concentration to adjust the amount of RNase One for the nuclease protection assay. The total mitochondrial lysate was divided into 4 samples (40 µl of volume, each containing approx. 680 µg of protein and 70 µg RNA). The maximum of protein content loaded on the sucrose gradient was 700 µg, hence the way the lysate was divided. All four samples were treated with RNase One as follows: 1.4 µl of RNase One (7U per reaction), 4 µl of 500 mM EDTA for 10 min at 20ºC in shaking thermoblock. Each sample was loaded on the 10-30 % sucrose gradient. RNA was isolated from each fraction and

those taken for further processing were chosen based on western blotting results with DAP3 and MRPL3 antibodies (Fig 5.9 A). DAP3 as a member of small mitoribosome subunit (SSU) is used as a marker for SSU position on the gradient, and MRPL3 as a marker for the large subunit, LSU. The highest accumulation together of both SSU and LSU marker proteins (fraction 5, 6 and 7) pointed at the most likely position of the monosome and protected mt-mRNA fragments. Also the fraction 4 was included in further experiments, as it appeared to contain a lot of DAP3 and MRPL3. However, this was an unlikely place on a gradient for a monosome and there was a possibility that this fraction contained fragmented subunits rather than an intact 55S.

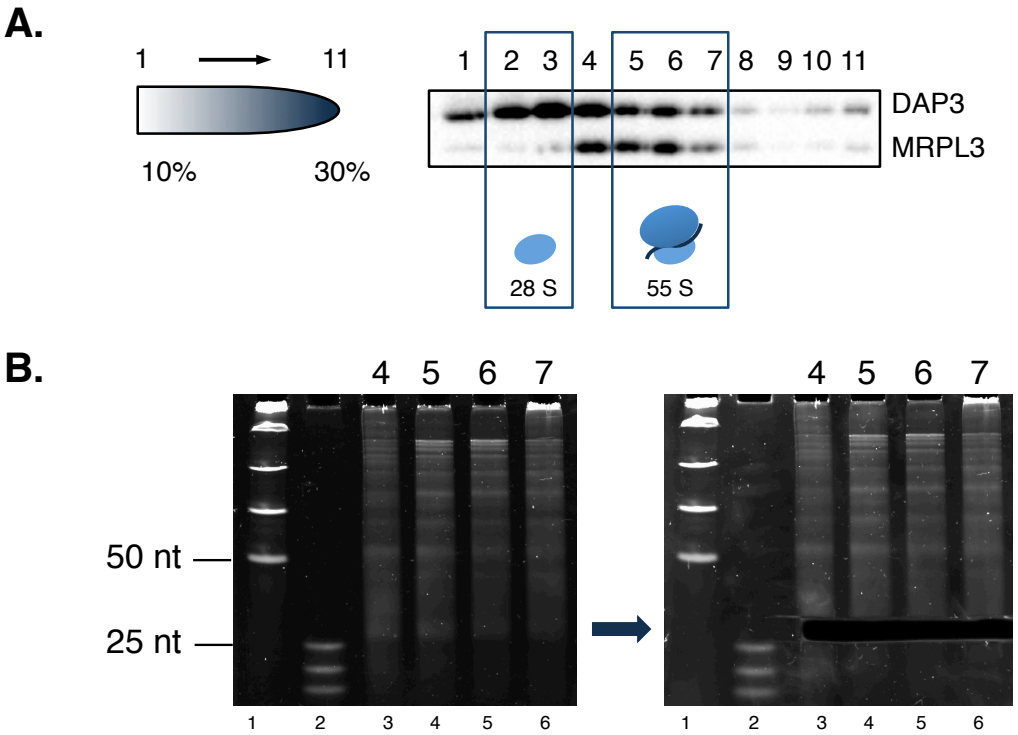

Figure 5.9. Generation and size separation of the mitoribosome footprints from HEK293 WT

The HEK293 mitochondrial lysate was treated with RNase One and ~680 µg separated on each 10-30% sucrose gradient (see 5.2). **A.** Western blot analysis of each fraction was used to confirm the position of the mitoribosomes and their RNA footprints (see 5.2 and Fig. 5.2). Immunostaining with antibodies for mitoribosomal proteins DAP3 and MRPL3 allowed estimation of fractions containing 28S SSU (DAP3) and 55S monosomes (DAP3+MRPL3), both boxed. **B.** Total RNA was isolated from fractions chosen in A) (fractions 4, 5, 6 and 7, as described in 5.2). Size separation of the mitoribosomal footprints was performed by electrophoresis in denaturing 15% PAG with urea (see 5.2). Two molecular ladders were separated together with the samples (low range ssRNA and microRNA, lane 1 and 2 respectively). After the separation RNA fragments corresponding in size to ~30 nt were excised from each sample (left panel, lanes 3-6). The gel after the removal of the fragments is presented in the right panel.

Next, RNA was isolated from the chosen fractions and the RNA pellets were resuspended with 10 µl of DEPC-H_2O. As the result of the prior RNase activity, the isolated RNA species contained a residual phosphate group on the 3' end. The subsequent polyadenylation requires a free 3' end of the molecule, hence 3'-dephosphorylation was required (Ingolia, 2010). As described in (Ingolia, 2010), a polynucleotide kinase (PNK) was used with a buffer devoid of ATP, to force the enzyme to catalyse the removal of the -$(PO)_3$ group from the 3' end of RNA. To each of the RNA samples 10 µl of the PNK reaction mix was added that consisted of: 6.75 µl of DEPC-H_2O, 2 µl 10X PNK buffer without ATP (NEB), 0.25 µl SUPERase-In, 1 µl T4 PNK (10U/ µl, NEB: #M0236). Samples were incubated for 1 hour at 37°C. In order to terminate the reaction and to prepare the samples for the size selection, 30 µl of the denaturing loading dye was added to each of them. The mitoribosomal footprints were separated via electrophoresis on the 18% denaturing PAG (Fig. 5.9 B). Two types of size markers were used (ssRNA low range marker, NEB and microRNA, NEB #N2102) to facilitate accurate selection of the 25~30 nt range of fragments from each sample (Fig. 5.9 B, right panel). Excision and elution of the RNA fragments was performed as described earlier. Purified mixture of RNA that most likely contained mitoribosomal footprints was next polyadenylated and the products of this reaction served directly as the template for the reverse transcription with the RT primer ("MITOPROF-RT").

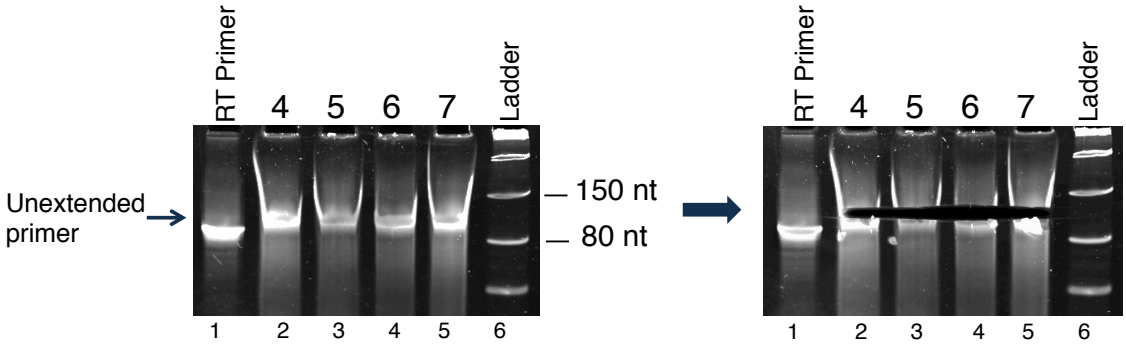

Figure 5.10. Mitoribosome footprints were converted into sequencing library

The generation of the library from the size separated ribosomal footprints was performed as described in 5.3. Products of reverse transcription of the RNA fragments isolated from the picked fractions 4-7 (lanes 2-5) were separated on the 18% denaturing PAGE. RT-Primer (lane 1) and low range ssRNA ladder (lane 6) were electrophoresed alongside. The anticipated-size products (depicted with an arrow) were retrieved from the gel as presented in the right panel.

The results of the reverse transcription (Fig. 5.10 left panel) varied slightly from the ones obtained during optimization step. The space above the primer band was obscured by the intense signal from the un-extended RT primer. It was difficult to definitely state that the reverse transcription was unsuccessful, hence the region of the gel above the primer in all sample lanes was removed (Fig. 5.10 right panel) and the cDNA was extracted as described previously.

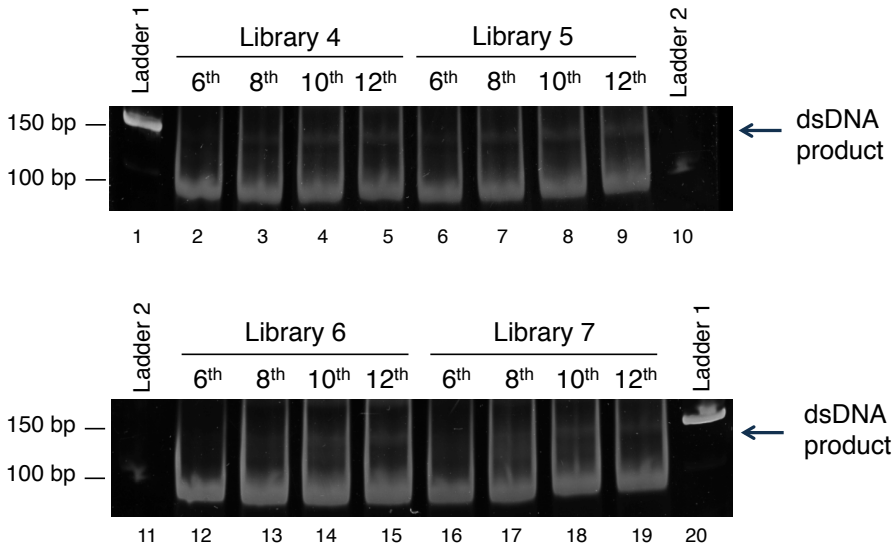

Figure 5.11. Selection of library PCR products based on the size and intensity of a signal

After the circularization, cDNA was amplified in PCR reaction and the double stranded DNA products were separated on the10% non-denaturing PAGE. All 4 samples (amplified for 6, 8, 10 or 12 cycles) from each reaction mix ("Library 4-7") were electrophoresed along the molecular weight markers (lanes 1, 10, 11 and 20).

Next all 4 samples were circularized (as described in 5.3 and Table 5.1). The products of these reactions were immediately amplified according to library PCR protocol (5.3, Tables 5.2 and 5.3). The only change made to the original PCR protocol was to increase of the amount of cycles (maximum 14 cycles instead of 12). It was changed in order to improve the amount of the final product. As during the optimization step, each reaction mix (now labelled "Library 4-7") was divided into 4 samples, each sample was placed in separate tube and amplified for different number of cycles (8, 10, 12 or 14). All 4 samples from each Library were separated on the 10% non-denaturing PAGE together with a size ladder (Fig. 5.11). Conditions of the electrophoresis were as described in 5.3. Amplification of cDNA was successful and resulted in the band of the expected size (about 140 bp depicted by the arrow). The lower-sized band of much greater intensity is the unamplified cDNA template. The very high

level of the template in comparison to the final product suggested that the amplification was weak and was a cause for the concern for quantity of the footprints in the libraries. For further steps of the procedure only the clearly visible bands of ~ 140 bp were chosen (Fig. 5.11, sample 8th, 10th and 12th from Library 4 and 5, sample 10th and 12th from Library 6 and 7, corresponding to lanes 3, 4, 5, 7, 8, 9, 14, 15, 18 and 19). Samples of DNA from one Library were pooled together and relabelled as 4 - 7. Next, the IonTorrent adapters were ligated to the purified samples. The conditions and components of the ligation were as described in 5.4 (detailed in Table 5.4. and 5.5). However, because of the low concentration of the template DNA (less than 5 ng/ µl) the Ion Xpress^{TM} Barcode adapters were diluted 1:9. Barcodes 4-7 were used and were assigned to the sample based on corresponding sample number (for sample 4 the barcode no. 4 was used and so on). Next the barcoded libraries were purified (as described in 5.4) using 400 µl of Agencourt AMPure reagent. After the purification, samples were amplified (conditions and reaction mix as described in Tables 5.6 and 5.7 but the number of PCR cycles was increased to 10 and purified one more time (5.4). Final products were kept at -20ºC until sequencing on IonTorrent (performed by dr. Helen Tuppen). All 4 samples were analysed in the same sequencing run and the results were aligned to mtDNA sequence by the IonTorrent software. Unfortunately, the results of the alignment, when viewed in IGV, showed very low number of reads aligning to the reference genome. This observation was consistent to all 4 samples. Therefore, the data was not sufficient for any down stream analysis. However, given the previous difficulties with sequencing of the "ND3 construct" this was most likely caused by the lack of recognition by IonTorrent software of the Illumina-compatible adapters (parts of RT primer " MITOPROF-RT"). In order to bypass the software's built-in filters the analysis had to be performed manually. This was performed by Dr Matthew Bashton from the Bioinformatics Support Unit. The raw sequencing data was first processed with homerTools software (http://homer.salk.edu/homer/ngs/homerTools.html) to remove the adapter sequences from both ends. Next, the poly(A) stretches were removed and the remaining sequences were aligned with the mtDNA using bowtie2 (http://bowtie-bio.sourceforge.net/bowtie2/index.shtml). Unfortunately, inspection of the data in IGV showed only very short sequences (4-5 bp) aligning to the genome. These results meant that the library products did not contain the expected-

sized products (30 bp). Finally, this was a confirmation that the preparation of the mitoribosome footprints had not resulted in the sufficient amount of material to produce a functional library and later, a mitoribosome profile.

5.6. Discussion

At the beginning of this project there was no published evidence of the application of the ribosome profiling in mitochondria. The original published protocols (Ingolia, 2010; Ingolia et al., 2012) described the use of this technique for studying cytosolic ribosomes only, hence the necessity to optimize the methodology to human mitoribosomes. The other principle of adjusting the pre-existing protocols was to change the sequencing platform from Illumina to IonTorrent. Although the IonTorrent is characterized by much lower throughput than the Illumina platform (10 Mb for 314 chip as opposed to 1500 Mb in MiSeq, Illumina benchtop sequencer(Loman et al., 2012), it would have been sufficient for the sequencing of a genome as small as the human mtDNA. The success of this approach was, however, dependent on reduction of the contamination with cytosolic ribosomal footprints. In that case even with low amount of reads, the majority of them would be derived from mitoribosomes and would form a complete ribosomal profile. In order to achieve that it was decided to isolate mitochondria prior to the RNase treatment.

Despite the promising results of the trial sequencing with *MT-ND3* fragment, the final experiment using the complete protocol did not yield sufficient amount of data to form mitoribosome profiles. It was most likely caused by too low an input of the ribosome footprints. This hypothesis is consistent with the observed low amounts of cDNA produced after reverse transcription (Fig. 5.10 A) and amplification (Fig. 5.11), which was not seen during the optimisation step (Fig. 5.6 and 5.7). It is important to note that when the library preparation methodology was optimized, the concentration of the initial RNA template (fragment of the *MT-ND3* transcript) was known and corresponded to the required amount described in (Ingolia, 2010). However, when the actual mitoribosome footprints were used the concentration of the initial template was unknown because the measurement step was omitted in order not to lose any of the material. The isolation of the mitoribosomes from the sucrose gradient is a crucial step, but it limits the size of the initial pool of mitoribosome footprints. The quality of the generated library depends on the correct digestion of the

mRNA and efficient isolation of the intact monosomes with protected mRNA fragments. The digested mitochondrial lysate separated on the sucrose gradient showed a shift in position of mitoribosomal subunits and monosomes in comparison to untreated samples (Fig. 5.2 and 5.9). A strong signal from the mt-SSU was detected, starting in fraction 2 after the RNase treatment, whereas in undigested sample it was fraction 4. Also the signal from mt-LSU was present in earlier fractions due to the enzymatic digestion, but there was only a '1 fraction' shift towards the top of the gradient. The change in the position of mitoribosomal could be explained by the activity of the RNase 1. The average molecular weight (MW) of mt-mRNAs could be estimated at approximately 0.5 MDa. The difference in MW between the SSU and LSU is also approximately 0.5 MDa, which results in the change of 1-2 fractions in position on a gradient (Fig. 5.2). Therefore, the shift in the position of where the mt-SSU and monosome were observed after the RNase digestion (2 fractions for SSU, 1 for monosome) was consistent with the loss of unprotected mt-mRNA. A difference in how big this shift was between mt-SSU and mt-LSU/monosome could be explained by a difference in ability to protect the transcript from the RNase. It is possible that, when bound with small mitoribosomal subunit, mRNA is more exposed than if associated with the LSU/ monosome and therefore more susceptible to the RNase activity. The evidence presented suggests that the RNase treatment was successful and resulted in removal of unprotected mRNA. However, the possibility of overdigestion cannot be completely excluded. Signal from the mt-SSU protein DAP3 was also present in the first fraction, although weaker than in the following ones. This signal represents free DAP3 proteins and could be interpreted as a result of disruption of the mitoribosome due to excessive RNase activity. The digestion with RNase requires further work, which should include investigation of the effect on mitoribosome composition over different time points. Comparison of the mitoribosomal subunits' migration would allow to select optimal conditions for the digestion that accomplish the removal of the mRNA without causing damage to the structure of the mitoribosome.

In order to continue the use of IonTorrent for deep sequencing, it would be advised to redesign the MITOPROF-RT primer so that it would contain the adapters suitable for sequencing with this platform. This would simplify the preparation of the library and ensure that the reads would not be discarded

by the software. The manual alignment of the data would provide an additional confirmation that viable sequencing reads are not being filtered out and discarded by the automated analysis pipeline.

Chapter 6

Mitoribosome profiling - Illumina protocol (collaboration with NKI, Amsterdam)

6.1. Introduction

My first attempt to optimize the ribosome profiling protocol for the application in mitochondria did not yield sufficiently satisfying results. Thus, proceeding with this project required a completely new approach and re-evaluating the principals of the chosen methodology. The acquisition of data that corresponded to ribosome profiling in mitochondria by a group based at the Netherlands Cancer Institute in Amsterdam gave the opportunity to start a collaboration to successfully establish the technique in Newcastle. The group was a part of Division of Gene Regulation led by Prof. Reuven Agami and their results were later published as the first ribosome profiling application in mitochondria (Rooijers et al., 2013). The publication contained a description of methodology used to generate and analyse mitoribosome footprints, as well as the general characterisation of the mitoribosome profiles. The major difference observed by (Rooijers et al., 2013) between the mitochondrial and cytosolic ribosomes footprints was the size. Mitoribosomes generated two populations of footprints of 27 and 33 nt in size, both of which were distributed in the same way across the transcripts and showed no differences in periodicity. Based on these two features it was concluded that both sizes of footprints were indeed generated by mitoribosomes and were not artefactual. To test the efficiency of this method the authors compared the mitoribosome profiles of the cells containing a homoplasmic mutation in mitochondrial $tRNA^{Trp}$ (m.5556G4A) relative to controls. The cell line harbouring the mutation was a transmitochondrial cybrid that was created by the transfer of mitochondria from a patient's fibroblasts carrying the mentioned $tRNA^{Trp}$ mutation into donor osteosarcoma cells devoid of their endogenous mtDNA (Smits et al., 2010a). Decrease in levels of aminoacylated-mt-$tRNA^{Trp}$, resulting from the destabilizing mutation was predicted to cause the stalling of mitoribosomes when translating tryptophan codons. Profiles of mitochondrial ribosome distribution in the mutant cell line were compared with control human osteosarcoma cells (143B). Results showed intensive stalling of mitoribosomes localized to tryptophan codons (represented by an increase in mitoribosome accumulation) due to reduction in $tRNA^{Trp}$ levels.

The basis of the collaboration with Prof. Agami's group was to apply their ribosome profiling protocol to analyse one of the cell lines generated in my host group. The cell line, called T1V1, was a *trans*-mitochondrial cybrid cell line

with homoplasmic point mutation in mt-tRNA^{Val} gene (1624C>T *MTTV*), which was transformed to inducibly express mitochondrial valyl-tRNA synthetase (VARS2) (Rorbach et al., 2008b). Mitochondria carrying the 1624C>T mutation were derived from a patient sample, where the biochemical phenotype included low activity of complex I and IV in skeletal and cardiac muscle (McFarland et al., 2002). The uninduced T1V1 cybrids displayed reduced level of mt-tRNA^{Val} that was a result of an accelerated degradation of the uncharged tRNA^{Val} form. Overexpression of VARS2L partially restored the level of mt-tRNA^{Val}. However, the trans-mitochondrial cybrids analysed in that study did not reflect the same severe biochemical defect as characterized patient skeletal muscles. In order to study cybrids with a phenotype more comparable to the patient's a new selection process was performed (Hornig-Do et al., 2014). Impaired growth on galactose containing medium was chosen as indicator of the defect in respiratory function and served to identify more suitable cybrid clones. As described above, the selected cell lines were transformed with VARS2 gene and their mitochondrial function was investigated between un- and induced cells. Induction of VARS2 expression resulted in an increase in activity and levels of fully-assembled complex I and IV. In addition an overall increase in levels of *de novo* mt-translation was observed. These data suggested that indeed the VARS2 expression resulted in partial recovery of the mitochondrial defect caused by mt-tRNA^{Val} mutation. The ability to induce the rescue of this T1V1 cell line phenotype was the reason for choosing it to conduct the first ribosome profiling experiments. Low levels of mt-tRNA^{Val} in uninduced cells were expected to cause the stalling of the mitoribosomes on valine codons, similar to the observed stalling on tryptophan codons in (Rooijers et al., 2013). The rescue due to the overexpression of the valyl-tRNA synthetase was predicted to alleviate this effect and confirm that the mitoribosome stalling was caused by mt-tRNA^{Val} deficiency.

Changes to ribosome speed of translation are widely studied and the advantages provided by ribosome profiling contributed to expanding the knowledge about this phenomenon. Application of the ribosome profiling in different organisms and detailed analysis of the ribosome distribution allowed identifying different mechanisms that regulate the rate of their movement. The methods used for identification of the elongation speed involves detection of the shifts in ribosome densities where the increase in the ribosome footprint is

associated with lower speed (Ingolia, 2014). The elongation speed varies across the transcripts and its measurement is a source of valuable information about the translation process *in vivo*. By comparison between the regions of high and low ribosome density or investigating ribosome profiles from different conditions numerous factors that cause these changes were identified. The general tendency for the ribosomes to slow down at first 30-40 codons downstream from the initiation site was observed in yeast (Ingolia et al., 2009). The slowing of ribosome elongation was also shown to facilitate the mechanics of the protein synthesis. In *C. elegans* the wobble codon positions were reported to cause ribosomal pausing (Stadler and Fire, 2011). In mammalian cells the decrease in elongation rate was observed as a consequence of co-translational folding of the nascent polypeptide (Han et al., 2012). Certain features of mRNA were proven to be affecting the speed of translation based on the ribosome profiling data. These included local folding of mRNA in mouse embryonic stem cells (Dana and Tuller, 2012) and Shine-Dalgarno-like sequences in bacterial genome (Li et al., 2012). Also the qualities of the nascent polypeptide chain, specifically positively charged residues, were identified as a cause for slowing of the ribosomes (Charneski and Hurst, 2013; Dana and Tuller, 2012). Different stress conditions were also shown to induce changes in ribosome progression. The heat shock (Shalgi et al., 2013), oxidative stress (Gerashchenko et al., 2012) and the accumulation of misfolded proteins (Liu et al., 2013) were reported to result in a characteristic ribosome arrest in the first 50 nt downstream from the start codon.

The following part of my project was aimed at learning the mitochondria-targeted ribosome profiling protocol from Prof. Agami's group by applying it to a cell line with a specific defect in mt-translation. The data analysis on the generated ribosome profiles was planned to identify the regions with accumulation of mitoribosomes and linked them with mt-tRNA^{Val} deficiency.

6.2. Generation of mitoribosome footprints from T1V1 cell line

As a part of collaboration with Prof. Agami's group I spent 3 weeks in Division of Gene Regulation, NKI in Amsterdam in order to learn the ribosome profiling protocol optimized for mitochondria. One of the fundamental differences between this protocol and the one I previously used (optimized for IonTorrent^{TM}, described in chapter 5) is the approach to generation of mitoribosome

footprints. This protocol does not require isolation of the mitochondria prior to the lysis and RNase treatment. Instead, the total cell lysate is subjected to RNase digestion and then separated on the sucrose gradient to enrich for mitoribosomes. As a result, the volume of the loaded samples exceeds the capacity of the gradients generally used in our lab. For this application a much bigger volume and also a different composition of the gradient was used. The gradient was prepared from two sucrose solutions (7% and 47%) in a buffer containing 20 mM Tris-HCl pH 7.8, 10 mM $MgCl_2$, and 100 mM KCl. The buffer was additionally supplemented with chloramphenicol (final concentration 100 µg/ml) and DTT (final concentration 2 mM). The solutions were combined in different proportions to give 5 different sucrose concentrations (Table 6.1). Each solution (2.3 ml) was carefully layered into the centrifuge tube without mixing, starting from the most dense and successively adding less concentrated sucrose solutions on top. Tubes were left overnight at 4ºC prior to the experiment to allow diffusing of the layers, which creates a linear sucrose gradient.

Table 6.1. Sucrose gradient preparation

Final concentration	7% sucrose (ml)	47% sucrose (ml)
7%	12	0
17%	8	4
27%	6	6
37%	4	8
47%	0	12

The T1V1 cell line and the control 143B parental cultured in 225 cm^2 flasks (see 2.1.1) were seeded in 15 cm dishes (5 for ribosome profiling and 1 for parallel RNAseq analysis per condition). Three days prior to the experiment, expression of VARS2L was induced by addition of tetracycline (final concentration 1 µg/ml) to cells from 1 set of dishes. The second set of T1V1 cells, as well as the 143B parental control were left untreated. When the induction was completed, all cells were treated with chloramphenicol by adding the antibiotic to the medium to final concentration of 100 µg/ml and incubation left to proceed for 15 min. Similarly to the previously described protocol, chloramphenicol is used to inhibit elongation of mitochondrial translation and prevent the “run off” of mitoribosomes during the procedure. This allowed mitoribosomes to maintain the exact position they were occupying at the beginning of the experiment.

Additionally, to maintain the effect of the initial treatment, all the buffers used in the following steps were supplemented with chloramphenicol (final concentration 100 µg/ml). To harvest cells after the treatment, plates were washed with PBS containing chloramphenicol and the cells were scraped off with a plastic scraper. Cells from the plates with the same experimental condition were pooled together and centrifuged. Cells collected from the plates designated for RNAseq analysis were resuspended in 5 ml Trizol reagent and stored at -20ºC. The cell pellets for ribosome profiling were resuspended in 1-1.2 ml of lysis buffer (20 mM Tris-HCl pH 7.8, 10 mM $MgCl_2$, 100 mM KCl, 1% Triton X-100, 1X complete protease inhibitor, 2mM DTT, 100 µg/ml chloramphenicol) depending on the size. Samples were incubated on ice for 15 min and then sheared by passing 6 times through the needle (25G). The lysed samples were then centrifuged (10 min, 560 xg, 4ºC). The procedure was repeated in case the supernatant was cloudy after the first centrifugation. The clear supernatant was transferred to a new tube and treated with RNase 1 (Ambion, final concentration 2.5 U/µl) for 45 min at room temperature with agitation. During this step the mRNA not protected by ribosomes was digested, allowing for generation of ribosome footprints. Depending on the volume of the lysis buffer used 1- 1.1 ml of each sample was designated for the sucrose gradient separation and the remaining part was stored at -20ºC.

In order to separate the ribosome protected fragments of mitochondrial mRNA only, the lysate treated with ribonuclease was loaded on previously prepared sucrose gradient. Each tube was topped up with the lysis buffer (to the final volume 13.4 ml). Samples were centrifuged in the ultracentrifuge (SW40Ti rotor) at 221632 x g, 4ºC for 2 h, with maximum acceleration and minimum deceleration. Next, each sample was divided into 14 fractions of 935 µl. During the centrifugation mitoribosomes were separated from the cytosolic ones due to the difference in their density. They were retained in the different phases of the sucrose, with mitoribosomes located closer to the top in the lower sucrose density. To confirm the exact position of whole mitoribosomes, which were predicted to contain protected fragments, 20 µl of each fraction were subjected to western blotting, using antibodies that would detect small (DAP3) and large (MRPL3) subunit proteins. Until the presence of mitoribosomes was confirmed, the remaining parts of all fractions were prepared for the storage and RNA isolation following proteinase treatment. In order to facilitate RNA isolation,

ribosomal proteins were digested with 0.2 mg/ml of proteinase K (PCR grade, Roche) supplemented by 1% SDS for 30 min at 45ºC. For storage and subsequent RNA isolation, Trizol LS reagent was added in proportion of 3:1.

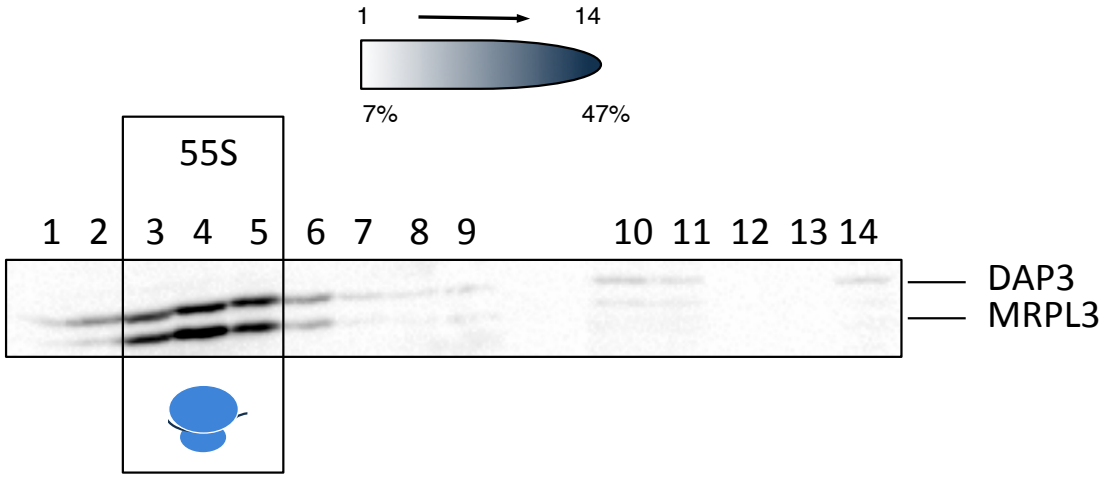

Figure 6.1. Separation of mitoribosomes by isokinetic sucrose gradient centrifugation

Cell lysate from 143B parental control cell line was separated on 7 - 47% sucrose gradient and after ultracentrifugation divided into 14 fractions. Each fraction was subjected to western blotting with antibodies specific to small and large mitoribosomal subunits (DAP3 and MRPL3 respectively). Fractions that contained monosomes were defined by presence of signal from both proteins (box labeled '55S').

Results of the western blot validation revealed the signals form DAP3 and MRPL3 (corresponding to the presence of small and large mitoribosome subunit respectively) coincided in fractions 3, 4 and 5. Both these proteins were detected with equally strong signals as these fractions contained the mitochondrial monosomes and most likely the 55S protected mRNA fragments.

6.3. Library preparation and deep sequencing

Size separation of mitoribosome footprints

Based on the results of the western blot analysis that determined the position of mitoribosomes on the gradient, only fractions 3, 4 and 5 were chosen for RNA isolation. The procedure was performed according to the manufacturer's instructions. RNA was precipitated in isopropanol with GlycoBlue. Pellets were washed with 75% ethanol and resuspended in 10 µl of loading dye (Gel loading buffer II, Ambion) to prepare the samples for size separation. According to the findings of Prof. Agami's group, the size of mitoribosome footprints varies from their cytosolic equivalents (Rooijers et al., 2013). There are two populations of

ribosome-protected fragments in mitochondria with 27 and 33 nt in length. Therefore, it was necessary that the cutoff for the size separation included all RNA fragments between 25 and 35 nt, a pool that would most likely contain mitoribosome footprints. In order to separate these fragments total RNA isolated from the selected sucrose gradient fractions was loaded on 10% denaturing polyacrylamide gel. The gel was electrophoresed in 1x TBE buffer at 150 V, and subsequently stained with SYBRGold (Fig. 6.2; method as in chapter 5.3.).

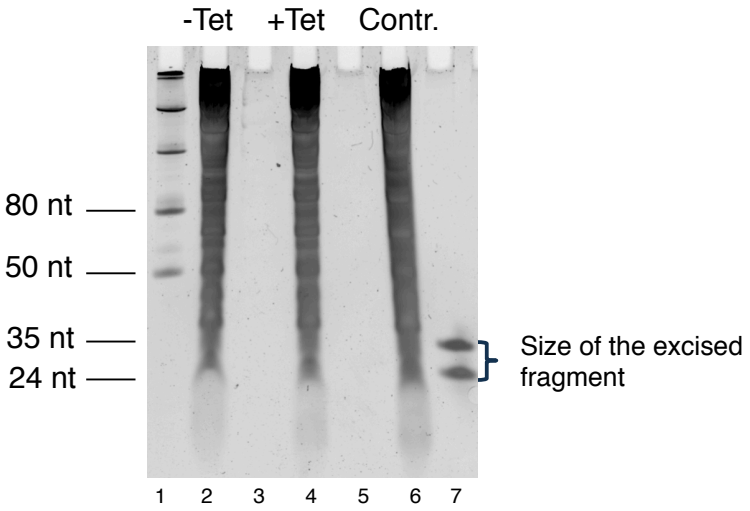

Figure 6.2. Size separation of the mitoribosome footprints

Mitoribosome footprints were generated in all three cell lines: mt-tRNA^{Val} mutant with (+Tet; lane 3), or without (-Tet; lane 2) VARS2L induction, and 143B control (Contr.; lane 6). Total RNA was isolated from the chosen sucrose gradient fractions that contained mitoribosomes, and loaded on 10% denaturing polyacrylamide gel. In addition to low range ssRNA ladder (lane 1), two oligo-RNA size markers were used (25 and 34-nt size, lane 7). The oligo-RNA fragments marked the borders of the area that was excised from each sample lane (2, 4 and 6) as it contained RNA fragments corresponding in size to the ribosome footprints.

From each lane a fragment of the gel corresponding to 24-35 nt size was removed. This size range was predicted to contain the mitoribosome footprints. In order to facilitate the elution of mRNA fragments from the gel, the excised pieces were first triturated by centrifugation through a pierced tube (as described in Ch. 5.3.). Elution buffer (0.3 M NaCl) was then added and the gel fragments were incubated overnight at 37ºC with vigorous shaking.

Table 6.2. Composition of 10% denaturing polyacrylamide gel

Component	Stock (30 ml)	Final conc.
urea	14.4 g	7M
40% acrylamide:bisacrylamide (19:1)	7.5 ml	10%
10x TBE	3 ml	1X
H_2O	8 ml	n.a.

The mixture was heated in the microwave oven to dissolve urea and then left at room temperature to cool down. For 1 gel, 10 ml of the stock solution was taken and 50 µl 10% APS and 10 µl TEMED was added. The rest of the stock solution was kept at room temperature.

Table 6.3. Sequences of the size markers

Size marker	Sequence
24 nt	5′ GCGUGUACUCCGAAGAGGAUCCAA 3′
35 nt	5′ GGCAUUAACGCGAACUCGGCCUACAAUAGUGAUGA 3′

Dephosphorylation of the 3' ends

When the elution process was completed, the buffer was separated from the gel pieces by centrifugation through cellulose acetate filters (1 minute, 16000xg, 4ºC). The RNA was then precipitated from the eluate by adding 1 ml of absolute ethanol with 3 µl glycogen (stock of 5 mg/ml concentration, Ambion AM9510, stored at -20ºC) and incubating at -20ºC for at least 2 h. After the incubation samples were centrifuged for 30 min, 21000xg at 4ºC. Pellets of RNA were resuspended in 25 µl 3'-dephosphorylation reaction mix (Table 6.4.). Residual phosphate moieties on 3' ends were the result of RNase 1 activity and it was necessary to remove them in order to facilitate ligation of the 3'-linker (Fig. 6.3 A). The reaction was performed by polynucleotide kinase, which in the absence of ATP (usage of the buffer devoid of this nucleotide) removed the phosphate group from the 3' ends of the RNA fragments. Under the described conditions the enzyme efficiency is low, even at the optimal temperature of 37ºC, hence the reaction time was extended to 5 h.

Table 6.4. Composition of the 3'-dephosphorylation reaction

Components	Volume
1.5x MES-buffer (in Table 6.5 below)	16.67 µl
T4 PNK [10 U/µl], NEB M0201S	1.25 µl
Nuclease-free H_2O	7.08 µl

Table 6.5. Composition of 1.5x MES-buffer (stored at -20ºC)

Components	Concentration
MES-NaOH pH 5.5	150 mM
NaCl	450 mM
$MgCl_2$	15 mM
ß-mercapthoethanol	15 mM

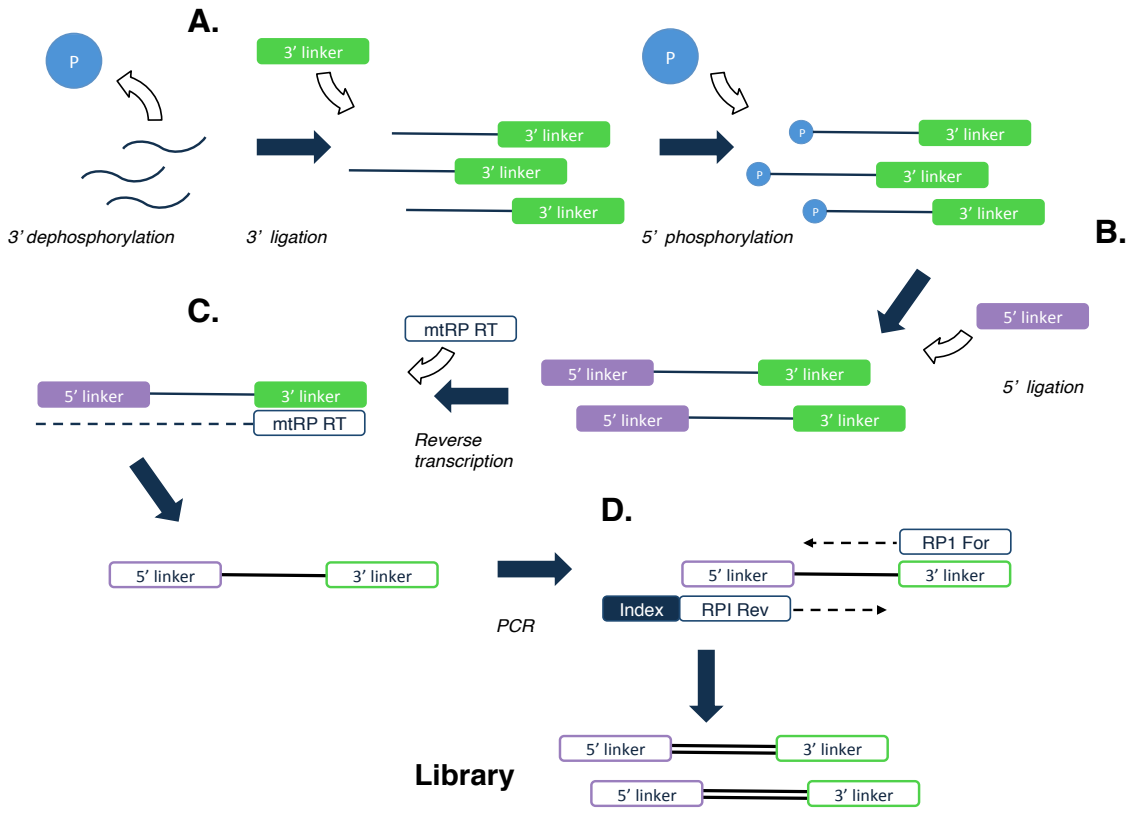

Figure 6.3. Overview of the library preparation method

A. The size separated mitoribosome footprints were first dephosphorylated at 3' end in order to bare the free hydroxyl groups and facilitate ligation of the 3'-linker. After the ligation, successfully extended fragments were separated via electrophoresis in 10% denaturing polyacrylamide gel. **B.** Purified fragments were then phosphorylated at the 5' end and the 5' linker was ligated. **C.** The size separation of the ligation products was repeated and the obtained RNA fragments were then reverse transcribed using a primer specific to the 3'-linker sequence. **D.** The cDNA was next amplified via PCR and the purified library was ready for sequencing.

Samples containing dephosphorylated RNA fragments were next purified through isolation with Trizol® reagent. 725 µl of Trizol® was added to each sample, followed by 150 µl chloroform. RNA isolation was performed according to manufacturer's instruction. Precipitated pellets were washed with 500 µl of 75% ethanol and stored at -20ºC until the next step, ligation of the 3'-end linker

(Fig. 6.3 A).

Ligation of the 3' linker

The sequence of this linker (Table 6.12 A) was designed to maximize the efficiency and specificity of the ligation. The first nucleotide at the 5' end contained ribose (adenylated) so the ligation would occur between two RNA species. The rest of the sequence was build of deoxyribonucleotides with the dideoxy-modification of the 3' end to prevent ligating on the 5' end of ribosome footprints library. The reaction buffer applied lacked ATP (Table 6.7) to ensure the ligation occurred at the 3' end only and with the linker in the right orientation as only its 5' end was adenylated. The RNA pellets were resuspended in 15 µl of reaction mix (Table 6.6 and 6.7). Reaction was performed for 2.5 h at 37ºC with agitation. In addition to the experimental and control samples, both size marker oligos (24 and 35 nt, sequences in Table 6.3) were also subjected to ligation. These samples served as a positive control of the ligation and the right-size markers for facilitating of the products selection.

Table 6.6. Composition of the 3' end ligation (15 µl) reaction.

Components [stock concentration]	**Volume**
3' linker [100 µM]	1.5 µl
10x T4 ligation buffer (custom)	1.5 µl
T4 RNA ligase I [20U/µl], NEB M0204S	2.25 µl
Nuclease-free H_2O	9.75 µl
Components of the positive control	**Volume**
3' linker [100 µM]	1.5 µl
10x T4 ligation buffer (custom)	1.5 µl
24 nt marker [20 µM]	2.6 µl
35 nt marker [20 µM]	1.3 µl
T4 RNA ligase I [20U/µl], NEB M0204S	2.25 µl
Nuclease-free H_2O	5.85 µl

Table 6.7. Composition of 10x T4 ligation buffer (custom, stored at -20ºC)

Components	**Concentration**
Tris-HCl, pH 7.8	500 mM
$MgCl_2$	100 mM
DTT	100 mM

After the reaction was completed, the products were resuspended in loading dye (10 µl, Gel loading buffer II, Ambion 8546G) and separated on a 10%

denaturing polyacrylamide gel. The composition of the gel (Table 6.2) and the electrophoresis conditions were the same as those used for size separation of the RNA isolated from the ribosomes (see Fig. 6.2; method as in chapter 6.3, “Size separation of the mitoribosome footprints”).

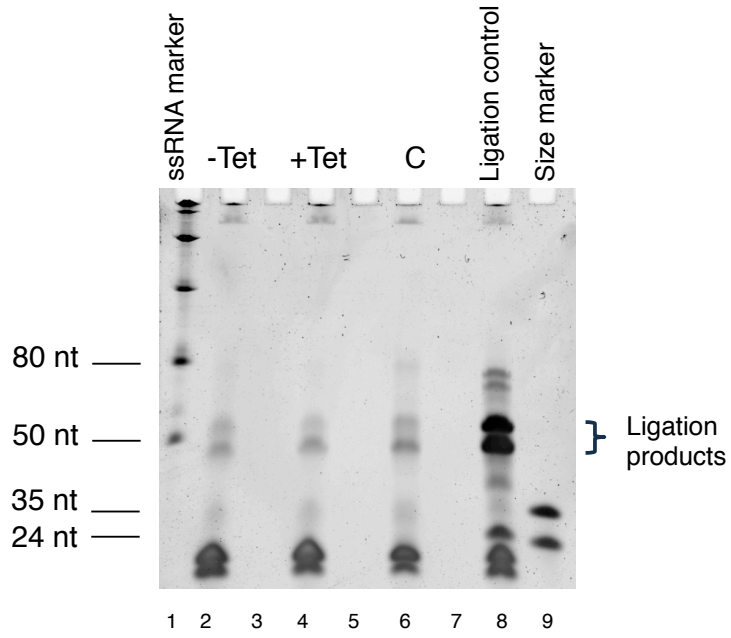

Figure 6.4. Size separation of the 3’ linker ligation products

Ligation products of the 3’ linker and isolated RNA fragments (potential ribosome footprints) were separated by 10% denaturing SDS PAGE. Reactions were performed on RNA fragments from 3 cell lines: $tRNA^{Val}$ mutant with (+Tet) or without VARS2L induction (-Tet) and wild type control (C). In addition, a positive control of the ligation reaction (lane 8) facilitated selection of the correct sized products (depicted by brackets). ssRNA low range (lane 1) and oligo (lane 9) size markers were used.

The expected product sizes of the 3’ linker ligation ranged between 44- 55 nt, extending the original 24-35 nt ribosomal footprints (Fig. 6.4). The main ligation products in experimental and control samples corresponded in size to the products in the positive control, which suggested that the reaction was successful. From each sample lane (Fig. 6.4 lanes 2, 4, 6 and 8) the gel area between 45 and 55 nt was excised. The products in the positive control samples were also included to serve the same purpose in following 5’ ligation step.

Phosphorylation of 5’ ends and ligation of the 5’ linker

RNA from gel pieces was eluted in the same way as described for size

separation of the footprints and prepared for the next step, which was phosphorylation of the 5' end of the fragments (Fig. 6.3 B). Addition of the phosphate group at 5' end was necessary for the ligation of the second linker (5' linker). The pellets of the precipitated RNA were resuspended in 14 µl of phosphorylation reaction mix (Table 6.8). Reactions were performed for 30 min at 37ºC with agitation.

Table 6.8. Composition of the 5'-phosphorylation reaction

Components [stock concentration]	Volume
10x PNK buffer, NEB	1.5 µl
ATP [4 mM]	3.6 µl
T4 PNK [10 U/µl] NEB M0201S	1.5 µl
Nuclease-free H_2O	7.5 µl

To purify the samples after phosphorylation, they were subjected to RNA isolation with Trizol®. As described previously ("Dephosphorylation of the 3' ends"), the whole of the reaction sample was combined with 725 µl of Trizol® reagent and the isolation was carried according to the manufacturer's instructions. Pellets were washed in 0.5 ml of 75% ethanol, dried and resuspended directly in 15 µl of 5'-ligation reaction mix (Table 6.9). The 5'-ligation reaction was performed at 22ºC, overnight with agitation.

Table 6.9. Composition of the 5' end ligation reaction.

Components	Volume
5' linker [100 µM] sequence in Table 6.11 B.	3.9 µl
10x T4 ligation buffer (custom), Table 6.7	1.5 µl
4 mM ATP	0.9 µl
T4 RNA ligase I [20U/µl], NEB M0204S	1.5 µl
Nuclease-free H_2O	7.2 µl

As in case of the 3' end ligation step, loading dye (10 µl) was added to the entire reaction product, which was then separated on 10 % denaturing polyacrylamide gels (Table 6.2). The preparation of the gels, conditions of electrophoresis and size markers were as described in "Size separation of the mitoribosome footprints". The expected product size following successful ligation was between 65-75 nt.

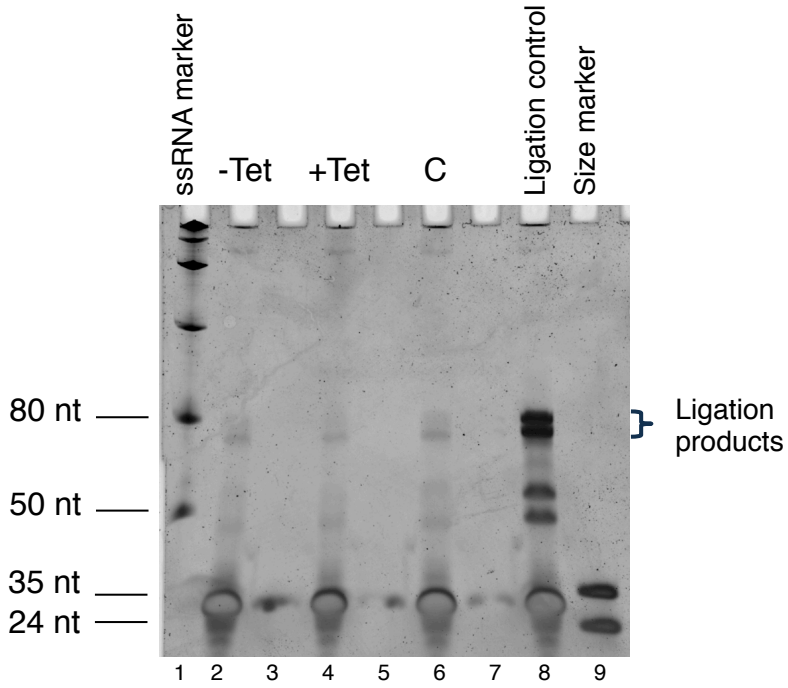

Figure 6.5. Size separation of the 5' linker ligation products

Products of the ligation of the second linker (5' linker) to the ribosome protected fragments were separated by 10% denaturing PAGE. The 5' linker was ligated to RNA from all samples: uninduced $tRNA^{Val}$ mutant (-Tet; lane 2), $tRNA^{Val}$ mutant induced to express VARS2L (+Tet; lane 4), wild type control (C; lane 6) and positive control reaction (ligated size markers; lane 8). The latter served as a reference for the size of the expected products and aided in their excision (depicted by brackets). The size markers used were ssRNA low range marker (lane 1) and oligo size markers (lane 9).

Results of the 5' ligation in the positive sample (Fig. 6.5, lane 8) showed the presence of the expected-sized product indicated that the procedure had been successful. Similar sized products were detected in all of the experimental and control samples although of the much lower intensity. Taken together these results indicated that the ligation of the 5' end linker was successful. The small amount of the final product was most likely due to the low levels of the template that was diminished after each size separation step. However, despite the low amount the ligation products, these were excised from gel and eluted as described above ("Size separation of the mitoribosome footprints"). Pellets of the precipitated samples were resuspended in 8 µl of water and prepared for reverse transcription (Fig. 6.3 C). The reaction was performed using SuperScript III kit (Invitrogen) with the conditions outlined in Table 6.10.

Table 6.10. Component and condition of the reverse transcription reaction

Components (all included in SuperScript III First-Strand Synthesis System 18080-051)	**Volume**
RNA sample	8 µl
dNTPs [10 mM]	1 µl
mtRPRT primer [100 µM] sequence in Table 6.11 B	1 µl
Samples were incubated for 5 min at 65ºC and then placed on ice	
10x buffer	2 µl
$MgCl_2$ [25 mM]	4 µl
0.1 M DTT	2 µl
SuperScript III [20 U/µl] Invitrogen	1 µl
RNase Out	1 µl
Temperature	**Time**
50ºC	50 min
85ºC	5 min
4ºC	∞

After the reverse transcription, samples were treated with 1 µl RNase H for 1 hour at 37ºC. Then they were purified with illustra Microspin G-50 spin columns (GE Healthcare) according to the manufacturer's instructions. Next, the purified samples were amplified in the PCR reaction (composition and conditions of the reaction in Tables 6.11. A and B) with primers specific to the linker sequences ligated to each end of the templates (Fig. 6.3 D). The forward primer (termed mtRPPCR RP1, Table 6.11 B) was universal for all samples, whereas three types of the reverse primers were used, each contained a different index sequence (one index sequence type per sample, Table 12 B). Use of the indexed primers allowed simultaneous sequencing of all libraries, since the reads originated from different samples they could easily be distinguished based on the index sequence. Index sequences embedded in primers were compatible with the Illumina platform and recognized by its software. After the sequencing, reads with one type of index were assigned to the specific sample.

Table 6.11. Component (A) and conditions (B) of the library PCR reaction

A.

Components	Volume
2x Phusion master mix with HF buffer, Thermo Scientific	50 µl
mtRPPCR RP1 Forward primer [25 µM] Table 6.12 B	1 µl
mtRPPCR RPIX* Reverse primer [25 µM]	1 µl
H_2O	18 µl
Template (cDNA)	30 µl
* X= index number	

B.

Stage	Temperature	Time
Hold	98˚C	30 s
19 cycles	94˚C	30 s
	60˚C	30 s
	72˚C	15 s
Hold	72˚C	10 min
Hold	4˚C	∞

Table 6.12. Linker (A) and primer (B) sequences

A.

Type	Name	Sequence (5'-3')
5' Linker (RNA)	RP RNA 5' adapter (RA5)	GUUCAGAGUUCUACAGUCCGACGAUC
3' Linker (DNA*)	RP RNA/DNA 3' Adapter (RA3)	5rApp*/TGGAATTCTCGGGTGCCAAGG/3ddC**

* 5rApp: adenylated ribonucleotide

** 3ddC: dideoxy modification in the 3' nucleotide

B.

Type	Name	Sequence (5'-3')	T_m
Reverse transcription	mtRPRTPrimer (RTP)	GCCTTGGCACCCGAGAATTCCA	53.5 °C
PCR Forward	mtRPPCR (RP1)	AATGATACGGCGACCACCGAGATCTACACGTTCAGAGTTCTACAGTCCGA	66.9 °C
PCR Reverse Index 1	mtRPPCR (RPI1)	CAAGCAGAAGACGGCATACGAGAT**[CGTGAT]**GTGACTGGAGTTCCTTGGCACCCGAGAATTCCA	70.7 °C
PCR Reverse Index 2	mtRPPCR (RPI2)	CAAGCAGAAGACGGCATACGAGAT**[ACATCG]**GTGACTGGAGTTCCTTGGCACCCGAGAATTCCA	70.7 °C
PCR Reverse Index 3	mtRPPCR (RPI3)	CAAGCAGAAGACGGCATACGAGAT**[GCCTAA]**GTGACTGGAGTTCCTTGGCACCCGAGAATTCCA	70.7 °C
PCR Reverse Index 4	mtRPPCR (RPI4)	CAAGCAGAAGACGGCATACGAGAT**[TGGTCA]**GTGACTGGAGTTCCTTGGCACCCGAGAATTCCA	70.7 °C

PCR Reverse Index 5	mtRPPCR (RPI5)	CAAGCAGAAGACGGCATACGAGA**[TCA CTG]**TGTGACTGGAGTTCCTTGGCACC CGAGAATTCCA	70.7 °C

[ ] contain the index sequence

The PCR products were purified using the Qiaquick PCR purification kit (Qiagen 28106) according to the manufactures protocol. The elution was performed with 25 µl of nuclease-free H_2O. The purified DNA was finally size separated using E-GEL Invitrogen system (G6400EU) with E-GEL EX with SybrGold 2% SizeSelect precast gel (Invitrogen G661002). Whole samples were loaded to the top row of wells, along the 10 µl 25 bp size marker (diluted to 200 µg/µl with nuclease-free water and stored at -20ºC, Invitrogen 10597-011). The E-Gel system utilizes precast gels set between two plastic plates, which allows omitting the running buffer. In addition, the real-time visualisation of the sample progress is possible as the gels are prestained with specific dyes (mainly SYBRGold) and placed on the transilluminator during the electrophoresis. For the size selection these gels have two rows of wells- top one to load the sample and the one in the middle where the product of the desired size can be selected and retrieved. For this purpose, the second row of wells was filled with 25 µl of the nuclease-free water so that the desired DNA species (approx. 130 bp) can be resuspended and removed from the gel. The samples were electrophoresed with the "2% select" pre-set program. When the expected size products (assessed based on the size marker) arrived in the second row of wells (after approx. 13 min) they were resuspended in the water and transferred in to a tube. These products contained purified, size selected library of potential mitochondrial ribosome footprints (RFs) and were stored at -20ºC prior to sequencing on HiSeq Illumina Platform.

6.4. Bioinformatics analysis of sequencing results

The library samples were sent to the Netherlands Cancer Institute, Amsterdam to be sequenced at the Genomics Core Facility. Samples were sequenced using mainly Illumina HiSeq2000 (samples from the first experiment were also sequenced in parallel on the MiSeq platform). As an additional control, data from a cell line used in published mitoribosome profiling study (Rooijers et al., 2013) labeled SRR935452 or SRR935453 depending on the type of sequencer it was sequenced with (raw data available at NCBI Gene Expression Omnibus under accession code GSE48933) were included.

The bioinformatics analysis of the raw data (from the first experiment) was performed by Dr. Mathew Bashton from the Bioinformatics Support Unit, Newcastle University. The protocol described below was developed by him and then used by Dr. Fei Gao from my host lab to analyze data from the following experiments. First, the adaptors were removed using cutaddapt with the options listed in Table 6.13.

Table 6.13. Adapter trimming options (based on the original methodology by (Rooijers et al., 2013)

Option	Function
-a TGGAATTCTCGGGTGCCAAGGAACTCCAGTCACATCACGATCTCGTATGCCGTCTTCTGCTTG	Removing the specified adapter adapter sequence from 3' ends. Used in my samples and SRR935453
-a TCGTATGCCGTCTTCTGCTTG	Removing the specified adapter adapter sequence from 3' ends. Used in SRR935452
-O 12	minimum overlap length between the read and adaptor is set as 12
-m 20	discards reads shorter than 20
-o *sample_name*_trimmed.fastq	The output file was named after the sample with _trimmed.fastq

Next, the outputfiles (*_trimmed.fastq) were aligned to decoy tRNA / rRNA sequences from nuclear and mitochondrial genomes. This operation was facilitating filtering out reads that originated from other than mRNA fragments. It was performed with bowtie2 with the options as presented in Tab. 6.14.

Table 6.14. Filtering out the tRNA / rRNA sequences (based on the original methodology by (Rooijers et al., 2013)

Option	Function
-p 4 –D 20 –R 10 –N 1 –L 20 –i C/1	Technical parameters for the alignment
--un *sample_name*_screened.fastq	Output file for the fastq sequences that do not align to decoy tRNA/ rRNA, i.e. potential RFs mRNA sequences
-x prescreen	The bowtie index decoy file with tRNAs and rRNAs, created prior to this analysis
-U *sample_name* _trimmed.fastq	Input file
-S *sample_name* _screened_out.sam	Output *.sam file with the filtered out sequences aligned with the decoy index

Further analysis was conducted using the *_screened.fastq files which were devoid of rRNA and tRNA sequences. This file was aligned to the mitochondrial genome. This reference file was created by Dr. Bashton and labeled HumanMT. The alignment was performed with bowtie2 using the following parameters (Table 6.15):

Table 6.15. Alignment with the mitochondrial genome (based on the original methodology by (Rooijers et al., 2013)

Option	Function
-p 10 -D20 -R 10 -N 1 -L 20 -i C,1	Technical parameters for the alignment
-x HumanMT	The bowtie index for humen mt-genome reference
-U *sample_name screened*_out.sam	Input file
-S *sample_name* _.sam	Output *.sam file with alignment to human mt-genome

From the alignment output file (*.sam) multimapping reads were removed and the resulting file was converted into *bam file using the following pipeline command:
samtools view -q 1 -bS *sample_name*_screened_out.sam -u | samtools sort - -f *sample_name* _screened.sorted.bam

The final *bam file was then indexed (as it is required by the visualization software, namely IGV) using the following command:
samtools index *sample_name* _screened.sorted.bam

It is important to point that the quality of the data was rather low with only ~ 1% of the reads originating in the mitochondrial mRNAs (approximately 1.5 $x10^5$, Appendix 1.4, Table A1, samples labeled '2553'). The retention of mitoribosome footprints was lower than expected and observed in Prof. Agami's lab (approximately 5 $x10^6$,' Appendix 1.4, Table A1, samples labeled 'SRR935452'). However, the quality of data did not render the data analysis impossible, hence the downstream analysis was commenced.
Once the alignment was completed, the resulting *.bam files were visualized in the IGV software. The brief visual inspection of the ribosome profiles allowed identifying regions that in mt-$tRNA^{Val}$ mutant cell line would accumulated higher

amounts of ribosome footprints (RFs) associated with the presence of valine codons. However, in order to quantify the actual ribosomal occupancy over these codons and compare it between the mutant and control cell lines a different approach was needed. This part of the analysis was performed by Dr. John Grady using R. The first questions to be answered were : 1) is the mt-tRNA^{Val} mutation in T1V1 cell line resulting in an increase of the RFs accumulation over the mt-valine codons consistent with mitoribosome stalling? 2) Is the mitoribosome stalling relieved to some extend in T1V1 cell line with VARS2 overexpression?

Estimation of the A-site position in the mitoribosomal footprints

First, it was important to establish methodology to identify the footprints generated by only these mitoribosomes that were actively translating valine codons. The presence of a valine codon in the footprint can be placed at any given position in a RF (Fig. 6.6 A position of the valine codon marked in blue). Valine codons at the 5' end of the footprint represent these sequences that were already translated, whereas Val codons at the far 3' end were not yet reached by the ribosome. Only the codons that were directly over the ribosomal A-site represent what sequence was currently translated by each ribosome at the time of experiment. In their publication (Rooijers et al., 2013) observed that in mt-tRNA^{Trp} mutant cell line there is a high concentration of RFs with Trp codon starting 15-18 nt from the 5' end. After further investigation they estimated that on average the mitoribosomal A-site was placed 17 nt from the 5' end of the RF. In order to test if the same relation is observed in my data, all RFs with valine codons were grouped according to the position at which these codons started (measured from the 5' end per each nucleotide: 1 - 30). Number of RFs in each of the groups was counted. Then the numbers were used to calculate what percentage of all RFs with any amino acid codon starting at that particular position in a footprint it constituted. The results of these calculations were than plotted for all cell lines (Fig. 6.6 B wild type "Control", uninduced T1V1 "Tet-", T1V1 with VARS2 induction "Tet+").

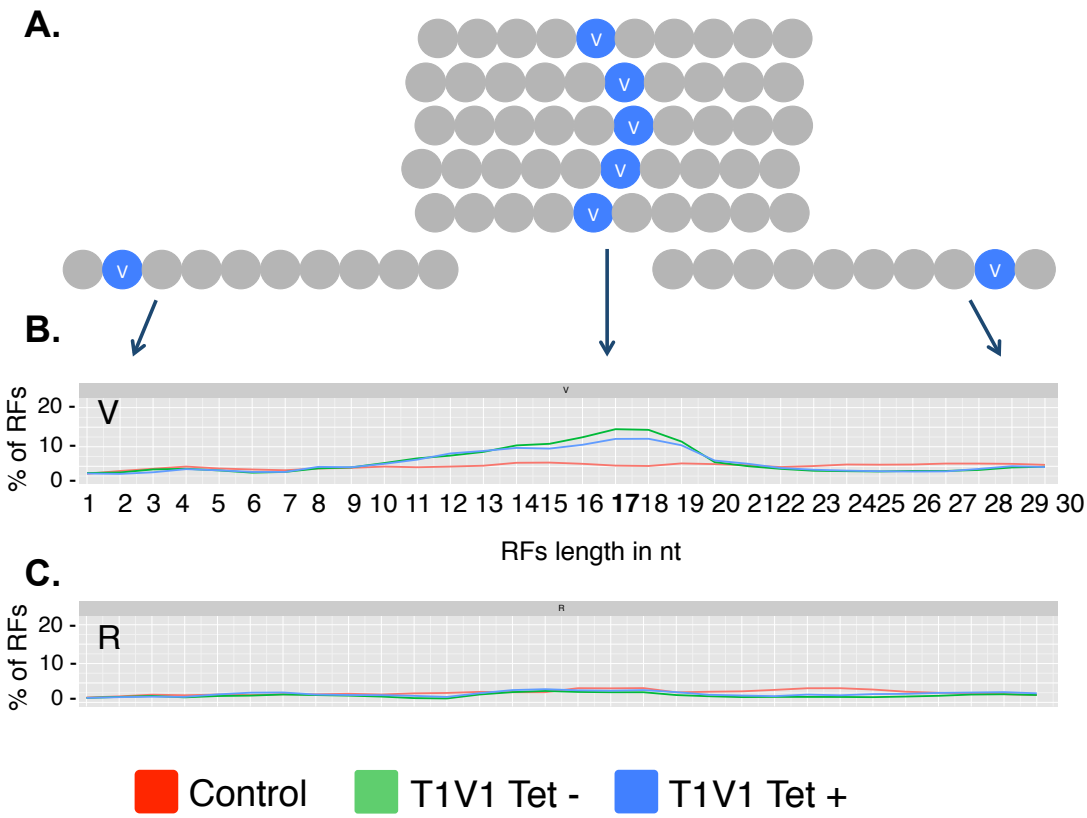

Figure 6.6. Estimation of the A-site position in ribosome footprints

A. Schematic illustrating how RFs containing valine codons were grouped and quantified. **B.** Plots showing quantification of RFs with valine codons at various positions were generated for all 3 cell lines: wild type control (Control, in red), T1V1 uninduced (Tet -, green), T1V1 induced (Tet+, blue). The x axis representing different offsets of all RFs containing valine codon which 5' end starts at any possible position (1-30 nt, 5' – 3') in a predicted-sized footprint. The y axis represents a number of RFs with valine codon starting at each particular position. This number is presented as a percentage of all footprints with an amino acid codon starting at that position. **C.** The same types of plots as in A. were generated for the arginine-containing RFs. The original plots (in B and C) were generated by Dr. John Grady.

Comparison of the percentage of the RFs containing valine between the analyzed cell lines showed the most striking difference in their number when the valine codon started 17 nt from the 5' end. In both T1V1 cell lines (with and without Tetracycline) the number of RFs with valine codon beginning at 17 nt was higher than in control. Interestingly, in control cell line the position of the valine codon in a footprint did not change what the proportion of all amino acid-encoding RFs they constitute. The position of the valine codon in RFs had an effect on their number only in T1V1 cell lines and when placed in the middle of RF. As a contrast, for arginine-containing RFs (Fig. 6.6 C), the position of this amino acid codon did not have an effect on their numbers, regardless of the cell line analysed. To investigate this further, number of RFs containing valine 17 nt

from 5' end was compared between cell lines. Results, shown as % of RFs with all amino acid codons at that position, were presented on a graph (Fig. 6.7).

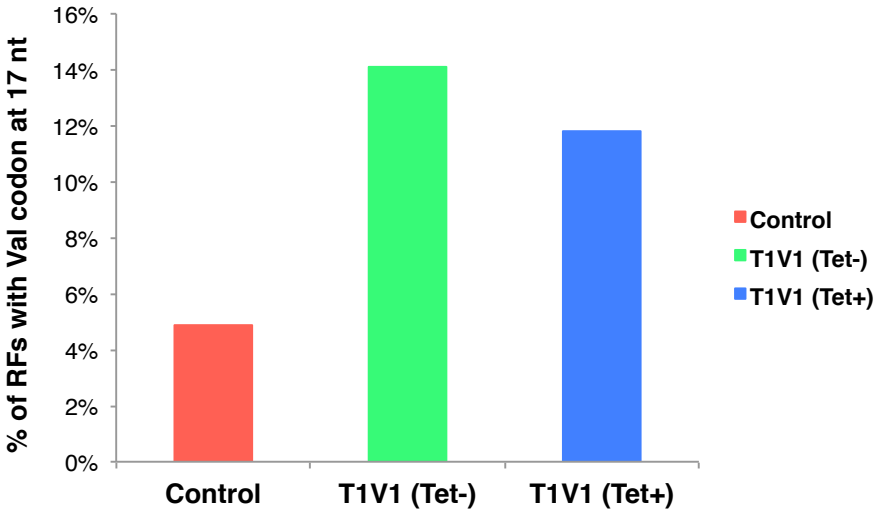

Figure 6.7. Proportion of RFs with valine codon beginning at 17 nt from 5' end

Number of RFs with valine codons beginning at the 17th nt from the 5' end were compare between all 3 cell lines: wild type control (Control, in red), T1V1 with (T1V1 Tet+, blue) and without (T1V1 Tet-, green) induction of VARS2 expression. Results were presented as percentage of RFs with aa-codons starting at that position.

The result showed that approximately 14% (Fig. 6.7, 'Tet-') and 12% ('Tet+') of all the footprints generated for these cell lines contained valine codon starting 17 nt from the 5' end. As opposed to control cell line where RFs with valine at that position constituted for only 5% of all RFs. Interestingly, there was very little variation between the induced and uninduced T1V1 cell lines. This result could have been explained by the failure to rescue the pathological phenotype, possibly caused by ineffective induction of VARS2L expression. This was suggested in the correspondence with Koos Rooijers, who performed additional analysis of these ribosome profiling data and founf no evidence of the VARS2L overexpression. Until this result was definitively confirmed with immunodetection of VARS2L levels, it was assumed that the induction of T1V1 was not successful and both samples (Tet- and Tet+) were treated as replicates of the mutant cell line. These results suggested that the estimation of the mitoribosomal A-site position at the 17th nt from the 5' end was most likely correct and that the mutation in mt-tRNA^{Val} was possibly causing the increase in ribosome accumulation over valine codons.

Is stalling depending on the type of valine codon?

In human mitochondrial DNA there are 4 codons encoding valine, namely GTA, GTC, GTG and GTT. In the (Rooijers et al., 2013), stalling of mitoribosomes on tryptophan codons in mt-tRNA^{Trp} mutant was more profound on one of the Trp triplets than on the other. In order to investigate if the accumulation of the mitoribosomes on valine codons would also be dependent on their type in T1V1 cells, the pool of RFs with valine in the A-site was divided into 4 categories based what Val codon they contained. The number of RFs in each category was calculated for all 3 cell lines and presented as a graph (Fig. 6.8, Control, T1V1 Tet- and T1V1 +Tet).

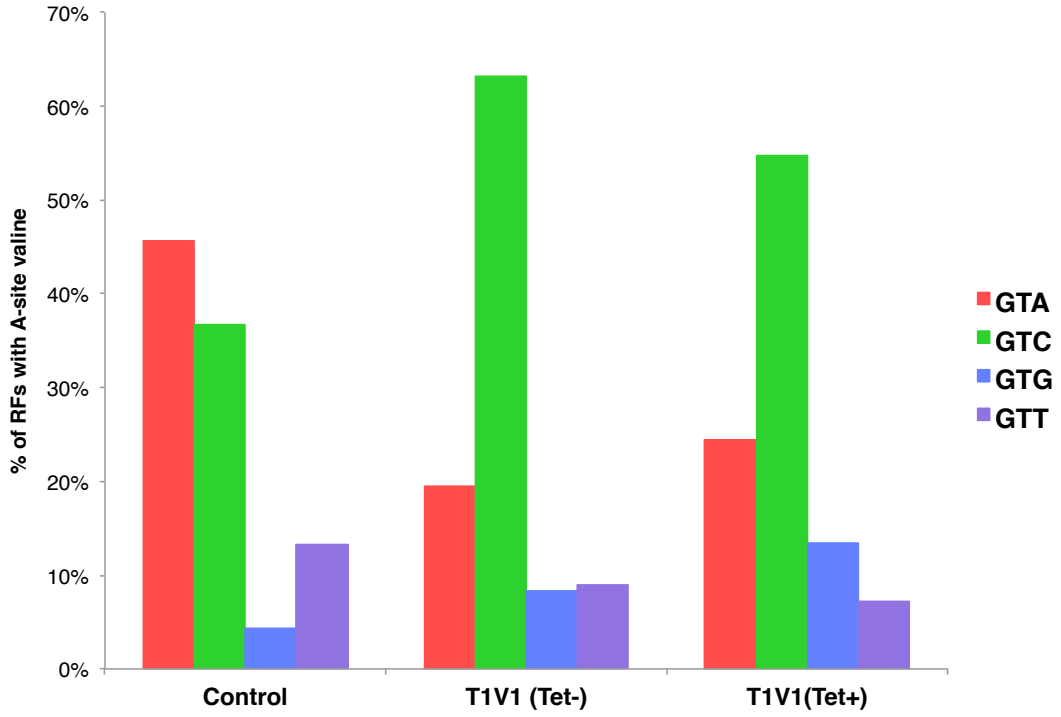

Figure 6.8. Quantification of RFs with A-site valine codon based on the type of the coding triplet

RFs with valine at the 17th nt from the 5' end were grouped according to the type of valine codon (GTA, GTC, GTG or GTT) at that position. Number of RFs in each category was presented as % of all RFs with valine at 17 nt. Graphs were generated for each of the cell lines: wild type control (Control), uninduced T1V1 (Tet-) and induced T1V1 (Tet+).

In wild type control majority (45%) of RFs with valine at A-site contained GTA codon at that position. The second most abundant codon was GTC. In both mutant cell lines, however, this proportion was different: approximately 60% (63% in Tet- and 55% in Tet+) of RFs with A-site valine contained GTC codon at that position. GTA codon was present at the A-site of 20% (Tet-) or 25%

(Tet+). The proportion of RFs with GTG and GTT codons in the A-site varied to much smaller extent between the cell lines (4-13% for both codons). In order to explain the change of A-site valine codon usage between the cell lines, first the proportion, number and position of different valine codons in human mtDNA were determined. It was important to calculate which of the valine codon types is more abundant in mtDNA and how are they distributed across different ORFs. The position of valine codons was marked in all mitochondrial gene templates, distinguishing between the types of the triplets (Fig. 6.9 A).

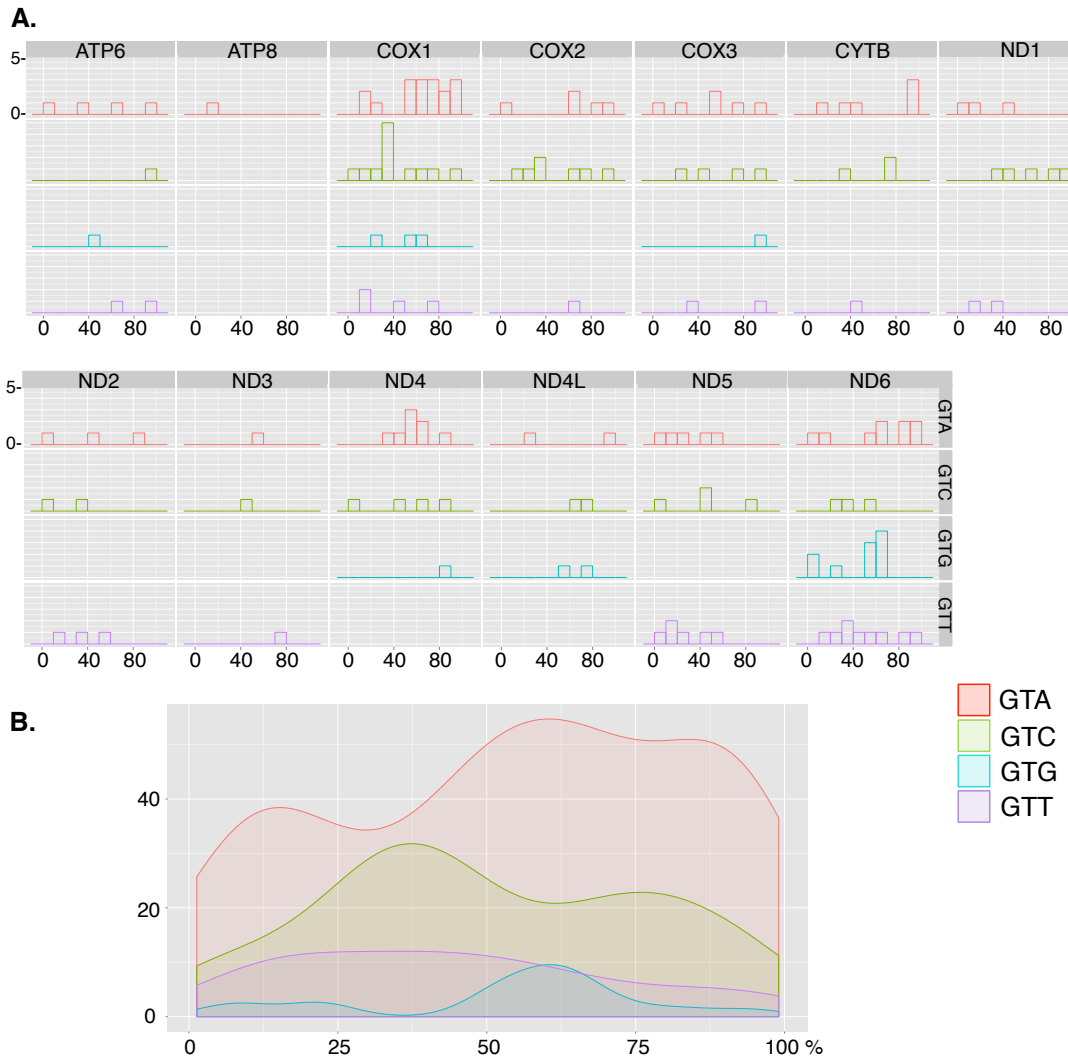

Figure 6.9. Position of valine codons in mtDNA

A. Positions of each type of valine codons were marked in all mitochondrial polypeptide genes. Panels represent the position of each valine codon separately. The full length of each gene is presented as 100%. The Y-axis represents the number of valine codons in the certain area. Image enlarged in appendix 1.1. **B.** Representation of the occurrence of different types of valine codons in mtDNA when all transcripts were superimposed. The original plots were generated by Dr. John Grady.

By merging the distribution patterns of individual valine codons across each gene (which full length is represented as 100%) a general density map was created (Fig. 6.9 B). On average in human mitochondrial genes, the most represented type of valine codon is GTA. It is also the triplet that is fully complementary to the mt-tRNA^{Val} anticodon (3' CAT 5'). All other 3 valine codons require wobble (other than classical Watson:Crick) base pairing at their 3rd position from 5' end. In the wild type control cell line, the GTA codon is also the most abundant in the RFs with the valine codon at position 17. In T1V1 cells, however, the proportion of valine codons in that position was shifted in favor of GTC, the second most abundant in the mtDNA. It is possible that the wobble base pairing of the 3rd (from 5' end) nucleotide of this codon (C) with the corresponding nucleotide of the anticodon (T) increases the time required by a ribosome to translate it. This also may be the reason why in the mutant T1V1 cell line where the charged mt-tRNA^{Val} level is lower than in the control, the time delay due to the wobble pairing is more prominent.

Distribution of RFs across mt-transcripts

In order to investigate if the potential staling on valine codons changes the distribution of mitochondrial ribosomes, the mitoribosome profiles were generated and compared between the cell lines. The number of RFs accumulating along the length of each mt-transcript was calculated and plotted to form histograms (Fig. 6.10 A). This resulted with separate mitoribosome profiles for each of the mt-transcripts. Regions in mt-genes with high concentration of valine codons, where identified by creating separate density maps, distinguishing between different types of these codons (as in Fig. 6.9 B). The valine codon density maps were created for each of the individual mt-transcripts (Fig. 6.10 B). Comparison of these two sets of data facilitated determination if the higher accumulation of RFs is corresponding with the places in mtDNA sequence where valine codons are more abundant.

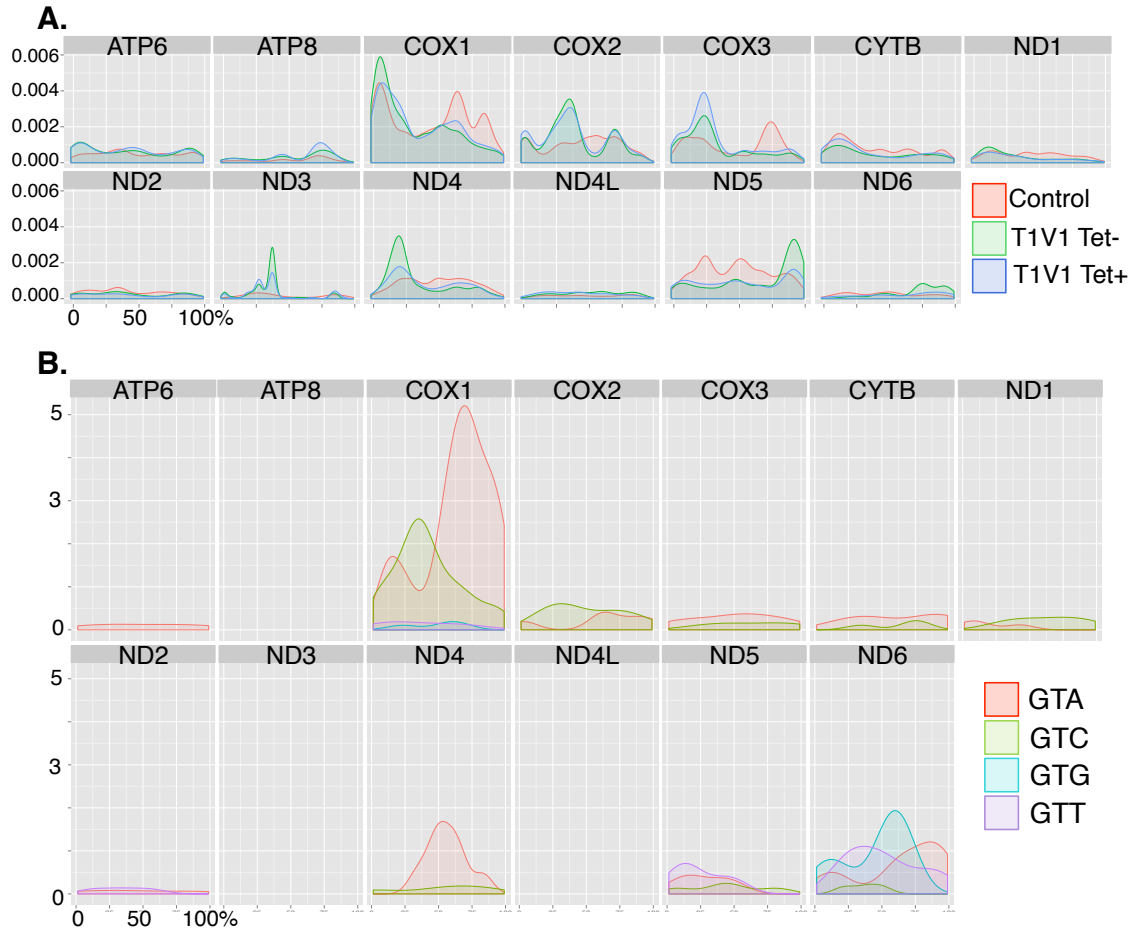

Figure 6.10. Distribution of mitoribosomes is not dependent on the position of valine codons

A. Density of the RFs across each mt-transcript was calculated and plotted for all 3 cell lines: wild type control (in red), uninduced T1V1 (Tet-, in green), unsuccessfully induced T1V1 (Tet+, in blue). The full length of each transcript was presented as 100%. **B.** Position of valine codons in mtDNA was marked for each type of codon separately. Amount of different Val codon was presented as density plots over the length of each mitochondrial transcript (length represented in %). Both images enlarged in appendix 1.2. The original plots were generated by Dr. John Grady.

The pattern of RFs distribution between the two T1V1 samples (Fig. 6.10 A Tet+ and Tet-) was very similar, further confirming that the rescue experiment with VARS2L expression was most likely unsuccessful. If these two samples were to be treated as identical repeats of the same cell line the observed similarities in ribosome profiles could suggest reproducibility of this method. Comparison of the mitoribosome profiles between the control and T1V1 cell lines shows differences in distribution of RFs in most of mt-transcripts (Fig. 6.10 A). These discrepancies in mitoribosome coverage were especially visible in COX1, COX2, COX3, ND3, ND4 and ND5. However, the regions with higher accumulation of RFs in T1V1 than control cells were not overlapping with the positions of valine codon-rich sequences in mtDNA (Fig. 6.10 B). For

example, the high number of valine codons in the 3' region of COX2 and in the middle of ND4 did not generate a higher number of RFs in T1V1 cells than in control cell line. Similar, the valine codon-rich ND6 sequence did not generate a high number of mitoribosomal RFs.

Finally the comparison of RFs profiles with valine triplets distribution was focused on GTC codons, which possibly had the highest stalling potential of all valine-encoding sequences in mutant cell lines (Fig. 6.8). The enrichment in GTC codons could have been a reason for the RFs accumulation visible as a peak approximately 25% in the COX2 transcript in T1V1 cell line. However, even higher number of GTC triplets in the second quarter of COX1 did not result in higher density of RFs. The changes of RFs distribution between control and T1V1 cell lines, visible in the general mitoribosome profiles were most likely caused by factors other than the presence of valine codons.

Repeat of mitoribosome profiling on T1V1 cell line

In addition to the samples analyzed in the preceding section, a second ribosome profiling experiment was performed on T1V1 cell line. This library included uninduced T1V1 and 143B wild type control. The sample from rescue experiment was omitted because of the concerns with possible lack of VARS2 expression. Sequencing results were analysed as described in '*Estimation of the A-site position in the mitoribosomal footprints'* and Fig. 6.6. The objective was to test if the estimation of the A-site position to be 17 nt from RFs' 5' end was correct and the new mutant sample would present similar valine codon-induced stalling. Number of RFs with 17 nt valine codons was calculated for both cell lines distinguishing between 4 Val coding sequences.

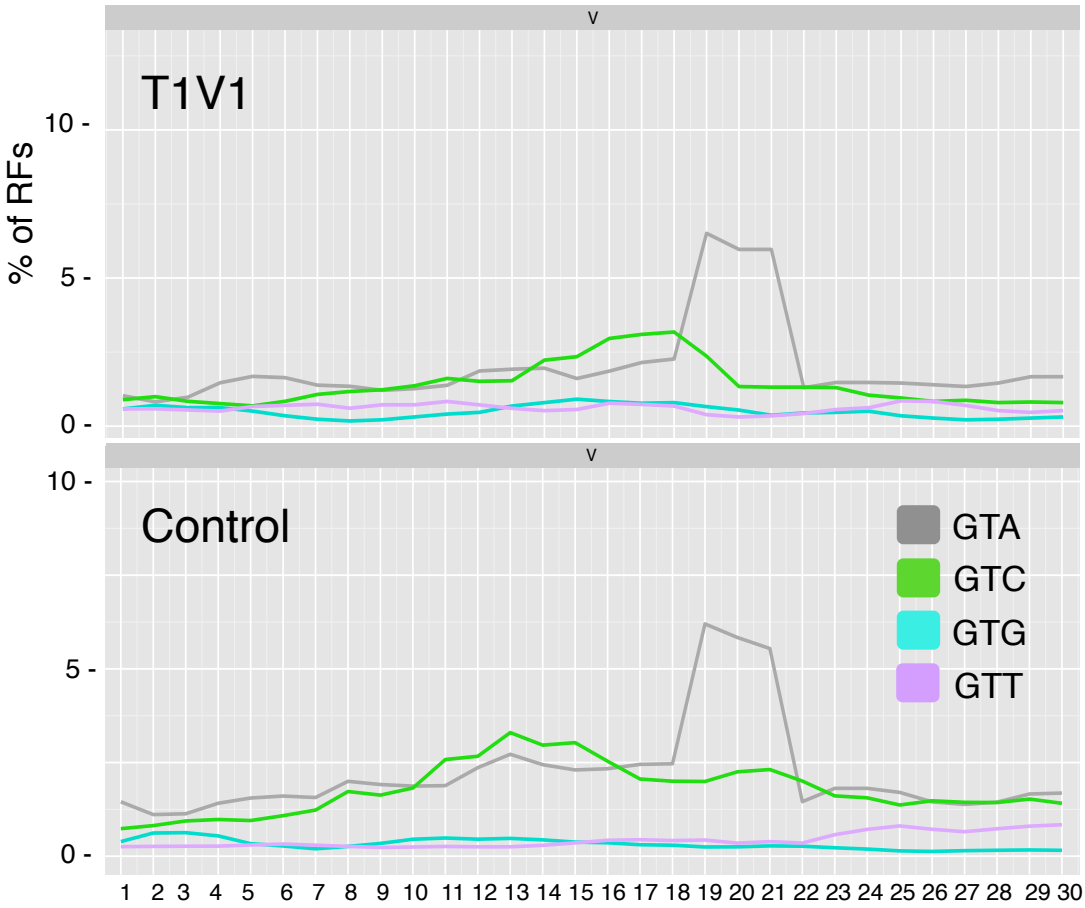

Figure 6.11. Position of different valine codons in RFs

Plots showing quantification of RFs with specific valine codon at various positions in T1V1 (upper panel) and control cell line (lower panel) were generated for each type of valine codon (GTA, GTC, GTG, GTT) separately. The x axis representing different offsets of all RFs containing one type of valine codon which 5' end starts at any possible position (1-30 nt, 5' – 3') in a predicted-sized footprint. The y axis represents a number of RFs with specific valine codon starting at each particular position. This number is presented as a percentage of all footprints with an amino acid codon starting at that position. The original plots were generated by Dr. John Grady.

Unlike in the first experiment (Fig. 6.6 B), for T1V1 cell line there was no strong enrichment in RFs with the valine codons beginning at 17th nt (Fig. 6.11 A). There was, however, a high accumulation of RFs with the GTA codon starting at 19th nt. This observation was made in both cell lines, hence it was most likely caused by a factor other than tRNA^{Val} level-induced stalling. To complete the investigation of potential stalling on valine codons, the RFs with Val sequences at the 17th position were then grouped based on the type of codon (as in 6.8). Quantification and comparison of the proportion of RFs with specific type of Val codon in the A-site is presented in Fig. 6.12.

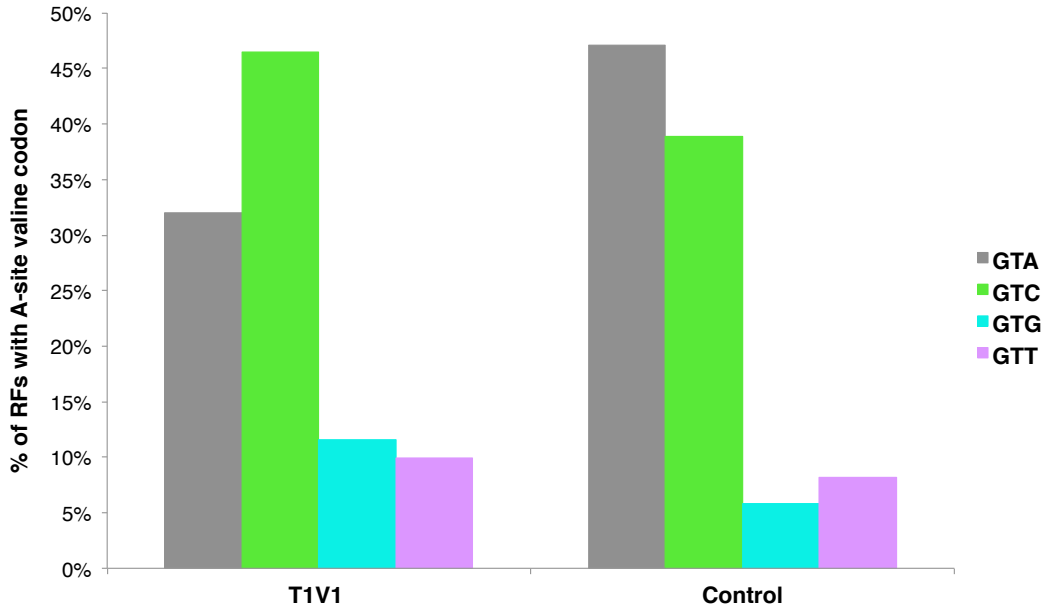

Figure 6.12. Quantification of RFs with A-site valine codon based on the type of the coding triplet

RFs with valine at the 17th nt from the 5' end were grouped according to the type of valine codon (GTA, GTC, GTG or GTT) at that position. Number of RFs in each category was presented as % of all RFs with valine at 17 nt. Graphs were generated for each of the cell lines: wild type control (Control), uninduced T1V1 (Tet-) and induced T1V1 (Tet+).

T1V1 sample analyzed in the first experiment (Fig. 6.8) was characterized with much higher proportion of A-site GTC-containing RFs than the control. Footprints of ribosomes translating valine, derived from wild type cells, were more enriched in GTA codons, which are also more abundant in mtDNA (Fig. 6.9). Analysis of the data from the repeated experiment also showed a change in the proportion of Val codons in favor of GTC in T1V1 cell line (Fig. 6.12). However, the change is not as dramatic as in the first experiment. The proportion of GTA and GTC-containing RFs in the control cell line (Fig. 6.12) is similar to the control in first experiment (Fig. 6.8)

Enrichment in RFs with valine codon at position 19 observed in both cell lines was unexpected, hence to investigate the matter further other amino acid coding sequences were analysed. The analysis was focused on finding other codons occupying a specific position within the footprint, which abundance was equally high in both cell lines. Such codons were identified, apart from valine, for methionine, alanine, histidine, glutamine and leucine (Fig. 6.13).

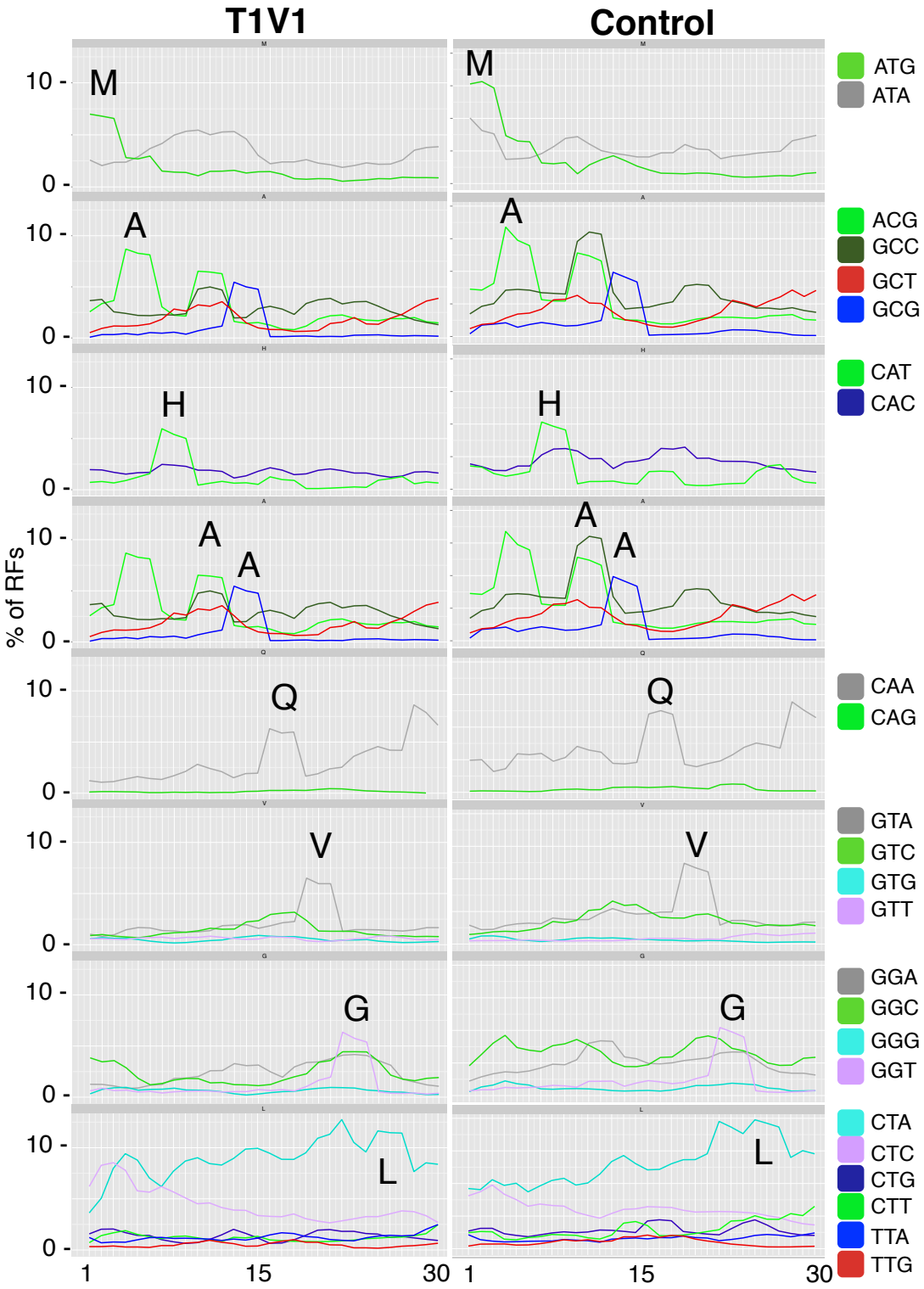

Figure 6.13. Comparison of different amino acids' positions in RFs shows a dominant pattern

Plots showing quantification of RFs with specific amino acid (M, A, H, Q, V, G and L) codons at various positions in T1V1 (left panel) and control cell line (right panel). A separate plot was generated for each of the coding triplets. The x axis representing different offsets of all RFs containing one type of valine codon which 5' end starts at any given position (1-30 nt, in 5' –> 3' direction) in a predicted-sized footprint. The y axis represents a number of RFs with specified codon starting at each particular position. This number is presented as a percentage of all footprints with an amino acid codon starting at that position. The original plots were generated by Dr. John Grady.

When the results for these amino acids were put together it was observed that they form a pattern. High number of RFs with methionine-ATG codon starting at the very 5' end prompted that the pattern may have been a specific polypeptide sequence. Indeed the MAHAAQVGL formed with the subsequent areas of high RFs densities is found at the beginning of COX2 sequence. To investigate participation of RFs from COX2 translation and compare it to other polypeptides, a number of RFs from each transcript was calculated. The results for each individual transcript were presented as percentage of all mt-transcripts (Fig. 6.14).

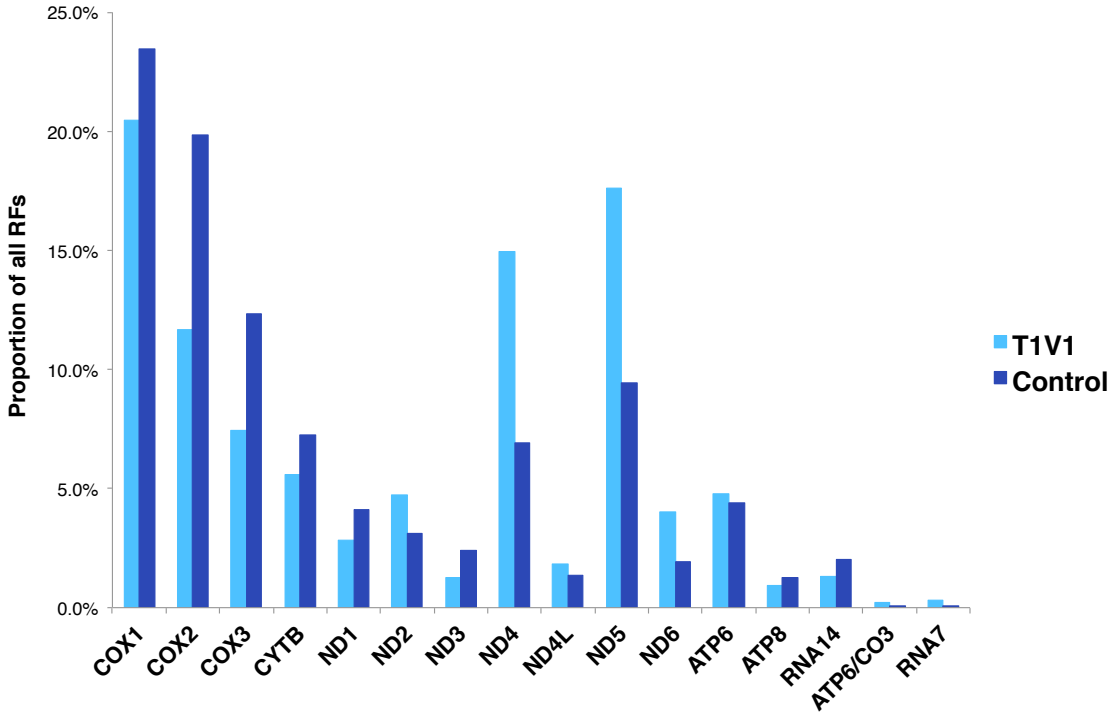

Figure 6.14. The ribosome footprint (RFs) abundance on each mt-ORF from the T1V1 and control cell lines.

The analysis was performed on data derived from T1V1 and control cell lines. The number of ribosome footprints (RFs) originating from mitochondrial ORF was calculated for each individual transcript. The results per ORF were presented as the percentage of the total number of mitochondrial RFs.

When mitoribosome abundance was compared between the transcripts, those captured on COX2 were second most represented group in control cell line and fourth in T1V1. The most abundant group of RFs in both cell lines was COX1. There was also a high number of RFs generated from COX3 (in control), ND5 (T1V1) and ND4 (T1V1). However, it was COX2 with its N-terminal sequence that seemed to have the most impact on the general population of RFs (Fig.

6.13).

In order to investigate the distribution of RFs across COX2, detailed mitoribosome profiles were generated for this ORF in both T1V1 and control cell lines (Fig. 6.15). For the comparison, similar profiles were also generated with data from the first experiment.

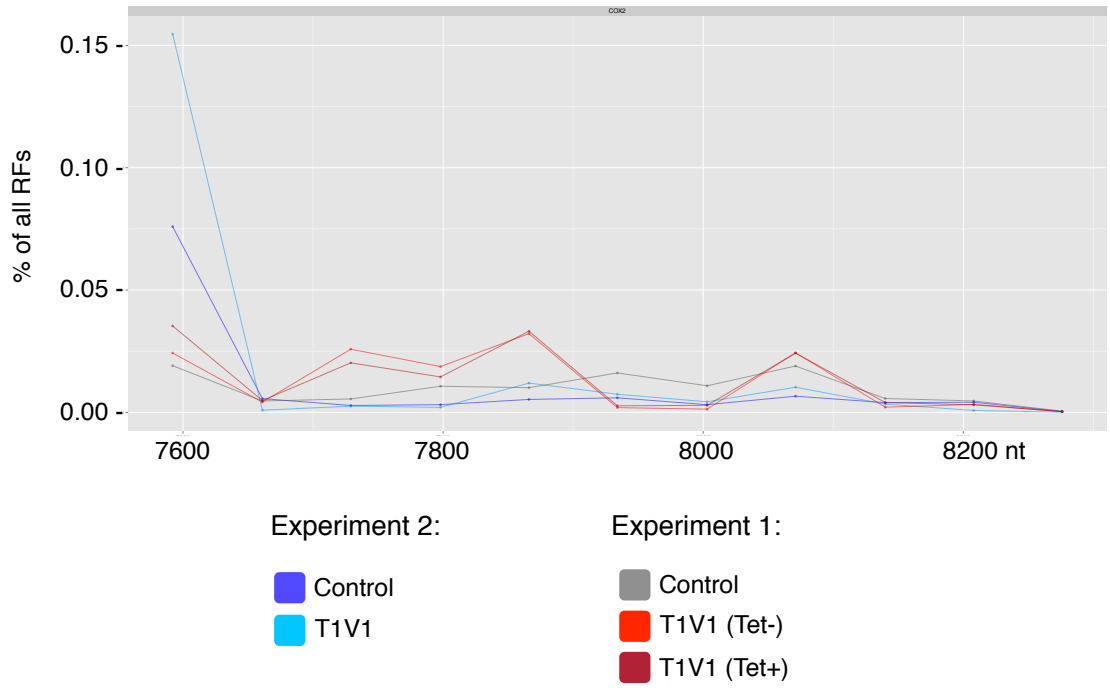

Figure 6.15. Distribution of RFs across *MT-CO2* in T1V1 and control cell lines from both ribosome profiling experiments

Distribution of the RFs across *MT-CO1* experiment 2 (T1V1 and control cell line) and experiment 1 (T1V1 –Tet, T1V1 +Tet and control) was plotted as a number of RFs (represented as a percentage of all RFs in experiment, Y axis) aligning to each position within this mt-mRNAs. The X axis presents the full length of the transcript in nucleotides. The original plot weas generated by Dr. Fei Gao.

In both cell lines analysed in the second experiment (Fig. 6.15, Control and T1V1) the majority of RFs was accumulated at the 5' end of the *MT-CO2* transcript (approximately first 50 nt). This result confirmed the pattern observed for RFs separated based on specific amino-acid codons (Fig. 6.13). The participation of RFs originating from the beginning of this transcript was so high that it was visible on individual aminoacid-coding sequences distribution. The high abundance of RFs from COX2 observed in general population of RFs (Fig. 6.14) was caused mainly by footprints from 5' end sequence. As they are the most highly represented across the whole length of transcript, their contribution was the most important. It also explained why the valine codon distribution

was different in the repeated experiment than in the first one (Fig. 6.6 B). The proportion of the RFs at the beginning of *MT-CO2* in all 3 cell lines from experiment 1 is much lower than in experiment 2 (Fig. 6.15). Therefore the pattern of valine-containing footprints distribution was a representation of all transcripts not just the COX2.

6.5. Complementary RNAseq analysis of T1V1 and control cell lines

Ribosome profiling data provide information on the occupancy of ribosomes across the transcript. If this analysis is combined with the measurement of the transcript levels through RNAseq, it can be used to assess the efficiency with which each transcript was translated. For this purpose, while preparing cells for the ribosome profiling (repeated experiment on T1V1 cell line), an additional plate (1x diam. 15 cm per condition) was cultured in parallel for RNAseq analysis. Control 143B and T1V1 uninduced cell lines were treated with chloramphenicol (100 µg/ml, as described in 6.2.) then washed with PBS with chloramphenicol, stripped and resuspended in 5 ml Trizol. The Trizol samples were stored at -20°C and then sent to the Netherlands Cancer Institute, Amsterdam to be sequenced at the Genomics Core Facility. The RNA isolation and subsequently the sequencing library was prepared with TruSeq RNA Sample Preparation Kit v2 (Illumina, detailed in (Rooijers et al., 2013). The sequencing of the libraries was performed with Illumina HiSeq2000 (single-read sequencing).

After receiving the raw data (Appendix 1.4, Table A2, samples 'rp2'), the high quality of data was confirmed with FastQC software (http://www.bioinformatics.babraham.ac.uk/projects/fastqc/). Having established that the quality of these data was sufficient for the analysis, I proceeded to perform the alignment with the reference genome using TopHat2 software (http://ccb.jhu.edu/software/tophat/index.shtml). The reference sequence was provided from GRCh37 human genome. The alignment results (accepted_hits.bam file in the TopHat output directories) for each of the individual samples were assembled into transcripts using Cufflinks (http://cole-trapnell-lab.github.io/cufflinks/). The output files of the transcriptome assembly (*.cuff) from both samples were then merged together into one file with Cuffmerge (http://cole-trapnell-lab.github.io/cufflinks/cuffmerge/). Finally, using Cuffdiff (http://cole-trapnell-lab.github.io/cufflinks/cuffdiff/) the differences in

transcript abundance between the two samples and their significance were calculated. The results (*_gene_exp.diff) were exported to excel for further analysis, i.e. comparison of the steady state levels of each mitochondrial transcript between the two cell lines. The level of individual mt-transcript expressed in FPKM, fragments per kb of transcript per million reads was presented on the plot (Fig. 6.16).

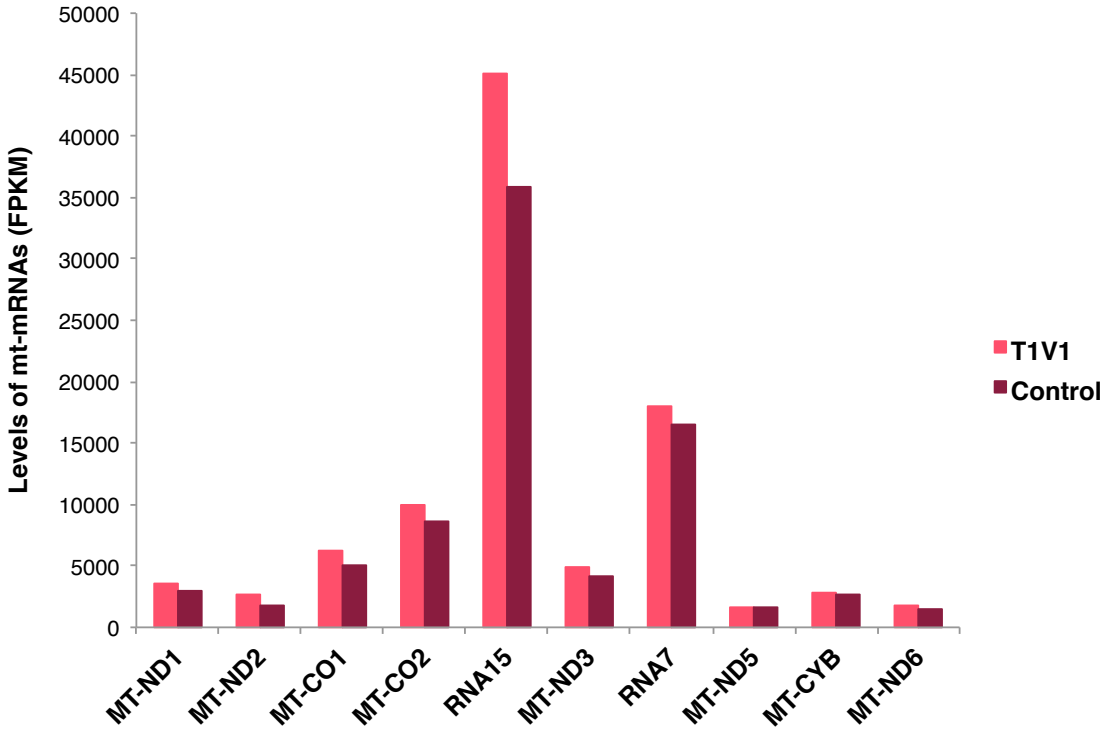

Figure 6.16. RNAseq analysis shows no varition in mt-mRNAs expression between T1V1 and control cell lines

Levels of each mt-mRNA expression (in FPKM), derived from the analysis with Cufflinks software, for both cell lines: T1V1 and Control are plotted pairwise to facilitate comparison.

There was very little variation in levels of mt-mRNAs between the samples, which suggested that the mutation in 1624C>T *MTTV* does not affect the steady state levels of mt-transcripts. In both cell lines the most abundant transcript was *RNA15*, which corresponds to *MT-ATP8*, *MT-ATP6* and *MT-CO3.* Second most represented transcript was *RNA7* (*MT-ND4* and *4L*), followed by *MT-CO2*. In order to compare the abundance of the specific templates with the number of RFs generated from it the RNAseq data (presented as % of all mt-transcript as in Fig. 6.16) was combined with RFs abundance data (Fig. 6.14). In RNAseq results the gene annotation for the mitochondrial transcripts in the reference

genome included two polycistronic transcripts (*RNA15* and *RNA7*) unlike during the ribosome profiling analysis. Therefore the RFs from transcripts forming *RNA15* and *7* were summed, including those aligning to the overlapping sequences, or spanning both transcripts. Having both ribosome profiling and RNAseq data sets prepared, they were utilized to calculate the translational efficiency (TE) ratio. For each transcript, the number of RFs originating from it (% of all RFs) was divided by this transcript's level (% of all mt-transcripts) giving its TE ratio. TE ratio was calculated for all mt-transcripts in both T1V1 (Fig. 6.17 A) and control (Fig. 6.17 B) cell lines. The higher the TE ratio value, the more mitoribosomes were captured translating it but with fewer of the available template. Therefore the high TE ratio value can be interpreted as high activity of translation of a particular transcript that would result in high level of synthesized protein. Alternatively, it can be caused by high level of stalling. The TE value that was close to 1 meant that the representation of RFs from this particular transcript is similar to how the level of this transcript is represented in the pool of all mt-transcripts.

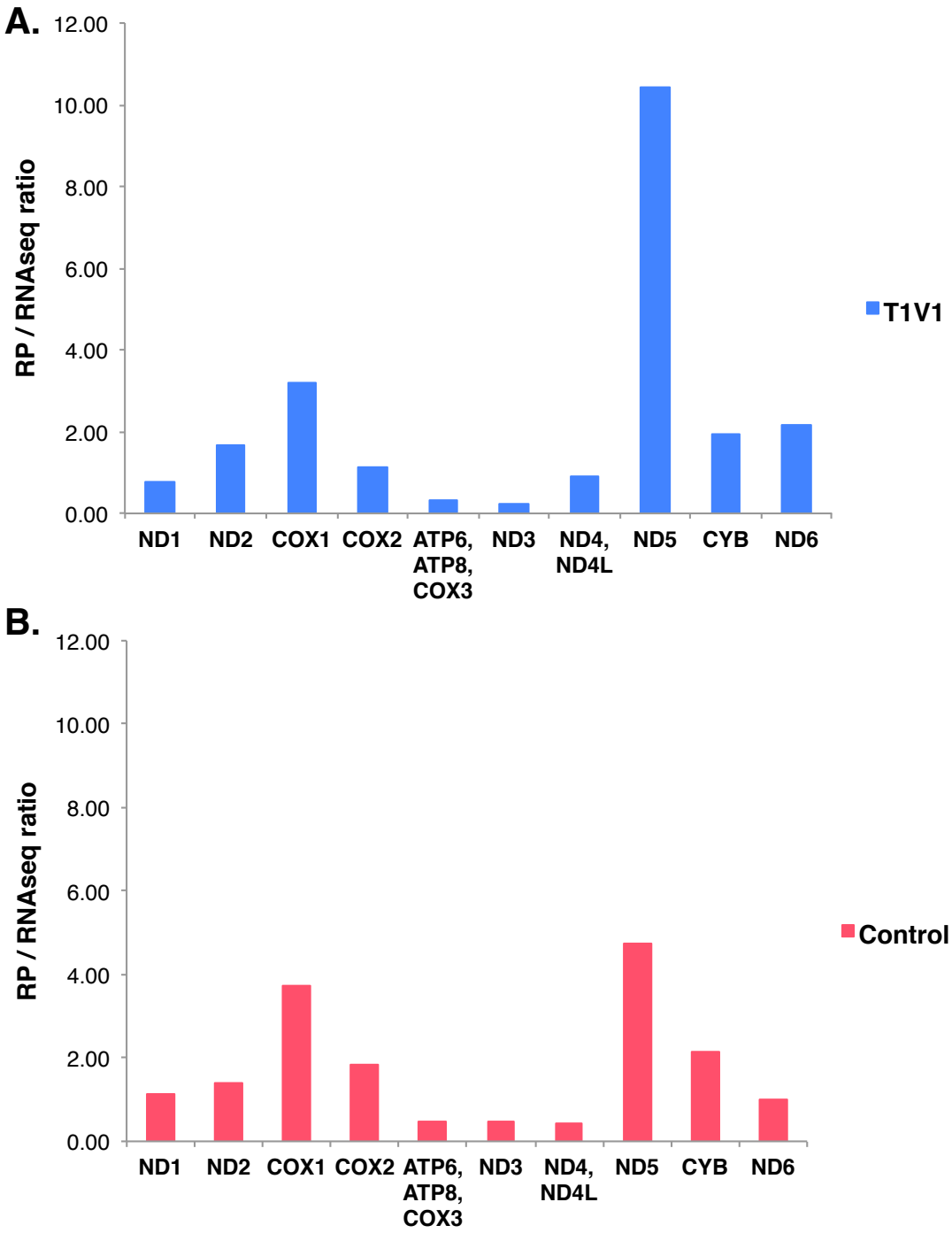

Figure 6.17. Comparison of the translation efficiency ratio shows differences between the cell lines

Translational efficiency (TE) values were calculated for each mt-ORF by dividing the RFs number originated from it (presented as % of all RFs) by the mt-mRNA levels (presented as % of all mt-transcripts). TE values for all mt-ORFs were generated for T1V1 (panel **A**) and control (**B**) cell lines separately.

In both cell lines the highest TE ratio value was observed in case of ND5, followed by COX1. In comparison ATP6-ATP8-COX3, ND4-ND4L and ND3 were characterized with low TE value (≤1), meaning the proportion of RFs from

these ORFs was lower, or equal the proportion of the template. This observation was especially interesting in case of the two polycistronic templates. Even though these templates' levels were high (Fig. 6.16) the amount of footprints originating from them was not proportional, which suggests low translational efficiency.

The TE value for COX2, an ORF that was a source of high number of ribosome footprints (Fig. 6.14), were not as high as expected. However, in addition to very high proportion of RFs, the level of *MT-COX2* was also relatively high (Fig. 6.16), hence the TE ratio value was between 1 (T1V1) and 2 (Control). Another interesting result was obtained for ND6. As the only polypeptide translated from the anti-sense template the ND6 is though to be expressed at a very low level. However, the calculation of TE showed the value of 1 (control) or 2 (T1V1) which is higher than ND3 of both polycistronic templates. This suggested that translation of ND6 might be more effective than previously assumed.

When comparing the results between the cell lines the most striking difference was observed in the ND5 TE value, which in T1V1 cells (Fig. 6.17 A) is 2x higher than in the control (Fig. 6. 17 B). In T1V1 cells, there was 10x more RFs generated from this transcript in comparison to what could be expected based on the transcript level. For some reason this template generated a very high amount of RFs, which was even higher in the T1V1 cell line.

6.6. Validation of VARS2L overexpression via qPCR and screening of different T1V1 clones

The comparison of the ribosome profiles of T1V1 samples did not show any significant changes between the induced and uninduced samples. It was an indication that the expression of the VARS2L protein, necessary for the rescue of low levels of mt-tRNA^{Val}, might not have been successful. In order to investigate if the induction with tetracycline was successful in causing the overexpression of VARS2L, the remaining cell lysate (retained after RNase treatment) was analyzed by western blotting and antibodies specific to VARS2L. In the original study on the T1V1 cell line the endogenous levels of VARS2L were very low and detection was only possible in samples where high amounts of mitochondrial proteins were used (100 µg of mitochondrial lysate). Since mitochondria were not isolated for the mitoribosomal profiling, such a blot could not been replicated in validation of the VARS2L induction as the only

remaining material from ribosome footprints generation was a total cell lysate. Thus, these total cell lysates from each sample (240 µg) were separated on the 8% SDS-PAGE (2.5.5), unfortunately this proved to be insufficient material to detect endogenous levels of VARS2L protein. However, there was no signal in any of the cell line samples, which suggested that the induction to cause overexpression of VARS2L did not work. In the absence of the positive control it was not possible to confirm if the lack of detection was caused by the antibodies not working. Instead, in order to definitely confirm the lack of the VARS2L overexpression, other than the western blot method had to be chosen. It was decided to use a real-time quantitative PCR (qPCR) instead. This method allowed for the measurement of the VARS2L mRNA levels in RNA isolated from cells used in ribosome profiling experiments and stored in Trizol. First, the primers specific to *VARS2L* gene were designed using the PrimerQuest on-line tool (http://eu.idtdna.com/Primerquest/Home/Index).

Table 6.16. VARS2L qPCR primer sequence

Type	Name	Sequence
Forward	VARS2LqPCRFor	5' CTGATGCAGAGGTTGTGGTAG 3'
Reverse	VARS2LqPCRRev	5' GCCCGTGTAGATGTGTGTATC 3'

The RNA was isolated from cells resuspended in the Trizol solution and stored (at -20°C) for RNAseq experiments. From thawed samples, 1 ml of Trizol solution was taken and incubated at room temp for 5 min. The isolation was performed according to manufacturer's instructions. From each samples 300 ng of RNA was taken and used as a template for cDNA synthesis. Reverse transcription was conducted with SuperScript VILO Master Mix (Invitrogen, Table 6.17).

Table 6.17. Component and condition of the reverse transcription reaction

Components	Volume
RNA sample (300 ng)	1 µl
SuperScript VILO Master Mix (Invitrogen, Cat. No: 11755050)	4 µl
H_2O	15 µl
Temperature	**Time**
25ºC	10 min
42ºC	60 min
85ºC	5 min
4ºC	∞

To test the efficiency of the designed VARS2L primers, a qPCR reaction was performed on a dilution series of the 143B control cDNA template. The dilutions used were as follows: 10^{-3}, 10^{-4}, 10^{-5} and 10^{-6}. The components and conditions of the reaction were as in 2.4.4.

The averaged C_T for each dilution was plotted and the slope of the standard curve was used to calculate the efficiency of the amplification:

$$E = 10^{\frac{-1}{slope}}$$

For a 100% efficiency of the reaction (when the amount of PCR product doubles which each cycle, E=2) the optimal slope of the standard curve should be -3.32. The slope of the standard curve calculated for VARS2L primers on 4 template dilutions was -3.33 (boxed in Fig 6.18), which corresponds with a 99% efficiency of the reaction.

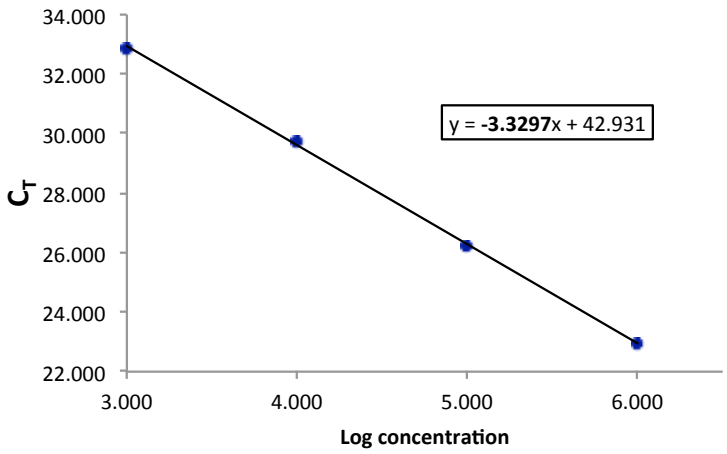

Figure 6.18. Calculation of the VARS2L primers amplification efficiency

Efficiency of the amplification with VARS2L primers was determined using qPCR with serial dilution of the cDNA template (10^{-3} - 10^{-6}). The averaged C_T (from 3 technical replicates) was calculated for each template dilution and plotted against the log of its concentration to generate a standard curve. The equation with a calculated slope of the standard curve is boxed above the trendline.

After the validation of the efficiency, primers were used for the actual experiment investigating the VARS2L overexpression in the cell samples used in ribosome profiling. The previously prepared cDNA samples (uninduced T1V1 "-Tet", induced "+Tet", and 143B control) were used as templates without dilution. The 18S rRNA served as a reference gene. The conditions of the reaction were the same as described (2.4.4). The averaged $C_{T\ for}$ VARS2L was compared between uninduced and induced cell lines and normalized to the

reference gene. The difference in expression of VARS2L was calculated using the following equation (Livak and Schmittgen, 2001):

$$2^{-\Delta\Delta C_T}$$

where:

$\Delta\Delta C_T = C_{T\,(VARS2L)} - C_{T\,(18S)}$

$\Delta C_{T\,(VARS2L)} = C_{T\,(VARS2L,\ +Tet)} - C_{T\,(VARS2L,\ -Tet)}$

$\Delta C_{T\,(18S)} = C_{T\,(18S,\ +Tet)} - C_{T\,(18S,\ -Tet)}$

The difference in the *VARS2L* mRNA levels between the induced and uninduced T1V1 cell line in both ribosome profiling experiments was 1.08 and 1.09 fold respectively. This indicated that in the supposedly induced cells the transcript levels were not significantly higher than endogenous levels. In order to identify the changes to mitoribosome profiles that could be caused by the mt-tRNA^{Val} deficiency, the T1V1 profiles had to be compared to 143B parental control.

Since these results indicated that there was no increase in VARS2L expression in any of the induced samples it meant there was no potential for rescue of the deleterious phenotype. This meant that without the VARS2L overexpression both T1V1 cell lines used in ribosome profiling experiments could only be treated as replicates of the mutant cell line. The analysis of VARS2L expression was also conducted on samples (induced and uninduced T1V1 cell lines) from the second ribosome profiling experiment. Results confirmed the lack of VARS2 overexpression in the induced sample. It was, therefore, excluded from the analysis and the uninduced T1V1 cells were compared against wild type control. It is not uncommon for cell lines to stop expressing proteins, particularly in lines that do not utilize the Flp-In cassette, as was the case with these lines. The cell line tested originated from one frozen aliquot that had been maintained in culture over an extended period of time. To investigate if other, previously preserved aliquots of T1V1 cells still retained the ability to inducibly express VARS2L, 3 more cell samples were tested. These were all aliquots of T1V1 cells but handled and stored by different people prior to my experiments. For the sake of this experiment they were labeled: “DYG” (frozen by Dyg Pertiwi Kamal), “HTH” (Dr. Hue Tran Hornig-Do) and “MW” (myself; the aliquot frozen before the ribosome profiling experiments). After three days of induction with

tetracycline, the total RNA was isolated and converted to cDNA as described above. Levels of VARS2L expression were tested and calculated by qPCR. Comparison of the results between induced and uninduced cells showed that only the “DYG” sample displayed an increase in expression of VARS2L to a level of 150% of control (Fig. 6.19 A). In order to eliminate inactive tetracycline as the cause, a parallel 3-day induction of the HEK-C12orf65-FLAG cell line was performed using the same aliquot of the reagent. Total cell lysate from induced and uninduced cells was separated by 15% SDS-PAGE and analysed via western blotting with antibodies specific to FLAG. The strong signal from C12orf65-FLAG samples (Fig. 6.19 panel B, lanes 1 and 3) indicates that the activity of the tetracycline aliquot used in experiments was sufficient to induce overexpression. Absence or a very low level of VARS2L expression in tested cell aliquots was not caused by inactive tetracycline.

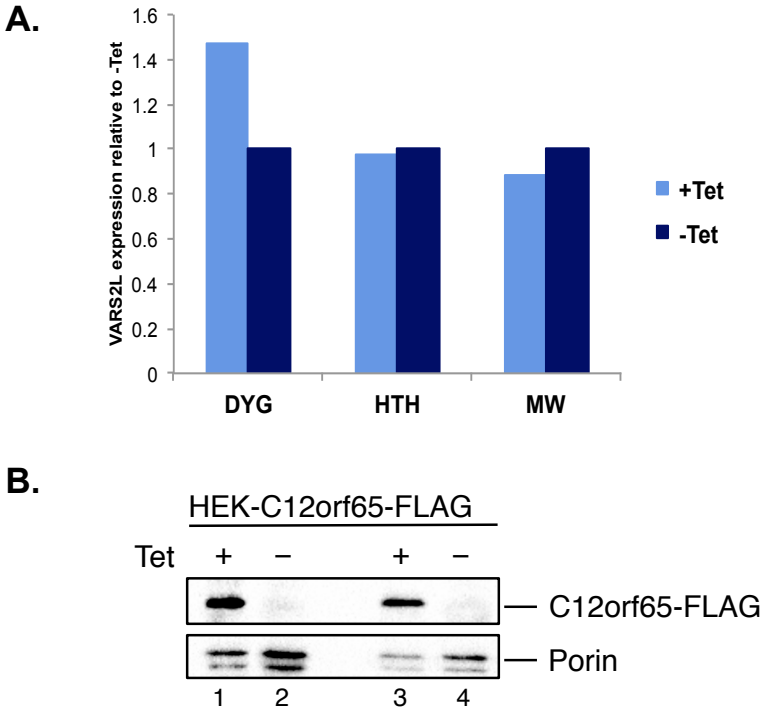

Figure 6.19. Screening for the VARS2L expression in different T1V1 cell aliquots

VARS2L induction was tested in three aliquots of T1V1 cell lines (DYG, HTH and MW), handled and stored in liquid nitrogen by different people, prior to the ribosome profiling experiments. Induction with 1 µg/mg tetracycline was conducted for 3 days, after which the levels of *VARS2L* transcript were measured with qPCR. **A**. Expression of VARS2L in induced cells was calculated based on the *VARS2L* levels normalized to 18S rRNA levels and represented in relation to endogenous expression in uninduced cells. **B.** Tetracycline activity was confirmed in a parallel experiment on HEK293 cell line stably transfected with C12orf65-FLAG. Total cell lysate (50 µg per lane) of both un- (lanes 2 and 4) and induced cells (lanes 1 and 3), was subjected to western blot analysis with antibodies specific to the FLAG tag. Detection of porin served as a loading control.

6.7. Generation of a WARS2 in pcDNA5/FRT/TO construct as a part of the collaboration with Professor Agami

The collaboration with Prof. Agami's group also involved a contribution from my host laboratory that would further substantiate their mitoribosomal profiling data. The objective of this work was to assist in the generation of a cell system similar to T1V1, where low levels of a given mutant mt-tRNA could be rescued by inducibly overexpressing the cognate aa-tRNA synthetase. The chosen subject for this system was the cell line harboring the homoplasmic mutation in mt-tRNA^{Trp} that had been used as the model for mitoribosome stalling in the publication (Rooijers et al., 2013). The potential rescue mechanism required generation of the construct containing mitochondrial tryptophanyl-tRNA synthetase (WARS2) in pcDNA5/FRT/TO vector. This construct could then be used for either transient or stable transfection of mammalian cells. The insert, comprising the full length WARS2 CDS (1082 bp), was generated via PCR from the pool of cDNA derived from 300 ng cell total RNA (2.3.1). Primers for this reaction were designed to include restriction sites for HindIII and XhoI enzymes at the 5' and 3' termini respectively (Fig 6.20). The FLAG encoding sequence was also added so that the resulting protein was tagged at C-terminus and was easily detected via western blotting.

Figure 6.20 Primers for WARS2 cloning

Primer sequences were designed to amplify full length WARS2 ORF. Highlighted are the digestion sites for the restriction enzymes (HindIII and XhoI) and the sequence encoding a protein tag (FLAG).

The insert was cloned into pcDNA5/FRT/TO vector via the XhoI/HindIII sites (2.3.4). Transformation of *E. coli* α- select chemically competent cells (2.2.1) with the generated construct resulted in 5 clones (designated as clones 5,

12, 13, 14, 16) that contained the full length of the insert (Fig 6.21 A lanes 7, 14, 15, 16 and 18). The correct integration and orientation of the insert in all 5 clones was confirmed by PCR amplification with the primers specific to the vector sequences flanking the insert (Fig. 6.10 C). Finally Sanger sequencing (2.3.9) of the isolated plasmids revealed that only clone 13 contained no mutations and therefore it was suitable for use in transfection of cell lines. The plasmid isolated from that clone was sent to the Netherlands Cancer Institute for future applications.

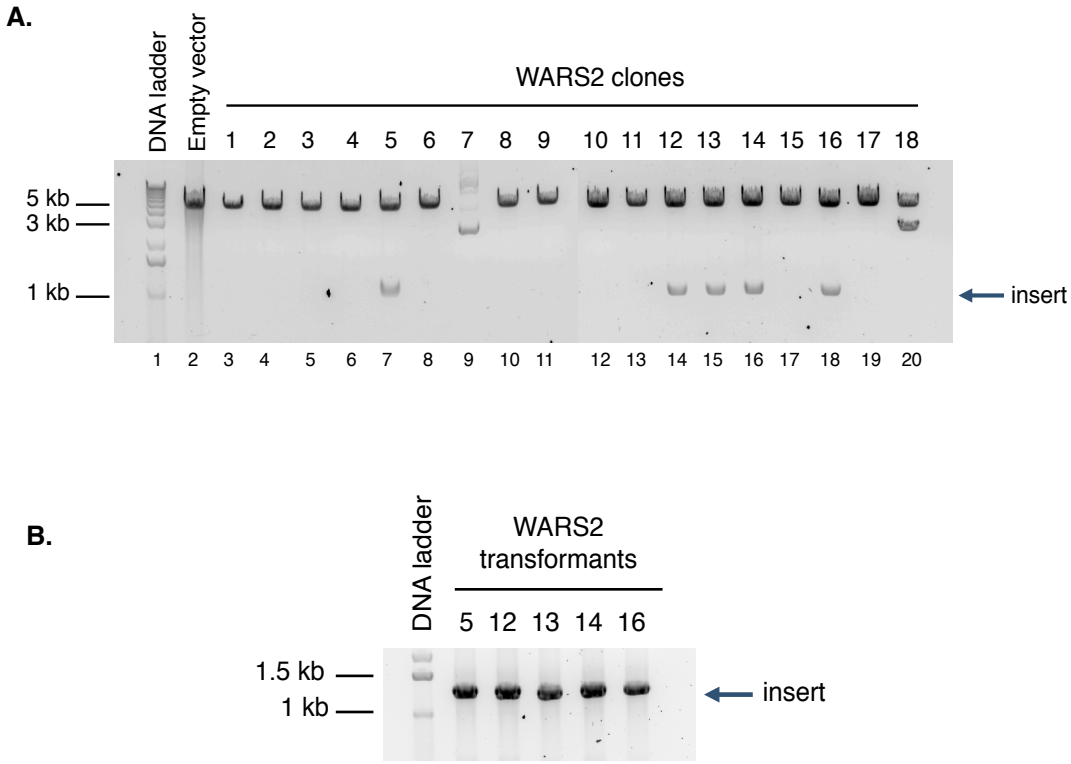

Figure 6.21. Cloning of the WARS2 into pcDNA5/FRT/TO

A. Plasmids isolated from 18 clones selected after transformation were digested with HindIII and XhoI enzymes (2.3.4) to confirm the presence of the insert (indicated by the arrow, (~1.1 kbp). An empty pcDNA5/FRT/TO vector digested with HindIII and XhoI was used as a negative control (lane 2). **B**. PCR products generated with vector specific primers flanking the insert (CMV-For and BGM-Rev, see Table 6.18) were separated by agarose gel (1%) electrophoresis to confirm the expected size of the insert in plasmids from 5 positive clones. The product is indicated by the arrow (> 1.1 kbp).

Table 6.18. PCR primers for pcDNA5/FRT/TO vector

Name	Sequence (5'-3')
CMV Forward	CGCAAATGGGCGGTAGGCGTG
BGH Reverse	TTAGAAGGCACAGTCGAGG3

6.8. Discussion

The changes to the mitoribosome profiling protocol that was developed for the sequencing with the IonTorrent (Ch. 5) were necessary, as it did not yield satisfactory results. Therefore, as a result of a collaboration with Prof. Agami's group, an entirely different protocol was introduced. This method characterized with simplified footprint generation step (6.2) and a library preparation method (6.3), with separate ligation reactions followed by electrophoresis, that allowed monitoring of the amount of product at most of the steps. Protocol was proven to be successful in analyzing mitochondrial translation including stalling of the mitoribosomes (Rooijers et al., 2013). The cell line selected to test this protocol, named T1V1, was characterized with lower level of aminoacetylated form of mt-tRNA^{Val} (Hornig-Do et al., 2014). This was a potential reason for mitoribosomes to stall on valine codons. The ability of T1V1 cell line to inducibly express VARS2L was an additional advantage as it provided the opportunity to perform the rescue experiment (Hornig-Do et al., 2014; Rorbach et al., 2008b). Therefore, this cell line was appropriate for first mitoribosome profiling application and to test the hypothesis of tRNA-induced stalling. The goal was to compare the mitoribosome profiles of uninduced T1V1 mutant cells with VARS2L-expressing cells and wild type control. Special focus was on the valine codons and the potential increase in mitochondrial ribosome footprints (RFs) accumulation. Unfortunately the rescue experiments (samples labeled 'T1V1 Tet+') were not successful as the induction of VARS2L expression failed. The loss of expression of the introduced gene in stable cell lines is not uncommon. While T1V1 cell line was generated, the stable transfection of VARS2L was performed on *trans*-mitochondrial cybrids containing the mt-tRNA^{Val} mutation (Rorbach et al., 2008b). This was not a Flp-In TRex cell line, which would contain the Flp cassette, hence it did not allow to control where the expression vector was integrated. With continuous passages of the cells, especially if the selection conditions (blastocidin^{S} addition to the medium) were not rigorously kept it is possible for the cell line to cease the expression of the introduced gene. Careful handling and extended monitoring of the expression levels for these cell lines would be advised if they will be used in the future.

However, even without the functional rescue system, the analysis of generated data was possible. Both mutant cell lines (Tet- and Tet+), treated as repeats of the same sample, were compared to the wild type control (ribosome

profiling data from (Rooijers et al., 2013). Investigation of the potential stalling due to the deficiency of the valyl-tRNA was commenced with identification of the footprints derived from mitoribosomes that were currently translating valine codons. This required estimation of the position of A-site in mitoribosomal footprints. In cytosolic ribosome profiling it was observed that within a given CDS the footprints' 5' ends would start abruptly 12 to 13 nt upstream of the start codon, corresponding to the position of the initiating ribosome. This observation led to the estimation of the A-site position within footprints as 15-16 nt from the 5' end (Ingolia et al., 2009). This method, however, could not be applied to the mitoribosome profiling data generated with the described protocol. Since human mitochondrial transcripts characterize with very short (maximum 3 nt) 5' UTRs (Anderson et al., 1981), mitoribosomes at the initiation stage possibly overhang from the 5' end of the mRNA. Therefore the fragment protected by the initiating mitoribosome is predicted to be much shorter (approximately 18 nt). The size selection step of the RNA fragments (6.2 and Fig. 6.2) includes only sequences between 25-35 nt so the footprints of the mitoribosome during initiation were most likely not selected.

Different offsets of valine-coding sequences were tested (with 5' at any possible position within RFs). The difference in the number of RFs between the mutant and control cell lines was visible when valine codons were positioned beginning at 17 nt, (Fig 6.6 B and 6.7). This position was assumed to be the beginning of the mitoribosomal A-site. The RFs with valine codon occupying it were treated as derived from the ribosomes in the state of translating and incorporating valine into the nascent polypeptide. The higher number of RFs with A-site valine codon suggested that the deficiency of charged $tRNA^{Val}$ was possibly causing mitoribosome stalling at Val sequences.

It is also possible that the type of the valine codon was influencing the potential valine-related stalling. In mutant cell lines, higher proportion of RFs with A-site valine contained the GTC codon (Fig. 6.8), even though it was not the most abundant valine triplet in human mtDNA (Fig. 6.9 B). In control cell line majority of these RFs contained the GTA codon at A-site, which was consistent with its frequency in mtDNA. The possible explanation for this result was that with the lower levels of charged mt-$tRNA^{Val}$ the stalling time of the mitoribosome over valine codon would be increased because of the wobble base pairing of the GTC (5'-3') and CAT (3'-5') of tRNA's anticodon. Similar situation was

observed in *C. elegans* where the G:U wobble base pairing caused accumulation of ribosomes higher than during G:C pairing (Stadler and Fire, 2011). However, if the potential stalling of mitoribosomes on valine codons in T1V1 cell lines was visible analyzing the A-site valine RFs, it was not evident in the general mitoribosome profiles. The changes to the distribution of RFs (all aligned footprints, Fig. 6.10 A) across mt-transcripts between T1V1 and control did not coincide with the position of most-valine rich sequences (Fig. 6.10 B). The tRNA-induced staling, if present, was not affecting the global distribution of mitoribosome footprints.

Interestingly in the repeated mitoribosome profiling experiment the valine codons had even less influence on stalling position of mitoribosomes. These samples (both T1V1 and control) had a very high abundance of RFs generated from the 5' end of the COX2 open reading frame. It obscured the pattern of valine position in RFs from T1V1 that in first experiment contained valine at position 17 (estimated mitoribosomal A-site) at much higher level than control (Fig. 6.6). The preponderance of GTC A-site codons over GTA in T1V1 cells was, however, present but to a lower extent (Fig. 6.12). The usage of valine A-site codons in control was as seen in the first experiment (Fig. 6.8).

The prevalence of 5' end of COX2 was visible when analysing the number of RFs with specific amino acids in regards to their position within footprints (Fig. 6.13). This effect was shared by both T1V1 and control cell lines. The majority of RFs contained methionine codon at their very 5' end (M), followed by the alanine starting 3 nt downstream (A), then histidine (H), finally forming a sequence that could be translated into first 9 codons of COX2 (MAHAAQVGL). The analysis of RFs originating from COX2 (Fig. 6.14) and their specific distribution across the template (Fig. 6.15) showed that indeed the number of RFs at the 5' end of ORF surpasses those from other position. The general number of RFs from COX2 is high in comparison to other ORFs and vast majority of these footprints comes from the 5' end sequence, which justifies the influence on amino acid coding sequences. None of the cell lines analysed in the first experiment showed such high proportion of RFs at the 5' terminus of COX2 (Fig. 6.15). Therefore the imbalance in favor of COX2 RFs was not observed.

The complementary RNAseq analysis allowed additional analysis of the translational efficiency. It enables comparison of the amount of ribosome

footprints between the ORFs eliminating the influence of the template levels. The most interesting results were obtained for ND5, which was characterized with the highest TE value in both cell lines (Fig. 6.17 A and B) due to high RFs abundance (Fig. 6.14) in comparison to low levels of *MT-ND5* transcript (Fig. 6.16). Therefore, it resulted in a very high TE value, which could be interpreted as though ND5 is translated at a very high rate. When comparing the TE value between T1V1 and control cell lines, the TE value for the former is 2x higher than in control, which would correspond to even grater efficiency of translation. However, analysis of *de novo* mt-protein synthesis in T1V1 cells performed by Hornig-Do and colleagues showed that levels of newly-synthesised ND5 are lower than in control (Hornig-Do et al., 2014). If ND5 is indeed translated at higher rate in T1V1 cells, its turnover rate must be very high. Alternatively, the high amount of ribosome footprints generated from ND5 ORF is a result of mitoribosome stalling. The later could be explained by the high number of valine codons present in *MT-ND5*, which could induce stalling in T1V1.

In conclusion, the general pool of RFs in repeated experiment was dominated by COX2 5'-terminal sequences. This cell line- independent effect was not observed in the first experiment. It is possible that this result was caused by a bias during the ligation or amplification step. The higher than expected level of contamination with non-mRNA sequences and therefore smaller pool of mitoribosomal footprints in repeated experiment (approximately 5 $x10^4$, Table A1, samples '2934 1 and 2') could be the one of the factors that makes it more prone to bias. In order to increase the reliability of the results the mitoribosome footprint retention should be improved, for example by depletion of rRNA from cDNA pool via hybridization to biotinylated complementary probes. After the removal of hybridized rRNA (through streptavidin affinity) the amplified pool would be enriched in mRNA, and increase the number of informative sequence data.

Chapter 7

Analysis of C12orf65-depleted cell line with mitoribosome profiling

7.1. Introduction

The questions that my project repeatedly posed referred to potential quality control and ribosome rescue systems that operate in human mitochondria. To obtain a better understanding of these mechanisms and to identify the potential factors involved (namely C12orf65) was a motivation to implement ribosome profiling on human mitochondria. However, quality control and rescue of stalled mitoribosomes are not the only aspects of mitochondrial translation that are still undefined. In fact the knowledge of the molecular mechanisms governing protein synthesis in human mitochondria is very superficial. Many basic steps of this process, which are well described in bacteria or in eukaryotic cytosol, remain unrevealed for mitochondria. There are various reasons for this, one of which is the lack of a well-established in vitro system to conduct the necessary investigations. So far, despite the numerous attempts, no reliable, complete in vitro system for mitochondrial translation has been established (Christian and Spremulli, 2012; Chrzanowska-Lightowlers et al., 2011). The knowledge generated up to now is based on in vitro experiments that used purified mitoribosomes and a few factors that may not constitute the actual components operating in vivo (Chrzanowska-Lightowlers et al., 2011). A further difficulty with working on mitochondrial gene expression is the lack of proven successful method of transforming human mitochondrial DNA. Without the ability to manipulate the mitochondrial genome scientists must rely on patient cell lines carrying a specific mtDNA mutation. However, access to such cell lines can be limited and the investigation is restricted to only the particular defects that arise and not those that might be designed to help determine molecular mechanisms, leaving no flexibility to the experiments. All of the factors mentioned above contribute to the fact that our understanding of the mechanisms regulating mitochondrial translation is very limited. That is why, in order to broaden our knowledge of mitochondrial protein synthesis, it was necessary to devise an alternative experimental approach. Ribosome profiling provides a suitable tool to thoroughly investigate mitochondrial protein synthesis as it provides a genome-wide analysis of translation in vivo, which has not yet been achieved with previous methods. The analysis of the ribosome profiling results usually focuses on 3 main themes: 1) identification of the sequences that were actively translated (rather than pre-selected candidates), 2) monitoring of the protein synthesis (speed of ribosome progression) and maturation in vivo, 3)

measuring the efficiency of the translation (and how it is regulated) (Ingolia, 2014). These 3 approaches could be applied equally well to mitochondrial translation. The first and so far the only published data on ribosome profiling in mitochondria focuses on technical aspects of the methodology and general quality of data only (Rooijers et al., 2013). The characterisation of the typical features of mt-translation was not an objective of this study. Therefore the gap in our knowledge of mitochondrial gene expression in humans is still open. The analysis of mitoribosome profiles could potentially serve to characterize common features of mt-translation. For example it could identify regions within transcripts that accumulate high numbers of mitoribosomes. This would help understand what causes a decrease in mt-translation elongation. In addition to investigating local differences in mitoribosomal distribution a total number of ribosome footprints per transcript can be informative. When compared with the levels of mt-mRNAs expression, the abundance of mitochondrial ribosome footprints (RFs) could provide the information of each transcript's translation efficiency. Finally, identification of unusual translational events is one of the most important features of ribosome profiling analysis (Ingolia, 2014). Since mitochondrial transcripts do not contain long sequences upstream the initiation codon (Anderson et al., 1981) they cannot be considered as templates for unanticipated translation as described in eukaryotic cytosol (Ingolia et al., 2009). However, there are other regions in mitochondrial transcripts that can be investigated with this method, for example the overlapping sequences of the bicistronic transcripts including that which encodes *MT-ATP8* and *MT-ATP6*. Detailed analysis of the mitoribosome profiles from this region could help shed new light on the mechanisms of translation from the bicistrons with overlapping open reading frames.

In the final part of my project I applied the optimized ribosome profiling to the cell line after C12orf65 depletion. The protocol was proven successful in analysis of the stalled mitoribosomes in the mt-tRNA^{Val} mutant cell line, as described in chapter 6. The mitoribosome profiles generated were compared between the two samples (C12orf65- depleted and control) and between individual transcripts. Although it was later discovered (chapter 3) that the depletion level obtained with siRNA treatment is not sufficient to generate visible changes to mitochondrial translation, mitoribosome profiling results were not discarded. The analysis was continued hoping that changes to

mitochondrial gene expression, not detected with metabolic labelling and northern blot, would be visible in mitoribosome profiles. Finally, in case there were no differences between the depleted and control samples, the generated data would be a valuable source of information about the normal distribution of mitoribosomes.

In addition to the ribosome profiling, a parallel RNAseq experiment was performed on the same RNA samples. The ribosome profiling results were complemented with the corresponding RNAseq analysis in order to compare the efficiency of each mt-mRNA translation.

7.2. Generation of the footprints and sequencing library

For this experiment wild type HEK293 cells were seeded in 12x diam. 15 cm dishes. Out of these 12 dishes, 6 were treated with C12orf65 siRNA (siC12) and the other 6 with non-targeting siRNA (NT). The protocol was as described in (2.1.4) but scaled up for the much bigger volume of used dishes. Thus, 4.5 ml of OptiMEM, 66.6 µl of siRNA (20 µM) and 36 µl lipofectamine were used per dish. The treatment lasted 3 days and was followed by the preparation of the mitoribosome footprints, which was conducted as described in the previous chapter (6.2).

Briefly: Cells were first treated with chloramphenicol (100 µg/ml) for 15 min in order to inhibit the translation elongation and secure ribosomes at the place they were currently translating. After the incubation the cells were washed with PBS-chloramphenicol, stripped and pelleted. For each condition 1 dish was used for the RNAseq analysis, where cell pellets were resuspended in 5 ml Trizol and stored at -20°C. Before freezing, from each sample 0.5 ml of the Trizol cell solution was taken and stored in a separate tube at -20°C for the qPCR to analyse C12orf65 depletion levels. For the ribosome profiling the remaining 5 dishes per conditions were used and these cells were lysed with the lysis buffer (1-1.2 ml, 20 mM Tris-HCl pH 7.8, 10 mM $MgCl_2$, 100 mM KCl, 1% Triton X-100, 1X complete protease inhibitor, 2 mM DTT, 100 µg/ml chloramphenicol) according to the protocol described in more details in 6.2. The clarified lysed (after centrifugation 10 min, 560 xg, 4ºC) was subjected to the RNase 1 digestion (Ambion, final concentration 2.5 U/µl) for 45 min at room temperature with agitation. This step was necessary to remove the mRNA, which was not protected by ribosomes, i.e. not actively translated. Samples

after the RNase treatment were separated on the 7 – 47% isokinetic sucrose gradient. The gradient samples were prepared prior to the experiment (details in 6.3), the composition of the buffer was as follows: 20 mM Tris-HCl pH 7.8, 10 mM $MgCl_2$, 100 mM KCl, chloramphenicol (100 µg/ml) and DTT (2 mM). The whole of the lysate treated with RNase 1 was loaded on to the top of the gradient, tubes were then balanced and topped up with the lysis buffer to give a final and identical volume of 13.4 ml. The centrifugation was performed in the Beckman ultracentrifuge (SW40Ti rotor) at 35300 rpm (221632 xg), 4ºC for 2 h, with maximum acceleration and minimum deceleration. Next, samples of 935 µl were taken from top to bottom giving 14 fractions. From each fraction 20 µl was saved for the western blotting analysis in order to identify fractions containing the monosomes with protected mRNA fragments (ribosome footprints, RFs). Immunodetection with DAP3 (small subunit protein) and MRPL3 (large subunit protein) antibodies allowed confirmation of which sucrose gradient fractions contained mitoribosomes and therefore the RFs. Fractions 3 – 6, where the anticipated position of the mitoribosome was, were then treated with proteinase K (0.2 mg/ml proteinase K, 1% SDS for 30 min at 45ºC). For storage and subsequent RNA isolation, Trizol LS reagent was added to each sample in proportion of 3:1.

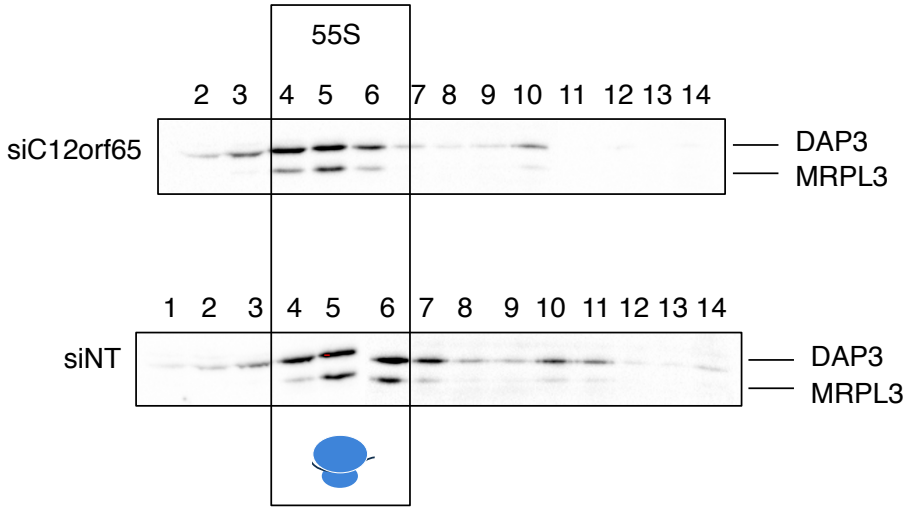

Figure 7.1. Separation of mitoribosomes by isokinetic sucrose gradient centrifugation

Cell lysates from HEK293 cells treated with C12orf65 siRNA (siC12orf65) or non-targeting siRNA (siNT) were subjected to digestion with RNase 1. Both samples were separated on 7 - 47% sucrose gradient and after ultracentrifugation divided into 14 fractions. Each fraction was subjected to western blotting with antibodies specific to small and large mitoribosomal subunits (DAP3 and MRPL3 respectively). Fractions that contained monosomes were defined by presence of signal from both proteins (box labelled “55S”).

The position of the mitoribosomes and potentially their RFs was estimated based on the presence of a strong signal from both mitoribosomal proteins (Fig. 7.1, DAP3, MRPL3). All fractions taken from both samples were analysed, except for the fraction 1 from the siC12orf65 sample, which was unfortunately lost during the fractionation. The position of the monosome was assigned to fractions 4 – 6 (Fig. 7.1, boxed and labelled “55S”) in both samples. The RNA was isolated from these selected fractions.

Library preparation

The selected fractions from the sucrose gradient (3 – 6) were pooled and then RNA isolated (as described in 6.3, ‘Size separation of mitoribosome footprints’). The RNA pellets were resuspended in 10 µl Gel loading buffer II (Ambion) and separated on a 10% denaturing PAG along with the ssRNA low range marker and 24-35 nt oligo size markers (sequences tabulated in Table 6.3). The composition of the gel (Table 6.2) and the electrophoresis conditions were as described in 6.3.

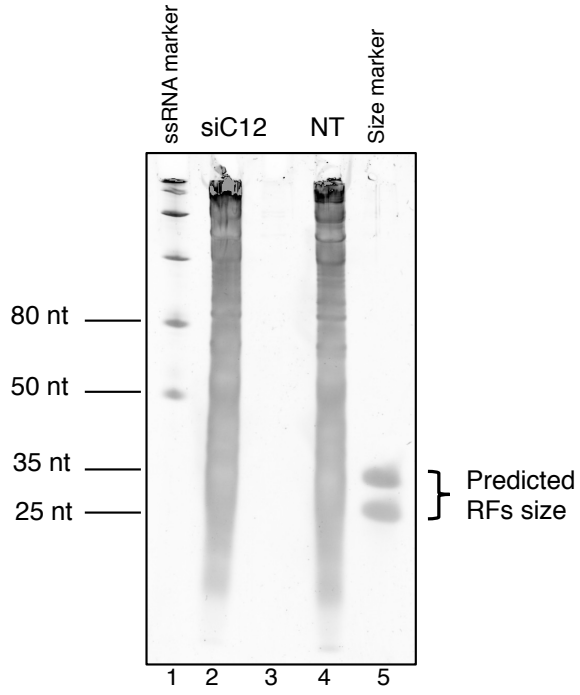

Figure 7.2. Isolation of mitoribosome footprints by size separation

Mitoribosome footprints were generated from cells treated with C12orf65 (siC12, lane 2) or non-targeting (NT, lane 4) siRNA. Total RNA was isolated from selected sucrose gradient fractions that contained mitoribosomes, and separated on 10% denaturing polyacrylamide gel. Low range ssRNA ladder (lane 1) and two were used (24 and 35-nt size, lane 5) as size markers. The RNA oligomers marked the borders of the area that was excised from each sample (lanes 2 and 4) as they spanned the expected size of the ribosome footprints.

From each sample (Fig. 7.2 lanes 2 and 4) a small area (Fig. 7.2, 25-35 nt, depicted by brackets and labelled “Predicted RFs size”) was excised and RNA extracted (as described in 6.3). RFs were predicted to be among these fragments, as it corresponded to their observed size (Rooijers et al., 2013) as described in 6.3. The eluted RNA was then precipitated in 96% ethanol supplemented with glycogen and the RNA pellet was resuspended in 25 µl of 3’-dephosphorylation reaction mix (Table 6.4 and 6.5). This step was necessary to remove the residual phosphate moieties left on the 3’ ends by the RNase 1 treatment and to facilitate the ligation of the first linker to the RNA fragments. The conditions of the dephosphorylation reaction as well as the subsequent purification of its products by Trizol isolation are described in 6.3. The RNA pellets precipitated after Trizol purification were resuspended in 15 µl of the 3’ end ligation mix (composition in Table 6.6). The reaction was performed for 2.5 h at 37ºC with agitation. In parallel to the experimental (siC12) and control (NT) samples, both size marker oligos (24 and 35 nt) were also subjected to ligation (as described in Table 6.6). The products of their ligation served as a positive control and generated the correctly sized markers to facilitate the selection of correctly ligated sample products. The products of the 3’ ligation were size separated by denaturing 10% PAGE (as described earlier and in 6.3). The comparison with the positive control (Fig. 7.3 A, Contr.) showed that the ligation in both samples (Fig. 7.3 A, siC12 and NT) had been successful. The products that had increased in size to 45-55 nt (Fig. 7.3 A, depicted with brackets, labelled ‘Ligation products’) from both experimental samples (siC12 and NT) and positive control (Contr.) were extracted from the gel (as described in 6.3). The precipitated RNA from each of these 3 samples was then phosphorylated at the 5’ end by resuspension in 14 µl of phosphorylation reaction mix (Table 6.8). Reactions were performed for 30 min at 37ºC with agitation.

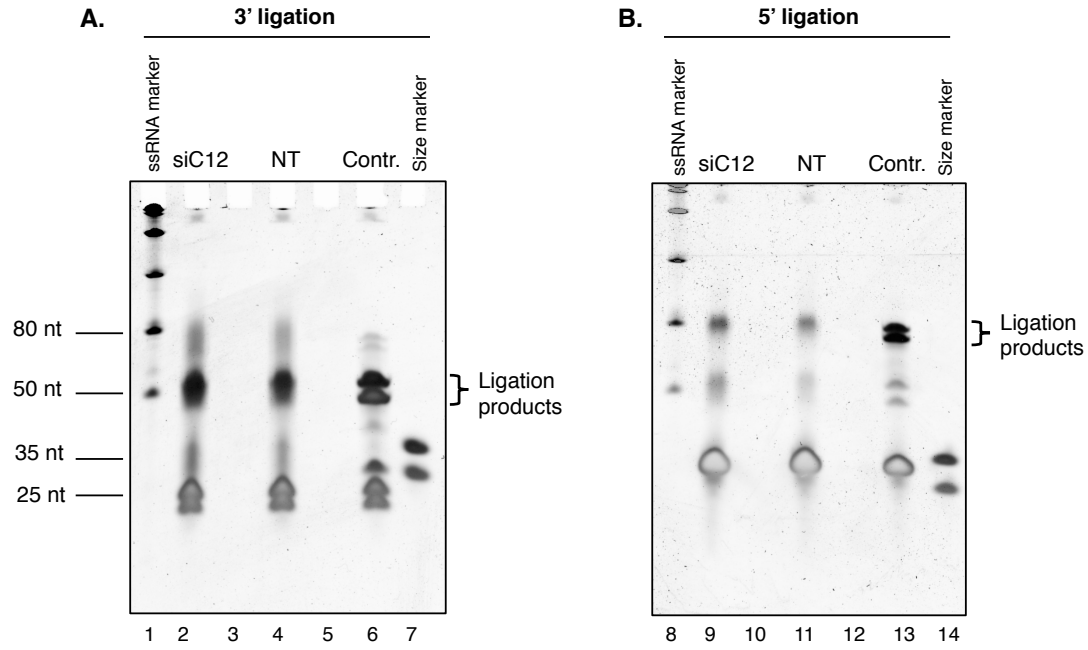

Figure 7.3. Isolation of successful 3' and 5' linker ligation products by size separation

A. The ligation reaction of the 3' linker and isolated RNA fragments (potential ribosome footprints) was separated by 10% denaturing SDS PAGE. Reactions were performed on RNA fragments from C12orf65 siRNA treated (siC12, lane 2), non-targeting siRNA treated (NT, lane 4) and a positive control of the ligation reaction (Contr. lane 6), which facilitated selection of the correct sized products (depicted by brackets). Low range (lane 1 ssRNA) and oligo (lane 7) size markers were used. **B.** The reaction of the ligation of the second linker (5' linker) was also separated by 10% denaturing SDS PAGE. Samples are as for A; siC12, lane 9; NT, lane 11 and the positive control, lane 13. All were subjected to ligation and the correct sized product is depicted by brackets. The low range ssRNA marker (lane 8) and 25-25 oligo size markers (lane 14) were used as in A.

After the phosphorylation step, the RNA was Trizol purified (details in 6.3) and then it was subjected to the ligation of the 5' end linker (as described in 6.3 'Phosphorylation of 5' ends and ligation of the 5' linker' and Tab.6.9). The products of the 5' end ligation were also size separated by 10% denaturing PAGE. In the positive control sample (Fig. 7.3 B, Contr.) and both experimental samples (Fig. 7.3 B, siC12 and NT) the products of the expected 65-75 nt size were present (Fig. 7.3 B depicted by brackets and labelled 'Ligation products'). This result confirmed that the ligation was successful, and the area of the gel with correctly sized products was extracted (Fig. 7.3 siC12 lane 9; NT lane 11). The RNA was eluted from the gel pieces and precipitated as described in 6.3. The pellets of the precipitated RNA were resuspended in 8 µl of the nuclease-free H_2O and used in the reverse transcription reaction (components and conditions listed in Table. 6.10). After the reverse transcription, samples were

treated with 1 µl RNase H for 1 hour at 37ºC and purified with illustra Microspin G-50 spin columns (GE Healthcare) according to the manufacturer's instructions. Next, the resulting cDNA was amplified in the PCR reaction with primers specific to the linker sequences ligated to each end of the templates (reaction conditions in Tables 6.11 A and B, primer sequences in Table 6.12 B). A single forward primer (termed mtRPPCR RP1) was used for both samples, whereas 2 different reverse primers were added to each sample (termed mtRPPCR RPI3 and 4). The reverse primers varied in the embedded index sequence (depicted by brackets in Table 6.12 B). The PCR products were purified with Qiaquick PCR purification kits (Qiagen, 28106) as described in 6.3. The purified products were separated using the E-GEL Invitrogen system (G6400EU) with E-GEL EX with SybrGold 2% SizeSelect precast gel (Invitrogen G661002) according to the protocol described in 6.3. Samples were electrophoresed together with the 25 bp size marker (diluted to 200 µg/µl with nuclease-free water and stored at -20ºC, Invitrogen 10597-011). The size selected dsDNA library products (approximately 130 bp in length) were resuspended in 25 µl of nuclease free water (added to the second row of wells, see 6.3.) and stored at -20ºC for shipment to Netherlands Cancer Institute (NKI), Amsterdam. The sequencing of the samples was performed in NKI's Genomics Core Facility with Illumina HiSeq2000 system.

7.3. Bioinformatics analysis of results

Before the sequencing results were obtained, the level of the C12orf65 depletion was determined with qPCR following reverse transcription with random hexamer primers (SuperScript® III First-Strand Synthesis System, 2.4.3) and analysed using C12orf65 –specific primers (C12RTFor and C12RTRev) as described in 3.5.

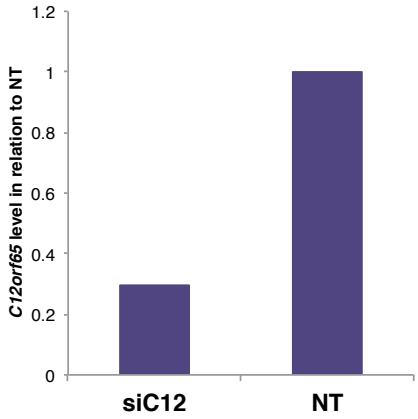

Figure 7.4. Determination of the level of C12orf65 depletion in the ribosome profling experiment

RNA from cells cultivated and treated in parallel to the ribosome profiling experiment was isolated and analysed with qPCR to estimate the level of C12orf65 depletion. C12orf65 levels were normalized to 18S rRNA levels and represented in relation to the expression in NT cells.

The results of the qPCR show that after 3 days of depletion with siC12orf65, approx. 30% (in comparison with NT control) of the C12orf65 still remained (Fig.7.4, 'siC12'). Although, the experiments described in 3.6 and 3.7 clearly show that 70% of depletion may not be enough to induce changes to mitochondrial translation, these experiments were performed later than ribosome profiling. Therefore, at the time of this profiling experiment there was no cause for concern regarding depletion levels. In order to investigate if the level of depletion could cause changes to the mitoribosomal profiles, the sequenced data was analysed.

The bioinformatics analysis of sequencing results was performed by Dr. Fei Gao according to the protocol developed by Dr. Bashton, as described in 6.4. The adapter sequences at the 3' end were removed with Cutadapt, then the trimmed reads were aligned with the decoy collective tRNA / rRNA reference sequences using bowtie2. The reads that did not align to the decoy sequences (*_screened.fastq) were aligned with actual reference genome, human mtDNA (HumanMT) with bowtie2. The resulting *.sam files were devoid of multimapping reads (with samtools view) and next converted into *.bam files (samtools sort). Finally the *.bam files were indexed (samtools index). As observed in ribosome profling experiments on T1V1 cell line (6.4), the final number of reads that aligned to mt-mRNAs was low (approximately 2 x10^4, Appendix 1.4, Table A1 '2934_3_ siC12_RP1 and 4_siNT').

The downstream analysis of the aligned reads, which contained a pool of the mitochondrial ribosome footprints (RFs) was collaboratively performed by Dr. John Grady and Dr. Fei Gao using R software.

Amino acid position within RFs

One of the interesting observations derived from the data obtained from ribosome profiling analysis of T1V1 cell line was unexpectedly high proportion of RFs from 5' terminus of COX2 ORF, namely MAHAAQVGL sequence (Fig. 6.13 and 6.15). It was determined by analysis of the position of different amino acid codons in RFs (Fig. 6.13). In order to investigate if the same pattern would be present in this experiment, a similar analysis (as in 6.4, 'Repeat of mitoribosome profiling on T1V1 cell line') was performed on siC12orf65 and NT cell lines (Fig. 7.5). The number of RFs with specific codons located at any given position was calculated for methionine, alanine, histidine, glutamine, valine, glycine and leucine encoding sequences (without distinguishing between particular triplets). Position of codons for each of these amino acids was plotted separately. Apart from siC12orf65 and NT cell lines, the plots were generated for the T1V1 and control cell lines (from both experiments) for comparison.

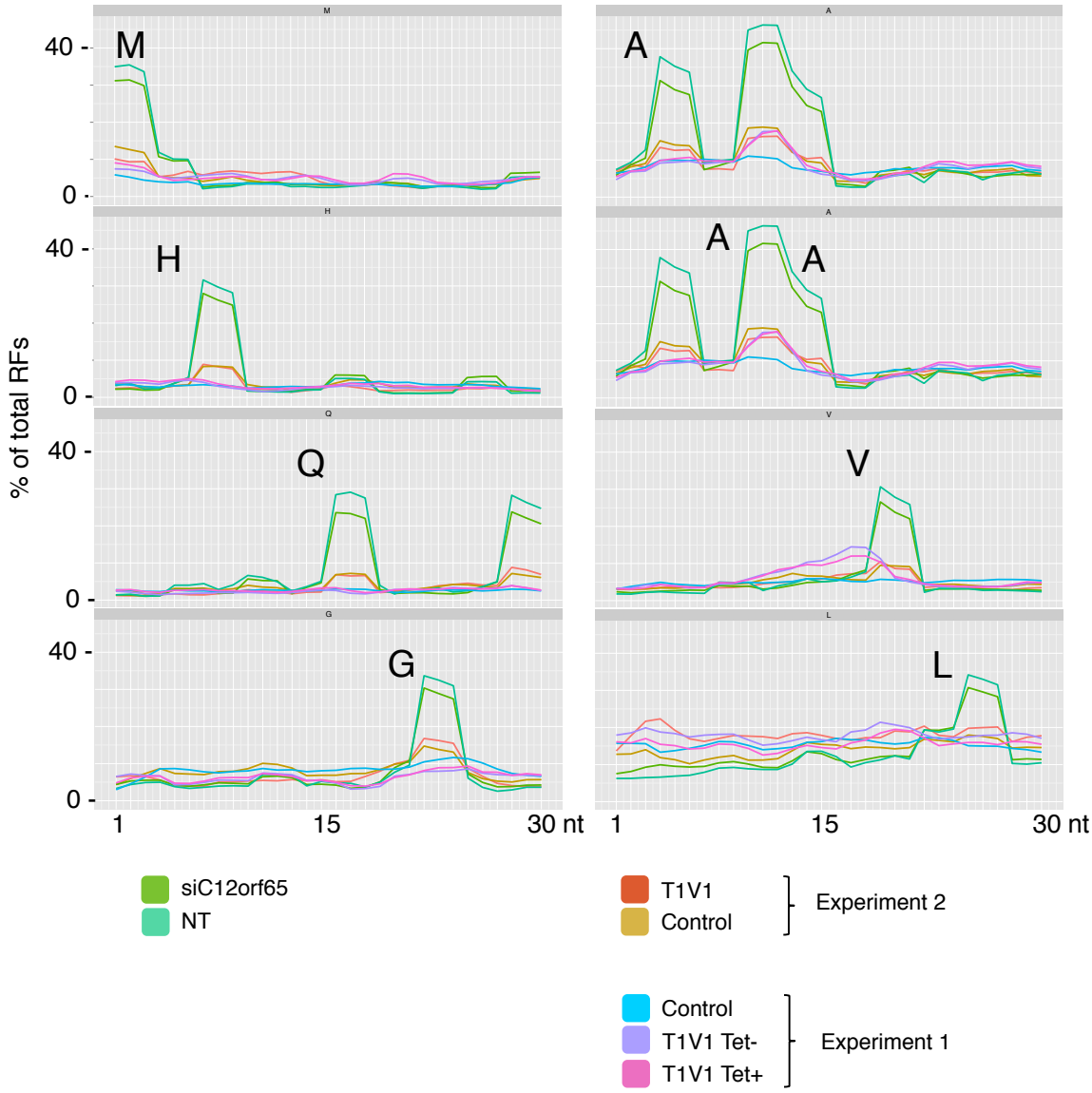

Figure 7.5. Comparison of different amino acids' positions in RFs shows a dominant pattern

Plots showing quantification of RFs with specific amino acid (M, A, H, Q, V, G and L) codons at various positions in siC12orf65 and non-targeting control cell lines. The T1V1 and control cell line data from previous experiments (6.4 and 6.5) were also included. The x axis representing different offsets of all RFs containing one type of valine codon which 5' end starts at any given position (1-30 nt, in 5' –> 3' direction) in a predicted-sized footprint. The y axis represents a number of RFs with specified codon starting at each particular position. This number is presented as a percentage of all footprints with an amino acid codon starting at that position. The original plots were generated by Dr. John Grady.

As in case of the results of repeated ribosome profiling on T1V1 there was a high number of RFs containing the MAHAAQVGL sequence. However their proportion in the total pool of all RFs was even higher in the siC12orf65 and NT cell lines than in the T1V1 and control. Therefore, the next step in analysis was to quantifiy the number of RFs originating from separate mt-ORFs.

Distribution of ribosomes between transcripts

The comparison of the number of RFs aligning to each mitochondrial transcript was performed on data from both siC12orf65 and NT cell lines. For each of the mt-mRNAs including the overlapping fragments open reading frames of *MT-ATP6* / *MT-ATP8* and *MT-ND4* / *MT-ND4L*, the number of RFs that originated from it representing the number of actively translating mitoribosomes, was calculated and presented as the percentage of the total number of mitochondrial RFs. The results were calculated for each mt-transcript in both cell lines and presented as histograms (Fig. 7.6 siC12orf65 treated 'siC12' and non-targeting control 'NT').

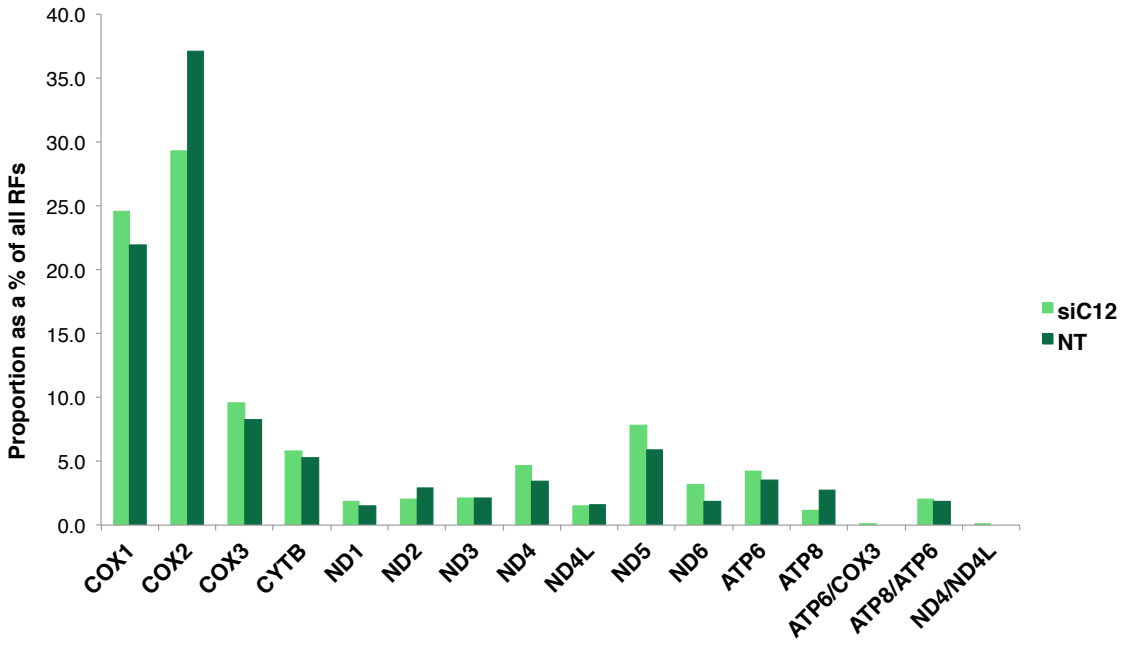

Figure 7.6. The Ribosome Footprint abundance on each mt-ORF from the C12orf65 depleted and control cell lines

The analysis was performed on data derived from cells treated with siC12orf65 (siC12) or non-targeting control (NT) siRNAs. The number of ribosome footprints (RFs) originating from mitochondrial ORF was calculated for each individual transcript. The results per ORF were presented as the percentage of the total number of mitochondrial RFs.

Comparing the RFs abundance between the two samples there were no striking differences in the number of mitoribosome footprints on each mt-transcript. It is important to remember that these were results of one experiment so the moderate variations (as seen in *MT-CO2*) may be sample-dependant. When examining the results for individual transcripts it was clear that the highest

number of RFs originated from *MT-CO1* (25% and 22%) and *MT-CO2* (29% and 37%).

Interestingly, there was also a number of RFs aligning to the overlapping region of *MT-ATP8* and *MT-ATP6* (*MT-ATP8/6*, Fig. 7.6). This 45 nt sequence is shared between 3' end of *MT-ATP8* and 5' end of *MT-ATP6*. The number of RFs aligning exclusively in that overlapping region (2%) was comparable to those from *MT-ATP8* (full length excluding the overlap) even though the overlapping fragment is much shorter than the rest of the ORF.

Distribution of RFs within each mt-transcript

The next analytical step was focused on how the RFs were distributed within individual transcripts. In order to investigate this, a separate mitoribosome profile was prepared for each mt-mRNA. The profiles were represented as histograms of RFs density across the length of the transcript. The number of mitoribosome footprints found at each point in the transcript was again expressed as the percentage of all annotated RFs. Patterns of RFs distribution were divided into 4 major groups based on the position of the major accumulation of RFs within the transcript: 1) within first 100 nt near the 5' terminus (Fig. 7.7 and 7.8), 2) 5' terminus but further then 100 nt (Fig. 7.9), 3) at 3' terminus (Fig. 7.10 and 7.11), 4) diverse (Fig. 7.12). These also show the variation between siC12orf65 depleted and non-targeting control (Fig. 7.6 siC12, NT).

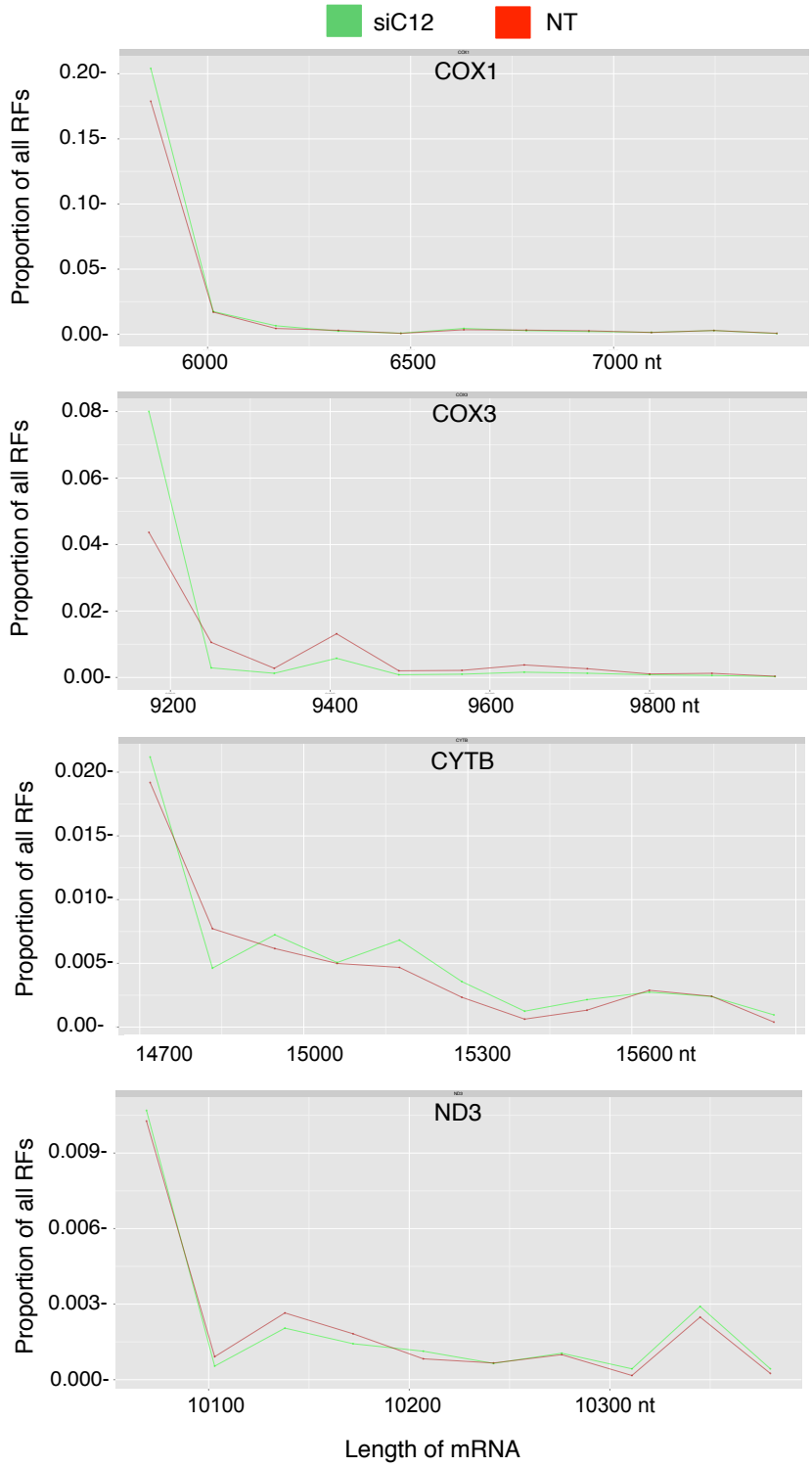

Figure 7.7. RFs distribution patterns showing accumulation near 5' terminus (first 100 nt) bigger in C12orf65 depleted cells

Distribution of the RFs across each mitochondrial transcript (mitoribosome profile) was presented as a number of RFs (percentage of all RFs in experiment, Y axis) aligning to each nucleotide position within a particular mt-mRNA. The X axis presents the length of the transcript in nucleotides and includes the mt-genome coordinates for each transcript. In order to facilitate comparison between the profiles, the x axis are of equal length, even though transcripts vary in length. The original plots were generated by Dr. Fei Gao.

The profiles that belong to the first category characterise with the highest number of RFs accumulated in the first 100 nt from the 5' terminus. This number was greater in either siC12orf65 cells (Fig. 7.7) or NT control (Fig. 7.8). However, the predominance of RFs in either cell line, even if present at the 5' terminus of a particular transcript, it was not necessary consistent across its whole length. As in case of COX3, CYTB and ND3 (Fig. 7.7) even though there was more RFs at first 100 nt in siC12orf65 cells, this proportion changed at different parts of the transcript.

The highest accumulation of RFs at 5' terminus in siC12orf65 cells was observed at COX1 and COX3 (Fig. 7.7). RFs from these two mt-mRNAs were also among the 3 most represented in total RFs pool (Fig. 7.6).

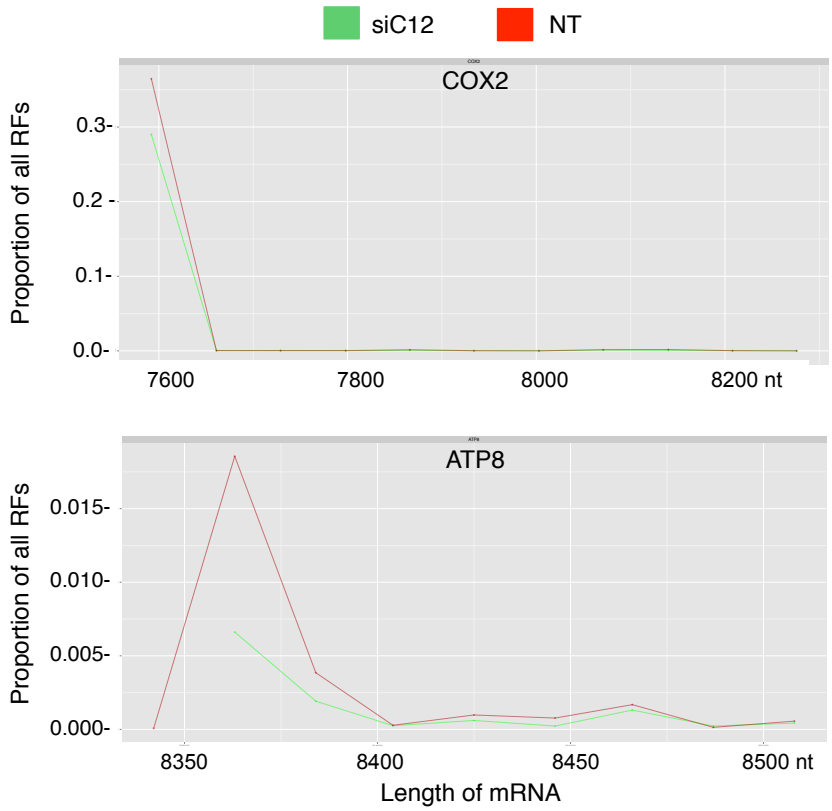

Figure 7.8. RFs distribution patterns showing accumulation near 5' terminus (first 100 nt) bigger in non-targeting cells

Distribution of the RFs across each mitochondrial transcript (mitoribosome profile) was presented as a number of RFs (percentage of all RFs in experiment, Y axis) aligning to each nucleotide position within a particular mt-mRNA. The X axis presents the length of the transcript in nucleotides and includes the mt-genome coordinates for each transcript. In order to facilitate comparison between the profiles, the x axis are of equal length, even though transcripts vary in length. The original plots were generated by Dr. Fei Gao.

It is unlikely that the high number of RFs at the 5' end represent initiating

mitoribosomes. As discussed in 6.8, the fraction of mitoribosome fragments is expected to contain smaller RNA species than these selected for the library preparation. Therefore the accumulation of RFs at 5' terminus is a result of other features of mRNA like specific amino acid codons that would attract higher numbers of mitoribosomes. However, it is also possible that the arrest of mitoribosomes near the 5' terminus of these ORFs is a form of regulation of translation.

The highest accumulation of RFs was not only observed at first 100 nt from 5' terminus. In ND1 and ND4 it was also present further downstream. This form of mitoribosomal footprints could be associated with potential interactions of the nascent polypeptide with the exit tunnel of the ribosome. Or, perhaps would signify the slower progression of the ribosome due to the interactions of the emerging peptide with the outside factors (as chaperons).

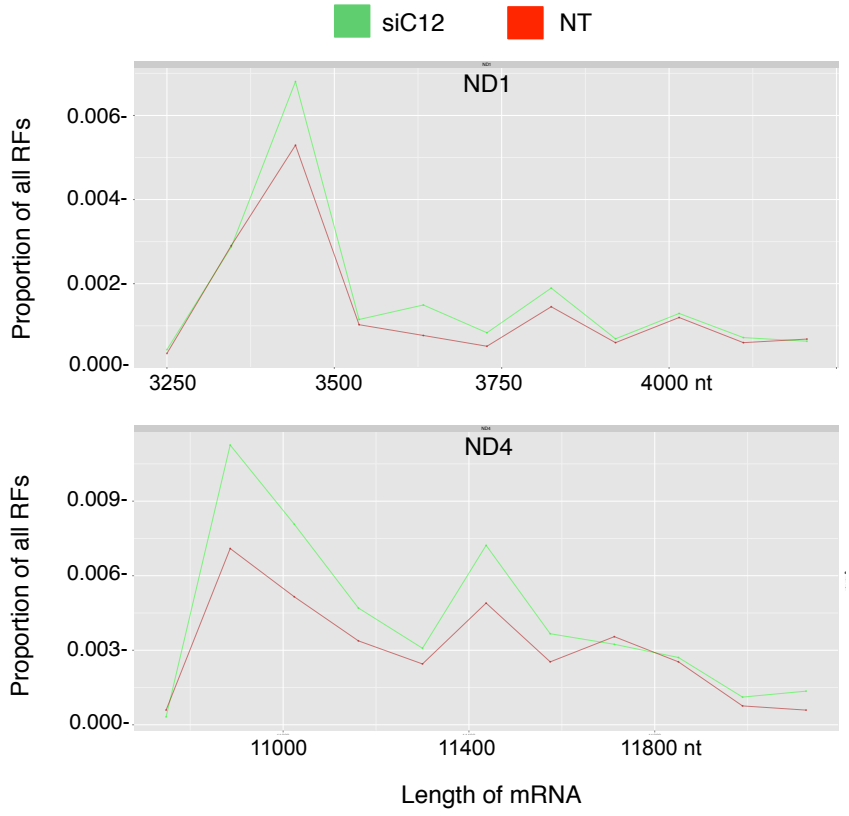

Figure 7.9. RFs distribution patterns showing accumulation further from 5' terminus (beyond 100 nt) bigger in C12orf65 depleted cells

Distribution of the RFs across each mitochondrial transcript (mitoribosome profile) was presented as a number of RFs (percentage of all RFs in experiment, Y axis) aligning to each nucleotide position within a particular mt-mRNA. The X axis presents the length of the transcript in nucleotides and includes the mt-genome coordinates for each transcript. In order to facilitate comparison between the profiles, the x axis are of equal length, even though transcripts vary in length. The original plots were generated by Dr. Fei Gao.

The regions of the highest accumulation of RFs were also observed at the 3' terminus of mRNAs (Fig. 7.10 and 7.11). The length of these regions varied from less than 100 nt (Fig. 7.10, ND6) to over 350 nt (Fig. 7.10 ND5) and increased with the length of the transcript. In majority cases the accumulation at 3' terminus was more profound in siC12orf65 treated cells (Fig. 7.10) but in ND2 (Fig. 7.11) it was dominating in non-targeting cells.

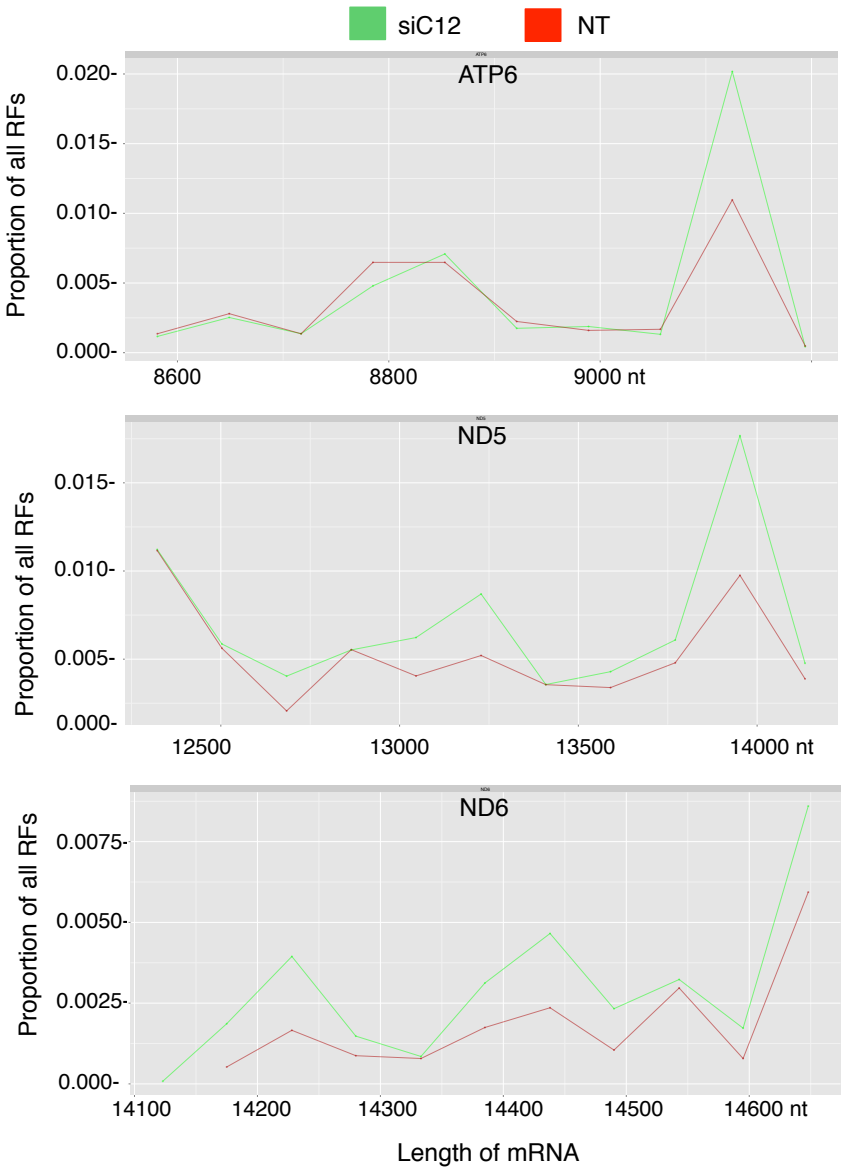

Figure 7.10. RFs distribution patterns showing accumulation near 3' terminus bigger in C12orf65 depleted cells

Distribution of the RFs across each mitochondrial transcript (mitoribosome profile) was presented as a number of RFs (percentage of all RFs in experiment, Y axis) aligning to each nucleotide position within a particular mt-mRNA. The X axis presents the length of the transcript in nucleotides and includes the mt-genome coordinates for each transcript. In order to facilitate comparison between the profiles, the x axis are of equal length, even though transcripts vary in length. The original plots were generated by Dr. Fei Gao.

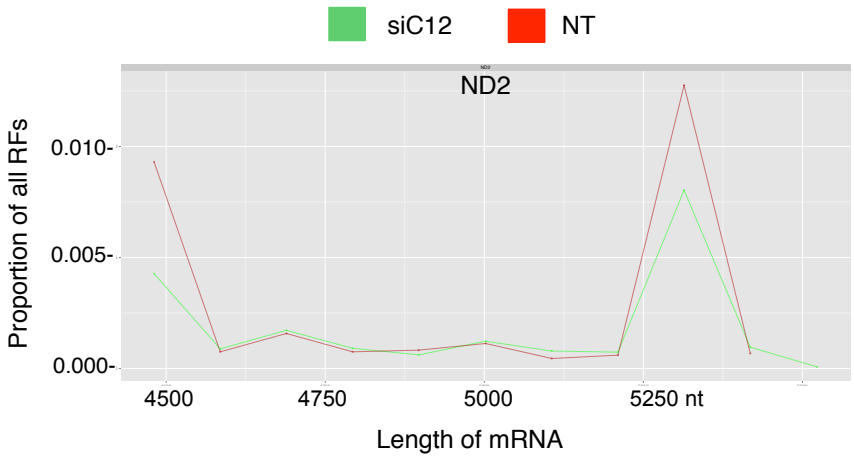

Figure 7.11. RFs distribution pattern showing accumulation near 3' terminus bigger in control cells

Distribution of the RFs across each mitochondrial transcript (mitoribosome profile) was presented as a number of RFs (percentage of all RFs in experiment, Y axis) aligning to each nucleotide position within a particular mt-mRNA. The X axis presents the length of the transcript in nucleotides and includes the mt-genome coordinates for each transcript. In order to facilitate comparison between the profiles, the x axis are of equal length, even though transcripts vary in length. The original plot was generated by Dr. Fei Gao.

Finally, the diverse pattern was observed in case of ND4L where there was not one dominating peak of RFs accumulation (Fig. 7.12). Instead there were two equally high peaks corresponding to two major accumulations of the RFs. This pattern was distinct from all presented above (Fig. 7.7- 7.11), possibly due to the small length of the transcript with low number of RFs. However, the distribution of RFs was similar in both siC12orf65 and NT treated cell lines suggesting that this is a normal pattern for this particular ORF.

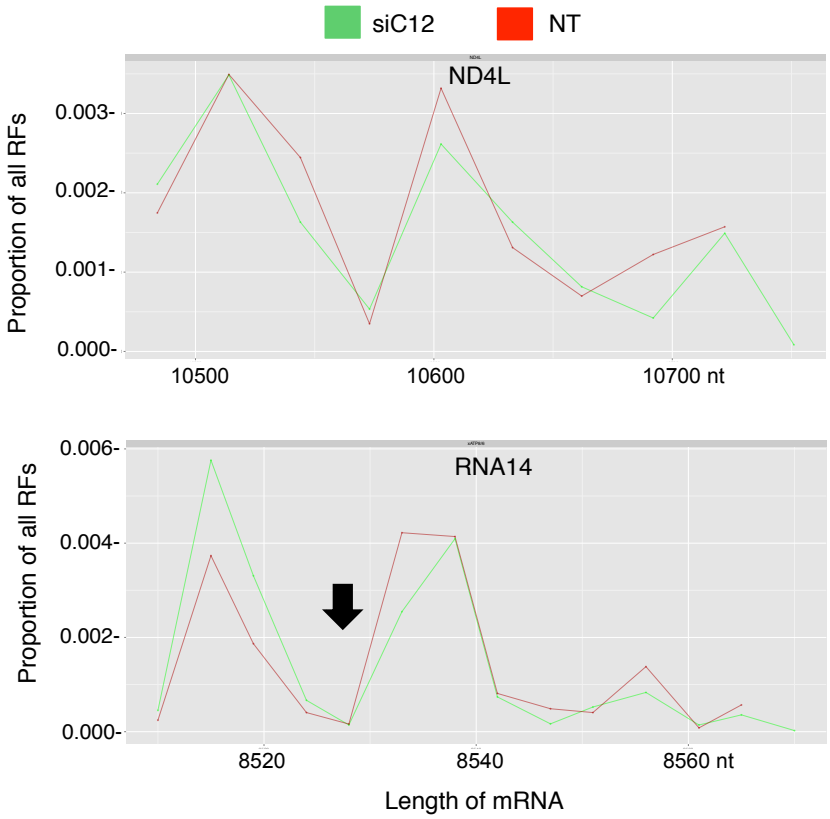

Figure 7.12. Diverse RFs distribution pattern in C12orf65 depleted and control cell lines

Distribution of the RFs across each mitochondrial transcript (mitoribosome profile) was presented as a number of RFs (percentage of all RFs in experiment, Y axis) aligning to each nucleotide position within a particular mt-mRNA. The X axis presents the length of the transcript in nucleotides and includes the mt-genome coordinates for each transcript. In order to facilitate comparison between the profiles, the x axis are of equal length, even though transcripts vary in length. The original plots were generated by Dr. Fei Gao.

A representation of RFs from the junction of *MT-ATP8* and *MT-ATP6* (Fig. 7.12, RNA14) was also included in this category. The distribution pattern showed that there were two distinct accumulations of RFs. The gap between them (pointed with an arrow) represents the start of *MT-ATP6* transcript, therefore the peak of RFs accumulation that starts after it is most likely composed of mitoribosomes that started translation of *MT-ATP6* and/or finish synthesis of *MT-ATP8*. The peak before the gap represents mitoribosomes that are only translating the latter ORF. It is also very interesting that this peak contains higher number of RFs in siC12orf65 treated cells than in NT control. It is possible that these RFs originate from mitoribosomes that are stalled on *MT-ATP8* as they wait for these initiating translation of *MT-ATP6* to progress.

In conclusion, the individual transcripts' mitoribosome profiles presented various patterns of RFs distribution that differed between each other and in some

cases between the two samples. There was no single rule for the way these differences were manifested though. It is the fact that these are results of one experiment and were generated from a low number of reads (Table A1). It is also possible that the C12orf65 depletion was not sufficient to remove residual activity and therefore may not have generated strong changes to the mitoribosome profiles. Therefore, further analysis was focused on characterisation of the general features of mt-translation based on the obtained data in the cell lines examined. Mitoribosome profiles of all mt-ORFs (obtained as described in Fig. 7.7-7.12) were merged together to form one profile per cell line (Fig. 7.13). The length of each transcript was presented as their actual size and they were aligned at the 5' ends. However, mt-ORFs vary in sizes, therefore not all of their 3' end align at the same point. The merged mitoribosome profiles were not only generated for siC12orf65 treated cells and non-targeting control but also for the T1V1 and control cell lines from previous experiments (6.4 and 6.5).

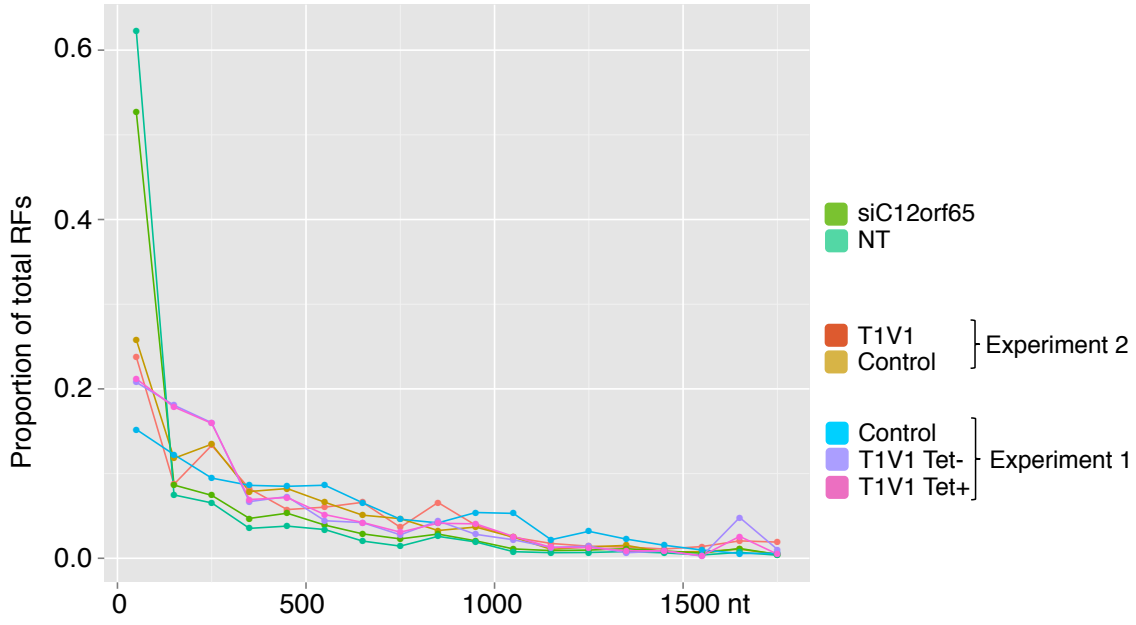

Figure 7.13. General mitoribosome profiles show similarities in RFs distribution in all tested cell lines

RFs distribution profiles for every mt-ORF were merged together to form a singular profile per one cell line. The x-axis represents the maximum length of the my-mRNA in nt, the Y-axis shows the proportion of total RFs aligning at each point. The general mitoribosome profile was generated for each sample analysed with ribosome profiling including siC12orf65 and non-targeting control (NT), T1V1 mutants and 143B control cells (from both experiments, 6.4 and 6.5). The original plot was generated by Dr. John Grady.

On average, in all cell lines investigated in this analysis the highest number of RFs accumulated approximately at first 100 nt of mt-ORF. This was a consistent trend regardless of the type of cell line and experiment. This feature was most prominent in siC12orf65 and NT cell lines, where it was most likely caused by COX1 and COX2 abnormally high accumulation of RFs. This result further confirms that such domination of RFs from COX1 and COX2 was specific to the siRNA treatment experiment but not to the C12orf65 depletion.

7.4. Complementary RNAseq analysis of C12orf65-depleted and control cell lines

In order to expand the analysis of mitoribosome distribution a complementary RNAseq experiment was conducted. The information on the level of each mt-mRNA when compared with the RFs distribution leads to more accurate measurement of ribosome accumulation. By eliminating the level of template as a factor influencing the number of RFs per ORF it allows assessing how many ribosomes were associated with each transcript. These ribosome footprints represent either a number of ribosomes actively translating the template or accumulated as a result of stalling.

HEK293 wild type (1x 15 cm dish per condition) cells were treated with siC12orf65 or NT siRNAs as in 7.2. The preparation of cell samples for the experiment was conducted as in 6.5. The library and sequencing was performed in Netherlands Cancer Institute, Amsterdam to be sequenced at the Genomics Core Facility with Illumina HiSeq2000 (single-read sequencing).

After receiving the raw data, I first confirmed their quality with FastQC software (http://www.bioinformatics.babraham.ac.uk/projects/fastqc/, Appendix 1.4 Table A2, samples 'rp1'). The quality value (Q) was generated per each bp of all reads. It represents the probability that the corresponding base call was incorrect on a scale of 0 – 40 (40 being the lowest probability of an error). The reports showed that both samples had a very high quality of sequencing across the whole length of reads, with Q ranged between 32 and 40 (Fig. 7.8). Having established that the raw data was of sufficient quality for the analysis, I proceeded to perform the alignment following the methodology as described in 6.5. The resulting differential expression data were exported to excel for further analysis as described below. First, the expression of C12orf65 was investigated

in order to confirm the RT-qPCR estimate of the level of C12orf65 depletion (detailed in 7.4 and Fig. 7.4).

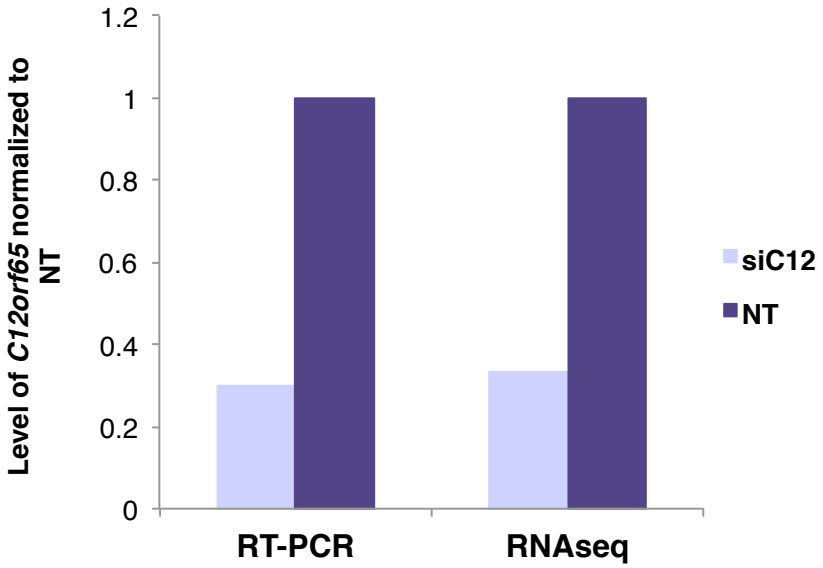

Figure 7.14. Comparison of the levels of C12orf65 depletion as estimated by RT-PCR and RNAseq

The level of *C12orf65* depletion was estimated based on the RNAseq measurement of the *C12orf65* transcript levels (RNAseq) in C12orf65 depleted cell line (siC12) and non-targeting control (NT) as described in the text. This was compared with the previously derived estimate from RT-qPCR by evaluating the histograms depicted above.

By analysing the levels of C12orf65 measured in control and depleted samples it was determined that approximately 30% of the transcript remained after 3 days of days treatment (Fig. 7.14 'RNAseq") which is consistent with previous observations from RT-PCR (Fig. 7.14 'RT-PCR' and Fig. 7.4). With this level of depletion confirmed, however, the possibility existed that C12orf65 was not being removed to a sufficient extent to cause changes to phenotype. Therefore, the first feature investigated was the comparison of the mitochondrial transcripts levels between the C12orf65 (Fig. 7.15, siC12) depleted and control (Fig. 7.15, NT) cell line. The level of each mt-mRNA was presented as the percentage of a total number of mitochondrial transcripts. In previous experiments by Dr. Pajak it was observed that the C12orf65 depletion resulted in an increase in steady state levels of mt-transcripts (3.1). Therefore, the analysis with RNAseq was aimed to examine if the same effect would be observed in this experiment.

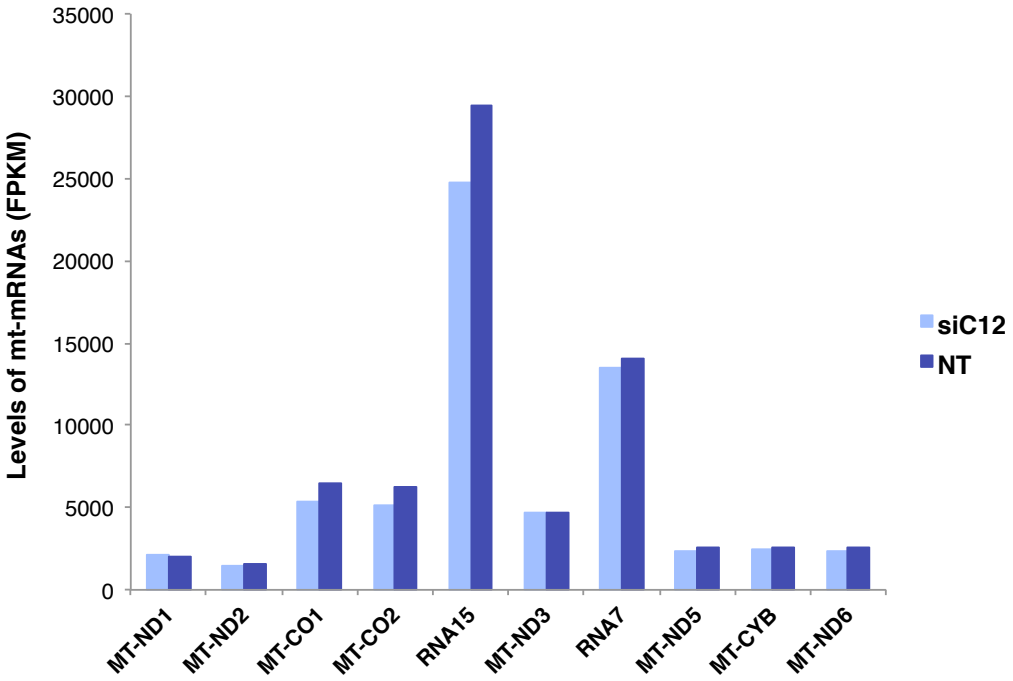

Figure 7.15. RNAseq analysis shows no varition in mt-mRNAs expression between siC12orf65-depleted and NT control cell lines

Levels of each mt-mRNA expression (in FPKM), derived from the analysis with Cufflinks software, for both cell lines: C12orf65-depleted (siC12) and non-targeting control (NT) are plotted pairwise to facilitate comparison.

Comparison of the mt-mRNAs between the two samples showed no changes to levels of ech mitochondrial transcript resulting from the C12orf65 depletion. As predicted after the confirmation of the percentage of depletion (Fig. 7.14) the remaining 30% of C12orf65 transcript (in comparison to NT control) was potentially sufficient to inhibit changes to mitochondrial gene expression.

The next step in analysis was to test the efficiency of translation of each transcript. This was assessed by comparison of the abundance of the mt-mRNA (represented as % of all mt-transcripts) with the abundance of the RFs (also as % of all mitochondrial RFs) originating from it. The analysis was performed on both cell lines (C12orf65-depleted 'siC12' and non-targeting control 'NT', Fig. 7.16). For each individual mt-ORF the number of RFs was divided by the level of the template mRNA. As described in 6.5, in order to merge the two data sets the annotation were first matched. The number of RFs from *MT-ATP6*, *MT-ATP8* and *MT-CO3* with overlapping regions were added and presented as one sample. The same operation was performed on *MT-ND4* and *MT-ND4L*.

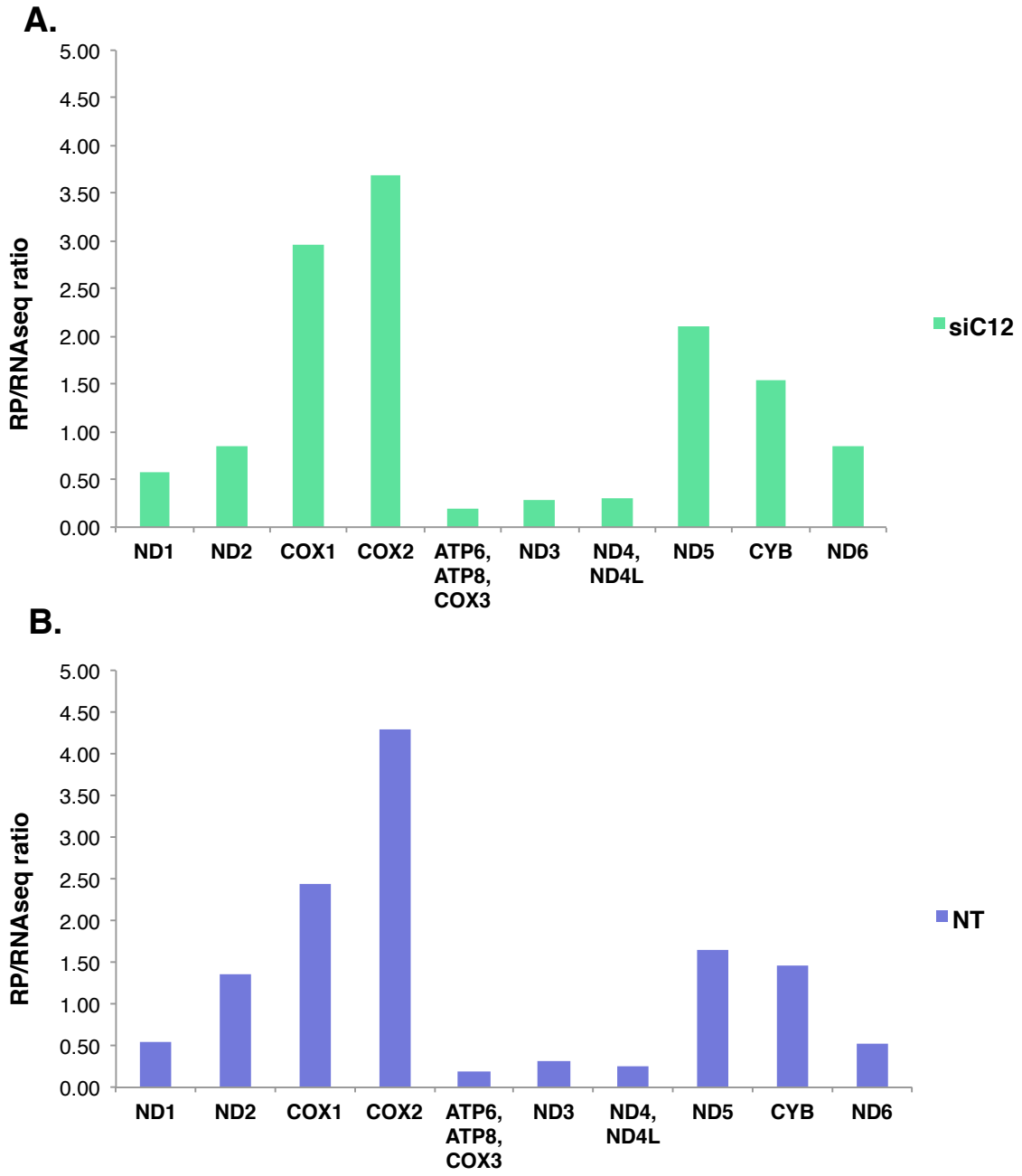

Figure 7.16. Comparison of the translation efficiency ratio shows little difference between the cell lines

Translational efficiency (RP/RNAseq ratio) values were calculated for each mt-ORF by dividing the RFs number originated from it (presented as % of all RFs) by the mt-mRNA levels (presented as % of all mt-transcripts). TE values for all mt-ORFs were generated for siC12orf65 treated (panel **A**) and non-targeting control (**B**) cell lines separately.

Comparison of translational efficiency ratio between the cell lines showed only moderate changes with slight increase in COX1, COX2, ND5 and ND6. The higher the TE ratio the more ribosomes were accumulated over the transcript. The number of mitoribosomes can be a reflection of the translational activity or a measure of staling. Unfortunately without validated results of *de novo* mt-

protein synthesis estimation (3.6) it is impossible to distinguish what is causing the increase in RFs number.

Within each cell line the highest RP/RNAseq ratio was observed in COX1 and COX2, which was most likely a direct effect of the accumulation of RFs in the 5' terminal region of these transcripts (Fig. 7.7 and 7.8). The disproportion in RFs accumulation between the beginning and the remaining part of COX1 and COX2 ORFs suggests that these footprints originated from mitoribosomes that did not complete translation. On the contrary, it seems that these mitoribosomes were arrested at the 5' terminus. Therefore the high RP/RNAseq ratio was not a result of higher translational activity associated with these ORFs. Interestingly, comparison of results for siC12orf65 and NT treated cells with previously analysed T1V1 and control (Fig. 6.17) showed differences between these two experiments. In T1V1 and control cells the TE ratio for ND5 was the highest of all mt-ORFs but in the siC12orf65 and NT control cell lines it was COX1 and COX2 that dominated. This observation suggests that such high proportion of COX1 and COX2 RFs was specific to the experiment and was not caused by depletion of C12orf65.

7.5. Discussion

The purpose of the last part of my project was to compare the mitoribosome profiles from cells depleted of C12orf65 and control treated with non-targeting siRNA. The experiment and the generated initial data showed some potentially problematic features. First, efficiency of the siRNA knockdown of C12orf65 was questionable. However, it was possible that 70% of depletion would be sufficient to induce changes detectable with ribosome profiling. If not, it was decided to use the generated data to characterize the mitoribosome profiles of control cells. Second, the quality of deep sequencing data was lower than expected, resulting in low number of reads aligning to the mtDNA (Table A1). However, it was sufficient to perform the downstream analysis. Mitoribosome footprints (RFs) were grouped and quantified based on the ORF they originated from. There was very little variation in general RFs numbers between cell lines. The potential increase in mitoribosomal stalling, even if present, was not detectable in this presentation of data. Comparison of individual mitoribosome profiles showed variations in the distribution of RFs between the cell lines but they were not uniform. There was not one singular pattern that would show

specific mitoribosome stalling due to lack of C12orf65. One possible explanation of this observation would be insufficient silencing of C12orf65 and a failure to generate the pathological phenotype. The efficiency of depletion, calculated based on the results of RT-qPCR, was at the level of 70% (Fig. 7.4). The result was later confirmed with RNAseq analysis (Fig. 7.14). The residual 30% of C12orf65 transcript could be the reason why there were very little differences in mitoribosomal occupancy between the cell lines. In addition, there was no difference between the levels of mt-transcripts as the increase observed by Dr. Pajak through Northern blot. As in my previous experiments on C12orf65 depletion, where *C12orf65* was not fully removed, there were no visible changes to the cellular phenotype (Fig. 3.7, 3.10 and 3.12). Steady state levels of mt-transcripts were unchanged, not displaying the anticipated increase in the same way it was observed on Northern blotting analysis of cells with 60% depletion (Fig. 3.12). This result confirms the necessity to increase the efficiency of depletion in order to observe the effect that lack of C12orf65 has on cells.

Although there seemed to be no effect on accumulation of RFs in C12orf65 depleted cells, the obtained data could be utilized as a source of information on normal mitoribosomes distribution. In general there was a tendency to accumulate high number of RFs in the first 100 nt (Fig. 7.13). As discussed in 6.8, due to the method of mitoribosome footprints size selection, these RFs most likely do not represent the initiating ribosomes. However, other factors specific to the translated transcript or the nascent polypeptide could generate these mitoribosome profiles. The progression of ribosomes can be affected by codon adaptation, secondary structures in mRNA and positively charged amino acids (Charneski and Hurst, 2013; Dana and Tuller, 2012). It is possible that some of these factors or a combination contributes to the observed accumulation of RFs at 5' terminus of majority of mt-transcripts. These could also explain the differences between individual mt-ORFs' profiles (Fig. 7.7 - 7.12). If repeated it would be interesting to investigate if the same patterns of RFs distribution would occur and with the same proportion between the siC12orf65 and NT cells.

The highest number of RFs was produced by mitoribosomes translating subunits of complex IV, namely COX1, COX2 and COX3 (Fig. 7.6). The detailed analysis of mitoribosomal profiles showed that in all 3 of these

ORFs the majority of RFs was accumulated at first 100 nt from 5' terminus (Fig. 7.7 and 7.8). In case of COX2, the high number of RFs at the 5' end was also reflected in analysis of amino acid coding distribution within footprints (Fig. 7.5). As in repeated experiment on T1V1 and control cells (6.5, Fig. 6.13) the proportion of RFs from 5' terminus of COX2 was so high it dominated the total pool of RFs. This was also a reason why footprints from COX2 were the most highly represented from all mt-ORFs (Fig. 7.6). This result confirmed that the unusually high number of COX2 5'end RFs was independent of the cell line. It was observed in HEK293 treated with both siC12orf65 and NT siRNAs as well as in 143B control and T1V1 cell lines. However, it was not observed in T1V1 cell lines analysed in ribosome profiling experiment performed in Amsterdam, nor in the 143B control cells in (Rooijers et al., 2013) (Fig. 6.15). It may be caused by the handling of cells or the conditions in which they were kept. The fact that this effect was the strongest in siRNA treated cells (Fig. 7.5) suggests that it might be connected to process of siRNA transfection itself. As described in 7.2 and 2.1.4 these cells were kept for 3 days in medium containing siRNA and lipofectamine, which was not replaced with fresh media. Maybe these conditions or the downstream steps of preparing cells for lysis caused the arrest of translation near the 5' terminus. This could be a form of regulation of translation that attenuates synthesis of proteins in conditions less than optimal.

This and other curious aspects of the data presented in this chapter require further investigation. However, it is crucial that in the future experiments the issue of low quality of the data would be addressed. Higher number of reads generated from mt-mRNA would provide the confidence that obtained data fully reflect the natural course of mitochondrial protein synthesis. A possible solution to the problem of low quality would be a differential subhybridisation with probes against mitochondrial and cytosolic rRNA. This additional step, performed on cDNA samples before PCR amplification, would enrich the library in mitochondrial mRNA fragments.

An increase in the number of the mitochondrial RFs is one of the ways to improve analysis of mitoribosomal stalling with ribosome profiling. Another approach should focus on finding a good model of stalling that would facilitate validation of different release factor candidates. The model used in this part of the project consisted of wild type cell line treated with siC12orf65. However, even if the depletion of C12orf65 was complete it is possible that the

changes to the level of mitoribosome stalling could only be moderate. In cells with wild type mtDNA the events of mitoribosome stalling could be sporadic and not easy to detect. It is also possible that in the absence of C12orf65 other factors as mtRF1 or ICT1 would act in its place. Therefore, in order to facilitate the analysis of mitoribosomal stalling, it should be performed on cells with pre-existing mitoribosome progression defect. Depletion of C12orf65 in such cell lines would allow narrowing the analysis to the regions where the stalling would be anticipated. An example of a cell line that could be utilized in this type of experiment is derived from a patient harbouring μΔ9205 mutation in *MT-ATP6* (Temperley et al., 2003). As a result of this mutation 2 bp is removed from the *MT-ATP6* stop codon rendering it non-functional. This mutation would potentially cause stalling at non-stop mRNA. This would be a great model to generate and investigate mitoribosome stalling. Comparison of the mitoribosomal footprints number over the 3' terminus of *MT-ATP6* between the cells with and without C12orf65 could provide the information on this protein's potential to alleviate stalling.

Finally, there is also a potential to improve the RNAseq data to make it more informative. In order to better characterize the common features of mt-translation, especially these concerning levels of each transcript translation these experiments should be repeated. It is advised for RNAseq data to include at least 3 biological repeats (Trapnell et al., 2012). This would allow averaging the results and allowing to eliminate experimental variation. In addition, the RNAseq analysis results that were described in this chapter only referred to the levels of mitochondrial transcript. However, the analysis was performed on the total RNA. Differential expression profiles could be further analysed to compare which nuclear genes were upregulated as a result of the C12orf65 depletion. These results could answer the question if, for example, mtRF1 or ICT1 would be expressed at higher levels to compensate for the loss of C12orf65.

Chapter 8

Final discussion

In my PhD project I focused on the characterisation of C12orf65 protein and exploring its putative role as a rescue factor for mitoribosomes. The second part of my project involved development of mitoribosome profiling, which was initiated to extend the investigation mentioned above. It was also designed to analyse general features on mitochondrial translation including mitoribosome distribution on mitochondrial transcripts.

The following chapter will summarise and discuss the most important results I have obtained for each area of my PhD project.

8.1. Characterisation of C12orf65

The investigation into the function of C12orf65 was based on experiments using siRNA-mediated depletion in conjunction with the analysis of skin fibroblasts that harbour the c.210A mutation in *C12orf65* gene from a patient presenting with mitochondrial disease. The panel of experiments using C12orf65 depletion were the continuation of work by Dr. Aleksandra Pajak whose most important observation was upregulation of mt-transcripts in the absence of C12orf65. This result was consistent with patient reports by (Antonicka et al., 2010) where the same effect was observed. My experiments, however, failed to repeat this result. In addition, none of the anticipated changes to phenotype (decrease in *de novo* mt-translation, loss of cell viability in GGQ mutants) were present. This was most likely caused by insufficient level of depletion (≤ 70%) as it was presented previously that ~90% of siRNA-mediated depletion can produce visibly negative effects on cells (Kogure et al., 2012).

Even though my experiments failed to demonstrate a phenotype due to incomplete depletion of C12orf65, they revealed an important feature of this protein. Based on results of antibody validation, where I tested different combinations or conditions, the endogenous levels of C12orf65 appear to be very low. However, even with this little amount of protein it is necessary to remove over 70% of it in order to observe the negative effects of depletion. One explanation could be that C12orf65, if engaged in mitoribosome rescue, is not the primary factor, indispensable to the process. This hypothesis is in line with results of ICT1 overexpression that partially rescued the mitochondrial defect in patient cells with C12orf65 mutation (Antonicka et al., 2010). Another possibility would be that only small amounts of C12orf65 are required for its function. It may be that mitoribosome stalling in cells with wild type mtDNA would not

necessary be a very frequent event. Therefore, the low levels of the factor that could potentially alleviate it would be sufficient.

The anticipated negative effects of C12orf65 absence on mitochondrial function were observed in the patient study. The c.210A mutation was predicted to result in a frameshift leading to a premature stop codon. The protein product of this mutated template would be truncated and devoid of the presumably catalytically-important GGQ motif. There is an indication that the truncation of C12orf65 does not trigger the nonsense-mediated decay as reflected by results of RT-qPCR (Antonicka et al., 2010) and western blotting (Haruo Shimazaki et al., 2012).

The results of characterisation of the patient samples that I studied were as follows:

- Impaired growth on galactose but not glucose containing medium
- Decrease in complex IV activity
- Disruption of complex I, IV and V assembly
- Decrease in steady state levels of CI and CIV subunits
- General decrease of *de novo* mt-protein synthesis
- Increase in steady state levels of mitochondrial mRNAs and rRNAs

These results clearly show disruption in mitochondrial protein synthesis, reflected in decrease of *de novo* translation, which leads to lower steady state levels of mitochondrial proteins and also of fully assembled complexes.

As demonstrated in yeast cytosolic translation, ribosome rescue is part of a complicated process that in addition to recycling ribosomal subunits, includes degradation of nascent polypeptide and defective mRNA template (Defenouillère et al., 2013). It is possible that a similar mechanism could operate in mitochondria and involves C12orf65 to promote the release of the polypeptide. One explanation could be that the truncation of C12orf65 affects the downstream components of the rescue pathway, namely the mRNA degradation. This could lead to disruption of transcript turnover, which could be a reason for the increase in steady state levels of mt-mRNAs and rRNAs.

Although it is not yet definitely confirmed, C12orf65 may associate with mitochondrial RNA processing granules (RPG). These distinct mitochondrial foci were shown to be sites of RNA processing, turnover and mitoribosome biogenesis (Antonicka et al., 2013; Antonicka and Shoubridge, 2015; Jourdain

et al., 2013). Recent publications on the composition of RNA granules did not list C12orf65 among proteins immunoprecipitated by GRSF1, a confirmed member of RNA granules (Antonicka and Shoubridge, 2015). However, when the IP of C12orf65 was performed GRSF1 was identified as a binding partner (Antonicka et al., 2013). This would suggest that the possible interaction between C12orf65 and the granules is weak and transient. C12orf65 may be directed to the processing granules to perform the mitoribosome rescue as all steps of this process can be implemented there.

8.2. Mitoribosome profiling

In order to facilitate the investigation of potential mitoribosome stalling, the method of ribosome profiling was selected. One of the objectives behind this choice was to design methodology to identify stalling of mitochondrial ribosomes. The developed protocol was validated on a T1V1 cell line where a defined mutation in mt-tRNA^{Val} gene was expected to cause stalling on valine codons in mt-mRNAs. This cell line provided also a potential rescue mechanism via the stably inducible expression of mitochondrial valyl-tRNA synthetase (VARS2) (Hornig-Do et al., 2014). Although the rescue experiment was not successful due to the lack of VARS2 overexpression, the results derived from the uninduced mutant and wild type control cell lines were sufficient to provide informative data.

The most important results of mitoribosome profiles' analysis in these cell lines allowed me to conclude that there is :

- Accumulation of ribosome footprints with A-site positioned valine is higher in the T1V1 mutant line than control cells
- Higher proportion of RFs with A-site GTC codon in the T1V1 mutant line than in control cells
- Dominance of ribosome footprints originating from the 5' terminal sequence of COX2 in the experiment repeats
- Higher ribosome footprints in the RNAseq ratio for ND5 in mutant cells.

My data arising from the mitoribosome profiling suggest that there is an increase in ribosome occupancy of valine codons in mutant cells consistent with stalling. Differences in accumulation of RFs over particular valine codon types between the mutant and control cell lines could be caused by the wobble

base-pairing affecting the speed of translation more in the mutant cells. However, the potential stalling of mitoribosomes due to deficiency of mt-tRNA^{Val} was not profound nor were all valine codon clusters associated with high density of RFs.

Further, the mitoribosome profiles obtained in the experimental repeats showed more stalling at the 5' terminus of COX2 than on valine codons. This could be a manifestation of a different physiological state of cells between the two experiments that triggered a regulatory mechanism as discussed in more detail below.

There is also another factor that could potentially influence the results of the mitoribosome profiles derived from T1V1 cells. According to the recently published cryo-EM structures of mt-LSU, the position in central protuberance that is usually occupied by the 5S rRNA in eubacteria and eukaryotes is taken up by a tRNA species in mitochondria. There is currently no consensus whether it is mt-tRNA^{Phe} (Greber et al., 2014) or mt-tRNA^{Val} (Brown et al., 2014). However, assuming that it is the latter it is possible that the shortage of mt-tRNA^{Val} could also affect the composition and/ or function of mitoribosome. If this were the case then mt-translation would be affected in a global way, which was indeed observed as a general decrease in *de novo* synthesis (Hornig-Do et al., 2014). In my experiments the potential effect of low mitoribosomal processivity was especially visible in ND5, where a very high ratio of RFs to transcript level did not result in higher levels of *de novo* synthesis. This protein is the largest of all those that are mitochondrially-encoded and it contains a high number of valines (third most enriched in valine residues). Both of these features could affect the function of potentially damaged mitoribosome in mitochondria with a shortage of tRNA^{Val}.

Final experiments were conducted on C12orf65 depleted cells and non-targeting control. Unfortunately, the level of depletion was again only 70%, which was previously proven to be insufficient to induce mitochondrial dysfunction. The mitoribosomal profiles of individual mt-ORFs varied in ribosomal distribution patterns as seen in the tRNA^{val} cell line. However, there was no single significant feature that would suggest an increase in mitoribosome stalling in the absence of C12orf65. This could be partially caused by incomplete depletion. It is also possible that a different model needs to be used, namely a cell line with pre-existing mt-translational defect, or an

increased efficiency of C12orf65 depletion. In that case depletion of C12orf65 would be more likely to cause a visible and easy to detect increase in mitoribosomal accumulation.

Interestingly, as observed in the experimental repeat of T1V1, both siC12orf65 and NT control cell lines were characterised by a high accumulation of RFs at the 5' region of *MT-CO1*, *MT-CO2* and *MT-CO3*. It is possible that cells were in less favourable physiological state at the day of experiment and this triggered a regulatory mechanism. This potential mechanism could repress protein synthesis by attenuation of translation at the 5' end of the transcript. It seems that expression of complex IV subunits is more sensitive to changes in physiological state than other mt-ORFs and is a subject to this regulation.

In conclusion the mitoribosome profiling protocol was proven successful in the analysis of patterns of translation in human mitochondria and also in mitoribosome stalling. However, there are certain aspects of the methodology that need further optimisation to produce higher quality and more extensive data. These include the removal of rRNA species from the library and optimisation of RNase treatment in order to reduce contamination with non-mRNA fragments. When these issues are resolved the protocol presented here would serve as a powerful tool to study mitochondrial translation in control and diseased states with details and depth that have never been achieved before.

References

Abo, T., Chadani, Y., 2014. The fail-safe system to rescue the stalled ribosomes in Escherichia coli. Front. Microbiol. 5.
Abrahams, J.P., Leslie, A.G., Lutter, R., Walker, J.E., 1994. Structure at 2.8 A resolution of F_1-ATPase from bovine heart mitochondria. Nature 370, 621–628.
Alkalaeva, E.Z., Pisarev, A.V., Frolova, L.Y., Kisselev, L.L., Pestova, T.V., 2006. *In vitro* reconstitution of eukaryotic translation reveals cooperativity between release factors eRF1 and eRF3. Cell 125, 1125–1136.
Allen, G.S., Zavialov, A., Gursky, R., Ehrenberg, M., Frank, J., 2005. The cryo-EM structure of a translation initiation complex from *Escherichia coli*. Cell 121, 703–712.
Amunts, A., Brown, A., Toots, J., Scheres, S.H.W., Ramakrishnan, V., 2015. Ribosome. The structure of the human mitochondrial ribosome. Science 348, 95–98.
Anderson, S., Bankier, A.T., Barrell, B.G., de Bruijn, M.H., Coulson, A.R., Drouin, J., Eperon, I.C., Nierlich, D.P., Roe, B.A., Sanger, F., Schreier, P.H., Smith, A.J., Staden, R., Young, I.G., 1981. Sequence and organization of the human mitochondrial genome. Nature 290, 457–465.
Andersson, S.G., Zomorodipour, A., Andersson, J.O., Sicheritz-Pontén, T., Alsmark, U.C., Podowski, R.M., Näslund, A.K., Eriksson, A.S., Winkler, H.H., Kurland, C.G., 1998. The genome sequence of *Rickettsia prowazekii* and the origin of mitochondria. Nature 396, 133–140.
Antonicka, H., Østergaard, E., Sasarman, F., Weraarpachai, W., Wibrand, F., Pedersen, A.M.B., Rodenburg, R.J., van der Knaap, M.S., Smeitink, J.A.M., Chrzanowska-Lightowlers, Z.M., Shoubridge, E.A., 2010. Mutations in *C12orf65* in Patients with Encephalomyopathy and a Mitochondrial Translation Defect. Am. J. Hum. Genet. 87, 115–122.
Antonicka, H., Sasarman, F., Nishimura, T., Paupe, V., Shoubridge, E.A., 2013. The mitochondrial RNA-binding protein GRSF1 localizes to RNA granules and is required for posttranscriptional mitochondrial gene expression. Cell Metab. 17, 386–398.
Antonicka, H., Shoubridge, E.A., 2015. Mitochondrial RNA Granules Are Centers for Posttranscriptional RNA Processing and Ribosome Biogenesis. Cell Rep.10, 920-932.
Arava, Y., Wang, Y., Storey, J.D., Liu, C.L., Brown, P.O., Herschlag, D., 2003. Genome-wide analysis of mRNA translation profiles in *Saccharomyces cerevisiae*. Proc. Natl. Acad. Sci. U. S. A. 100, 3889–3894.
Atkinson, G.C., Baldauf, S.L., Hauryliuk, V., 2008. Evolution of nonstop, no-go and nonsense-mediated mRNA decay and their termination factor-derived components. BMC Evol. Biol. 8, 290.
Ballard, J.W.O., Whitlock, M.C., 2004. The incomplete natural history of mitochondria. Mol. Ecol. 13, 729–744.
Barends, S., Wower, J., Kraal, B., 2000. Kinetic parameters for tmRNA binding to alanyl-tRNA synthetase and elongation factor Tu from *Escherichia coli.* Biochemistry (Mosc.) 39, 2652–2658.
Becker, T., Armache, J.-P., Jarasch, A., Anger, A.M., Villa, E., Sieber, H., Motaal, B.A., Mielke, T., Berninghausen, O., Beckmann, R., 2011. Structure of the no-go mRNA decay complex Dom34–Hbs1 bound to a stalled 80S ribosome. Nat. Struct. Mol. Biol. 18, 715–720.
Berk, A.J., Clayton, D.A., 1974. Mechanism of mitochondrial DNA replication in mouse L-cells: asynchronous replication of strands, segregation of circular daughter molecules, aspects of topology and turnover of an

initiation sequence. J. Mol. Biol. 86, 801–824.
Bertram, G., Innes, S., Minella, O., Richardson, J., Stansfield, I., 2001. Endless possibilities: translation termination and stop codon recognition. Microbiol. Read. Engl. 147, 255–269.
Bogenhagen, D., Clayton, D.A., 1977. Mouse L cell mitochondrial DNA molecules are selected randomly for replication throughout the cell cycle. Cell 11, 719–727.
Bogenhagen, D.F., Clayton, D.A., 2003. The mitochondrial DNA replication bubble has not burst. Trends Biochem. Sci. 28, 357–360.
Bonawitz, N.D., Clayton, D.A., Shadel, G.S., 2006. Initiation and beyond: multiple functions of the human mitochondrial transcription machinery. Mol. Cell 24, 813–825.
Brandman, O., Stewart-Ornstein, J., Wong, D., Larson, A., Williams, C.C., Li, G.-W., Zhou, S., King, D., Shen, P.S., Weibezahn, J., Dunn, J.G., Rouskin, S., Inada, T., Frost, A., Weissman, J.S., 2012. A ribosome-bound quality control complex triggers degradation of nascent peptides and signals translation stress. Cell 151, 1042–1054.
Brown, A., Amunts, A., Bai, X., Sugimoto, Y., Edwards, P.C., Murshudov, G., Scheres, S.H.W., Ramakrishnan, V., 2014. Structure of the large ribosomal subunit from human mitochondria. Science 346, 718–722.
Buchert, R., Uebe, S., Radwan, F., Tawamie, H., Issa, S., Shimazaki, H., Henneke, M., Ekici, A.B., Reis, A., Abou Jamra, R., 2013. Mutations in the mitochondrial gene *C12ORF65* lead to syndromic autosomal recessive intellectual disability and show genotype phenotype correlation. Eur. J. Med. Genet. 56, 599–602.
Cai, Y.C., Bullard, J.M., Thompson, N.L., Spremulli, L.L., 2000. Interaction of mitochondrial elongation factor Tu with aminoacyl-tRNA and elongation factor Ts. J. Biol. Chem. 275, 20308–20314.
Carr-Schmid, A., Pfund, C., Craig, E.A., Kinzy, T.G., 2002. Novel G-protein complex whose requirement is linked to the translational status of the cell. Mol. Cell. Biol. 22, 2564–2574.
Cecchini, G., 2003. Function and structure of complex II of the respiratory chain. Annu. Rev. Biochem. 72, 77–109.
Celsi, F., Pizzo, P., Brini, M., Leo, S., Fotino, C., Pinton, P., Rizzuto, R., 2009. Mitochondria, calcium and cell death: A deadly triad in neurodegeneration. Biochim. Biophys. Acta BBA - Bioenerg. 1787, 335–344.
Chadani, Y., Ito, K., Kutsukake, K., Abo, T., 2012. ArfA recruits release factor 2 to rescue stalled ribosomes by peptidyl-tRNA hydrolysis in *Escherichia coli.* Mol. Microbiol. 86, 37–50.
Chadani, Y., Ono, K., Kutsukake, K., Abo, T., 2011. *Escherichia coli* YaeJ protein mediates a novel ribosome-rescue pathway distinct from SsrA- and ArfA-mediated pathways. Mol. Microbiol. 80, 772–785.
Chadani, Y., Ono, K., Ozawa, S., Takahashi, Y., Takai, K., Nanamiya, H., Tozawa, Y., Kutsukake, K., Abo, T., 2010. Ribosome rescue by *Escherichia coli* ArfA (YhdL) in the absence of trans-translation system. Mol. Microbiol. 78, 796–808.
Chan, D.C., 2006. Mitochondrial fusion and fission in mammals. Annu. Rev. Cell Dev. Biol. 22, 79–99.
Chang, J.H., Tong, L., 2011. Mitochondrial poly(A) polymerase and polyadenylation. Biochim. Biophys. Acta BBA - Gene Regul. Mech. 1819, 992–997.

Charneski, C.A., Hurst, L.D., 2013. Positively charged residues are the major determinants of ribosomal velocity. PLoS Biol. 11, e1001508.
Christian, B.E., Spremulli, L.L., 2010. Preferential selection of the 5'-terminal start codon on leaderless mRNAs by mammalian mitochondrial ribosomes. J. Biol. Chem. 285, 28379–28386.
Christian, B.E., Spremulli, L.L., 2012. Mechanism of protein biosynthesis in mammalian mitochondria. Biochim. Biophys. Acta BBA - Gene Regul. Mech. 1819, 1035–1054.
Chrzanowska-Lightowlers, Z.M.A., Pajak, A., Lightowlers, R.N., 2011. Termination of Protein Synthesis in Mammalian Mitochondria. J. Biol. Chem. 286, 34479–34485.
Chujo, T., Ohira, T., Sakaguchi, Y., Goshima, N., Nomura, N., Nagao, A., Suzuki, T., 2012. LRPPRC/SLIRP suppresses PNPase-mediated mRNA decay and promotes polyadenylation in human mitochondria. Nucleic Acids Res. 40, 8033–8047.
Clayton, D.A., 1991. Replication and transcription of vertebrate mitochondrial DNA. Annu. Rev. Cell Biol. 7, 453–478.
Cole, S.E., LaRiviere, F.J., Merrikh, C.N., Moore, M.J., 2009. A Convergence of rRNA and mRNA Quality Control Pathways Revealed by Mechanistic Analysis of Nonfunctional rRNA Decay. Mol. Cell 34, 440–450.
Craigen, W.J., Caskey, C.T., 1986. Expression of peptide chain release factor 2 requires high-efficiency frameshift. Nature 322, 273–275.
Crofts, A.R., 2004. The cytochrome *bc*1 complex: function in the context of structure. Annu. Rev. Physiol. 66, 689–733.
Dana, A., Tuller, T., 2012. Determinants of translation elongation speed and ribosomal profiling biases in mouse embryonic stem cells. PLoS Comput. Biol. 8, e1002755.
Defenouillère, Q., Yao, Y., Mouaikel, J., Namane, A., Galopier, A., Decourty, L., Doyen, A., Malabat, C., Saveanu, C., Jacquier, A., Fromont-Racine, M., 2013. Cdc48-associated complex bound to 60S particles is required for the clearance of aberrant translation products. Proc. Natl. Acad. Sci. U. S. A. 110, 5046–5051.
Demeshkina, N., Jenner, L., Westhof, E., Yusupov, M., Yusupova, G., 2012. A new understanding of the decoding principle on the ribosome. Nature 484, 256–259.
Des Georges, A., Hashem, Y., Unbehaun, A., Grassucci, R.A., Taylor, D., Hellen, C.U.T., Pestova, T.V., Frank, J., 2014. Structure of the mammalian ribosomal pre-termination complex associated with eRF1.eRF3.GDPNP. Nucleic Acids Res. 42, 3409–3418.
Doma, M.K., Parker, R., 2006. Endonucleolytic cleavage of eukaryotic mRNAs with stalls in translation elongation. Nature 440, 561–564.
Dontsova, M., Frolova, L., Vassilieva, J., Piendl, W., Kisselev, L., Garber, M., 2000. Translation termination factor aRF1 from the archaeon *Methanococcus jannaschii* is active with eukaryotic ribosomes. FEBS Lett. 472, 213–216.
Duarte, I., Nabuurs, S.B., Magno, R., Huynen, M., 2012. Evolution and Diversification of the Organellar Release Factor Family. Mol. Biol. Evol.29, 3497-3512.
Dubrovsky, E.B., 2004. *Drosophila* RNase Z processes mitochondrial and nuclear pre-tRNA 3' ends *in vivo*. Nucleic Acids Res. 32, 255–262.
Dudkina, N.V., Kouřil, R., Peters, K., Braun, H.-P., Boekema, E.J., 2010. Structure and function of mitochondrial supercomplexes. Biochim.

Biophys. Acta BBA - Bioenerg. 1797, 664–670.
Dunn, J.G., Foo, C.K., Belletier, N.G., Gavis, E.R., Weissman, J.S., 2013. Ribosome profiling reveals pervasive and regulated stop codon readthrough in *Drosophila melanogaster*. eLife 2, e01179.
Durand, M., Chevrie, K., Chassignol, M., Thuong, N.T., Maurizot, J.C., 1990. Circular dichroism studies of an oligodeoxyribonucleotide containing a hairpin loop made of a hexaethylene glycol chain: conformation and stability. Nucleic Acids Res. 18, 6353–6359.
Embley, T.M., Martin, W., 2006. Eukaryotic evolution, changes and challenges. Nature 440, 623–630.
Falkenberg, M., Gaspari, M., Rantanen, A., Trifunovic, A., Larsson, N.-G., Gustafsson, C.M., 2002. Mitochondrial transcription factors B1 and B2 activate transcription of human mtDNA. Nat. Genet. 31, 289–294.
Falkenberg, M., Larsson, N.-G., Gustafsson, C.M., 2007. DNA replication and transcription in mammalian mitochondria. Annu. Rev. Biochem. 76, 679–699.
Fisher, R.P., Lisowsky, T., Parisi, M.A., Clayton, D.A., 1992. DNA wrapping and bending by a mitochondrial high mobility group-like transcriptional activator protein. J. Biol. Chem. 267, 3358–3367.
Freistroffer, D.V., Pavlov, M.Y., MacDougall, J., Buckingham, R.H., Ehrenberg, M., 1997. Release factor RF3 in *E.coli* accelerates the dissociation of release factors RF1 and RF2 from the ribosome in a GTP-dependent manner. EMBO J. 16, 4126–4133.
Frey, T.G., Mannella, C.A., 2000. The internal structure of mitochondria. Trends Biochem. Sci. 25, 319–324.
Fritsch, C., Herrmann, A., Nothnagel, M., Szafranski, K., Huse, K., Schumann, F., Schreiber, S., Platzer, M., Krawczak, M., Hampe, J., Brosch, M., 2012. Genome-wide search for novel human uORFs and N-terminal protein extensions using ribosomal footprinting. Genome Res. 22, 2208–2218.
Frolova, L.Y., Tsivkovskii, R.Y., Sivolobova, G.F., Oparina, N.Y., Serpinsky, O.I., Blinov, V.M., Tatkov, S.I., Kisselev, L.L., 1999. Mutations in the highly conserved GGQ motif of class 1 polypeptide release factors abolish ability of human eRF1 to trigger peptidyl-tRNA hydrolysis. RNA N. Y. N 5, 1014–1020.
Gagliardi, D., Stepien, P.P., Temperley, R.J., Lightowlers, R.N., Chrzanowska-Lightowlers, Z.M.A., 2004. Messenger RNA stability in mitochondria: different means to an end. Trends Genet. TIG 20, 260–267.
Gagnon, M.G., Seetharaman, S.V., Bulkley, D., Steitz, T.A., 2012. Structural Basis for the Rescue of Stalled Ribosomes: Structure of YaeJ Bound to the Ribosome. Science 335, 1370–1372.
Garza-Sánchez, F., Gin, J.G., Hayes, C.S., 2008. Amino acid starvation and colicin D treatment induce A-site mRNA cleavage in *Escherichia coli*. J. Mol. Biol. 378, 505–519.
Gerashchenko, M.V., Lobanov, A.V., Gladyshev, V.N., 2012. Genome-wide ribosome profiling reveals complex translational regulation in response to oxidative stress. Proc. Natl. Acad. Sci. 109, 17394–17399.
Gesteland, R.F., Atkins, J.F., 1996. Recoding: dynamic reprogramming of translation. Annu. Rev. Biochem. 65, 741–768.
Glick, B., Schatz, G., 1991. Import of proteins into mitochondria. Annu. Rev. Genet. 25, 21–44.
Gouy, M., Gautier, C., 1982. Codon usage in bacteria: correlation with gene

expressivity. Nucleic Acids Res. 10, 7055–7074.
Graille, M., Chaillet, M., van Tilbeurgh, H., 2008. Structure of Yeast Dom34: A Protein Related To Translation Termination Factor eRF1 And Involved In No-Go Decay. J. Biol. Chem. 283, 7145–7154.
Graille, M., Séraphin, B., 2012. Surveillance pathways rescuing eukaryotic ribosomes lost in translation. Nat. Rev. Mol. Cell Biol. 13, 727–735.
Gray, M.W., 1999. Mitochondrial Evolution. Science 283, 1476–1481.
Gray, M.W., Burger, G., Lang, B.F., 1999. Mitochondrial evolution. Science 283, 1476–1481.
Graziewicz, M.A., Longley, M.J., Copeland, W.C., 2006. DNA polymerase gamma in mitochondrial DNA replication and repair. Chem. Rev. 106, 383–405.
Greber, B.J., Bieri, P., Leibundgut, M., Leitner, A., Aebersold, R., Boehringer, D., Ban, N., 2015. The complete structure of the 55S mammalian mitochondrial ribosome. Science 348, 303-308.
Greber, B.J., Boehringer, D., Leibundgut, M., Bieri, P., Leitner, A., Schmitz, N., Aebersold, R., Ban, N., 2014. The complete structure of the large subunit of the mammalian mitochondrial ribosome. Nature 515, 283-286.
Greber, B.J., Boehringer, D., Leitner, A., Bieri, P., Voigts-Hoffmann, F., Erzberger, J.P., Leibundgut, M., Aebersold, R., Ban, N., 2013. Architecture of the large subunit of the mammalian mitochondrial ribosome. Nature 505, 515-519.
Grohmann, K., Amairic, F., Crews, S., Attardi, G., 1978. Failure to detect “cap” structures in mitochondrial DNA-coded poly(A)-containing RNA from HeLa cells. Nucleic Acids Res. 5, 637–651.
Guydosh, N.R., Green, R., 2014. Dom34 Rescues Ribosomes in 3′ Untranslated Regions. Cell 156, 950–962.
Handa, Y., Hikawa, Y., Tochio, N., Kogure, H., Inoue, M., Koshiba, S., Güntert, P., Inoue, Y., Kigawa, T., Yokoyama, S., Nameki, N., 2010. Solution Structure of the Catalytic Domain of the Mitochondrial Protein ICT1 That Is Essential for Cell Vitality. J. Mol. Biol. 404, 260–273.
Handa, Y., Inaho, N., Nameki, N., 2010. YaeJ is a novel ribosome-associated protein in *Escherichia coli* that can hydrolyze peptidyl-tRNA on stalled ribosomes. Nucleic Acids Res. 39, 1739–1748.
Han, Y., David, A., Liu, B., Magadán, J.G., Bennink, J.R., Yewdell, J.W., Qian, S.-B., 2012. Monitoring cotranslational protein folding in mammalian cells at codon resolution. Proc. Natl. Acad. Sci. U. S. A. 109, 12467–12472.
Haque, M.E., Elmore, K.B., Tripathy, A., Koc, H., Koc, E.C., Spremulli, L.L., 2010. Properties of the C-terminal tail of human mitochondrial inner membrane protein Oxa1L and its interactions with mammalian mitochondrial ribosomes. J. Biol. Chem. 285, 28353–28362.
Haque, M.E., Grasso, D., Spremulli, L.L., 2008. The interaction of mammalian mitochondrial translational initiation factor 3 with ribosomes: evolution of terminal extensions in IF3mt. Nucleic Acids Res. 36, 589–597.
Harbauer, A.B., Zahedi, R.P., Sickmann, A., Pfanner, N., Meisinger, C., 2014. The protein import machinery of mitochondria-a regulatory hub in metabolism, stress, and disease. Cell Metab. 19, 357–372.
Hayes, C.S., Keiler, K.C., 2010. Beyond ribosome rescue: tmRNA and co-translational processes. FEBS Lett. 584, 413–419.
Hell, K., Neupert, W., Stuart, R.A., 2001. Oxa1p acts as a general membrane insertion machinery for proteins encoded by mitochondrial DNA. EMBO J. 20, 1281–1288.

Herr, A.J., Gesteland, R.F., Atkins, J.F., 2000. One protein from two open reading frames: mechanism of a 50 nt translational bypass. EMBO J. 19, 2671–2680.
Holt, I.J., Lorimer, H.E., Jacobs, H.T., 2000. Coupled leading- and lagging-strand synthesis of mammalian mitochondrial DNA. Cell 100, 515–524.
Holzmann, J., Frank, P., Löffler, E., Bennett, K.L., Gerner, C., Rossmanith, W., 2008. RNase P without RNA: Identification and Functional Reconstitution of the Human Mitochondrial tRNA Processing Enzyme. Cell 135, 462–74.
Hornig-Do, H.T., Montanari, A., Rozanska, A., Tuppen, H.A., Almalki, A.A., Abg-Kamaludin, D.P., Frontali, L., Francisci, S., Lightowlers, R.N., Chrzanowska-Lightowlers, Z.M., 2014. Human mitochondrial leucyl tRNA synthetase can suppress non cognate pathogenic mt-tRNA mutations. EMBO Mol. Med. 6, 183–193.
Hsieh, A.C., Liu, Y., Edlind, M.P., Ingolia, N.T., Janes, M.R., Sher, A., Shi, E.Y., Stumpf, C.R., Christensen, C., Bonham, M.J., Wang, S., Ren, P., Martin, M., Jessen, K., Feldman, M.E., Weissman, J.S., Shokat, K.M., Rommel, C., Ruggero, D., 2012. The translational landscape of mTOR signalling steers cancer initiation and metastasis. Nature 485, 55-61.
Huang, W.M., Ao, S.Z., Casjens, S., Orlandi, R., Zeikus, R., Weiss, R., Winge, D., Fang, M., 1988. A persistent untranslated sequence within bacteriophage T4 DNA topoisomerase gene 60. Science 239, 1005–1012.
Hüttemann, M., Lee, I., Samavati, L., Yu, H., Doan, J.W., 2007. Regulation of mitochondrial oxidative phosphorylation through cell signaling. Biochim. Biophys. Acta BBA - Mol. Cell Res. 1773, 1701–1720.
Huynen, M.A., Duarte, I., Chrzanowska-Lightowlers, Z.M.A., Nabuurs, S.B., 2012. Structure based hypothesis of a mitochondrial ribosome rescue mechanism. Biol. Direct 7, 14.
Ingolia, N.T., 2010. Genome-Wide Translational Profiling by Ribosome Footprinting. In: Methods in Enzymology. Elsevier, 470, 119–142.
Ingolia, N.T., 2014. Ribosome profiling: new views of translation, from single codons to genome scale. Nat. Rev. Genet. 15, 205–213.
Ingolia, N.T., Brar, G.A., Rouskin, S., McGeachy, A.M., Weissman, J.S., 2012. The ribosome profiling strategy for monitoring translation *in vivo* by deep sequencing of ribosome-protected mRNA fragments. Nat. Protoc. 7, 1534–1550.
Ingolia, N.T., Ghaemmaghami, S., Newman, J.R.S., Weissman, J.S., 2009. Genome-wide analysis *in vivo* of translation with nucleotide resolution using ribosome profiling. Science 324, 218–223.
Ingolia, N.T., Lareau, L.F., Weissman, J.S., 2011. Ribosome Profiling of Mouse Embryonic Stem Cells Reveals the Complexity and Dynamics of Mammalian Proteomes. Cell 147, 789–802.
Isken, O., Maquat, L.E., 2007. Quality control of eukaryotic mRNA: safeguarding cells from abnormal mRNA function. Genes Dev. 21, 1833–1856.
Ito, K., Uno, M., Nakamura, Y., 2000. A tripeptide “anticodon” deciphers stop codons in messenger RNA. Nature 403, 680–684.
Jackson, R.J., Hellen, C.U.T., Pestova, T.V., 2012. Termination and post-termination events in eukaryotic translation. Adv. Protein Chem. Struct. Biol. 86, 45–93.
Janssen, B.D., Hayes, C.S., 2009. Kinetics of Paused Ribosome Recycling in *Escherichia coli*. J. Mol. Biol. 394, 251–267.

Jones, C.N., Wilkinson, K.A., Hung, K.T., Weeks, K.M., Spremulli, L.L., 2008. Lack of secondary structure characterizes the 5' ends of mammalian mitochondrial mRNAs. RNA N. Y. N 14, 862–871.
Jørgensen, F., Kurland, C.G., 1990. Processivity errors of gene expression in *Escherichia coli.* J. Mol. Biol. 215, 511–521.
Jourdain, A.A., Koppen, M., Wydro, M., Rodley, C.D., Lightowlers, R.N., Chrzanowska-Lightowlers, Z.M., Martinou, J.-C., 2013. GRSF1 regulates RNA processing in mitochondrial RNA granules. Cell Metab. 17, 399–410.
Jungreis, I., Lin, M.F., Spokony, R., Chan, C.S., Negre, N., Victorsen, A., White, K.P., Kellis, M., 2011. Evidence of abundant stop codon readthrough in *Drosophila* and other metazoa. Genome Res. 21, 2096–2113.
Kaushal, P.S., Sharma, M.R., Booth, T.M., Haque, E.M., Tung, C.-S., Sanbonmatsu, K.Y., Spremulli, L.L., Agrawal, R.K., 2014. Cryo-EM structure of the small subunit of the mammalian mitochondrial ribosome. Proc. Natl. Acad. Sci. 111, 7284-7289.
Keiler, K.C., Shapiro, L., Williams, K.P., 2000. tmRNAs that encode proteolysis-inducing tags are found in all known bacterial genomes: A two-piece tmRNA functions in *Caulobacter*. Proc. Natl. Acad. Sci. U. S. A. 97, 7778–7783.
Keiler, K.C., Waller, P.R., Sauer, R.T., 1996. Role of a peptide tagging system in degradation of proteins synthesized from damaged messenger RNA. Science 271, 990–993.
Kirby, D.M., Thorburn, D.R., Turnbull, D.M., Taylor, R.W., 2007. Biochemical Assays of Respiratory Chain Complex Activity. In: Methods in Cell Biology. Elsevier, 80, 93–119.
Kisselev, L.L., Buckingham, R.H., 2000. Translational termination comes of age. Trends Biochem. Sci. 25, 561–566.
Koc, E.C., Spremulli, L.L., 2002. Identification of mammalian mitochondrial translational initiation factor 3 and examination of its role in initiation complex formation with natural mRNAs. J. Biol. Chem. 277, 35541–35549.
Kogure, H., Handa, Y., Nagata, M., Kanai, N., Güntert, P., Kubota, K., Nameki, N., 2014. Identification of residues required for stalled-ribosome rescue in the codon-independent release factor YaeJ. Nucleic Acids Res. 42, 3152–3163.
Kogure, H., Hikawa, Y., Hagihara, M., Tochio, N., Koshiba, S., Inoue, Y., Güntert, P., Kigawa, T., Yokoyama, S., Nameki, N., 2012. Solution structure and siRNA-mediated knockdown analysis of the mitochondrial disease-related protein C12orf65. Proteins 80, 2629-2642.
Konecki, D.S., Aune, K.C., Tate, W., Caskey, C.T., 1977. Characterization of reticulocyte release factor. J. Biol. Chem. 252, 4514–4520.
Kontos, H., Napthine, S., Brierley, I., 2001. Ribosomal pausing at a frameshifter RNA pseudoknot is sensitive to reading phase but shows little correlation with frameshift efficiency. Mol. Cell. Biol. 21, 8657–8670.
Korhonen, J.A., Gaspari, M., Falkenberg, M., 2003. TWINKLE Has 5' -> 3' DNA helicase activity and is specifically stimulated by mitochondrial single-stranded DNA-binding protein. J. Biol. Chem. 278, 48627–48632.
Kuhn, K.M., DeRisi, J.L., Brown, P.O., Sarnow, P., 2001. Global and specific translational regulation in the genomic response of *Saccharomyces cerevisiae* to a rapid transfer from a fermentable to a nonfermentable carbon source. Mol. Cell. Biol. 21, 916–927.

Kurita, D., Sasaki, R., Muto, A., Himeno, H., 2007. Interaction of SmpB with ribosome from directed hydroxyl radical probing. Nucleic Acids Res. 35, 7248–7255.
Lang, B.F., Burger, G., O'Kelly, C.J., Cedergren, R., Golding, G.B., Lemieux, C., Sankoff, D., Turmel, M., Gray, M.W., 1997. An ancestral mitochondrial DNA resembling a eubacterial genome in miniature. Nature 387, 493–497.
Lang, B.F., Gray, M.W., Burger, G., 1999. Mitochondrial genome evolution and the origin of eukaryotes. Annu. Rev. Genet. 33, 351–397.
Lang, B.F., Jakubkova, M., Hegedusova, E., Daoud, R., Forget, L., Brejova, B., Vinar, T., Kosa, P., Fricova, D., Nebohacova, M., Griac, P., Tomaska, L., Burger, G., Nosek, J., 2014. Massive programmed translational jumping in mitochondria. Proc. Natl. Acad. Sci. U. S. A. 111, 5926–5931.
LaRiviere, F.J., Cole, S.E., Ferullo, D.J., Moore, M.J., 2006. A Late-Acting Quality Control Process for Mature Eukaryotic rRNAs. Mol. Cell 24, 619–626.
Laurberg, M., Asahara, H., Korostelev, A., Zhu, J., Trakhanov, S., Noller, H.F., 2008. Structural basis for translation termination on the 70S ribosome. Nature 454, 852–857.
Lee, C.C., Timms, K.M., Trotman, C.N., Tate, W.P., 1987. Isolation of a rat mitochondrial release factor. Accommodation of the changed genetic code for termination. J. Biol. Chem. 262, 3548–3552.
Lee, S., Liu, B., Lee, S., Huang, S.-X., Shen, B., Qian, S.-B., 2012. Global mapping of translation initiation sites in mammalian cells at single-nucleotide resolution. Proc. Natl. Acad. Sci. U. S. A. 109, E2424–2432.
Li, G.-W., Oh, E., Weissman, J.S., 2012. The anti-Shine–Dalgarno sequence drives translational pausing and codon choice in bacteria. Nature 484, 538–541.
Lill, R., 2009. Function and biogenesis of iron–sulphur proteins. Nature 460, 831–838.
Litonin, D., Sologub, M., Shi, Y., Savkina, M., Anikin, M., Falkenberg, M., Gustafsson, C.M., Temiakov, D., 2010. Human Mitochondrial Transcription Revisited: Only TFAM And TFB2M Are Required For Transcription Of The Mitochondrial Genes *In Vitro*. J. Biol. Chem. 285, 18129–18133.
Liu, B., Han, Y., Qian, S.-B., 2013. Cotranslational response to proteotoxic stress by elongation pausing of ribosomes. Mol. Cell 49, 453–463.
Liu, M., Spremulli, L., 2000. Interaction of mammalian mitochondrial ribosomes with the inner membrane. J. Biol. Chem. 275, 29400–29406.
Livak, K.J., Schmittgen, T.D., 2001. Analysis of Relative Gene Expression Data Using Real-Time Quantitative PCR and the $2^{-\Delta\Delta CT}$ Method. Methods 25, 402–408.
Li, X., Yagi, M., Morita, T., Aiba, H., 2008. Cleavage of mRNAs and role of tmRNA system under amino acid starvation in *Escherichia coli*. Mol. Microbiol. 68, 462–473.
Loman, N.J., Misra, R.V., Dallman, T.J., Constantinidou, C., Gharbia, S.E., Wain, J., Pallen, M.J., 2012. Performance comparison of benchtop high-throughput sequencing platforms. Nat. Biotechnol. 30, 434–439.
Lynch, M., Koskella, B., Schaack, S., 2006. Mutation pressure and the evolution of organelle genomic architecture. Science 311, 1727–1730.
Martinou, J.-C., Youle, R.J., 2011. Mitochondria in Apoptosis: Bcl-2 Family Members and Mitochondrial Dynamics. Dev. Cell 21, 92–101.

Mašek, T., Valášek, L., Pospíšek, M., 2011. Polysome analysis and RNA purification from sucrose gradients. Methods Mol. Biol. Clifton NJ 703, 293–309.
Masters, B.S., Stohl, L.L., Clayton, D.A., 1987. Yeast mitochondrial RNA polymerase is homologous to those encoded by bacteriophages T3 and T7. Cell 51, 89–99.
McFarland, R., Clark, K.M., Morris, A.A.M., Taylor, R.W., Macphail, S., Lightowlers, R.N., Turnbull, D.M., 2002. Multiple neonatal deaths due to a homoplasmic mitochondrial DNA mutation. Nat. Genet. 30, 145–146.
Mears, J.A., Sharma, M.R., Gutell, R.R., McCook, A.S., Richardson, P.E., Caulfield, T.R., Agrawal, R.K., Harvey, S.C., 2006. A structural model for the large subunit of the mammalian mitochondrial ribosome. J. Mol. Biol. 358, 193–212.
Meaux, S., Van Hoof, A., 2006. Yeast transcripts cleaved by an internal ribozyme provide new insight into the role of the cap and poly(A) tail in translation and mRNA decay. RNA N. Y. N 12, 1323–1337.
Metodiev, M.D., Lesko, N., Park, C.B., Cámara, Y., Shi, Y., Wibom, R., Hultenby, K., Gustafsson, C.M., Larsson, N.-G., 2009. Methylation of 12S rRNA is necessary for *in vivo* stability of the small subunit of the mammalian mitochondrial ribosome. Cell Metab. 9, 386–397.
Mitra, K., Wunder, C., Roysam, B., Lin, G., Lippincott-Schwartz, J., 2009. From the Cover: A hyperfused mitochondrial state achieved at G1-S regulates cyclin E buildup and entry into S phase. Proc. Natl. Acad. Sci. 106, 11960–11965.
Montoya, J., Christianson, T., Levens, D., Rabinowitz, M., Attardi, G., 1982. Identification of initiation sites for heavy-strand and light-strand transcription in human mitochondrial DNA. Proc. Natl. Acad. Sci. U. S. A. 79, 7195–7199.
Montoya, J., Ojala, D., Attardi, G., 1981. Distinctive features of the 5'-terminal sequences of the human mitochondrial mRNAs. Nature 290, 465–470.
Moore, S.D., Sauer, R.T., 2007. The tmRNA system for translational surveillance and ribosome rescue. Annu. Rev. Biochem. 76, 101–124.
Morozov, Y.I., Parshin, A.V., Agaronyan, K., Cheung, A.C.M., Anikin, M., Cramer, P., Temiakov, D., 2015. A model for transcription initiation in human mitochondria. Nucleic Acids Res. 43, 3726–3735.
Müller, M., Mentel, M., van Hellemond, J.J., Henze, K., Woehle, C., Gould, S.B., Yu, R.-Y., van der Giezen, M., Tielens, A.G.M., Martin, W.F., 2012. Biochemistry and evolution of anaerobic energy metabolism in eukaryotes. Microbiol. Mol. Biol. Rev. MMBR 76, 444–495.
Nagaike, T., 2005. Human Mitochondrial mRNAs Are Stabilized with Polyadenylation Regulated by Mitochondria-specific Poly(A) Polymerase and Polynucleotide Phosphorylase. J. Biol. Chem. 280, 19721–19727.
Nakamura, Y., Ito, K., Isaksson, L.A., 1996. Emerging understanding of translation termination. Cell 87, 147–150.
Namy, O., Rousset, J.-P., Napthine, S., Brierley, I., 2004. Reprogrammed genetic decoding in cellular gene expression. Mol. Cell 13, 157–168.
Ngo, H.B., Kaiser, J.T., Chan, D.C., 2011. The mitochondrial transcription and packaging factor TFAM imposes a U-turn on mitochondrial DNA. Nat. Struct. Mol. Biol. 18, 1290–1296.
Nosek, J., Tomaska, L., Burger, G., Lang, B.F., 2015. Programmed translational bypassing elements in mitochondria: structure, mobility, and evolutionary origin. Trends Genet. TIG 31, 187–194.

Nosek, J., Tomáška, L., Fukuhara, H., Suyama, Y., Kováč, L., 1998. Linear mitochondrial genomes: 30 years down the line. Trends Genet. 14, 184–188.
Nunnari, J., Suomalainen, A., 2012. Mitochondria: In Sickness and in Health. Cell 148, 1145–1159.
O'Brien, T.W., 1971. The general occurrence of 55 S ribosomes in mammalian liver mitochondria. J. Biol. Chem. 246, 3409–3417.
O'Brien, T.W., 2002. Evolution of a protein-rich mitochondrial ribosome: implications for human genetic disease. Gene 286, 73–79.
O'Brien, T.W., 2003. Properties of human mitochondrial ribosomes. IUBMB Life 55, 505–513.
Ogle, J.M., Ramakrishnan, V., 2005. Structural insights into translational fidelity. Annu. Rev. Biochem. 74, 129–177.
Oh, E., Becker, A.H., Sandikci, A., Huber, D., Chaba, R., Gloge, F., Nichols, R.J., Typas, A., Gross, C.A., Kramer, G., Weissman, J.S., Bukau, B., 2011. Selective ribosome profiling reveals the cotranslational chaperone action of trigger factor *in vivo*. Cell 147, 1295–1308.
Ojala, D., Montoya, J., Attardi, G., 1981. tRNA punctuation model of RNA processing in human mitochondria. Nature 290, 470–474.
Old, S.L., Johnson, M.A., 1989. Methods of microphotometric assay of succinate dehydrogenase and cytochrome *c* oxidase activities for use on human skeletal muscle. Histochem. J. 21, 545–555.
Ott, M., Herrmann, J.M., 2010. Co-translational membrane insertion of mitochondrially encoded proteins. Biochim. Biophys. Acta 1803, 767–775.
Pedersen, K., Zavialov, A.V., Pavlov, M.Y., Elf, J., Gerdes, K., Ehrenberg, M., 2003. The bacterial toxin RelE displays codon-specific cleavage of mRNAs in the ribosomal A site. Cell 112, 131–140.
Perales-Clemente, E., Fernández-Vizarra, E., Acín-Pérez, R., Movilla, N., Bayona-Bafaluy, M.P., Moreno-Loshuertos, R., Pérez-Martos, A., Fernández-Silva, P., Enríquez, J.A., 2010. Five entry points of the mitochondrially encoded subunits in mammalian complex I assembly. Mol. Cell. Biol. 30, 3038–3047.
Pisareva, V.P., Skabkin, M.A., Hellen, C.U.T., Pestova, T.V., Pisarev, A.V., 2011. Dissociation by Pelota, Hbs1 and ABCE1 of mammalian vacant 80S ribosomes and stalled elongation complexes. EMBO J. 30, 1804–1817.
Pisarev, A.V., Skabkin, M.A., Pisareva, V.P., Skabkina, O.V., Rakotondrafara, A.M., Hentze, M.W., Hellen, C.U.T., Pestova, T.V., 2010. The role of ABCE1 in eukaryotic posttermination ribosomal recycling. Mol. Cell 37, 196–210.
Pohjoismäki, J.L.O., Holmes, J.B., Wood, S.R., Yang, M.-Y., Yasukawa, T., Reyes, A., Bailey, L.J., Cluett, T.J., Goffart, S., Willcox, S., Rigby, R.E., Jackson, A.P., Spelbrink, J.N., Griffith, J.D., Crouch, R.J., Jacobs, H.T., Holt, I.J., 2010. Mammalian Mitochondrial DNA Replication Intermediates Are Essentially Duplex but Contain Extensive Tracts of RNA/DNA Hybrid. J. Mol. Biol. 397, 1144–1155.
Preis, A., Heuer, A., Barrio-Garcia, C., Hauser, A., Eyler, D.E., Berninghausen, O., Green, R., Becker, T., Beckmann, R., 2014. Cryoelectron microscopic structures of eukaryotic translation termination complexes containing eRF1-eRF3 or eRF1-ABCE1. Cell Rep. 8, 59–65.
Pyle, A., Venkateswaran, R., Marina, B., Veronika, B., Aurora, G.-D., Agnes, H.,

L, B.E., Tania, S., Jennifer, D., Gail, E., David, M., Patrick, Y.W.M., Konstantinos, D., Mauro, S.-K., Helen, G., Hanns, L., Veronika, K., W, T.R., F, C.P., Rita, H., 2014. Behr's Syndrome is Typically Associated with Disturbed Mitochondrial Translation and Mutations in the *C12orf65* Gene. J. Neuromuscul. Dis. 1, 55–63.

Reyes, A., Kazak, L., Wood, S.R., Yasukawa, T., Jacobs, H.T., Holt, I.J., 2013. Mitochondrial DNA replication proceeds via a “bootlace” mechanism involving the incorporation of processed transcripts. Nucleic Acids Res. 41, 5837–5850.

Richter, R., Pajak, A., Dennerlein, S., Rozanska, A., Lightowlers, R.N., Chrzanowska-Lightowlers, Z.M.A., 2010a. Translation termination in human mitochondrial ribosomes. Biochem. Soc. Trans. 38, 1523–1526.

Richter, R., Rorbach, J., Pajak, A., Smith, P.M., Wessels, H.J., Huynen, M.A., Smeitink, J.A., Lightowlers, R.N., Chrzanowska-Lightowlers, Z.M., 2010b. A functional peptidyl-tRNA hydrolase, ICT1, has been recruited into the human mitochondrial ribosome. EMBO J. 29, 1116–1125.

Rizzuto, R., Pinton, P., Carrington, W., Fay, F.S., Fogarty, K.E., Lifshitz, L.M., Tuft, R.A., Pozzan, T., 1998. Close contacts with the endoplasmic reticulum as determinants of mitochondrial Ca^{2+} responses. Science 280, 1763–1766.

Robberson, D.L., Kasamatsu, H., Vinograd, J., 1972. Replication of mitochondrial DNA. Circular replicative intermediates in mouse L cells. Proc. Natl. Acad. Sci. U. S. A. 69, 737–741.

Roche, E.D., Sauer, R.T., 1999. SsrA-mediated peptide tagging caused by rare codons and tRNA scarcity. EMBO J. 18, 4579–4589.

Rooijers, K., Loayza-Puch, F., Nijtmans, L.G., Agami, R., 2013. Ribosome profiling reveals features of normal and disease-associated mitochondrial translation. Nat. Commun. 4, 2886.

Rorbach, J., Richter, R., Wessels, H.J., Wydro, M., Pekalski, M., Farhoud, M., Kuhl, I., Gaisne, M., Bonnefoy, N., Smeitink, J.A., Lightowlers, R.N., Chrzanowska-Lightowlers, Z.M.A., 2008a. The human mitochondrial ribosome recycling factor is essential for cell viability. Nucleic Acids Res. 36, 5787–5799.

Rorbach, J., Yusoff, A.A., Tuppen, H., Abg-Kamaludin, D.P., Chrzanowska-Lightowlers, Z.M.A., Taylor, R.W., Turnbull, D.M., McFarland, R., Lightowlers, R.N., 2008b. Overexpression of human mitochondrial valyl tRNA synthetase can partially restore levels of cognate mt-$tRNA^{Val}$ carrying the pathogenic C25U mutation. Nucleic Acids Res. 36, 3065–3074.

Ruzzenente, B., Metodiev, M.D., Wredenberg, A., Bratic, A., Park, C.B., Cámara, Y., Milenkovic, D., Zickermann, V., Wibom, R., Hultenby, K., Erdjument-Bromage, H., Tempst, P., Brandt, U., Stewart, J.B., Gustafsson, C.M., Larsson, N.-G., 2012. LRPPRC is necessary for polyadenylation and coordination of translation of mitochondrial mRNAs. EMBO J. 31, 443–456.

Sasarman, F., Brunel-Guitton, C., Antonicka, H., Wai, T., Shoubridge, E.A., LSFC Consortium, 2010. LRPPRC and SLIRP interact in a ribonucleoprotein complex that regulates posttranscriptional gene expression in mitochondria. Mol. Biol. Cell 21, 1315–1323.

Schaeffer, D., van Hoof, A., 2011. Different nuclease requirements for exosome-mediated degradation of normal and nonstop mRNAs. Proc. Natl. Acad. Sci. U. S. A. 108, 2366–2371.

Shalgi, R., Hurt, J.A., Krykbaeva, I., Taipale, M., Lindquist, S., Burge, C.B., 2013. Widespread regulation of translation by elongation pausing in heat shock. Mol. Cell 49, 439–452.
Sharma, M.R., Koc, E.C., Datta, P.P., Booth, T.M., Spremulli, L.L., Agrawal, R.K., 2003. Structure of the mammalian mitochondrial ribosome reveals an expanded functional role for its component proteins. Cell 115, 97–108.
Shimazaki, H., Takiyama, Y., Ishiura, H., Sakai, C., Matsushima, Y., Hatakeyama, H., Honda, J., Sakoe, K., Naoi, T., Namekawa, M., Fukuda, Y., Takahashi, Y., Goto, J., Tsuji, S., Goto, Y., Nakano, I., 2012. A homozygous mutation of C12orf65 causes spastic paraplegia with optic atrophy and neuropathy (SPG55). J. Med. Genet. 49, 777–784.
Shimizu, Y., 2012. ArfA Recruits RF2 into Stalled Ribosomes. J. Mol. Biol. 423, 624-631.
Shimizu, Y., 2014. Biochemical aspects of bacterial strategies for handling the incomplete translation processes. Front. Microbiol. 5, 170.
Shoemaker, C.J., Eyler, D.E., Green, R., 2010. Dom34:Hbs1 Promotes Subunit Dissociation and Peptidyl-tRNA Drop-Off to Initiate No-Go Decay. Science 330, 369–372.
Smeitink, J., van den Heuvel, L., DiMauro, S., 2001. The genetics and pathology of oxidative phosphorylation. Nat. Rev. Genet. 2, 342–352.
Smits, P., Mattijssen, S., Morava, E., van den Brand, M., van den Brandt, F., Wijburg, F., Pruijn, G., Smeitink, J., Nijtmans, L., Rodenburg, R., van den Heuvel, L., 2010a. Functional consequences of mitochondrial tRNA Trp and tRNA Arg mutations causing combined OXPHOS defects. Eur. J. Hum. Genet. EJHG 18, 324–329.
Smits, P., Smeitink, J., van den Heuvel, L., 2010b. Mitochondrial translation and beyond: processes implicated in combined oxidative phosphorylation deficiencies. J. Biomed. Biotechnol. 2010, 737385.
Soleimanpour-Lichaei, H.R., Kühl, I., Gaisne, M., Passos, J.F., Wydro, M., Rorbach, J., Temperley, R., Bonnefoy, N., Tate, W., Lightowlers, R., Chrzanowska-Lightowlers, Z., 2007. mtRF1a Is a Human Mitochondrial Translation Release Factor Decoding the Major Termination Codons UAA and UAG. Mol. Cell 27, 745–757.
Sologub, M., Litonin, D., Anikin, M., Mustaev, A., Temiakov, D., 2009. TFB2 is a transient component of the catalytic site of the human mitochondrial RNA polymerase. Cell 139, 934–944.
Somogyi, P., Jenner, A.J., Brierley, I., Inglis, S.C., 1993. Ribosomal pausing during translation of an RNA pseudoknot. Mol. Cell. Biol. 13, 6931–6940.
Sparks, K.A., Dieckmann, C.L., 1998. Regulation of poly(A) site choice of several yeast mRNAs. Nucleic Acids Res. 26, 4676–4687.
Spiegel, R., Mandel, H., Saada, A., Lerer, I., Burger, A., Shaag, A., Shalev, S.A., Jabaly-Habib, H., Goldsher, D., Gomori, J.M., Lossos, A., Elpeleg, O., Meiner, V., 2014. Delineation of C12orf65-related phenotypes: a genotype–phenotype relationship. Eur. J. Hum. Genet. 22, 1019-25.
Sprinzl, M., 1994. Elongation factor Tu: a regulatory GTPase with an integrated effector. Trends Biochem. Sci. 19, 245–250.
Stadler, M., Fire, A., 2011. Wobble base-pairing slows *in vivo* translation elongation in metazoans. RNA N. Y. N 17, 2063–2073.
Steitz, J.A., 1969. Polypeptide Chain Initiation: Nucleotide Sequences of the Three Ribosomal Binding Sites in Bacteriophage R17 RNA. Nature 224, 957–964.

Szyrach, G., Ott, M., Bonnefoy, N., Neupert, W., Herrmann, J.M., 2003. Ribosome binding to the Oxa1 complex facilitates co-translational protein insertion in mitochondria. EMBO J. 22, 6448–6457.
Tate, W.P., Brown, C.M., 1992. Translational termination: “stop” for protein synthesis or “pause” for regulation of gene expression. Biochemistry (Mosc.) 31, 2443–2450.
Temperley, R.J., Seneca, S.H., Tonska, K., Bartnik, E., Bindoff, L.A., Lightowlers, R.N., Chrzanowska-Lightowlers, Z.M.A., 2003. Investigation of a pathogenic mtDNA microdeletion reveals a translation-dependent deadenylation decay pathway in human mitochondria. Hum. Mol. Genet. 12, 2341–2348.
Temperley, R.J., Wydro, M., Lightowlers, R.N., Chrzanowska-Lightowlers, Z.M., 2010. Human mitochondrial mRNAs--like members of all families, similar but different. Biochim. Biophys. Acta 1797, 1081–1085.
Temperley, R., Richter, R., Dennerlein, S., Lightowlers, R.N., Chrzanowska-Lightowlers, Z.M., 2010. Hungry Codons Promote Frameshifting in Human Mitochondrial Ribosomes. Science 327, 301–301.
Thorvaldsdóttir, H., Robinson, J.T., Mesirov, J.P., 2013. Integrative Genomics Viewer (IGV): high-performance genomics data visualization and exploration. Brief. Bioinform. 14, 178–192.
Timmis, J.N., Ayliffe, M.A., Huang, C.Y., Martin, W., 2004. Endosymbiotic gene transfer: organelle genomes forge eukaryotic chromosomes. Nat. Rev. Genet. 5, 123–135.
Tomecki, R., Dmochowska, A., Gewartowski, K., Dziembowski, A., Stepien, P.P., 2004. Identification of a novel human nuclear-encoded mitochondrial poly(A) polymerase. Nucleic Acids Res. 32, 6001–6014.
Trapnell, C., Roberts, A., Goff, L., Pertea, G., Kim, D., Kelley, D.R., Pimentel, H., Salzberg, S.L., Rinn, J.L., Pachter, L., 2012. Differential gene and transcript expression analysis of RNA-seq experiments with TopHat and Cufflinks. Nat. Protoc. 7, 562–578.
Trobro, S., Åqvist, J., 2007. A Model for How Ribosomal Release Factors Induce Peptidyl-tRNA Cleavage in Termination of Protein Synthesis. Mol. Cell 27, 758–766.
Tsuboi, M., Morita, H., Nozaki, Y., Akama, K., Ueda, T., Ito, K., Nierhaus, K.H., Takeuchi, N., 2009. EF-G2mt is an exclusive recycling factor in mammalian mitochondrial protein synthesis. Mol. Cell 35, 502–510.
Tucci, A., Liu, Y.-T., Preza, E., Pitceathly, R.D.S., Chalasani, A., Plagnol, V., Land, J.M., Trabzuni, D., Ryten, M., on behalf of UKBEC, Jaunmuktane, Z., Reilly, M.M., Brandner, S., Hargreaves, I., Hardy, J., Singleton, A.B., Abramov, A.Y., Houlden, H., 2013. Novel *C12orf65* mutations in patients with axonal neuropathy and optic atrophy. J. Neurol. Neurosurg. Psychiatry 85, 486-92.
Unseld, M., Marienfeld, J.R., Brandt, P., Brennicke, A., 1997. The mitochondrial genome of *Arabidopsis thaliana* contains 57 genes in 366,924 nucleotides. Nat. Genet. 15, 57–61.
Van Belzen, N., Diesveld, M.P., van der Made, A.C., Nozawa, Y., Dinjens, W.N., Vlietstra, R., Trapman, J., Bosman, F.T., 1995. Identification of mRNAs that show modulated expression during colon carcinoma cell differentiation. Eur. J. Biochem. FEBS 234, 843–848.
Van Belzen, N., Dinjens, W.N., Eussen, B.H., Bosman, F.T., 1998. Expression of differentiation-related genes in colorectal cancer: possible implications for prognosis. Histol. Histopathol. 13, 1233–1242.

Van Hoof, A., Frischmeyer, P.A., Dietz, H.C., Parker, R., 2002. Exosome-mediated recognition and degradation of mRNAs lacking a termination codon. Science 295, 2262–2264.
Verma, R., Oania, R.S., Kolawa, N.J., Deshaies, R.J., 2013. Cdc48/p97 promotes degradation of aberrant nascent polypeptides bound to the ribosome. eLife 2, e00308.
Vivanco-Domínguez, S., Bueno-Martínez, J., León-Avila, G., Iwakura, N., Kaji, A., Kaji, H., Guarneros, G., 2012. Protein Synthesis Factors (RF1, RF2, RF3, RRF, and tmRNA) and Peptidyl-tRNA Hydrolase Rescue Stalled Ribosomes at Sense Codons. J. Mol. Biol. 417, 425–439.
Vogel, R.O., Smeitink, J.A.M., Nijtmans, L.G.J., 2007. Human mitochondrial complex I assembly: a dynamic and versatile process. Biochim. Biophys. Acta 1767, 1215–1227.
Weixlbaumer, A., Jin, H., Neubauer, C., Voorhees, R.M., Petry, S., Kelley, A.C., Ramakrishnan, V., 2008. Insights into translational termination from the structure of RF2 bound to the ribosome. Science 322, 953–956.
Wen, J.-D., Lancaster, L., Hodges, C., Zeri, A.-C., Yoshimura, S.H., Noller, H.F., Bustamante, C., Tinoco, I., 2008. Following translation by single ribosomes one codon at a time. Nature 452, 598–603.
Wesolowska, M.T., Richter-Dennerlein, R., Lightowlers, R.N., Chrzanowska-Lightowlers, Z.M.A., 2014. Overcoming stalled translation in human mitochondria. Front. Microbiol. 5, 374.
Wilson, W.C., Hornig-Do, H.-T., Bruni, F., Chang, J.H., Jourdain, A.A., Martinou, J.-C., Falkenberg, M., Spåhr, H., Larsson, N.-G., Lewis, R.J., Hewitt, L., Baslé, A., Cross, H.E., Tong, L., Lebel, R.R., Crosby, A.H., Chrzanowska-Lightowlers, Z.M.A., Lightowlers, R.N., 2014. A human mitochondrial poly(A) polymerase mutation reveals the complexities of post-transcriptional mitochondrial gene expression. Hum. Mol. Genet. 23, 6345–6355.
Withey, J.H., Friedman, D.I., 2003. A salvage pathway for protein synthesis: tmRNA and *trans* -translation. Annu. Rev. Microbiol. 57, 101–123.
Woriax, V.L., Bullard, J.M., Ma, L., Yokogawa, T., Spremulli, L.L., 1997. Mechanistic studies of the translational elongation cycle in mammalian mitochondria. Biochim. Biophys. Acta 1352, 91–101.
Yasukawa, T., Yang, M.-Y., Jacobs, H.T., Holt, I.J., 2005. A bidirectional origin of replication maps to the major noncoding region of human mitochondrial DNA. Mol. Cell 18, 651–662.
Yoshikawa, S., Muramoto, K., Shinzawa-Itoh, K., Aoyama, H., Tsukihara, T., Ogura, T., Shimokata, K., Katayama, Y., Shimada, H., 2006. Reaction mechanism of bovine heart cytochrome *c* oxidase. Biochim. Biophys. Acta 1757, 395–400.
Young, D.J., Edgar, C.D., Murphy, J., Fredebohm, J., Poole, E.S., Tate, W.P., 2010. Bioinformatic, structural, and functional analyses support release factor-like MTRF1 as a protein able to decode nonstandard stop codons beginning with adenine in vertebrate mitochondria. RNA N. Y. N 16, 1146–1155.
Zavialov, A.V., Hauryliuk, V.V., Ehrenberg, M., 2005. Splitting of the posttermination ribosome into subunits by the concerted action of RRF and EF-G. Mol. Cell 18, 675–686.
Zhang, Y., Spremulli, L.L., 1998. Identification and cloning of human mitochondrial translational release factor 1 and the ribosome recycling factor. Biochim. Biophys. Acta 1443, 245–250.

Publications arising

Publications arising from my PhD project:

Wesolowska, M.T., Richter-Dennerlein, R., Lightowlers, R.N., Chrzanowska-Lightowlers, Z.M.A., 2014. Overcoming stalled translation in human mitochondria. Front. Microbiol. 5.

Manuscript in preparation:

Adult onset Leigh syndrome in the intensive care setting: a novel presentation of a *C12orf65* related mitochondrial disease,

Maria Wesolowska, Grainne S. Gorman, Charlotte Alston, Aleksandra Pajak, Angela Pyle, Langping He, Helen Griffin, Patrick F. Chinnery, James A.L. Miller, Andrew M. Schaefer, Robert W. Taylor, Robert N Lightowlers and Zofia M Chrzanowska-Lightowlers.

Future publications:

Characterization of normal mitochondrial translation by mitoribosome profiling.

Appendices

Appendix 1.1.

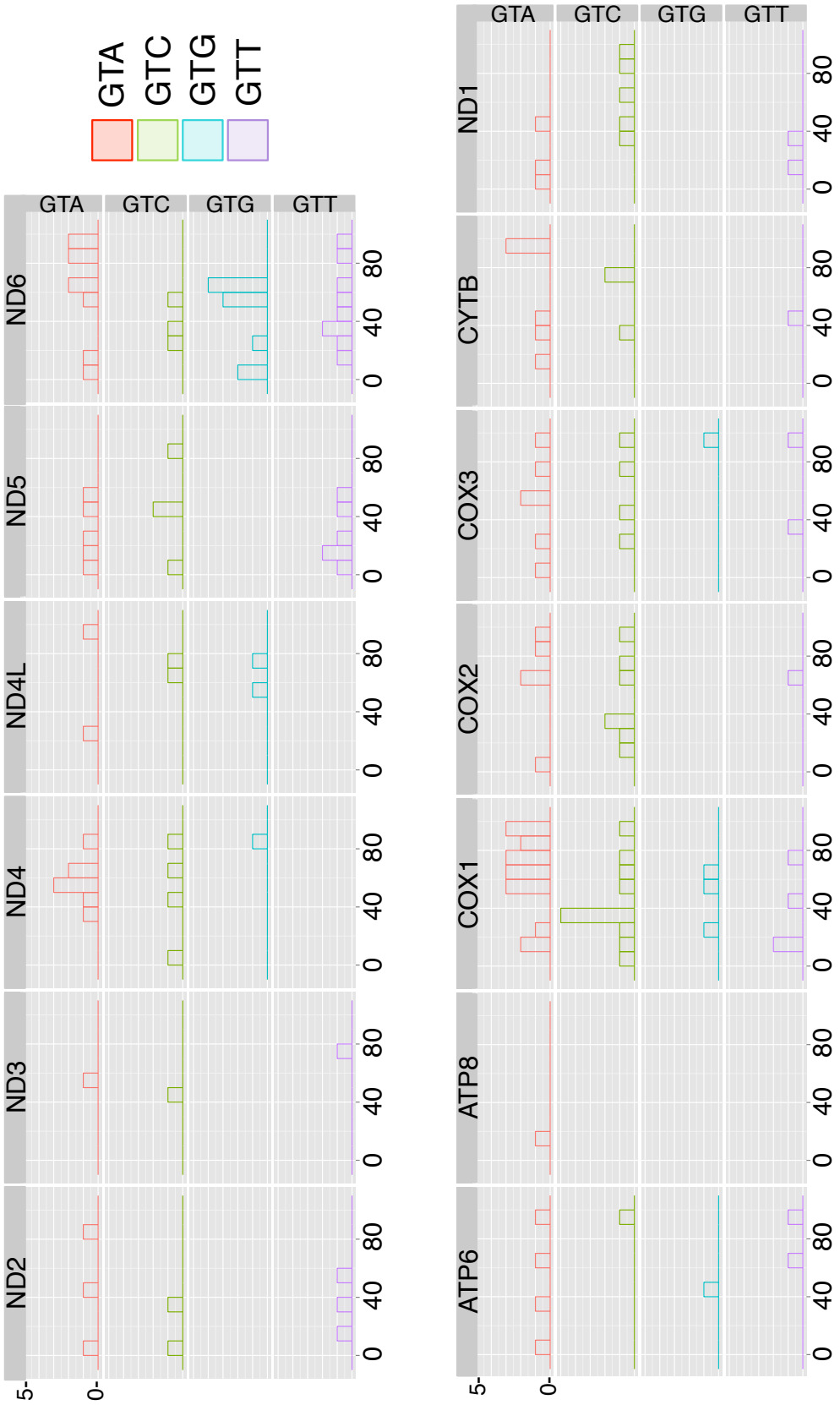

Figure A1. Position of valine codons in mtDNA (enlarged Fig. 6.9 A)

Marked positions of valine codons in all mitochondrial polypeptide genes. Position of each valine codon type is represented in a separate panel.

Appendix 1.2.

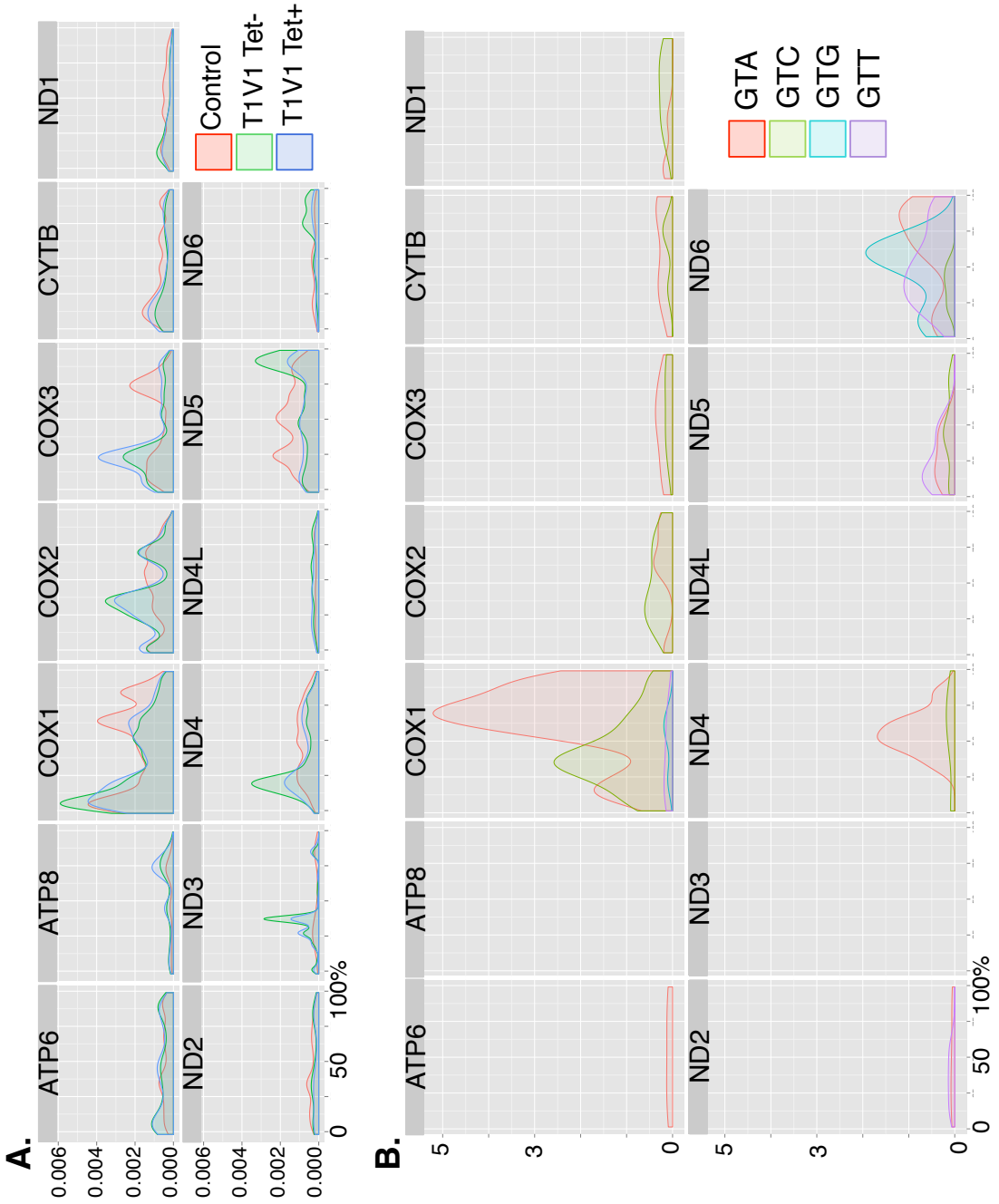

Figure A2. Distribution of mitoribosomes is not dependent on the position of valine codons (enlarged Fig. 6.10)

A. Density of the RFs across each mt-transcript was calculated and plotted for all 3 cell lines: wild type control (in red), uninduced T1V1 (Tet-, in green), unsuccessfully induced T1V1 (Tet+, in blue). The full length of each transcript was presented as 100%. **B.** Position of valine codons in mtDNA was marked for each type of codon separately. Amount of different Val codon was presented as density plots over the length of each mitochondrial transcript (length represented in %).

Appendix 1.3.

List of all sequencing raw data files generated in this project.

T1V1 ribosome profiling first experiment:
2553_1_Tet_-_ATCACGA_L004_R1_001.fastq
2553_2_Tet_Plus_CGATGTA_L004_R1_001.fastq
('Tet-' uninduced T1V1, 'Tet plus' failed T1V1 rescue)

T1V1 ribosome profiling second experiment:
2934_1_RP2_-Tet__A_ATCACGA_L005_R1_001.fastq
2934_2_RP2_Control__A_TTAGGCA_L005_R1_001.fastq
('-Tet ' uninduced T1V1, 'Control' 143B parental)

C12orf65 depletion ribosome profiling experiment:
2934_3_siC12_RP1__A_TGACCAA_L005_R1_001.fastq
2934_4_siNT_RP1__A_ACAGTGA_L005_R1_001.fastq

T1V1 RNAseq experiment (complementary to the second T1V1 ribosome profiling experiment):
3206_rp2_-tet_atcacga_l008_r1_001.fastq
3206_rp2_control_ttaggca_l008_r1_001.fastq

C12orf65 depletion RNAseq experiment (complementary to ribosome profiling experiment):
3206_sint_rp1_gatcaga_l008_r1_001.fastq
3206_sic12_rp1_acttgaa_l008_r1_001.fastq

Appendix 1.4.

Table A1. Number of reads in mitoribosome profiling samples at various steps of alignment

Sample	Reads raw data	Reads after screening	Reads aligned to mt-mRNA
SRR935452	183,299,160	43,210,341 (23.72%)	5,689,430 (13.17%)
2553_1_Tet	62,039,090	4815136 (7,77%)	163,588 (3.4%)
2553_2_Tet_Plus	50,296,184	3,341,448 (6.65%)	131,646 (3.9%)
2934_1_RP2_Tet	33,452,085	7,597,643 (23.52%)	26,970 (0.35%)
2934_2_RP2_Control	50,942,344	20,477,944 (42.68%)	76,575 (0.37%)
2934_3_ siC12_RP1	40,484,160	6,075,251 (15.6%)	36,359 (0.6%)
2934_4_ siNT_RP1	33,453,267	7,334,514 (22.6%)	12,489 (0.49%)

Column 3 ('Reads after screening') presents number of reads that did not align to the decoy reference genome (containing tRNA and rRNA sequences)

Percentage values are calculated in relation to the value in the preceeding column.

Data in sample SRR935452 come from experiments described in (Rooijers et al., 2013)

Table A2. Number of reads in RNAseq samples (fastq)

Sample	Total reads
3206_rp2_-tet	49,451,300
3206_rp2_control	45,584,649
3206_sint_rp1	48,447,645
3206_sic12_rp1	48,167,239

Appendix 1.5.

frontiers in
MICROBIOLOGY

PERSPECTIVE ARTICLE
published: 18 July 2014
doi: 10.3389/fmicb.2014.00374

Overcoming stalled translation in human mitochondria

Maria T. Wesolowska, Ricarda Richter-Dennerlein†, Robert N. Lightowlers and Zofia M. A. Chrzanowska-Lightowlers*

Wellcome Trust Centre for Mitochondrial Research, Institute for Cell and Molecular Biosciences, Newcastle University, Medical School, Newcastle upon Tyne, UK

Edited by:
Kenneth C. Keiler, Pennsylvania State University, USA

Reviewed by:
Tatsuhiko Abo, Okayama University, Japan
Umesh Varshney, Indian Institute of Science, India

Correspondence:
Zofia M. A. Chrzanowska-Lightowlers, Wellcome Trust Centre for Mitochondrial Research, Institute for Cell and Molecular Biosciences, Newcastle University, Medical School, Framlington Place, NE2 4HH, Newcastle upon Tyne, UK
e-mail: zofia.chrzanowska-lightowlers@ncl.ac.uk

†Present address:
Ricarda Richter-Dennerlein, Department of Cellular Biochemistry, University Medical Centre Göttingen, Humboldtallee 23, D-37073 Göttingen, Germany

Protein synthesis is central to life and maintaining a highly accurate and efficient mechanism is essential. What happens when a translating ribosome stalls on a messenger RNA? Many highly intricate processes have been documented in the cytosol of numerous species, but how does organellar protein synthesis resolve this stalling issue? Mammalian mitochondria synthesize just thirteen highly hydrophobic polypeptides. These proteins are all integral components of the machinery that couples oxidative phosphorylation. Consequently, it is essential that stalled mitochondrial ribosomes can be efficiently recycled. To date, there is no evidence to support any particular molecular mechanism to resolve this problem. However, here we discuss the observation that there are four predicted members of the mitochondrial translation release factor family and that only one member, mtRF1a, is necessary to terminate the translation of all thirteen open reading frames in the mitochondrion. Could the other members be involved in the process of recycling stalled mitochondrial ribosomes?

Keywords: mitochondria, release factor, ICT1, ribosome rescue, ribosome stalling, protein synthesis, translation

INTRODUCTION

Maintaining the efficiency and accuracy of protein synthesis is one of the most important aspects of cell survival. The translation of mRNAs into polypeptides is a complex multistep process that involves many proteins and RNA species. Consequently there are many points at which protein synthesis can be disrupted with consequent detrimental effects on cell viability (Zaher and Green, 2009). One step at which this process can fail is when the ribosome ceases to progress along the open reading frame within the transcript, termed stalling. The reasons for this are multiple and varied. Elongation arrest can be an important regulatory step such as is seen in the binding of signal recognition particles (SRP) to emergent nascent peptides. Docking of the SRP to its receptor in the endoplasmic reticulum (ER) membrane facilitates co-translational translocation and the nascent peptide is immediately inserted into the ER membrane prior to any folding event (Walter et al., 1981). Structural or sequence elements within the mRNA may cause pausing, as will the lack of sufficient charged tRNAs. In bacteria, examples of each of the events have been shown to trigger degradation of the mRNA on which the ribosome has paused (reviewed in Deana, 2005). In certain cases, however, there is potential for translational arrest to be more harmful, or more specifically that not alleviating the arrest or the cause of it, can be detrimental. For example, stalled ribosomes sequester tRNAs within the A, P, and E-sites thereby limiting their availability, impeding normal translation (Manley, 1978; Jørgensen and Kurland, 1990). Bacterial ribosomes can also stall by colliding with the RNA polymerase ahead of them, which has itself stalled on its template. The phenomenon of translational arrest caused by ribosome stalling appears to occur in bacteria and in the cytosol of eukaryotes, and although under-researched it is also likely to affect mitochondrial protein synthesis. Because of the detrimental effects that can result from stalling and the relative frequency of premature termination events, organisms have developed different strategies to rescue these ribosomes.

Eubacteria have developed a number of mechanisms (reviewed in Janssen and Hayes, 2012) but the best characterized is *trans*-translation promoted by tmRNA (reviewed in Moore and Sauer, 2007). This system, present in all eubacteria utilizes a molecule that folds to present two very different domains. The 5′ domain resembles a tRNA, which is recognized and aminoacylated by alanyl-tRNA synthetase. Aborted nascent peptides are transferred from the P-site tRNA to the alanine on this upstream tRNA-like structure, resulting in an (peptidyl)-alanyl-tmRNA. The downstream element of the tmRNA then acts as an mRNA, where the first triplet, or resume codon, generally encodes an alanine (Kapoor et al., 2011). Protein synthesis is resumed with the addition of an approximately 10 amino acid tag, before terminating in a conventional stop codon. The aberrantly translated peptide is able to leave the ribosome through the conventional mechanism, thereby rescuing the stalled components. This system is found in all known bacterial genomes, either a single tmRNA or as two pieces that bind to resemble tmRNA (Keiler et al., 2000).

The elegance of this arrangement is that it relieves the stall and tags the truncated/aberrant protein, effectively targeting it as a substrate for degradation. *Trans*-translation also requires the essential binding partner SmpB, which with tmRNA rescues ribosomes stalled on RNA templates that either lack a stop codon or have stalled during the elongation phase for other reasons. Alternative rescue pathways identified in *Escherichia coli* require the activity of protein factors ArfA or ArfB (YaeJ) that both utilize translation termination mechanisms to release arrested ribosomes (Chadani et al., 2010; Handa et al., 2010b; Abo and Chadani, 2014). The two mechanisms differ. ArfA requires recruitment of the translation termination factor RF2, whilst YaeJ retains the GGQ motif characteristic of release factors (RFs) and directly stimulates the ribosome dependent catalysis of the ester bond between the peptide and the P-site tRNA (Chadani et al., 2012). In eukaryotes, no homologs of the tmRNA system have been found, but a different mechanism has been identified to tackle the same problem. Characterized in the yeast cytosolic compartment, this system employs the protein Dom34, a homolog of the eukaryotic release factor (eRF1) but lacking the characteristic GGQ motif and codon recognition capability (Lee et al., 2007; Graille et al., 2008). Dom34 can act in concert with either a GTPase, Hbs1, or an ATPase, Rli1. In a codon-independent manner, it releases ribosomes from truncated transcripts or those that have failed to release the mRNA at the stop codon and have migrated into the 3′UTR (Guydosh and Green, 2014). Although mitoribosomes are likely to encounter similar issues that cause stalls, similar to the eukaryote cytosol no tmRNA species has been found in mammalian mitochondria. Curiously, a circularly permuted gene resembling the upstream tRNA-like fragment was identified in the primitive mitochondrial genome of *Reclinomonas americana* (Keiler et al., 2000). However, since no accompanying open reading frame for the tag peptide could be found, it seems unlikely that any mitochondrial genome has retained this apparatus. We are left, therefore, with no mechanistic data on precisely how stalled ribosomal complexes are resolved in mitochondria.

MITOCHONDRIAL RIBOSOMES, STALLING, AND PREDICTING POTENTIAL RESCUE MECHANISMS

Our understanding of all the critical recognition elements and *trans*-acting proteins responsible for mitochondrial translation lags behind the characterization in bacteria and the eukaryotic cytosol. Many of the aspects that are still unknown include the mechanisms that exert quality control of protein synthesis and rescue ribosome stalling. Given the presumed α-proteobacterial origin (Gray et al., 1999) of the organelle, the prediction is often that processes in mitochondria will strongly resemble those from their bacteria origins (Smits et al., 2010). The existing models of translation in mitochondria are, therefore, based on those of bacteria. However, despite evident similarities between the two processes, they are not identical and certain unique features of mitochondrial translation make direct comparison more complicated (reviewed in Christian and Spremulli, 2012).With respect to the ribosome rescue mechanisms, one important consideration is the structure and composition of the mitoribosome. Mitochondrial ribosomes are often compared to their prokaryotic counterparts (Sharma et al., 2003), however, mitoribosomes vary enormously depending on their organism of origin (Rackham and Filipovska, 2014). Although all consist of a small and a large subunit there can be variations in their size, RNA to protein ratio, and composition. Throughout their evolution, mitoribosomes have acquired many distinct structural characteristics, including the unusually high protein to rRNA ratio, caused by shortening of rRNA and recruitment of additional proteins (Sharma et al., 2003). Although many of the mitoribosome proteins (MRPs) have bacterial homologs, almost half of them are specific to mitochondria (Sharma et al., 2003; Koc et al., 2010). These unique MRPs are mostly situated on the outer surface of the mitoribosome some of which compensate for the loss of rRNA domains or missing bacterial proteins (Sharma et al., 2003). These new protein also form an extended peptide exit tunnel, the central protuberance and line the mRNA entry site, which differs in structure from the prokaryotic counterparts (Sharma et al., 2003; Greber et al., 2013; Kaushal et al., 2014). Recent publications describing high resolution cryo-electron microscopy (cryo-EM) structures of both the mammalian 39S large (Greber et al., 2013) and 28S small mitoribosomal subunits (Kaushal et al., 2014) confirm the unique aspects of mitoribosome architecture derived from these mitospecific RPs. Any potential ribosome rescue mechanism in mitochondria might be predicted to reflect these global changes to the structural features and composition of the mammalian 55S particle. However, analysis of mitochondrial proteins that have bacterial homologs with known function, and comparable structures may still be the best way to begin the search for potential mitoribosome rescue factors. Other approaches include looking for factors that transiently interact with the mitoribosome, or through bioinformatics analyses. Use of the last two methods have helped to identify the most likely candidates, namely members of the mitochondrial RF family (Rorbach et al., 2008; Richter et al., 2010).

MITOCHONDRIAL RELEASE FACTOR FAMILY

There are two types of release factors: those that are capable of mRNA sequence recognition (class 1 RFs) and those that are not (class 2). Class 1 RFs effect translation termination by sampling the ribosomal A-site and remaining transiently associated when they recognize a cognate STOP codon. Their function is to release the completed polypeptide from the ribosome by catalyzing the cleavage of the ester bond between the P-site tRNA and the terminal amino acid of the nascent peptide. Eubacteria utilize two different RFs, RF1 and RF2, to recognize the 3 universal STOP triplets (Oparina, 2005). In contrast, archaebacteria and eukaryotic cytosol both contain a single, omnipotent class 1 RF (named aRF1 and eRF1 respectively) that recognizes all three of the canonical STOP codons, UAA, UAG, and UGA (Ito et al., 2002; Seit-Nebi et al., 2002). Large scale phylogenetic analysis has examined the evolution and diversification of RF proteins and identified that members are present in both plastids and mitochondria (Duarte et al., 2012).

Human mitochondria use only UAA and UAG as terminating triplets, as UGA has been recoded to tryptophan. In combination with the altered characteristics of the mammalian mitoribosome this might predict the need for a reduced number of RFs. It is

perhaps a surprise, therefore, that bioinformatics classifies four proteins as members of the human mitochondrial RF family, namely mtRF1, mtRF1a, ICT1, and C12orf65. The first to be identified solely by database searches was mtRF1 (Zhang and Spremulli, 1998). The sequence recognition domains differed from the consensus, supporting the assumption that mtRF1 functioned as a single RF that recognized the four codons that at the time were assumed to function as stop codons. This premise was absorbed into the literature until mtRF1a was identified, with decoding domains that more closely resembled the consensus, and biochemical characterization confirming its recognition of UAA and UAG as stop codons (Soleimanpour-Lichaei et al., 2007). The second confounding assumption that had been accepted in the literature was that AGA and AGG were also stop codons. Since these followed the final coding triplet in mitochondrial transcripts *MTCO1* and *MTND6* respectively, this was not an unreasonable interpretation of the human mitochondrial genome (Anderson et al., 1981). More recent investigations in whole cells have shown that physiologically neither of these are stop codons. Although both codons are unassigned, they function to promote a -1 frameshift, to position UAG in the A-site for conventional termination by mtRF1a (Temperley et al., 2010).

Since mtRF1a is sufficient to terminate translation of all 13 open reading frames, what are the functions of the remaining 3 mitochondrial RF family members? Is there any evidence that they can still function as RFs? These proteins were grouped together due to similarities in their sequence and structures that they share with RFs from bacteria and the eukaryotic cytosol (Duarte et al., 2012). In particular all four family members display high conservation of the GGQ domain that is critical for catalyzing peptidyl-tRNA hydrolysis (PTH; Frolova et al., 1999). For the RF to trigger ester bond cleavage the GGQ domain must be positioned in the peptidyl transferase center of the ribosome (PTC), which occurs when the RF undergoes a major conformational change from a closed to open conformation (Vestergaard et al., 2001; Petry et al., 2005; Laurberg et al., 2008). In order to prevent RFs from displaying PTH activity too early, the conformational change that promotes peptidyl-tRNA hydrolysis is dependent on stop codon recognition (Shaw and Green, 2007; Laurberg et al., 2008). The required sequence specificity is dictated by another conserved domain, which comprises amino acid stretches that come together in space. This domain deviates from the consensus in mtRF1, both in amino acid content and by being extended in length. The hypothesis predicated on these changes, is that the extra bulk of the sequence recognition domain can fill the space in the A-site normally occupied by the mRNA. Three dimensional modeling shows that mtRF1 could occupy this cavity and synchronously extend the GGQ motif into the PTC to rescue ribosomes that have stalled with an incomplete peptide anchored to a mis-processed or partially degraded mRNA lacking a termination codon (Huynen et al., 2012). In contrast the codon recognition domain is absent in both ICT1 and C12orf65, the two remaining members of the mitochondrial RF family. Despite this, the retention of the GGQ motif in all family members strongly suggests they have all retained the ribosome dependent ability to release peptides from a P-site anchored tRNA. That they play an important role in translation is further substantiated as intra-organellar protein synthesis is impaired when ICT1 or C12orf65 are depleted or mutated (Antonicka et al., 2010; Richter et al., 2010). These observations suggest that mtRF1, C12orf65, and ICT1 are likely to function on stalled ribosomes or large subunits with peptidyl-tRNA still anchored within, allowing them to be recycled for a new round of translation.

ICT1 is intriguing as it has been incorporated into the mitoribosome as a permanent fixture. This would appear to be dangerous, as ICT1 displays codon independent PTH activity, which *a priori* could cause premature peptide release (Richter et al., 2010). Since this does not occur physiologically, the associated PTH activity of ICT1 must be carefully controlled with an as yet undefined specificity. The current hypothesis is that ICT1 must function in ribosome rescue but whether this occurs at stalling events within ORFs or on truncated transcripts is not yet clear. ICT1 does, however, have a bacterial homolog, YaeJ, which has been shown to be involved in release of arrested ribosomes (Gagnon et al., 2012). Below we will compare and contrast and see if there are useful parallels to be drawn to elucidate the potential role of ICT1 in mitochondrial ribosome rescue.

YaeJ

ArfB or YaeJ, is conserved among eukaryotes and is present in many Gram-negative species (Handa et al., 2010b). Its potential role in ribosome rescue was indicated by its structural similarity to RF1 and RF2 and the presence of the GGQ motif, characteristic of ribosome dependent PTH activity (Frolova et al., 1999). Convincing evidence for its function in ribosome rescue derived from studies in *E. coli* where YaeJ overexpression in strains lacking tmRNA and ArfA suppressed the lethal phenotype (Chadani et al., 2011). Subsequently YaeJ was shown to have direct PTH activity on stalled ribosomes both *in vitro* (Handa et al., 2010b) and *in vivo* (Handa et al., 2010b; Chadani et al., 2011), which was lost when the GGQ was mutated to GAQ (Chadani et al., 2011). This indicated that no auxiliary factors were required, in contrast to ArfA that needs to co-opt RF2 for activity. As with ICT1, the protein lacks domains 2 and 4 of a standard RF, thereby losing codon-recognition consistent with its ability to rescue ribosomes stalled on mRNA lacking STOP codons (Chadani et al., 2011). Structural analysis by the Steitz group has detailed the critical interactions that drive ribosomal rescue. The N-terminal globular domain is bound in the A-site and is joined to the C-terminus via a flexible linker (Gagnon et al., 2012). Although the C-terminus was thought to be an unstructured, it has a basic residue-rich tail that was necessary to facilitate interaction with the ribosome (Handa et al., 2010b; Chadani et al., 2011; Gagnon et al., 2012; Kogure et al., 2014). Gagnon et al. (2012) have shown that once positioned within the mRNA entry channel, it forms an α-helix. Their data suggest that the YaeJ tail can sample the mRNA channel and thereby determine whether or not the ribosome has stalled on a non-stop transcript or is still translating (Gagnon et al., 2012). If the ribosome is stalled on non-stop mRNA or an endonucleolytically cleaved transcript, the basic residues of the YaeJ tail could interact with negatively charged rRNA nucleotides lining the tunnel. Such binding to the ribosome would cause structural rearrangements within YaeJ,

similar to those following codon recognition of a standard RF, placing the GGQ domain within the PTC, facilitating peptidyl-tRNA hydrolysis (Gagnon et al., 2012). The data is clear that YaeJ is an important protein in ribosome rescue, but does it follow that the human mitochondrial ortholog plays a similar role?

ICT1

First reported, under the name of DS-1, as a transcript down-regulated during *in vitro* differentiation of a colon carcinoma cell line, immature colon carcinoma transcript-1 (ICT1; Van Belzen et al., 1995, 1998) had no connection to any potential mitochondrial function. Subsequent research by our group investigating ribosome recycling in human mitochondria, identified ICT1 as associated with mtRRF (Rorbach et al., 2008). Subsequently, the available data and bioinformatic analyses classified ICT1 in the prokaryote/mitochondrial RF family (uniprot Q14197). At ~175 amino acids post-maturation ICT1 is smaller than standard RFs due mainly to the loss of the codon recognition elements. It does, however, retain the GGQ motif that has been confirmed as functional, as GSQ and AGQ mutations affect growth and activity (Richter et al., 2010). As mentioned above, this work confirmed that ICT1 is not just mitochondrial but has actually become an integrated component of the

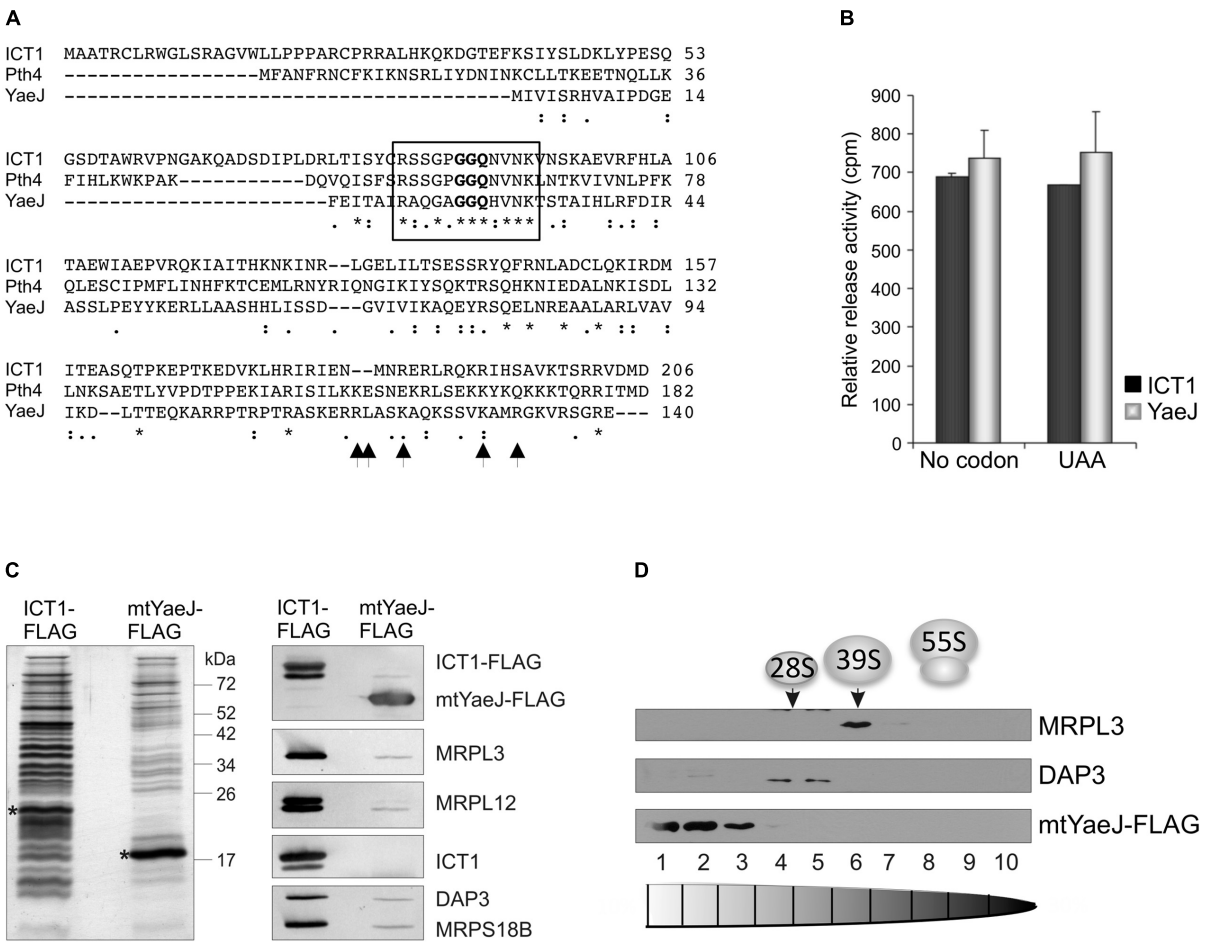

FIGURE 1 | ICT1 as a mitochondrial translation rescue factor and its possible orthologs. (A) *Alignment of human ICT1 (14197) with the Pth4 ortholog from S. pombe (Q9HDZ3) and YaeJ ortholog from E. coli (E2QFB9).* Identity is indicated by (*), high levels of similarity by (:) and lower levels by (·). The conserved GGQ region is boxed and the YaeJ residues that are required for PTH activity and are highly conserved between bacterial species are indicated by arrows. **(B)** *Release activity of recombinant YaeJ and ICT1.* PTH activity was tested on 70S ribosomes primed with either no RNA or UAA triplet in the A-site. **(C)** *Mitochondrial targetted YaeJ-FLAG shows interaction with human mitochondrial ribosomal proteins.* FLAG tag mediated immunoprecipitations of ICT1 and mitochondrially targeted YaeJ were performed on lysates of HEK293 cell lines induced for 3 days. The elution fractions (10%) were separated by SDS PAGE and analyzed by silver staining (left panel, FLAG protein indicated by *) or western blot (right panel). Antibodies against MRPL3, MRPL12, ICT1, DAP3, and MRPS18B were used to determine the relative levels of coimmunoprecipitated ribosomal proteins. The presence of FLAG tagged protein in each elution was confirmed by anti-FLAG antibodies. **(D)** *Mitochondrially-targeted YaeJ-FLAG does not co-migrate with the 39S LSU.* Lysate (700 μg) of mtYaeJ-FLAG expressing cells was separated on an isokinetic sucrose gradient. Fractions were analyzed by western blot using antibodies against the 39S LSU (MRPL3) and the 28S SSU (DAP3). The distribution of mtYaeJ-FLAG was determined by applying FLAG antibodies. Methods for panels **(B–D)** were essentially as described in Richter et al. (2010), except a YaeJ-FLAG construct was used to generate a HEK293T overexpression line instead of the ICT1 FLAG.

large ribosomal subunit. Recent cryo-EM coupled with cross-linked mass spectroscopy confirmed this observation and positions ICT1 at the central protruberance, close to MRPL15, -18, and -49 (Greber et al., 2013). Perhaps not surprisingly, depletion of ICT1 causes disruption of the mitoribosomal structure and subsequent *de novo* synthesis of mitochondrially encoded proteins (Richter et al., 2010). The combination of these characteristics make ICT1 a codon-independent but ribosome-dependent and ribosome-integrated peptidyl-tRNA hydrolase.

Analysis of ICT1 solution structure may provide more insight into the role of the protein (Handa et al., 2010a). The three distinct regions are the N-terminal mitochondrial targeting signal, the structured catalytic domain containing the GGQ motif, and an unstructured C-terminal extension rich in positively charged amino acids. The topology of the GGQ domain is β1-β2-α1-β3-α2, which follows the bacterial RF2 pattern with the exception of the α1 inserted between β2 and β3 that is not present in the latter (Handa et al., 2010a). Loss of the codon recognition domain appears to be replaced by a C-terminal extension, somewhat reminiscent of YaeJ.

YaeJ vs. ICT1

Comparisons of ICT1 and YaeJ structure and sequence alignment show both similarities and differences (**Figure 1A**; Handa et al., 2010a; Gagnon et al., 2012; Kogure et al., 2014). Identity and similarity are strong in the GGQ domains. The N-termini differ as would be expected, as ICT1 is a mitochondrially destined protein. Although an inserted region (α_i) is common to both the structure that follows differs, in YaeJ this is a β-strand in contrast to a 3_{10} helix in ICT1 (Kogure et al., 2014). The inserted α-helices share structure but differ in amino acid sequence, they are a characteristic and conserved feature for these two proteins that distinguish them from class I RFs (Kogure et al., 2014). An important feature for ribosome binding and activity in YaeJ was the length and amino acid composition of the linker and C-terminal region and critical residues for PTH activity are conserved between ICT1 and YaeJ (Kogure et al., 2014). The conserved similarities that link these two proteins whilst simultaneously distinguishing them from other RFs, suggest a conserved function and mechanism. As with Kogure et al. (2014) we could show codon-independent release activity by using recombinant YaeJ in *in vitro* assays with 70S ribosomes (**Figure 1B**). We, therefore, looked to see whether the similarities in these proteins were sufficient for YaeJ to substitute for ICT1 in the mitoribosome. To test this hypothesis, we generated cell lines that could inducibly express a mitochondrially targeted YaeJ (reported here) or the potential yeast mitochondrial RF, *Schizosaccharomyces pombe* Pth4 (reported in Dujeancourt et al., 2013). Each was generated with a C-terminal FLAG tag to facilitate efficient immunoprecipitation (IP). The immunoprecipitated protein was specifically and competitively eluted using FLAG peptide and in ach case demonstrated an association with the mitoribosome, but neither was as efficient as ICT1 at immunoprecipitating MRPs (**Figure 1C**). Each cell line was induced to express either YaeJ or Pth4 and the cell lysates were separated by isokinetic sucrose gradient (as in Richter et al., 2010). In neither case did the expressed protein migrate in fractions with the mt-LSU polypeptides (**Figure1D**). Similar results were derived for mtRRF-FLAG (Rorbach et al., 2008), supportive of an interaction with mitoribosome mediated by transient A-site entry, akin to YaeJ interaction with the bacterial ribosome (**Figure 2**; Gagnon et al., 2012; Kogure et al., 2014) rather than mitoribosome integration. This suggests that these proteins may take part in ribosome rescue but by different mechanisms. The integration of ICT1 into the mitoribosome and the cryo-EM data positioning it near the central protuberance would preclude unrestricted access of the GGQ motif to the PTC (Greber et al., 2013). This might indicate the pathway in which ICT1 is involved, as without significant conformational changes in the mitoribosome it would not be able to exert PTH activity (**Figure 2**). Such structural rearrangements of the 55S might potentially occur to release tRNA from prematurely discharged peptidyl-tRNA complexes, or if subunit dissociation occurs prior to release of the peptide. Further data is required to confirm the substrate and mechanism of ICT1 in the rescue of stalled translation in human mitochondria.

DISCUSSION

This "perspective" aims to highlight how perplexing post-transcriptional gene expression in mitochondria can be. Translation will not be an error free process but the exact nature of those errors, have yet to be determined. Mitochondrial ribosomes from different organisms can vary dramatically, and those in mammals are currently the most significantly different from the norm. This

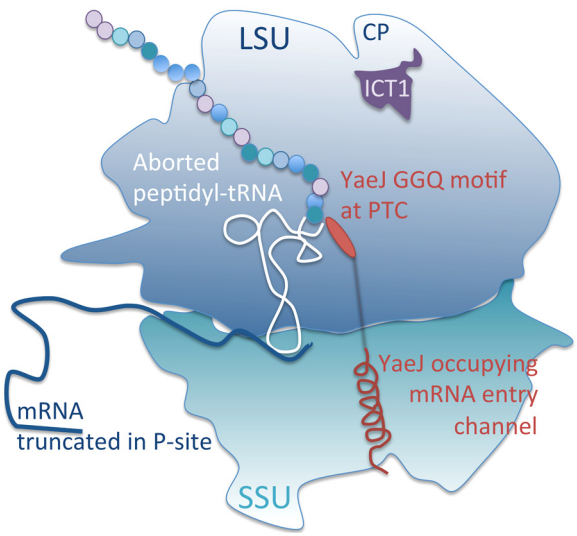

FIGURE 2 | Schematic of a composite ribosome to show relative positions occupied by ICT1 and YaeJ. Truncated mRNA lacking an A-site codon allows ingress of YaeJ such that the C-terminal α-helix aligns within the mRNA entry channel in the small subunit (SSU). This positions the GGQ motif at the peptidyl transferase centre (PTC) allowing cleavage of the ester bond between the P-site tRNA and the truncated polypeptide (as described in Kogure et al., 2014). The aborted product is then released via the polypeptide exit site in the large subunit (LSU). ICT1 by contrast is located at the central protuberance (CP) precluding its interaction with the nascent peptide without a large scale conformational change of the ribosome (as described in Greber et al., 2013).

alone would be enough to stymie progress but the lack of a robust transfection mechanism and the lack of a robust *in vitro* translation system makes study of mammalian mitochondrial translation processes a technical quagmire.

Lessons that we learnt from bacterial studies are unfortunately limited, as described above. Despite similarities between YaeJ and ICT1 and their common divergence from standard RFs, we cannot assume a similar mechanism using the bacterial paradigm, as the integration of ICT1 into the mitoribosome excludes a similar mechanism of action. Since bacteria have more than one rescue pathway, it seems probable that mitochondria will too. Thus far bioinformatics has narrowed the plausible candidates for mitochondrial rescue factors to members of mitochondrial RF family. In addition to ICT1, the feature conferring ribosome dependent PTH activity, the GGQ motif, is present in mtRF1 and C12orf65, neither of which have characterized functions. The latter shares sequence similarities with ICT1 (Kogure et al., 2012), moreover, evidence for its importance comes from clinical data where patients harboring mutations in C12orf65 manifest clear defects in mt-protein synthesis (Antonicka et al., 2010; Shimazaki et al., 2012; Spiegel et al., 2014). However, as discussed above, sharing similarities is not sufficient to infer function and confirmation of mtRF1 and C12orf65 as mitoribosome rescue factors will require evidence of their direct involvement in relieving ribosome stalling. This cannot be accomplished without initially developing a method to analyse stalled mammalian mitoribosomes. A promising approach to allow precisely such analyses comes from recent data using a patient cell line with a mutation in *MT-TY*, the gene encoding mitochondrial $tRNA^{Trp}$. Greater accumulation of mitoribosomes on Trp codons was detected, inferring mitoribosome arrest due to the shortage of the aminoacylated wild type mt-$tRNA^{Trp}$ (Rooijers et al., 2013). We are currently analysing mitoribosome distribution in the absence of the potential rescue factors, to confirm whether or not they indeed play a role in alleviating mitoribosome stalling.

AUTHOR CONTRIBUTIONS

Maria T. Wesolowska – performing the mitoribosome profiling described in the discussion and assistance in writing the manuscript. Ricarda Richter-Dennerlein – performed the experimental work reported herein. Robert N. Lightowlers – contributed to the manuscript, design of experiments and grant holder of funding supporting the co-authors. Zofia M. A. Chrzanowska-Lightowlers – main contributor to the manuscript, design of experiments and grant holder of funding supporting the co-authors.

ACKNOWLEDGMENTS

This work was supported by the Wellcome Trust [096919/Z/11/Z] and the Biotechnology and Biological Sciences Research Council [BB/F01/5895/1] whom Robert N. Lightowlers and Zofia M. A. Chrzanowska-Lightowlers would like to thank for continuing support.

REFERENCES

Abo, T., and Chadani, Y. (2014). The faIL-safe system to rescue the stalled ribosomes in *Escherichia coli*. *Front. Microbiol.* 5:156. doi: 10.3389/fmicb.2014.00156

Anderson, S., Bankier, A. T., Barrell, B. G., de Bruijn, M. H., Coulson, A. R., Drouin, J., et al. (1981). Sequence and organization of the human mitochondrial genome. *Nature* 290, 457–465. doi: 10.1038/290457a0

Antonicka, H., Østergaard, E., Sasarman, F., Weraarpachai, W., Wibrand, F., Pedersen, A. M. B., et al. (2010). Mutations in C12orf65 in patients with encephalomyopathy and a mitochondrial translation defect. *Am. J. Hum. Genet.* 87, 115–122. doi: 10.1016/j.ajhg.2010.06.004

Chadani, Y., Ito, K., Kutsukake, K., and Abo, T. (2012). ArfA recruits release factor 2 to rescue stalled ribosomes by peptidyl-tRNA hydrolysis in *Escherichia coli*. *Mol. Microbiol.* 86, 37–50. doi: 10.1111/j.1365-2958.2012.08190.x

Chadani, Y., Ono, K., Kutsukake, K., and Abo, T. (2011). *Escherichia coli* YaeJ protein mediates a novel ribosome-rescue pathway distinct from SsrA- and ArfA-mediated pathways. *Mol. Microbiol.* 80, 772–785. doi: 10.1111/j.1365-2958.2011.07607.x

Chadani, Y., Ono, K., Ozawa, S., Takahashi, Y., Takai, K., Nanamiya, H., et al. (2010). Ribosome rescue by *Escherichia coli* ArfA (YhdL) in the absence of trans-translation system. *Mol. Microbiol.* 78, 796–808. doi: 10.1111/j.1365-2958.2010.07375.x

Christian, B. E., and Spremulli, L. L. (2012). Mechanism of protein biosynthesis in mammalian mitochondria. *Biochim. Biophys. Acta* 1819, 1035–1054. doi: 10.1016/j.bbagrm.2011.11.009

Deana, A. (2005). Lost in translation: the influence of ribosomes on bacterial mRNA decay. *Genes Dev.* 19, 2526–2533. doi: 10.1101/gad.1348805

Duarte, I., Nabuurs, S. B., Magno, R., and Huynen, M. (2012). Evolution and diversification of the organellar release factor family. *Mol. Biol. Evol.* 29, 3497–3512. doi: 10.1093/molbev/mss157

Dujeancourt, L., Richter, R., Chrzanowska-Lightowlers, Z. M., Bonnefoy, N., and Herbert, C. J. (2013). Interactions between peptidyl tRNA hydrolase homologs and the ribosomal release factor Mrf1 in S. pombe mitochondria. *Mitochondrion* 13, 871–880. doi: 10.1016/j.mito.2013.07.115

Frolova, L. Y., Tsivkovskii, R. Y., Sivolobova, G. F., Oparina, N. Y., Serpinsky, O. I., Blinov, V. M., et al. (1999). Mutations in the highly conserved GGQ motif of class 1 polypeptide release factors abolish ability of human eRF1 to trigger peptidyl-tRNA hydrolysis. *RNA* 5, 1014–1020. doi: 10.1017/S1355838299 99043X

Gagnon, M. G., Seetharaman, S. V., Bulkley, D., and Steitz, T. A. (2012). Structural basis for the rescue of stalled ribosomes: structure of YaeJ bound to the ribosome. *Science* 335, 1370–1372. doi: 10.1126/science.1217443

Graille, M., Chaillet, M., and van Tilbeurgh, H. (2008). Structure of yeast Dom34: a protein related to translation termination factor erf1 and involved in no-go decay. *J. Biol. Chem.* 283, 7145–7154. doi: 10.1074/jbc.M708224200

Gray, M. W., Burger, G., and Lang, B. F. (1999). Mitochondrial evolution. *Science* 283, 1476–1481. doi: 10.1126/science.283.5407.1476

Greber, B. J., Boehringer, D., Leitner, A., Bieri, P., Voigts-Hoffmann, F., Erzberger, J. P., et al. (2013). Architecture of the large subunit of the mammalian mitochondrial ribosome. *Nature* 505, 515–519. doi: 10.1038/nature12890

Guydosh, N. R., and Green, R. (2014). Dom34 Rescues Ribosomes in 3′ Untranslated Regions. *Cell* 156, 950–962. doi: 10.1016/j.cell.2014.02.006

Handa, Y., Hikawa, Y., Tochio, N., Kogure, H., Inoue, M., Koshiba, S., et al. (2010a). Solution structure of the catalytic domain of the mitochondrial protein ICT1 that is essential for cell vitality. *J. Mol. Biol.* 404, 260–273. doi: 10.1016/j.jmb.2010.09.033

Handa, Y., Inaho, N., and Nameki, N. (2010b). YaeJ is a novel ribosome-associated protein in *Escherichia coli* that can hydrolyze peptidyl-tRNA on stalled ribosomes. *Nucleic Acids Res.* 39, 1739–1748. doi: 10.1093/nar/gkq1097

Huynen, M. A., Duarte, I., Chrzanowska-Lightowlers, Z. M. A., and Nabuurs, S. B. (2012). Structure based hypothesis of a mitochondrial ribosome rescue mechanism. *Biol. Direct* 7, 14. doi: 10.1186/1745-6150-7–14

Ito, K., Frolova, L., Seit-Nebi, A., Karamyshev, A., Kisselev, L., and Nakamura, Y. (2002). Omnipotent decoding potential resides in eukaryotic translation termination factor eRF1 of variant-code organisms and is modulated by the interactions of amino acid sequences within domain 1. *Proc. Natl. Acad. Sci. U.S.A.* 99, 8494–8499. doi: 10.1073/pnas.142690099

Janssen, B. D., and Hayes, C. S. (2012). "The tmRNA ribosome-rescue system," in *Advances in Protein Chemistry and Structural Biology (Elsevier)*, 151–191. Available at: http://linkinghub.elsevier.com/retrieve/pii/B9780123864970000050 [Accessed May 29, 2014].

Jørgensen, F., and Kurland, C. G. (1990). Processivity errors of gene expression in *Escherichia coli*. *J. Mol. Biol.* 215, 511–521. doi: 10.1016/S0022-2836(05)80164-0

Kapoor, S., Samhita, L., and Varshney, U. (2011). Functional significance of an evolutionarily conserved alanine (GCA) resume codon in tmRNA in *Escherichia coli*. *J. Bacteriol.* 193, 3569–3576. doi: 10.1128/JB.01446-10

Kaushal, P. S., Sharma, M. R., Booth, T. M., Haque, E. M., Tung, C.-S., Sanbonmatsu, K. Y., et al. (2014). Cryo-EM structure of the small subunit of the mammalian mitochondrial ribosome. *Proc. Natl. Acad. Sci. U.S.A.* 111, 7284–7289. doi: 10.1073/pnas.1401657111

Keiler, K. C., Shapiro, L., and Williams, K. P. (2000). tmRNAs that encode proteolysis-inducing tags are found in all known bacterial genomes: a two-piece tmRNA functions in *Caulobacter*. *Proc. Natl. Acad. Sci. U.S.A.* 97, 7778–7783. doi: 10.1073/pnas.97.14.7778

Koc, E. C., Haque, M. E., and Spremulli, L. L. (2010). Current views of the structure of the mammalian mitochondrial ribosome. *Isr. J. Chem.* 50, 45–59. doi: 10.1002/ijch.201000002

Kogure, H., Handa, Y., Nagata, M., Kanai, N., Güntert, P., Kubota, K., et al. (2014). Identification of residues required for stalled-ribosome rescue in the codon-independent release factor YaeJ. *Nucleic Acids Res.* 42, 3152–3163. doi: 10.1093/nar/gkt1280

Kogure, H., Hikawa, Y., Hagihara, M., Tochio, N., Koshiba, S., Inoue, Y., et al. (2012). Solution structure and siRNA-mediated knockdown analysis of the mitochondrial disease-related protein C12orf65. *Proteins* 80, 2629–2642. doi: 10.1002/prot.24152

Laurberg, M., Asahara, H., Korostelev, A., Zhu, J., Trakhanov, S., and Noller, H. F. (2008). Structural basis for translation termination on the 70S ribosome. *Nature* 454, 852–857. doi: 10.1038/nature07115

Lee, H. H., Kim, Y.-S., Kim, K. H., Heo, I., Kim, S. K., Kim, O., et al. (2007). Structural and functional insights into Dom34, a key component of no-go mRNA decay. *Mol. Cell* 27, 938–950. doi: 10.1016/j.molcel.2007.07.019

Manley, J. L. (1978). Synthesis and degradation of termination and premature-termination fragments of β-galactosidase in vitro and in vivo. *J. Mol. Biol.* 125, 407–432. doi: 10.1016/0022-2836(78)90308-X

Moore, S. D., and Sauer, R. T. (2007). The tmRNA system for translational surveillance and ribosome rescue. *Annu. Rev. Biochem.* 76, 101–124. doi: 10.1146/annurev.biochem.75.103004.142733

Oparina, N. J. (2005). Common and specific amino acid residues in the prokaryotic polypeptide release factors RF1 and RF2: possible functional implications. *Nucleic Acids Res.* 33, 5226–5234. doi: 10.1093/nar/gki841

Petry, S., Brodersen, D. E., Murphy, F. V. IV, Dunham, C. M., Selmer, M., Tarry, M. J., et al. (2005). Crystal structures of the ribosome in complex with release factors RF1 and RF2 bound to a cognate stop codon. *Cell* 123, 1255–1266. doi: 10.1016/j.cell.2005.09.039

Rackham, O., and Filipovska, A. (2014). Supernumerary proteins of mitochondrial ribosomes. *Biochim. Biophys. Acta* 1840, 1227–1232. doi: 10.1016/j.bbagen.2013.08.010

Richter, R., Rorbach, J., Pajak, A., Smith, P. M., Wessels, H. J., Huynen, M. A., et al. (2010). A functional peptidyl-tRNA hydrolase, ICT1, has been recruited into the human mitochondrial ribosome. *EMBO J.* 29, 1116–1125. doi: 10.1038/emboj.2010.14

Rooijers, K., Loayza-Puch, F., Nijtmans, L. G., and Agami, R. (2013). Ribosome profiling reveals features of normal and disease-associated mitochondrial translation. *Nat. Commun.* 4:2886. doi: 10.1038/ncomms3886

Rorbach, J., Richter, R., Wessels, H. J., Wydro, M., Pekalski, M., Farhoud, M., et al. (2008). The human mitochondrial ribosome recycling factor is essential for cell viability. *Nucleic Acids Res.* 36, 5787–5799. doi: 10.1093/nar/gkn576

Seit-Nebi, A., Frolova, L., and Kisselev, L. (2002). Conversion of omnipotent translation termination factor eRF1 into ciliate-like UGA-only unipotent eRF1. *EMBO Rep.* 3, 881–886. doi: 10.1093/embo-reports/kvf178

Sharma, M. R., Koc, E. C., Datta, P. P., Booth, T. M., Spremulli, L. L., and Agrawal, R. K. (2003). Structure of the mammalian mitochondrial ribosome reveals an expanded functional role for its component proteins. *Cell* 115, 97–108. doi: 10.1016/S0092-8674(03)00762-1

Shaw, J. J., and Green, R. (2007). Two distinct components of release factor function uncovered by nucleophile partitioning analysis. *Mol. Cell* 28, 458–467. doi: 10.1016/j.molcel.2007.09.007

Shimazaki, H., Takiyama, Y., Ishiura, H., Sakai, C., Matsushima, Y., Hatakeyama, H., et al. (2012). A homozygous mutation of C12orf65 causes spastic paraplegia with optic atrophy and neuropathy (SPG55). *J. Med. Genet.* 49, 777–784. doi: 10.1136/jmedgenet-2012-101212

Smits, P., Smeitink, J., and van den Heuvel, L. (2010). Mitochondrial translation and beyond: processes implicated in combined oxidative phosphorylation deficiencies. *J. Biomed. Biotechnol.* 2010, 737385. doi: 10.1155/2010/737385

Soleimanpour-Lichaei, H. R., Kühl, I., Gaisne, M., Passos, J. F., Wydro, M., Rorbach, J., et al. (2007). mtRF1a is a human mitochondrial translation release factor decoding the major termination codons UAA and UAG. *Mol. Cell* 27, 745–757. doi: 10.1016/j.molcel.2007.06.031

Spiegel, R., Mandel, H., Saada, A., Lerer, I., Burger, A., Shaag, A., et al. (2014). Delineation of C12orf65-related phenotypes: a genotype–phenotype relationship. *Eur. J. Hum. Genet.* doi: 10.1038/ejhg.2013.284 [Epub ahead of print].

Temperley, R., Richter, R., Dennerlein, S., Lightowlers, R. N., and Chrzanowska-Lightowlers, Z. M. (2010). Hungry codons promote frameshifting in human mitochondrial ribosomes. *Science* 327, 301. doi: 10.1126/science.1180674

Van Belzen, N., Diesveld, M. P., van der Made, A. C., Nozawa, Y., Dinjens, W. N., Vlietstra, R., et al. (1995). Identification of mRNAs that show modulated expression during colon carcinoma cell differentiation. *Eur. J. Biochem. FEBS* 234, 843–848. doi: 10.1111/j.1432-1033.1995.843_a.x

Van Belzen, N., Dinjens, W. N., Eussen, B. H., and Bosman, F. T. (1998). Expression of differentiation-related genes in colorectal cancer: possible implications for prognosis. *Histol. Histopathol.* 13, 1233–1242.

Vestergaard, B., Van, L. B., Andersen, G. R., Nyborg, J., Buckingham, R. H., and Kjeldgaard, M. (2001). Bacterial polypeptide release factor RF2 is structurally distinct from eukaryotic eRF1. *Mol. Cell* 8, 1375–1382. doi: 10.1016/S1097-2765(01)00415-4

Walter, P., Ibrahimi, I., and Blobel, G. (1981). Translocation of proteins across the endoplasmic reticulum. I. Signal recognition protein (SRP) binds to in-vitro-assembled polysomes synthesizing secretory protein. *J. Cell Biol.* 91(2 Pt 1), 545–550. doi: 10.1083/jcb.91.2.545

Zaher, H. S., and Green, R. (2009). Fidelity at the molecular level: lessons from protein synthesis. *Cell* 136, 746–762. doi: 10.1016/j.cell.2009.01.036

Zhang, Y., and Spremulli, L. L. (1998). Identification and cloning of human mitochondrial translational release factor 1 and the ribosome recycling factor. *Biochim. Biophys. Acta* 1443, 245–250. doi: 10.1016/S0167-4781(98)00223-1

Conflict of Interest Statement: The authors declare that the research was conducted in the absence of any commercial or financial relationships that could be construed as a potential conflict of interest.

Received: 07 June 2014; paper pending published: 20 June 2014; accepted: 03 July 2014; published online: 18 July 2014.

*Citation: Wesolowska MT, Richter-Dennerlein R, Lightowlers RN and Chrzanowska-Lightowlers ZMA (2014) Overcoming stalled translation in human mitochondria. Front. Microbiol. **5**:374. doi: 10.3389/fmicb.2014.00374*

This article was submitted to Microbial Physiology and Metabolism, a section of the journal Frontiers in Microbiology.